SEGREGATED AND RANDOM NETWORK FORMATION OF MWCNT AND NANOSILICA IN NR AND XNBR

Thesis submitted to

Cochin University of Science and Technology

in partial fulfilment of the requirements

for the award of the degree of

Doctor of Philosophy

Neena George

Department of Polymer Science and Rubber Technology

Cochin University of Science and Technology

Kochi- 682 022, Kerala, India

May 2017

Segregated and Random Network formation of MWCNT and Nanosilica in NR and XNBR

Ph. D Thesis

Author

Neena George
Assistant Professor,
Department of Chemistry
Govt. College Chittur, Palakkad - 678104
Kerala, India
E-mail: ninleo07@gmail.com

Supervising teachers

Dr. Rani Joseph
Professor (Rtd.)
Department of Polymer Science and
Rubber Technology
Cochin University of Science
and Technology
Cochin- 682 022, Kerala, India
E-mail: rani@cusat.ac.in

Dr. A. Mathiazhagan
Associate Professor
Department of Ship Technology
Cochin University of Science
and Technology
Cochin- 682 022, Kerala, India
E-mail: alagan@cusat.ac.in

Department of Polymer Science and Rubber Technology
Cochin University of Science and Technology
Cochin- 682 022, Kerala, India

May 2017

Certificate

This is to certify that the thesis entitled **"Segregated and Random Network formation of MWCNT and Nanosilica in NR and XNBR"** is a report of the original work carried out by **Smt. Neena George** under our supervision and guidance in the Department of Polymer Science and Rubber Technology, Cochin University of Science and Technology, Cochin-22. No part of the work reported in this thesis has been presented for any other degree from any other institution. All the relevant corrections and modifications suggested by the audience during the pre-synopsis seminar and recommended by the Doctoral committee have been incorporated in the thesis.

Supervising teachers

Dr. Rani Joseph
Professor (Retired)
Department of Polymer Science and
Rubber Technology
Cochin University of Science
and Technology
Cochin- 682 022, Kerala, India
E-mail: rani@cusat.ac.in

Dr. A. Mathiazhagan
Associate Professor
Department of Ship Technology
Cochin University of Science
and Technology
Cochin- 682 022, Kerala, India
E-mail: alagan@cusat.ac.in

Cochin-22
15/05/2017

Declaration

I hereby declare that the thesis entitled "**Segregated and Random Network formation of MWCNT and Nanosilica in NR and XNBR**", is the original work carried out by me under the supervision of **Dr. Rani Joseph** (Professor, Retired, Department of Polymer Science and Rubber Technology) and under the co-guidance of **Dr. A. Mathiazhagan** (Associate Professor, Department of Ship Technology) Cochin University of Science and Technology, Cochin-22 and has never been included in any other thesis submitted previously for the award of any degree.

Cochin – 22   **Neena George**
15/05/2017

Dedicated to...

My Ammichi 'Mettilda'
and Mummy 'Mary'

Acknowledgements

This thesis would not have been possible without the generous contribution of many people who were always there when I needed them the most. I take this opportunity to acknowledge them and extend my sincere gratitude for successful completion of my Ph.D Thesis.

First and foremost, I would like to thank God Almighty for enabling my life's long cherished dream to come true. Without his blessings, this achievement would not have been possible.

I especially thank my research guide Prof. Dr. Rani Joseph for her continuous support, motivation and care that she has given me throughout my research work. Teacher, you are very special to me and I would say like my mother … and I do freely share my emotions with you. You are my inspiration and your knowledge and experience in the polymer field are really amazing. Your guidance and deep insights helped me at various stages of my research.

I thank Dr. A. Mathiazhagan (Associate Professor, Department of Ship Technology, Cochin University of Science and Technology), my co-guide for his valuable suggestions and motivation. Whenever I met him he gave me instructions and tips for completing the research and thesis on time.

I am thankful to Dr. Honey John (Head of the Dept. of Polymer Science and Rubber Technology) for providing necessary facilities for the completion of my research work. She was always there with a helping hand, clearing my doubts and correcting research papers. My deep gratitude to Dr. Sunil K. Narayanankutty (Former Head of the Dept. of Polymer Science and Rubber Technology) for his philosophical approach and discussions that I loved always and made me happy after meeting him. I am thankful to all the retired faculty members of PSRT; Dr. K. E. George for his special concern and sincere corrections of my thesis, Dr. Philip Kurian, Dr. Eby Thomas Thachil for their whole-hearted support and well wishes.

 I express my sincere gratitude to Dr. C. P. Reghunathan Nair (Emeritus Professor, PSRT) for his valuable suggestions during my synopsis submission.

I convey my sincere thanks to the present faculty members of PSRT; Dr. Thomas Kurian (for his concern and prayers for me), Dr. Prasanth Raghavan, Dr. Sailaja G. S., Dr. Jayalatha Gopalakrishnan, Dr. Jinu Jacob George, Dr. Jyothishkumar P. and

Neena George

Preface

Conductive polymer composites with random conductive networks generally require high loadings of filler at the insulator/conductor transition. But highly loaded polymer composites exhibit inferior mechanical properties. A new class of polymer composites namely segregated conductive polymer composites (s-CPCs) have been emerged to solve this problem. s-CPCs contain conductive fillers segregated in the perimeters of the polymeric granules instead of being randomly distributed throughout.

Carbon nanotubes (CNTs) have attracted great deal of interest among researchers since their discovery due to their unique mechanical, electrical and thermal properties. Due to large surface energy and strong interaction, CNTs are difficult to be uniformly dispersed in polymer matrix by simple mechanical mixing. But good dispersion is essential for ensuring enhanced mechanical and electrical properties at low filler loadings.

In the present work both non covalent modification and covalent modification of the Multiwalled carbon nanotubes (MWCNTs) have been done to get their stable aqueous dispersions. Sonication assisted latex stage mixing of the aqueous dispersions of the fillers to the rubber has been done to get uniform and homogenous distribution of fillers in the rubber. Composite preparation was done by film casting. It is expected that the nanofillers will be pushed to the periphery of rubber particles when water gets evaporated. This ensures the formation of a web like segregated network of fillers in the composite.

Processing methods may influence the filler morphology and properties of the composites. To compare the filler morphology under different processing methods an alternate method involving co-coagulation of the rubber latex with nanofillers followed by mixing the dried coagulum in Haake mixer was also tried. The web-like network of nanofillers present in

the coagulum is likely to be broken by the intense shear forces inside the internal mixer. The final sample will contain uniformly distributed filler particles in the rubber matrix. To investigate the role of polarity of rubber in determining the filler morphology, the study was also conducted using polar XNBR latex.

The thesis entitled "**Segregated and Random Network formation of MWCNT and Nanosilica in NR and XNBR**" consists of 8 chapters. The chapters from 3 to 7 are divided into two parts.

The significance of fabricating polymer composites having segregated network of conducting nanofillers is discussed in **Chapter 1.** An introduction on the polymers viz. NR and XNBR and nanofillers viz. MWCNTs and nanosilica, used in the study is also included. The specific objectives of the work are also presented in this chapter.

A detailed description of the materials used and the methods employed for the present study is given in **Chapter 2**.

Natural rubber/multiwalled carbon nanotube composite with segregated network is described in **Chapter 3**. **Part A** is focussed on noncovalent modification of MWCNTs using non-ionic surfactant and optimization of surfactant concentration and sonication energy. The fabrication of NR composites having segregated network of surfactant coated MWCNTs by latex stage processing followed by film casting and curing is described in **Part B**. The evaluation of microstructure, morphology, mechanical and electrical properties of the composites is also reported.

Natural rubber/carboxylated multiwalled carbon nanotube composite with segregated network is presented in **Chapter 4**. Covalent modification of MWCNTs by H_2SO_4/HNO_3 treatment in order to disperse the nanotubes in water without adding any surfactant is explored in **Part A.** The preparation of NR/carboxylated MWCNT composites through latex stage processing

and the studies on morphology, mechanical and electrical properties are described in **Part B**

The use of nanosilica as reinforcing filler in natural rubber latex is discussed in **Chapter 5**. The role of processing method in determining filler morphology inside a polymer and its effect in the properties of the composites is also given in the chapter. The preparation and mechanical properties of NR/nanosilica composites with segregated network is presented in **Part A**. The effect of Haake mixing on the silica network in NR is discussed in **Part B**.

The effect of hybrid filler on the dielectric properties of NR/MWCNTR composites is described in **Chapter 6**. Nanosilica decorated MWCNTs (CS hybrid) were prepared and characterized by TEM, FTIR and UV-vis spectroscopy and utilized for the fabrication of composites with NR resulting in segregated (NRCSF) and random filler network (NRCSH). The study of mechanical and electrical properties of the NR/CS hybrid composites with segregated hybrid filler network is given in **Part A** and the NRCSH composites with random network of hybrid fillers are studied in **Part B.**

The preparation and evaluation of mechanical and electrical properties of the MWCNTR composites with carboxylated acrylonitrile butadiene rubber (XNBR) are presented in **Chapter 7**. The XCF composites with segregated structure are discussed in **Part A** and XCH composites with random structure are described in **Part B.**

The summary and conclusions of the study are given in **Chapter 8**.

▓▓ Contents ▓▓

Chapter 3
NATURAL RUBBER/MULTIWALLED CARBON NANOTUBE
COMPOSITES WITH SEGREGATED NETWORK.........................73 - 115

Chapter 5
NANOSILICA AS REINFORCING FILLER IN NATURAL
RUBBER LATEX .... 153 - 194

Chapter 6
NANOSILICA DECORATED MULTIWALLED
CARBON NANOTUBES (CS HYBRIDS) IN
NATURAL RUBBER LATEX .... 195 - 252

Part A
NR/CS HYBRID COMPOSITES WITH SEGREGATED NETWORK

Part B
NR/CS HYBRID COMPOSITES WITH RANDOM NETWORK

Chapter 7

CARBOXYLATED MULTIWALLED CARBON
NANOTUBES IN CARBOXYLATED NITRILE
BUTADIENE RUBBER LATEX .... 253 - 303

Part A
XNBR/CARBOXYLATED MWCNT COMPOSITES WITH
SEGREGATED NETWORK

Part B
XNBR/CARBOXYLATED MWCNT COMPOSITES WITH
RANDOM NETWORK

Chapter 8

…..ജി൘…..

List of Abbreviations and Symbols

AC	Alternating Current
ASTM	American Society for Testing and Materials
BET	Brunauer – Emmet – Teller
CB	Carbon black
CBS	N – cyclohexyl – 2 – benzothiazole sulphenamide
CMC	Critical micelle concentration
CNT	Carbon nanotube
Cp	Capacitance
CPC	Conductive polymer composite
CRI	Cure rate index
CS hybrid	Nanosilica carboxylated multiwalled carbon nanotube hybrid
CTAB	Cetyl trimethyl ammonium bromide
CVD	Chemical vapour deposition
DC	Direct current
DLS	Dynamic light scattering
DMA	Dynamic mechanical analyzer
DRC	Dry rubber content
DTG	Differential thermogravimetry
DWCNT	Double walled carbon nanotube
ε_0	Permittivity of free space
ε	Permittivity
E'	Storage modulus
ε''	Imaginary part of permittivity
E''	Loss modulus
EDS	Electron dispersive X-ray spectroscopy
EMI	Electromagnetic interference
ε_r	Relative permittivity
FTIR	Fourier transform infrared spectroscopy
GNS	Graphene nanosheets
GO	Graphene oxide
HRTEM	High resolution transmission electron microscopy
HXNBR	Hydrogenated carboxylated acrylonitrile-butadiene rubber
I	Current strength

2θ	Diffraction angle
k	Dielectric constant
MEK	Methyl ethyl ketone
M_H	Maximum torque
M_L	Minimum torque
MOR	Morpholino thiobenzthiazyl sulfonamide
MWCNT	Multiwalled carbon nanotube
MWCNTR	Oxidised/Carboxylated multiwalled carbon nanotube
MWS	Maxwell – Wagner – Sillars
NaDDBs	Sodium dodecyl benzene sulphonate
NBR	Nitrile rubber
NR	Natural rubber
NRCSF	Natural rubber/carboxylated multiwalled carbon nanotube-nanosilica hybrid composite prepared by latex stage mixing
NRCSH	Natural rubber/carboxylated multiwalled carbon nanotube-nanosilica hybrid composite prepared by latex coagulation
NRSF	Natural rubber nanosilica composite prepared by latex stage mixing
NRSH	Natural rubber nanosilica composite prepared by latex coagulation method
PEDOT:PSS	poly(3,4-ethylenedioxythiophene):poly(styrene sulfonate)
phr	Parts by weight per hundred parts of rubber
Qt%	Mol percentage uptake
R	Resistance
RGO	Reduced graphene oxide
RPA	Rubber process analyzer
SBR	Styrene butadiene rubber
s-CPC	Segregated conductive polymer network
SDBS	Sodium dodecyl benzene sulphonate
SDS	Sodium dodecyl sulphate
SE	Shielding effectiveness
SE_A	Absorption shielding effectiveness
SEM	Scanning electron microscopy
SE_R	Reflection shielding effectiveness
Si69	Bis (triethoxysilylpropyl) tetra sulphide
SP	Styrenated phenol

SWCNT	Singlewalled carbon nanotube
T_{10}	Scorch time
T_{90}	Optimum cure time
TEOS	Tetraethoxysilane
TGA	Thermogravimetric analysis
TMTD	Tetramethyl thiuram disulphide
TQ	2, 2, 4 – trimethyl – 1 2 – dihydro quinoline
TSC	Total solid content
UV – vis	Ultraviolet – visible spectroscopy
VL	Polyethylene oxide condensate
XCF	Carboxylated nitrile rubber/carboxylated multiwalled carbon nanotube composite prepared by latex stage mixing
XCH	Carboxylated nitrile rubber/carboxylated multiwalled carbon nanotube composite prepared by latex coagulation
XNBR	Carboxylated nitrile rubber
XPS	X – ray photo electron spectroscopy
XRD	X – ray diffraction
ZDC	Zinc diethyl thiocarbamate
σ	Electrical conductivity, nominal stress
σ^{*}	Reduced stress
ϕ	Filler volume fraction
ϕ_c	Percolation volume fraction
χ	Rubber solvent interaction parameter

.....ೞ೧ೱ.....

Chapter 1

INTRODUCTION

Rubber is a fascinating material due to its ability to undergo large elastic deformations, i.e. the ability to return to its original shape even after large elongation[1]. Rubbers can be classified as natural and synthetic. Natural rubber (NR) is the only biosynthesised rubber and is one of the important elastomer in terms of versatility, high tensile strength, flexibility and elasticity[2]. But NR has very poor resistance to flame, oil and weather, and to overcome these drawbacks different synthetic rubbers were developed. But both natural and synthetic rubbers in raw form do not possess sufficient mechanical strength and hence need to be vulcanised and reinforced with fillers for commercial applications[3,4]. Commonly used reinforcing fillers in rubber include finely divided particulates such as carbon black, silica or clay. These conventional fillers have to be added in large quantities (a minimum of 20 - 30 wt%) to achieve the required reinforcement, which makes the processing difficult and also increases the weight of the final product. The increased demand for light weight, high performance rubber products paved

the way to the use of nanofillers in rubber industry. In the last few decades rubber nanocomposites have attracted researchers and industrialists alike, due to their superior properties[5] compared to the rubber composites containing conventional fillers. Unique properties of the nanofillers enable large improvement in properties at low filler loading resulting in light weight products with high performance.

The essential conditions to obtain enhanced properties for polymer nanocomposites are the uniform distribution of the filler in the polymer matrix and strong polymer-filler interaction. So it is necessary to ensure good dispersion of nano-fillers in the rubber to obtain desirable properties. Carbon nanotubes are one of the promising nanofillers since they can impart mechanical reinforcement and electrical conductivity at low concentrations. Many studies are concentrating in the field of carbon nanotube-rubber composites on account of their wide range of applications[6-10]. Most of the studies reveal the difficulty in obtaining a homogeneous dispersion due to severe agglomeration of carbon nanotubes in the rubber matrix. For the same reason, efforts made to reinforce rubber with carbon nanotubes by conventional mill mixing method were found to be ineffective. Latex nanocomposites prepared by mixing the dispersions of nanofillers to the polymer latices have become attractive nowadays. This is due to better performance resulting from the homogeneous dispersion of nanofillers in the latex matrix[11].

Compared to intrinsically conducting polymers, electrically conductive polymer composites (CPCs) developed by mixing polymer with conductive filler have generated significant interest due to their ease of processing, low-cost and tunable electrical properties. They have been used in many applications as conductors, sensors, anti-static materials and electromagnetic interference (EMI) shields[12-14]. In ordinary CPCs with random network of conductive fillers insulator to conductor transition can be achieved only at high

filler loading resulting in high electrical percolation threshold. In 1971 Turner and co-workers introduced the concept of "segregated conductive network" for nickel particle/high-density polyethylene (HDPE) composites[15]. Segregated conductive polymer composite (s-CPC) contains conductive fillers that are segregated in the perimeters of the polymeric granules instead of being randomly distributed throughout the bulk CPC material. From thereon s-CPCs have generated considerable interest because of their ultralow percolation concentration (0.005–0.1 vol%), superior electrical conductivity (up to 10^6 S/m), and reasonable electromagnetic interference (EMI) shielding effectiveness (above 20 dB) at low filler loadings[16-18].

The study proposes fabrication of rubber nanocomposites by adopting latex stage mixing of the nanofillers viz. multiwalled carbon nanotubes and nanosilica with natural rubber (NR) and carboxylated nitrile rubber (XNBR). The formation of segregated conductive network of fillers inside the composites is also analysed in detail. A general introduction is given in the following sections about NR and XNBR lattices, MWCNTs, nanosilica, polymer nanocomposites, latex nanocomposites and significance of segregated conductive polymer nanocomposites.

1.1 Polymer latices

Latex is defined as a stable colloidal dispersion of a polymeric substance in an aqueous medium. The dispersion medium is usually a dilute aqueous solution containing substances such as electrolytes, surface-active compounds, hydrophilic polymers, and initiator residues[19]. Almost all latices contain spherical polymer particles. Sometimes partial agglomeration of the polymer particles may occur resulting in particles of irregular shape. NR latex contains particles having size in the range 0.05-5 μm. Compared to NR, latex particles in synthetic latex are smaller in size and hence possess larger surface area.
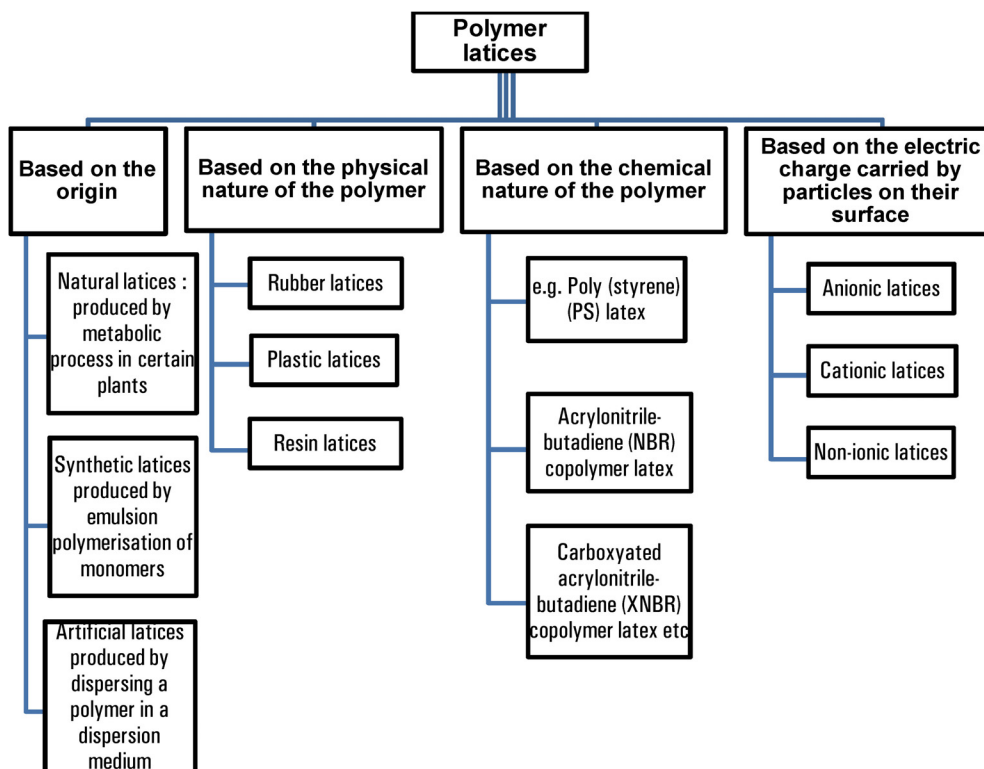
Fig. 1.1 Classification of polymer latices

The term 'latex' has been broadened in recent years and refers to a stable dispersion of a polymer in aqueous medium. Polymer latices are classified into different groups as given in Fig. 1.1.

1.1.1 Natural rubber (NR) latex

NR latex is a white colloidal suspension collected from *Hevea brasiliensis* tree by the 'tapping' process (Fig.1.2.A). NR latex contains rubber and non-rubber particles like proteins, lipids, minerals, carbohydrates and cytoplasmic C-serum[20]. Proteins and lipids constitute about 2% of the latex[21,22] and these have significant role in maintaining the stability of the latex system. NR particles are mainly spherical with hydrophobic core of polyisoprene

surrounded by a monolayer of proteins and lipids[23,24] (Fig. 1.2.C). The thickness of the monolayer is around 1.5-4.0 nm[25]. It is estimated that there are more than 1300 protein spots in the latex and nearly 600 in rubber particles[26]. Dai et al. reported 186 different proteins in rubber particles in 2013[27]. The colloidal stability of fresh field NR latex is primarily due to the presence of adsorbed proteins and phospholipids on the surface of the rubber particles. In the case of commercial ammonia preserved centrifuged latex, the latex particles are stabilised mainly by the adsorbed fatty acid anions, hydrolysis products of phospholipids[28,29].
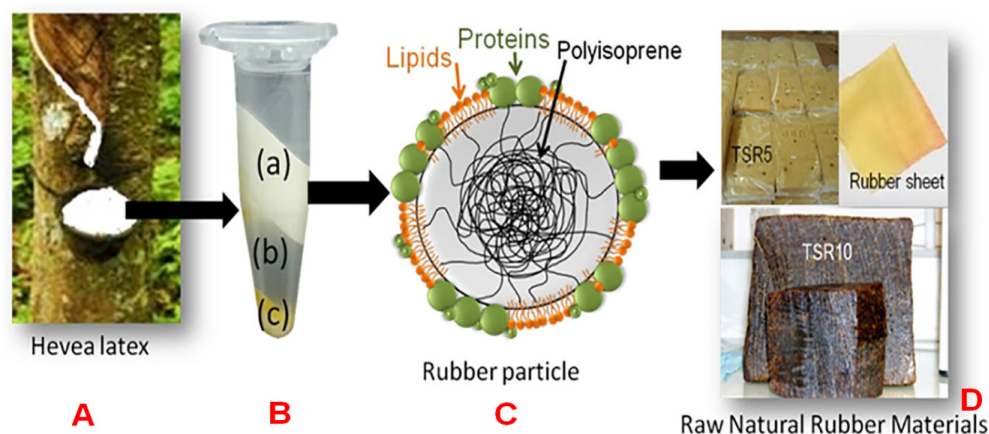
Fig. 1.2 (A) NR latex from *Hevea brasiliensis* tree (B) Composition of centrifuged NR latex: (a) cream, (b) C-serum and (c) bottom fraction/ lutoids (C) Schematic representation of a rubber particle (D) Raw dry rubber materials from NR latex

NR latex can be converted into useful products either by latex compounding in the case of dipped goods or can be allowed to coagulate and processed into dry forms for marketing. Natural rubber is chemically cis-1,4polyisoprene (Fig. 1.3). High green strength exhibited by NR is credited to its ability to crystallise on stretching. This ability, known as strain induced crystallisation is attributed to the stereoregularity in NR[30-32].
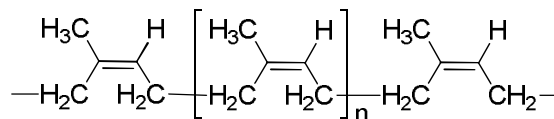
Fig. 1.3 Chemical structure of NR (cis-1,4 polyisoprene)

1.1.2 Synthetic latices

Synthetic latices are produced by the emulsion polymerization of monomers. Most of the synthetic latices are copolymers rather than homopolymers. The total solid content (TSC) of synthetic latices is around 35-55%. The latex contains exactly spherical polymer particles with a narrow size distribution (50-150 nm in diameter). Particles of synthetic latex are smaller than NR latex particles and are usually of a single type with simple structure unless deliberate attempts have been made to produce particles of complex structure. Chemical composition of the synthetic latex is simple and is controllable by the producer. Because of the absence of proteinaceous substances synthetic latices do not undergo spontaneous coagulation and putrefaction. Small amounts of microbicides are added to keep them sterile and to prevent any infection by microorganisms.

Synthetic latices are classified as synthetic rubber, synthetic plastic, artificial synthetic and functionalised synthetic latices. Functionalised synthetic latices are synthetic latices which are modified by introducing functional groups (<10 %) like carboxylic acid, sulfonic acid amine amide etc. A few examples of synthetic latices include styrene-butadiene copolymer latices, acrylonitrile-butadiene copolymer latices, polychloroprene latices, polyvinyl acetate latices and latices of copolymers of vinyl acetate. Polychloroprene and acrylic rubber latices are noted for their high chemical resistance. Carboxylated SBR and NBR latices exhibit superior mechanical properties and high resistance to wear and tear. They also show reduced swelling in hydrocarbon oils.

1.1.2.1 Carboxylated nitrile rubber (XNBR) latex

Carboxylated nitrile rubber (XNBR) latex is a modified version of nitrile rubber (NBR) latex. It is a terpolymer of acrylonitrile, butadiene and monomers like acrylic and methacrylic acids[33]. Randomly distributed carboxyl groups (usually less than 10%) along the hydrocarbon chain can provide additional curing sites that can form ionic cross links with metal ions (eg. Zn, Mg, Ca ions)[34,35]. These ionic cross links are formed along with covalent sulphur bonds when a mixed curing system of metal oxides along with sulphur is employed (Fig.1.4).
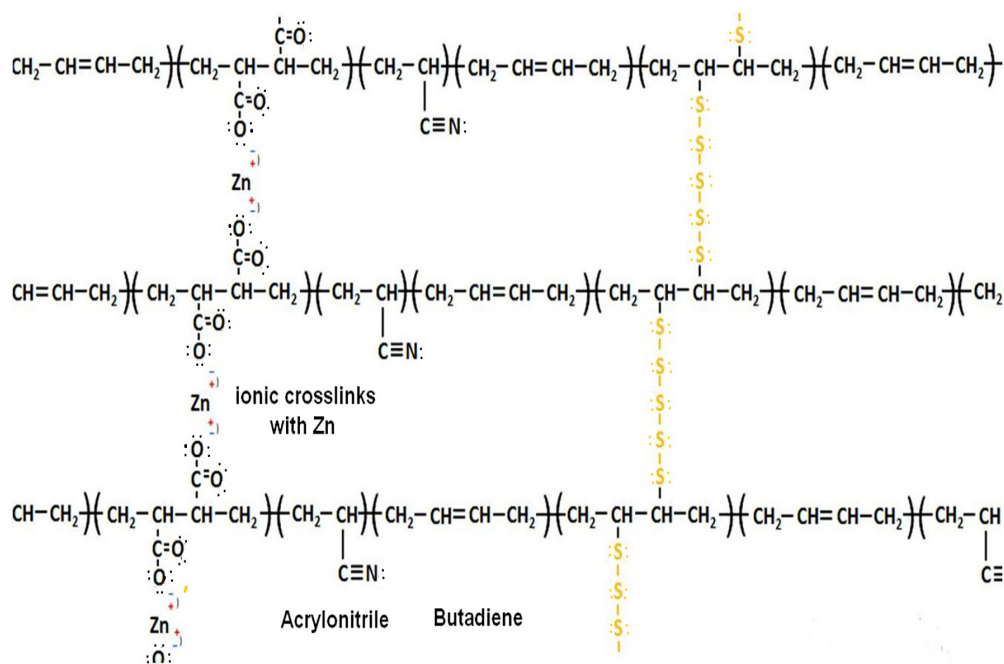
Fig. 1.4 Chemical structure of crosslinked XNBR

The ionic crosslinks can aggregate and form nanometer size domains that phase-separate from the rubber matrix and can act both as cross links and fillers leading to high reinforcement[36]. XNBR shows enhanced tensile strength, elastic modulus, hardness and exceptional tear and abrasion resistance compared to non carboxylated nitrile rubber. These properties

along with excellent oil resistance make them suitable for making hoses, oil well drilling parts, and conveyor belts, hose covers etc. Polar nature of XNBR adds the advantage of improved affinity towards fillers having polar functionalities on their surface.

1.1.3 Artificial latices

Artificial latices are manufactured by dispersing the bulk polymer in aqueous medium. The dispersion can be prepared by three methods viz. solution emulsification, phase inversion and polymer neutralisation. E.g. latices of rubbers such as polyurethane, silicone, chlorosulphonated polyethylenes, epichlorohydrin etc.

1.2 Fillers

Fillers are usually added to polymers to reduce the cost or to improve properties. Rubber industry makes use of a number of particulate fillers which can be categorised as reinforcing and non-reinforcing. Non-reinforcing fillers are usually added to reduce the cost of rubber products as they do not exhibit any reinforcing action. Examples for non-reinforcing fillers are mica, chalk powder, titanium dioxide, calcium carbonate and silicates of calcium and zinc. Reinforcing fillers can enhance the performance of the vulcanised rubber compounds by improving stiffness, abrasion resistance, tensile and tear strength. Carbon blacks and silica are the most commonly used reinforcing fillers in rubber industry.

1.3 Nanofillers

Recent advancements in nanotechnology have resulted in the realisation of different nanofillers capable of imparting excellent performance to the host rubber matrix at very low concentration. Nanofillers can be classified into one dimensional (1D), two dimensional (2D) and three dimensional (3D) based on their physical geometry.

- 1D nanofillers: They are in the form of cylinders, fibres and rods e.g. carbon nanotubes (CNTs), carbon nanofibres, gold or silver nanotubes, cellulose whiskers etc.

- 2D nanofillers: These have the shape of plates e.g. nanoclay, graphene etc.

- 3D nanofillers: These are in the form of spherical particles e.g. carbon black (CB), silica, zinc oxide and alumina.

1.3.1 Carbon nanotubes (CNTs)

The discovery of CNTs by Sumio Ijima in 1991[37] opened up a new era in materials science. These are fascinating structures with incredible mechanical, electrical and thermal properties[38]. High strength, light weight and flexibility have made them interesting candidates for structural reinforcement in materials research[39]. CNTs consist of graphene sheets rolled into cylinders. CNTs with aspect ratio (length to diameter ratio) of upto $(1.32 \times 10^8):1$ have been reported by Wang et al. They have diameters in the order of few nanometers and their length can reach upto18 centimeters[40]. Depending on the number of graphene sheets CNTs are classified into single walled (SWCNT), double walled (DWCNT) and multi walled carbon nanotubes (MWCNTs) as given in Fig.1.5. SWCNTs contain single sheet of graphene rolled into a seamless cylinder while MWCNTs consist of two or more concentric cylindrical shells with interlayer distance of about 0.34 nm. DWNT is s a special type of MWCNT wherein only two concentrically rolled up graphene sheets are present. There are two models for the structures of MWCNTs. According to the Russian Doll model, sheets of graphene are arranged in concentric cylinders, whereas, in the Parchment model, a single sheet of graphene is rolled in around itself resembling a rolled newspaper.
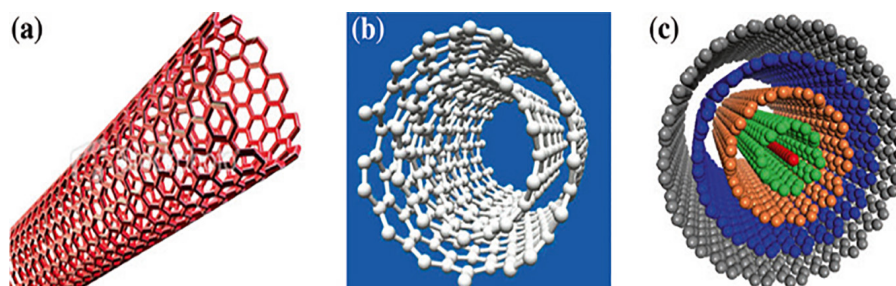
Fig. 1.5 Structures of (a) single-walled, (b) double-walled, and (c) multi-walled CNTs

CNTs are synthesised by different methods which include electric arc discharge[42], laser ablation[43] and chemical vapour deposition[44]. Individual CNTs are 200-300 times stronger than steel, lighter than aluminium and much better conductors than copper. Properties of CNTs are listed in Table 1.1.

Table 1.1 Theoretical and experimental properties of CNTs[45]

Properties	SWCNT	MWCNT
Dimensions (nm)	Diameter as low as ~1 nm, length up to 5 cm	Diameter 10 to 50 nm
Density (g cm^{-3})	0.8	1.8
Elastic modulus (TPa)	Theoretically 1.5; Experimentally0.6-1.5	0.4-0.95 (arc-discharge); 0.01-0.45 (CVD)
Tensile strength (GPa)	13-52	11-63 (arc discharge); 10 (CVD)
Electrical conductivity (S/cm)	10^2-10^6	10^3-10^5
Electron mobility (cm^2/(V s))	10^5	10^4-10^5
Thermal conductivity (W/m K)	3000	3500
Thermal expansion (10^{-6}/K)	negligible	negligible
Thermal stability (°C)	>700 (in air)	>600 (in air), 2800 (in vacuum)
Specific surface area (m^2/g)	>1000	>50

High tensile strength and elastic modulus of CNTs can be credited to the strong sp^2 carbon-carbon bonds in the graphene sheet. Unique mechanical strength exhibited by CNTs make them attractive substitutes for conventional fillers used for reinforcing polymer composites. Despite the excellent

mechanical, electrical and thermal properties, utilization of full potential of CNTs is limited by poor dispersion and weak interfacial bonding between the nanotubes and polymers. A suitable solution to this problem is to improve compatibility between the nanotubes and polymers by physical and chemical treatments of CNTs. The modifications on CNTs will be discussed later in the chapter.

MWCNTs are more attractive from the stand point of affordability when compared to SWCNTs. Although their aspect ratios are lower than those of SWCNTs, MWCNTS are available in large quantities with higher purity and at reasonable prices. Moreover the best candidates for polymer reinforcement are small diameter MWCNTs. This is because of the tendency of SWCNTS to bundle resulting in poor reinforcement. Inherent properties of the MWCNTs will be preserved even after chemical treatment unlike in SWCNTs since only the outer walls on MWCNTs undergo modification protecting the inner walls.

1.3.1.1 Modification and dispersion of carbon nanotubes

Disaggregation and uniform dispersion are two key factors required for the effective utilisation of nanotube properties to develop novel high performance composites. Usually pristine nanotubes remain highly bundled due to the presence of strong van der Waals attraction energy (ca. 500 eV/μm of tube-tube contact). This is the main challenge in processing involving CNTs[46]. Dispersing CNTs in a medium involves two steps: viz. separation of the nanotube bundles and then stabilisation of the individual tubes in the medium.

Ultrasonication is one of the methods employed in dispersing the nanotubes in a suitable medium. But mere ultrasonication of CNTs in water does not give thermodynamically stable dispersions since the individualized CNTs can still undergo re-aggregation to form bundles. Manufacturing techniques such as melt blending[47], in situ polymerisation in the presence of

CNTs[48] and solution mixing[49] are also reported to be effective in improving the dispersion of nanotubes in a polymer matrix.

Another method for effective dispersion is the modification of carbon nanotube surface. Both covalent and non-covalent modifications are employed to obtain good dispersion of carbon nanotubes in the polymer matrix[50].

1.3.1.1.a *Covalent modification*

Covalent methods involve functionalisation of nanotubes with different chemical moieties to enhance their compatibility with the polymer melt/solution or any solvent. In covalent modification functional groups are created on the end caps as well as on the side walls of the nanotubes. These functional groups improve the interfacial bonding between CNTs and the matrix leading to improvement in mechanical properties of the composites. Functionalised CNTs form stable suspensions by the mechanism of steric or electrostatic repulsions or both[51].

Covalent functionalisation of CNTs involves the creation of defects on the nanotube surface followed by functionalisation from the defects. According to Smalley et al.[52], sonication in the presence of strong acid mixture creates defects on the surface of CNTs and subsequent attack by the acid at the point of defect can cut the nanotubes. The cut ends will be rich in oxygen containing functionalities and assists in getting stable aqueous dispersions. Oxidation is a type of covalent modification which produces carboxyl and hydroxyl groups on the side walls as well as on the end caps[53]. Chemical oxidation of MWCNTs with different oxidizing agents is studied by Datsyuk et al.[54] and they have reported the difference in functionalisation yield and defect population on each treatment. According to them degree of functionalisation is more when acidic reagents like nitric acid or a mixture of sulphuric acid and hydrogen peroxide is used. Along with increase in quantity of carboxyl and hydroxyl groups, defect population was also high in this case. Different methods of covalent functionalisation of CNTs are illustrated in Table 1.2.

Table 1.2 Different methods of functionalisation of CNTs[55]

Methodology	Mode of reaction	Addend	Degree of functionalisation	Mode of attachment
Benzene diazonium salt	The diazonium salt reacts with Carbon atoms of CNT	aryl	1 addend in every 10 carbons	Aryl groups attaches to sidewall of CNTs
Diazonium in oleum	The diazonium salt reacts with Carbon atoms of CNT	aryl	1 addend in every 20 carbons	Aryl groups attaches to sidewall of CNTs
Fluorination	Fluorine gas is passed in to CNTs and then nucleophilic substitution with alkyl amino functionalities	amino group or alkyl or aryl group	1 addend in every 2 carbons	Creates side wall amino functional groups and also subsequent reaction with RMgBr/RLi creates alkyl or aryl group
Plasma treatment	By passing CF_4 gas via plasma treatment, which enhances the reactivity with aliphatic amines	alkyl or aryl group	1 addend in every 2 carbons	Gives fluorinated CNTs which on subsequent reaction creates alkyl/aryl groups.
Radical Chemistry	Reaction with free radicals created in situ.	alkyl	1 addend in every 6 carbons	Alkyl or aryl radicals get attach to sidewalls.
Billups reaction	Reductive alkylation reactions involving reaction with Li/NH_3 and RI	alkyl,aryl	1 addend in every 17 carbons	Give alkylated CNTs and results in complete exfoliation.
Prato reaction	1,3 dipolar cycloaddition of azomethine ylides to CNTs	pyrrolidine	1 addend in every 100 carbons	N-methylpyrrolidine derivative or pyrrolidinofullerene or pyrrolidino fullerene in 82% yield.
Bingel reaction	Haloderivative of malonate ion is reacted with a base and thereafter with CNTs	cyclopropane	1 addend in every 50 carbons	Cyclopropyl group formed as a result of the reaction get attached to the sidewalls
Nitrene	Nitrene is reacted with CNTs	cyclopropane	1 addend in every 25 carbons	Cycloaddition of nitrene to CNTs
Dichlorocarbene	CCl_2 is reacted with CNTs	cyclopropane	1 addend in every 25 carbons	Cycloaddition of carbene to CNTs

Functionalisation of CNTs can be identified by Raman spectroscopy, FTIR spectroscopy etc. Degree of functionalisation can be understood by

thermogravimetric analysis (TGA) and X-ray photoelectron spectroscopy (XPS). Morphological analysis using Transmission electron microscopy (TEM) and scanning electron microscopy (SEM) gives idea about diameter and atomic force microscopy (AFM) helps to find out the length and disentanglement of the tubes. One disadvantage of covalent functionalisation is that inherent optical, electrical and thermal properties of the tubes may be affected since these properties depend on the π conjugation. Aggressive chemical functionalisation can lead to structural defects in nanotubes leading to inferior mechanical and electrical properties.

1.3.1.1.b *Non-covalent modification*

Non-covalent method of modification is preferred over covalent method since the π system in graphene sheets remains undisturbed and inherent properties of the nanotubes are preserved[56]. The method involves the physical adsorption or wrapping of the modifiers on the surface of CNTs. This is stabilised by the π-π interactions possible between the graphitic walls of CNTs and conjugated polymers, as well as polymers with free electron pairs on the hetero atoms[57]. In non-covalent approach a number of surfactants have been reported to be useful in getting good aqueous dispersions of nanotubes[58]. Surfactants have hydrophilic polar as well as hydrophobic nonpolar part. They can get adsorbed on the nanotube surface through hydrophobic tail extending their hydrophilic head towards polar solvents making CNTs soluble[59].

Use of low molecular weight ionic surfactants for dispersing CNTs and graphene to prepare conductive nanocomposites has been reported by Tkalya et al.[60] Rastogi et al.[61] have reported comparative study on dispersion of MWCNTs with four surfactants - Tween 20, Tween 80, Triton X100 and sodium dodecyl sulphate (SDS). Triton X100 has provided maximum dispersion and minimum dispersing power was observed for SDS. They have also optimised CNT to surfactant ratio for stable dispersion. Anand et al.[62] have compared the dispersion efficiency of various surfactants sodium

dodecyl benzene sulphonate (NaDDBs), SDS, polyvinyl alcohol (PVA) and sodium benzoate for SWCNTs. NaDDBs is reported to be more effective due to the presence of aromatic ring along with longer alkyl chain.

Vigolo et al.[63] have used SDS surfactant for dispersing SWCNTs and they have reported an optimum concentration of SDS for getting homogeneous dispersion of SWCNTs in water. At this intermediate concentration electrostatic repulsion between adsorbed surfactants stabilises the CNTs against van der Waals attraction. Stabilisation mechanism of dispersions of CNTs and graphene in water for different ionic surfactants can be better understood from the works of Smith[64], Sun[65] and Loyta[66]. The research of Richard[5] is helpful to understand the assembly of surfactants on the surface of carbon nanotubes. Thermal and laser ablation are also used for the surface modification of CNTs[67].

1.3.2 Silica

Silica is a naturally occurring compound, with the chemical formula of SiO_2, usually found in sand, quartz and perlite. These natural forms are non-reinforcing and have been used as fillers only to reduce cost. Important naturally occurring silica are amorphous silica, crystalline silica, diatomaceous silica (fossil origin) and microcrystalline silica. Synthetic silica are reinforcing in nature and falls into different types like precipitated, pyrogenic (fumed), aerogels and hydrogels. Three most commonly used silica types in rubber-based compounds are fumed silica, precipitated silica and ground silica. Types of silica particles generally used in rubber and their properties are given in Table 1.3. Primary particle of precipitated silica is about 15-20 nm and that of fumed silica is about 15 nm in size. High surface forces of small primary particles cause agglomeration and they form secondary particles. These can further agglomerate to form chain like tertiary structures. Usually the conventional mill mixing methods are not efficient enough to disperse the primary particles in the rubber[68].

Table 1.3 Properties of generally used silica particles[69]

Category	Size (nm)	Primary size in rubber (nm)	Pore size (nm)	Specific area (m^2/g)	Density (g/cm^3)
Fumed silica	5-50	5-50	N/A	50-600	2.2
Arc silica	5-500	50	N/A	25-300	2.2
Precipitated	5-100	10-80	30	30-800	2.0
Xerogels	3-20	50	2-20	250-1000	2.0
Aerogels	3-20	50	25	250-400	2.0

Silica contains silicon and oxygen atoms arranged in a tetrahedral structure. The surface of amorphous silica particle contains silanol groups (-Si-OH) and can be of three types: isolated or free silanol, the germinal silanol (two –OH on the same silicon atom) and vicinal silanol (-OH on the adjacent silicon atoms) as shown in Fig. 1.6. Hydrophobic siloxane groups (Si-O-Si) are also present on the silica surface. Isolated hydroxyl groups are present on dehydrated silica, pyrogenic silica and only small amount is present on precipitated silica. Vicinal hydroxyl groups have stronger reinforcement effect. Silica adsorbs water due to the presence of polar hydroxyl groups on the surface. The amount of water adsorption is directly related to the number of surface hydroxyl groups[70].
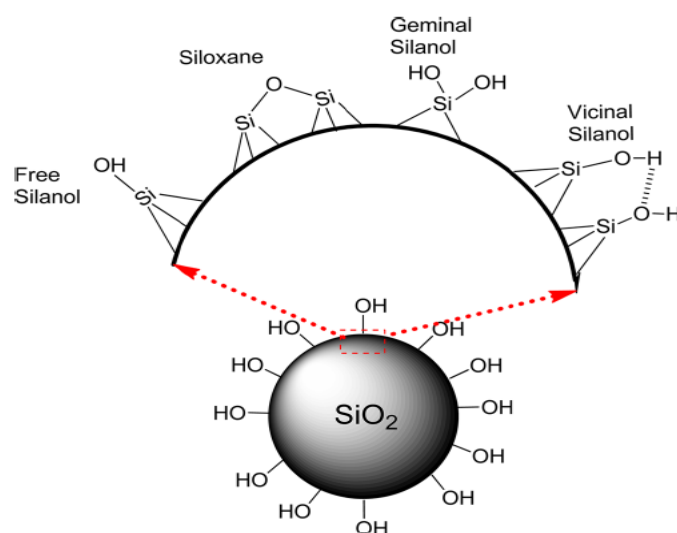
Fig. 1.6 Classification of silanol groups on the surface of silica particles

There is another class of silica known as colloidal silicas which are suspensions of fine amorphous, nonporous and typically spherical silica particles in a liquid phase[71]. Colloidal silicas are most often prepared in a multi-step process where an alkali-silicate solution is partially neutralized, leading to the formation of silica nuclei. The subunits of colloidal silica particles are typically in the range of 1 to 5 nm.

If the pH is reduced below 7 or if salt is added, then the units tend to fuse together in chains. These products are often called silica gels. If the pH is kept slightly on the alkaline side of neutral, then the subunits stay separated, and they gradually grow. These products are often called precipitated silica or silica sols. Hydrogen ions from the surface of colloidal silica tend to dissociate in aqueous solution, yielding a high negative charge. Substitution of some of the Si atoms by Al is known to increase the negative colloidal charge, especially when it is evaluated at pH below the neutral point. Because of the very small size, the surface area of colloidal silica is very high.

The colloidal suspension is stabilized by pH adjustment and then concentrated, usually by evaporation. The maximum concentration obtainable depends on the particle size. For example, 50 nm particles can be concentrated to greater than 50 wt% solids while 10 nm particles can only be concentrated to approximately 30 wt% solids before the suspension becomes too unstable.

Colloidal silica is usually used in concrete densifiers, as an abrasive, as high temperature binder, textile fibre coating, abrasion resistance coatings etc. No reports are available in the literature on the use of these materials as reinforcing filler in rubber.

1.4 Rubber nanocomposites

Elastomeric polymers and rubbers are widely used for various applications including tires, shock-absorbers, gaskets and seals for energy,

structural, electronic and electrical requirements. The high and reversible deformability of elastomers along with good strength, stress relaxation resistance, creep and long fatigue life make them attractive material in industry. Raw rubbers do not have sufficient strength for commercial applications. Therefore fillers like carbon black (CB), silica and metal oxides are usually employed for their effective reinforcement. Stiffness and toughness of the vehicle tyres and shock mounts are enhanced by the addition of fillers. The incorporation of fillers in elastomers can also improve the processability, fracture resistance and stress transfer. The main problem with rubber composites of conventional fillers is that property improvement can be achieved only at high filler loadings.

Rubber nanocomposites have attracted great attention for the past few years due to their superior mechanical, thermal and electrical properties. Nano particles can reinforce rubbers at very small loading due to their very small size and large surface area. Properties like tensile strength, modulus, thermal stability, elasticity, and processability and barrier properties are improved by the incorporation of nanofillers. Nanoparticles used in the preparation of rubber nanocomposites include layered silicates, carbon nanotubes, graphene, nanosilica etc.

Many data are available in the literature showing that the use of clay in rubber improves mechanical properties of the rubber. Rezende et al.[72] studied the mechanical properties of natural rubber-clay nanocomposites by uniaxial deformations. Wu et al.[73] used co-coagulating process for the preparation of NBR, SBR, NR, and XNBR /clay nanocomposites and studied the difference between intercalated and exfoliated structures. Kim et al.[74] and Kader et al.[75] respectively have studied the effect of organo modified clay and unmodified clay in NBR. Reinforcing effect of clay on rubbers like NR[76,77], SBR[78,79], XNBR[80,81] have reported by many researchers.

Superior mechanical and electrical properties of carbon nanotubes enable them to be used as reinforcing filler in rubber instead of traditional fillers. Research reports also support the significant improvement in mechanical and electrical properties of rubbers at very small concentrations of CNTs[82-84]. Significant improvement in physical properties is reported for SBR/CNT composites[85,86]. Zhou et al.[87] have adopted combination of spray drying method and mechanical mixing process to prepare SBR/CNT composites. They have reported improvement in crosslink density of SBR with CNT addition and subsequent increase in mechanical properties of the composites. Perez et al.[88] have used HNO_3 treated CNTs in the preparation of NBR and SBR composites. Compared to SBR/CNT composites NBR/CNT composites showed improvement in properties like resistance to solvent swelling, storage and loss moduli and glass transition temperature due to the strong interaction between the carboxyl and hydroxyl groups on the CNT surface and nitrile groups on NBR. Chen et al.[89] prepared SBR /MWCNT composites by processing in a two roll mill and found an increase in the mechanical properties like tensile strength, tear strength, hardness and abrasion resistance of the composite.

Geometry of the CNTs is different compared to the fillers like CB or silica because of high aspect ratio and inert surface. Therefore the reinforcement mechanism of carbon nanotubes in rubber is mainly due to the physical entanglement and networking effect.[90] NR/MWCNT composites with significant enhancement in mechanical strength are reported by Atieh et al.[91]. Abdullateef et al.[92] have reported the use of acid modified MWCNTs as reinforcing filler in NR. In addition to CNT modification, if the rubber is also modified by suitable means, interactions between the rubber and nanotube will be enhanced leading to good dispersion. Nakaramontri et al.[93] have studied the properties of composites by adding CNTs to three types of NR viz. NR, ENR and maleated NR. They observed that ENR/CNT

composites showed better mechanical strength compared to the other two because of the strong interactions between the functional groups on CNTs and epoxide groups on ENR.

CNT filled silicone based elastomers are studied by Frogley et al. [94] and the composites are found to have improved initial modulus and they have correlated the reinforcement with interfacial interactions and orientation of nanotubes inside rubber using strain dependent polarized Raman spectroscopy measurements. A simple and eco-friendly method of preparation of polychloroprene rubber composites with ionic liquid modified CNTs is done by Subramaniam et al. [95]. The prepared composites were of high electrical conductivity (0.1 S/cm), tensile modulus and stretchability (>500%). Raman spectroscopy and TEM analysis confirm an improved dispersion of CNTs in the matrix as well as formation of secondary filler-filler network which explains the high conductivity of the composite.

Graphene has excellent mechanical and electrical properties which make them attractive nanofiller for the preparation of advanced polymer nanocomposites. Zhan et al. [96] have prepared NR/graphene composites by ultrasonically assisted latex mixing method. Wang et al.[97] have studied NBR/nanographite composites prepared by latex compounding method and mechanical mixing. Graphene/natural rubber (GE/NR) nanocomposites prepared by a modified latex mixing method combined with in situ chemical reduction have been reported by Xing et al. [98]. Wu et al. [99] have studied the influence of three different sized graphene oxide sheets GO) on the properties of NR. The results indicate that addition of GO remarkably increased the modulus of NR with smallest sheet giving maximum reinforcement.

Silica is one of the widely used reinforcing filler in rubber industry. Composites filled with silica is reported to have better performance regarding mechanical and thermal properties compared to the corresponding neat rubbers[100,101]. The main application of silica is in passenger tire tread

compounds and commonly used silica for this purpose is precipitated amorphous silica. The silica particles provide excellent we traction, winter performance and good reduction in rolling resistance in comparison to carbon black[102].

Fumed silica nanoparticles are widely used in the reinforcement of rubber usually by melt compounding. But due to the self-aggregation nature of silica nanoparticles they form aggregates of size 300-400 nm in rubber. The shear forces during the melt compounding cannot break down these aggregates to nano level. This problem can be solvent to great extent by in situ precipitation of silica nanoparticles in rubber. In situ precipitation of silica in epoxidised natural rubber (ENR), styrene butadiene rubber (SBR) and butadiene rubber (BR) by sol gel process in the presence and absence of silane coupling agents was investigated by Kohjiya et al. [103] Improvement in tensile and dynamic mechanical properties and morphology study by TEM have proved that the in situ generated silica is better than conventionally added silica. NR/nanosilica composites were prepared by Lin et al. [104] using in-situ generation and coagulation method. The composites with well dispersed silica nanoparticles had good mechanical properties and further improvement in properties was observed when silane coupling agent (Si69) was added.

Silane coupling agents are commonly used in all rubber-tread compounding formulations containing more than 15 phr of silica in order to enhance the compatibility between rubber and silica[105]. Works on NR/nanosilica composites without using silane coupling agents have reported. One among such work is by George et al. [106] on the usage of ENR as a reinforcement modifier for NBR/silica system. Similar work was reported by Cataldo et al.[107] in which ENR has been used for the composite preparation and they have compared the properties with NR/silica system. The authors suggest that NR with some degree of epoxidation gives better

performance due to the possibility of interaction between epoxy groups on ENR and silanol groups on silica.

1.5 Fabrication of rubber nanocomposites

In the fabrication of high performance rubber nanocomposites dispersion of nanoparticles in the rubber matrix plays an important role. Uniform dispersion and strong interaction between the nanotubes and rubber are two key factors that ensure efficient load transfer from the matrix to the nanotubes. Likewise, alignment and orientation of conducting fillers influences the electrical properties and electrical percolation threshold. So the method of nanocomposite preparation has to be chosen carefully in order to get composites with desirable mechanical and electrical properties[108].

Different types of preparation methods of rubber nanocomposites are given below.

1.5.1 Solution mixing

This method involves the dissolution of both rubber and filler in separate suitable solvents. The two solutions are then homogeneously mixed by high energy sonication or mechanical agitation. Dry composite samples are obtained on evaporation of the solvent. Khalid et al.[109] and Fakhru'l-Razi et al.[110] have prepared NR/CNT composites by solvent casting method using toluene as the solvent. They have reported improvement in mechanical properties of the rubber credited to the uniform distribution of CNTs in the rubber matrix.

1.5.2 Freeze drying

In this process polymer solution containing filler is frozen in a cold bath and thereafter frozen solvent is removed by sublimation under vacuum. This leads to the formation of porous structures. This method is not widely used in the preparation of rubber/CNT composites. Yu et al. [111] have

synthesised CNT/polystyrene latex composites by freeze drying followed by compression moulding.

1.5.3 Melt blending

This method involves high temperature shear mixing in which elastomers are mixed in internal mixers or two roll mills along with nanofillers. This is the most preferred composite preparation method in industry since it is easy to scale up and also devoid of the usage of solvents. The intense shear forces in the internal mixer or between the two rollers in a mill assist in dispersing the nanotubes efficiently in the matrix. This method is widely used for the preparation of thermoplastics based composites also. Das et al. have succeeded in getting good dispersion of CNTs in styrene butadiene rubber (SBR)/butadiene rubber (BR) blend by melt mixing method[112]. Verge et al. [113] prepared acrylonitrile butadiene rubber (NBR)/CNT composites by melt blending method. They highlight the possibility of grafting of NBR onto the CNT surface by a free radical mechanism.

1.5.4 Spray drying

Here a suspension of nanofillers, elastomer and curing agents is homogeneously mixed and then spray dried to obtain composite powders. This method is successful in getting fine dispersion of nanoparticles in the elastomers. Zhou et al. have used this method for the preparation of SBR/CNT powders with diameter of about 5-10 μm and succeeded in improving the hardness, tear strength and tensile strength to a significant amount.

1.5.5 In situ polymerisation

Here, in situ polymerisation of the monomers is done within the nanofiller suspensions. This is an efficient and easy method to fabricate nanocomposites with uniformly distributed nanoparticles. This method ensures the covalent bond formation between the nanofillers and monomers in addition to the bonds between the monomers, provided fillers should

contain reactive functional groups. Strong matrix–filler interaction possible in these composites leads to enhanced mechanical strength as reported in literature. Wang et al.[114] have fabricated polyurethane (PU) elastomer/CNT composite by in situ polymerisation with hydroxyl modified MWCNTs. They report significant increase in the conductivity for the composite and applied these composites as electrodes in a pressure sensor.

1.5.6 Latex stage compounding

In latex stage compounding method nanoparticles are mixed with the rubber latex along with curing agents. Curing agents are added to the rubber latex as aqueous dispersions. The latex compound containing nanofillers can either be allowed to dry to form films or they can be coagulated and compression moulded. Another common method is to prepare a masterbatch of latex with filler which is then subjected to coagulation. The dried coagulum is further processed in a two roll mill or using an internal mixer.

Mao et al.[115] prepared graphene oxide/styrene butadiene rubber composites by aqueous phase mixing of colloidal solution of GO with SBR latex and small loadings of butadiene-styrene-vinyl pyridine (VPR) latex, followed by their co-coagulation. Complete exfoliation of GO sheets with improvement in mechanical and gas barrier properties was attained for the composite. They also report high wear resistance and low rolling resistance which make them suitable for green tyre application. Latex compounding method has been successfully applied for the preparation of SBR/graphene[116], NR/layered silicates[117] and NR/GO nanocomposites[96]. XNBR/GO composites with high mechanical and gas barrier properties were prepared by using latex co-coagulation method[118]. XNBR/expanded graphite composite[119] and XNBR/nanoclay composite[120] preparations using latex compounding technique have been reported.

1.5.6.1 Rubber latex/carbon nanotube composites

In order to ensure uniform dispersion of CNTs in the rubber matrix, nanocomposites based on the rubber latex have been studied my many researchers. This involves the incorporation of aqueous dispersions of CNTs in the rubber latex and further processing the mixture. Peng et al. [121] have prepared self-assembled NR/MWCNT composites using latex compounding technique. They have functionalised MWCNTs by H_2SO_4/HNO_3 treatment, mixed with poly (diallyl dimethyl ammonium chloride) and incorporated in pre-vulcanised NR latex. The mixture is cast on glass plates and dried to get the composites. It is found that MWCNTs are homogeneously dispersed in the NR matrix and imparted marked improvement in mechanical properties on account of the strong adhesion between NR and MWCNTs. NR-SWCNT nanocomposites have been prepared through latex stage mixing method by Anand et al.[62] They report good mechanical and electrical properties for the prepared composite. Ponnamma et al. [122] have correlated the dispersion of MWCNTs in NR latex with rheological properties of nanocomposites. They have used different types of surfactants for dispersing MWCNTs in NR latex and investigated the interfacial interaction between nanotube surface and rubber matrix. Their report illustrates the role of a dispersing agent in reducing the aggregation of nanotubes and achieving good dispersion in the rubber latex.

1.5.6.2 Rubber latex/nanosilica composites

Fumed silica nanoparticles usually exist as large aggregates in the composites due to the high surface free energy and strong H-bonding interaction. Latex based nanosilica composites can solve this problem to a great extent. Poompradub et al.[123] have prepared in situ generated silica in the NR latex by sol-gel technique using tetraethoxysilane (TEOS). A high concentration of (54 phr) well dispersed nanosilica could be obtained by this method. Li et al. [124] have developed latex compounding and self-assembly

technique to prepare NR/nanosilica composite in which silica nanoparticles are homogeneously distributed in the rubber matrix as spherical nano clusters. The self-assembly was assisted by the addition of poly (diallyldimethylammonium chloride) (PDDA) and the electrostatic adsorptive interactions between the NR latex particles, PDDA chains and nanosilica particles act as the driving force for the self-assembly. NR based nanocomposites exhibiting good mechanical and thermal properties can be prepared by the latex compounding technique involving the addition of nanosilica in the form of aqueous dispersions[125,126].

1.6 Electrically conductive polymer composites (CPCs)

Electrically conductive polymer composites (CPCs) are the composites that contain single or hybrid conductive fillers (eg. metallic, carbonaceous and conducting polymeric particles) dispersed in a single polymer or a polymer blend. These have attracted considerable attention of researchers and industry for several decades[127,128]. Their easy processability, low cost and tunable electrical properties make them suitable for applications like conductors, sensors, anti-static materials and electromagnetic interference (EMI) shielding[129]. Based on the electrical resistivity, CPCs are classified into different types suitable for different applications (Fig. 1.7).

Fig. 1.7 Classification of CPC materials according to their electrical resistivity and applications

Electrical conductivity of CPCs relies on the continuous network of conductive fillers inside the insulating polymer. When the conductive filler concentration reaches a critical value, the material exhibits an insulator/ conductor transition which is characterised by a tremendous increase in the electrical conductivity. This critical volume fraction is defined as the percolation threshold, ϕ_c. As the filler concentration increases conductivity increases gradually until a plateau is reached. The following power law explains the electrical conductivity of a CPC material[130].

$$\sigma = \sigma_0(\phi - \phi_c)^t \quad \text{...} (1.1)$$

where 'σ' is the conductivity of the composite, σ_0 is the proportionality constant depending on the intrinsic conductivity of the filler, ϕ is the filler volume fraction, ϕ_c is the percolation volume fraction and t is the critical exponent that depend on the dimensionality of the conductive networks in CPC. $t \approx 2$ and $t \approx 1.3$ respectively for three-dimensional (3D) and two-dimensional (2D) conductive networks. Experimental values may sometimes show deviations from the proposed t values.

Carbon nanotubes (CNTs) and graphene nanosheets (GNS) are promising conductive nanofillers because of their high aspect ratio, but their extreme agglomeration tendency during processing in polymers leads to relatively high ϕ_c. This causes inferior mechanical properties, high melt viscosities and production cost. Therefore the major challenge in the fabrication of high performance CPC materials is to reduce ϕ_c.

1.7 Segregated conductive polymer composites

The concept of "segregated conductive network" was initially proposed by Turner and co-workers in 1971 for the segregated network of nickel particles in high-density polyethylene (HDPE) composites[15].

In segregated CPC (s-CPC) materials, the conductive fillers are primarily located at the interfaces between the polymeric matrix particles, instead of

being randomly arranged throughout the entire CPC system, as shown in Fig. 1.8. Compared to conventional CPCs, this special structure requires only vary small amount of conductive fillers to form initial conducting channels. Therefore s-CPCs are characterised by ultralow percolation threshold. Lowest percolation threshold available in the literature is the one reported by Gupta et al. [131] for segregated conductive network of CB in acrylonitrile–butadiene–styrene (ABS) (ϕ_c ~0.0054 vol%).
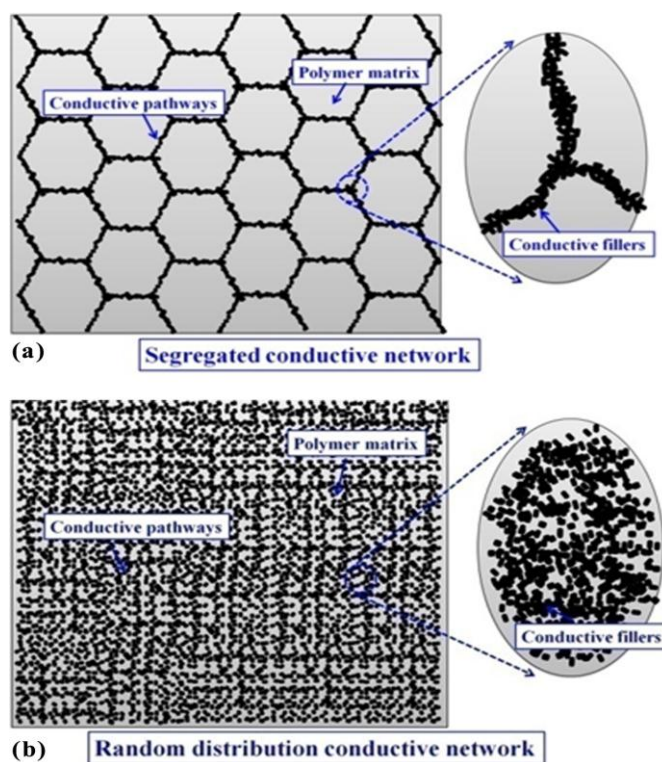
Fig. 1.8 Schematic illustration of (a) segregated and (b) random distribution conductive fillers in a CPC

The mechanism of formation of a segregated conductive network depends on a polymeric matrix with an exclusionary microstructure in which conductive fillers are allotted a constrained volume. This increases the effective density of the conductive pathways even at low filler

concentrations. In brief, this interesting structure provides an efficient paradigm for forming a well-established conductive network with minimal filler loading.

1.7.1 Preparation of s-CPCs

Different processing methods adopted in the preparation of s-CPCs are shown in Fig. 1.9. There are three approaches commonly used. One method is to compress a mixture of polymer granules and conductive fillers (Fig. 1.9a) [132]. This method is very simple since it involves only mixing and compaction. Various conductive fillers like metallic particles, CB, CNTs, and GNSs have been distributed on the surface of the polymeric particles using this method[133-135]. The polymers suitable for this method should possess high melt viscosities to preserve the segregated structure during hot compression moulding. Filler concentration cannot exceed 10 wt % in this method due to processing difficulties.

The second method is called latex technology in which conductive fillers are dispersed within a polymeric latex[136,137]. The conductive fillers will be retained within the interstitial space between latex particles on drying (Fig. 1.9b). Merits of this process include: (i) compared to dry or solution mixing fairly good dispersion of conductive fillers at the surface of the latex particles (ii) low cost and environment friendly process where water is used as the solvent (iii) no limitation to the filler concentration in the composite (can vary from 0 to 100 wt%)[138]. The third processing method is by the selective distribution of conductive fillers at the interfaces of immiscible polymer blends through melt blending (Fig. 1.9c). This is the most preferred method in industry due to the simplicity of melt blending. But the formation of segregated network in this case depends on thermodynamic coefficients (e.g., interfacial energy between the polymer matrices and conductive fillers) and kinetics parameters (e.g., mixing procedures and sequence, blending time, and shear strength) [139].
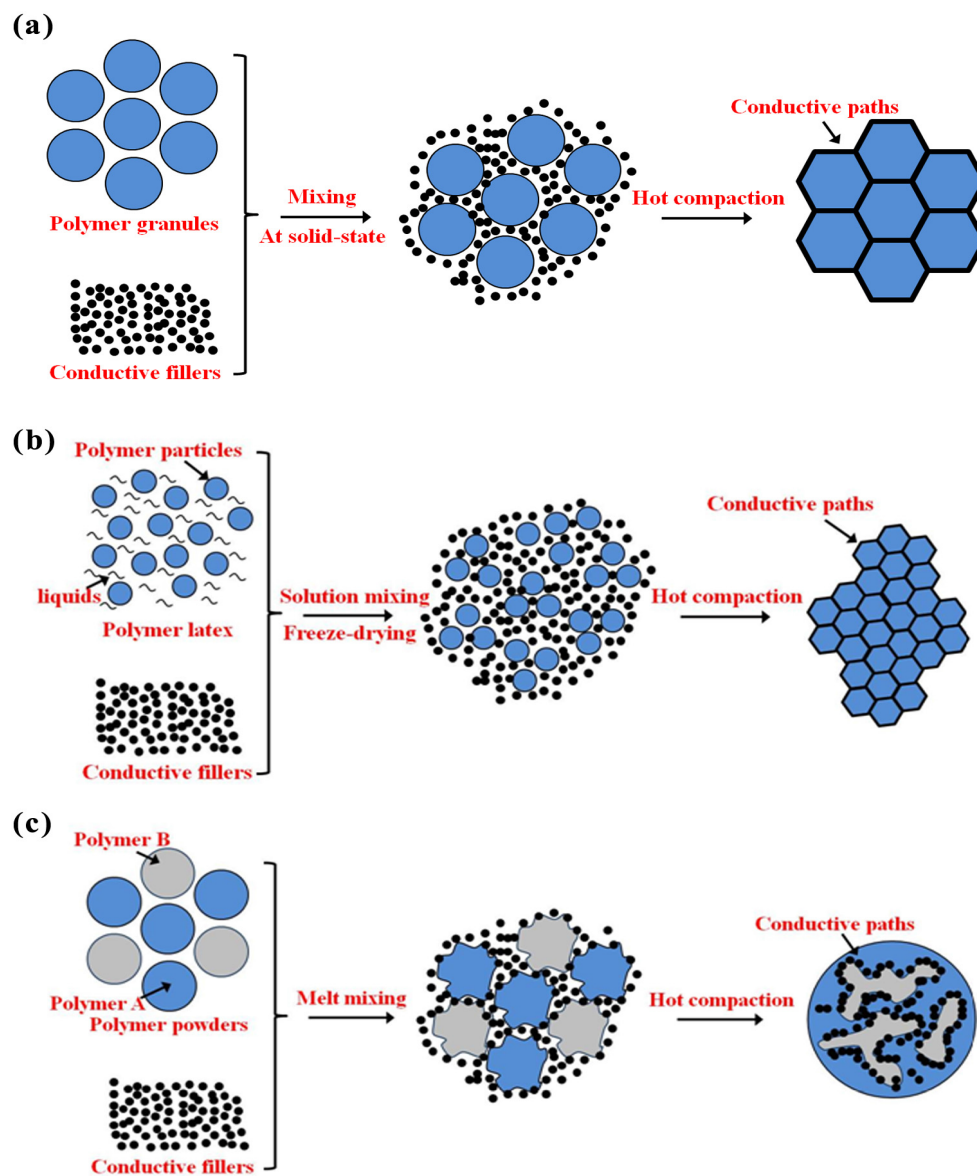
Fig. 1.9 Schematic for the fabrication of the s-CPCs by: (a) dry -mixing, (b) latex technology, and (c) melt-blending methods

1.7.2 Ultralow percolation threshold (ϕ_c)

s-CPCs are fascinating structures among conductive composites due to their ultralow percolation threshold (ϕ_c). The difference in electrical conductivity behaviour and electrical percolation of CNT filled composites with segregated and random networks is given in Fig. 1.10.[140].
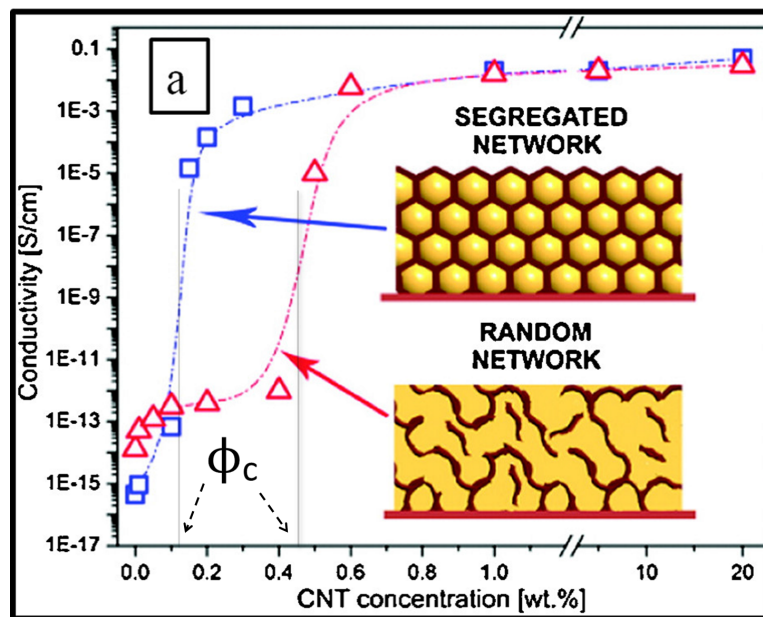
Fig. 1.10 **Electrical conductivity as a function of CNT weight fraction in CPCs with segregated and random network [*Adapted from Ref. 140*]**

s-CPCs generally exhibit ϕ_c below 0.5 vol% and the value depends on the type of conductive fillers, their electrical characteristics, dispersion quality and morphology of filler networks. Molecular weight, modulus and particle size of the polymeric matrices and processing methods also influence ϕ_c. For example the percolation threshold of UHMWPE/CB composite decreased with the increase of the molecular weight of UHMWPE, and with the decrease of the particle size of CB[134]. s-CPCs produced by latex technology and melt blending usually possess higher ϕ_c than those prepared by dry or

solution mixing method[141]. However, maximum electrical conductivity (σ_{max}) of the s-CPCs prepared by dry and melt-blending methods is usually lower than that of the materials fabricated using latex technology.

For the past few years researches are going on towards tailoring segregated structures to get ultralow ϕ_c[142,143]. The majority of s-CPCs consist of high melt viscosity polymers such as polymethyl methacrylate (PMMA)[144], polystyrene (PS)[111], ultrahigh molecular weight polyethylene (UHMWPE)[145], polyvinyl acetate (PVAc)[146] etc, because they can preserve the network of conductive fillers in interfacial regions during processing. Of late high-aspect-ratio conductive fillers like carbon nanotubes and graphene nanosheets have attracted significant attention over the low-aspect ratio fillers like CB, metallic particles and graphite flakes. The reason for the popularity of high aspect ratio fillers is their superior electrical conductivity and ease of formation of networks at low volume content.

1.7.3 s-CPCs based on NR and XNBR

s-CPCs based on Poly (acrylonitrile-co-butadiene-co-styrene) (ABS)[131], polymethyl methacrylate (PMMA)[147], polypropylene (PP)[148], polycarbonate (PC)[149], polystyrene (PS)[150], polyvinyl acetate (PVAc)[151], ultrahigh molecular weight polyethylene (UHMWPE)[152] and polyvinylidene difluoride (PVDF)[153] have been reported previously. But reports on s-CPCs based on rubber matrices are limited in the literature. Rubber composites with segregated network of graphene nanoplates are reported by a few. Wu et al.[154] have developed polyaniline@cellulose nanowhiskers (PANI@CNs)/natural rubber (NR) nanocomposites by latex mixing method followed by co-coagulation. PANI@CNs nanohybrids selectively located in the interstitial space between NR microspheres and organized into a 3D hierarchical multiscale conductive network structure in NR matrix and the composite exhibited high mechanical properties and low percolation threshold. Potts et al.[155] have

succeed in fabricating NR composite with weblike morphology consisting of reduced graphene oxide platelet networks between the latex particles and found that network morphology was highly beneficial for thermal and electrical conductivity properties but unfavourable for getting good mechanical properties. Vulcanised graphene/natural rubber composites with a conductive segregated network exhibiting good electrical conductivity, water vapor permeability and high mechanical strength are prepared by self-assembly in latex and static hot pressing by Zhan et al. [156].

Tian et al. [157] report carboxylated nitrile rubber (XNBR)/ graphene oxide nanosheet (GONS) composite with promising dielectric properties. They have used latex mixing method in which GONS are encapsulated on XNBR latex spheres followed by thermal reduction of GONS. The same group has reported thermally reduced graphene oxide (RGO) @ carbon nanosphere (CNS)/XNBR composites having segregated filler structure with high dielectric constant (k), low dielectric loss, low elastic modulus and large actuated strain at a low electric field[158]. To the best of our knowledge there have been no reports in the literature regarding CNT composites based on NR or XNBR with segregated filler network structure.

1.7.4 Properties and applications of s-CPCs

1.7.4.1 Mechanical properties

Although the segregated structures allow for the formation of efficient conductive networks at extremely low filler loadings, the interfacial segregation of the conductive fillers largely prevents molecular diffusion between the polymer domains. Moreover, agglomerated conductive fillers also inevitably appear, forming microvoids along the segregated conductive pathways. These two aspects create many structural flaws that harm the mechanical behaviours of the s-CPC materials. Apart from the enhanced modulus of the s-CPCs that may originate from the stiffness of the segregated conductive

networks, few successful examples with mechanical improvement have been reported[159,160]. These reports explain why only a few s-CPC materials have been employed in specific applications to date.

There are two major strategies for strengthening s-CPC materials: improving the dispersion of the conductive fillers and intercalating polymer chains into segregated conducting pathways. To improve the uniform dispersion of conductive fillers efficiently on the surfaces of polymer particles, latex technology is usually recommended. Through a crosslinking technique, rubber-based s-CPCs always exhibit superior strength and reinforcement effects over the plastic based s-CPCs[161] due to the micro-void free segregated conductive networks and the powerful adhesive interactions between the polymer granules induced by the vulcanisation of rubber matrix. Additionally, the synergistic effects of hybrid filler on enhancing the storage modulus of the s-CPCs have also been observed, which originated from the excluded volume effect[146].

1.7.4.2 Electrical properties

It has been previously mentioned that the ultralow electrical percolation threshold makes the s-CPCs attractive among the conductive polymer composites. The electrical properties depend on the morphology of conductive filler network inside the polymer matrix. The s-CPCs can find application as stretchable conductors. Stretchable conductors can maintain high electrical conductivity even in a highly stretched condition[162,163]. This special type of CPC is desirable for applications in robot arm joints, wearable displays, flexible electronics, dielectric elastomer actuators and stretchable solar cells, as well as in medical implants for health monitoring, disease diagnostics and biological actuation. s-CPCs are reported to possess very good dielectric properties, viz. high dielectric constant, low dielectric loss and low elastic modulus facilitating the application as dielectric elastomer actuators[164].

s-CPCs can also be used in applications like strain sensors, temperature sensors, self-regulated heaters and over-current protectors. This is based on the fact that application of strain or increase in temperature can cause change in the segregated conductive network structure and subsequent change in electrical conductivity of the composite. It has been widely reported that CPCs can sense vapour or liquid chemicals[165]. Sensing is achieved through a change in the local conductive network on exposure to various chemicals, including water, methanol, toluene, chloroform or tetrahydrofuran (THF). An increase in the resistivity of the CPCs could be observed upon exposure to these chemicals.

1.7.4.3 EMI shielding properties

CPCs have also been widely used for EMI shielding applications[166]. However, the high filler loading required for adequate shielding capabilities (at least above $\sim$20 dB) in conventional CPCs adversely affects the economic feasibility and mechanical performance. Reducing the filler content without compromising the electrical conductivity and EMI shielding efficiency remains a considerable challenge. Forming a segregated conductive network might resolve this problem. Nevertheless, few reports concerning shielding materials based on s-CPCs have been published[167, 168]. Interestingly, the EMI shielding behaviours of the reported s-CPCs often follow an absorption-dominant shielding mechanism. As illustrated schematically in Fig. 1.11, the s-CPC has a "special foam structure" with dense conductive filler layers that act as highly conductive "struts" and polymer domain that act as "microcells", forming numerous interactive interfaces[169]. The incident electromagnetic microwaves that enter the s-CPCs are attenuated by reflecting and scattering many times between these "strut-cell" interfaces and conductive filler surfaces. This hinders the escape of the waves from the s-CPC material before being dissipated as heat and therefore, s-CPCs have great potential as high performance EMI shielding materials.
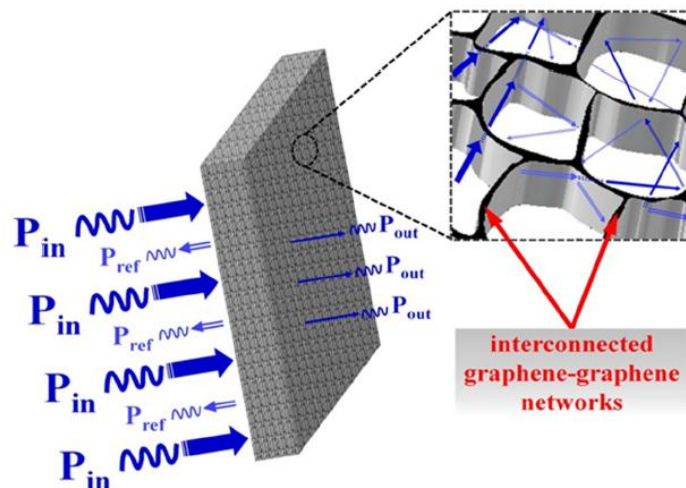
Fig. 1.11 Schematic representation of microwave transfer across the GNS/PS s-CPC material *[Adapted from Ref.169]*

1.8 Objectives of the work

Two types of composites, one containing the segregated and the other containing random network of MWCNTs and nanosilica in NR and XNBR are proposed to be developed to ensure efficient dispersion. The fillers are proposed to be added as aqueous dispersions to the rubber latex and then processed by adopting two methods viz. film casting and co-coagulation followed by mixing in an internal mixer. The effect of processing method on the filler distribution and properties are proposed to be studied with special emphasis on mechanical, thermal, solvent barrier and electrical properties.

The specific objectives of the present work are:

- To modify MWCNT by surfactant and acid treatment in order to improve its dispersion in water.

- To optimise the concentration of surfactant and sonication time required for preparing stable aqueous dispersions of MWCNTs.

- To develop rubber nanocomposites with segregated network of nanofillers.

- To investigate the effect of Haake mixing on the segregated structure of nanofillers.

- To understand the morphology of nanofillers in the composites using TEM, SEM and strain sweep studies.

- To study the effect of latex stage mixing of CNTs and nanosilica on the mechanical properties of NR and XNBR.

- To understand the role of segregated network of conducting fillers in lowering the electrical percolation threshold.

- To study the dielectric properties and AC conductivity of the nanocomposites.

- To prepare rubber nanocomposites with high dielectric constant and low dielectric loss.

- To compare the physical and electrical properties of the composites with segregated and random network of conducting nanofillers.

- To investigate the thermal stability and solvent resistance of MWCNT and nanosilica filled NR and XNBR nanocomposites.

References

[1] Gent, A. N., (Ed) J.E. Mark, B. Erman and F. Eirich. (1994). in Science and Technology of Rubber, 2nd edn,.. Academic Press, San Diego.

[2] Roberts, A. D. (1988). *Natural rubber science and technology*. Oxford University Press.

[3] Bateman, L. (1963). The Chemistry and Physics of Rubber-Like Substances. Maclaren & Sons, London.

[4] Kraus, G. (1965). Reinforcement of Elastomers. Interscience, New York.

[5] Thomas, S., & Maria, H. J. (2016). Progress in Rubber Nanocomposites. *Woodhead: Sawston, Cambridge, UK*.

[6]   Das, A., Kasaliwal, G. R., Jurk, R., Boldt, R., Fischer, D., Stöckelhuber, K. W., & Heinrich, G. (2012). Rubber composites based on graphene nanoplatelets, expanded graphite, carbon nanotubes and their combination: a comparative study. *Composites Science and Technology*, *72*(16), 1961-1967.

[7]   Sui, G., Zhong, W., Yang, X., & Zhao, S. (2007). Processing and Material Characteristics of a Carbon-Nanotube-Reinforced Natural Rubber. *Macromolecular Materials and Engineering*, *292*(9), 1020-1026.

[8]   Yue, D., Liu, Y., Shen, Z., & Zhang, L. (2006). Study on preparation and properties of carbon nanotubes/rubber composites. *Journal of materials science*, *41*(8), 2541-2544.

[9]   Kueseng, K., & Jacob, K. I. (2006). Natural rubber nanocomposites with SiC nanoparticles and carbon nanotubes. *European Polymer Journal*, *42*(1), 220-227.

[10]   Bokobza, L., & Kolodziej, M. (2006). On the use of carbon nanotubes as reinforcing fillers for elastomeric materials. *Polymer International*, *55*(9), 1090-1098.

[11]   Kong, L., Chen, Y., Peng, Z., & Li, P. (2008). Latex-based nanocomposites. *Progress in polymer nanocomposite research*, 83-104.

[12]   Villmow T, Pegel S, John A, Rentenberger R, Pötschke P. (2011). Liquid sens-ing: smart polymer/CNT composites. *Mater Today*, 14:340–5.

[13]   Antunes, R. A., De Oliveira, M. C., Ett, G., & Ett, V. (2011). Carbon materials in composite bipolar plates for polymer electrolyte membrane fuel cells: A review of the main challenges to improve electrical performance. *Journal of Power Sources*, *196*(6), 2945-2961.

[14]   Dang, Z. M., Yuan, J. K., Zha, J. W., Zhou, T., Li, S. T., & Hu, G. H. (2012). Fundamentals, processes and applications of high-permittivity polymer–matrix composites. *Progress in Materials Science*, *57*(4), 660-723.

[15]   Malliaris, A., & Turner, D. T. (1971). Influence of particle size on the electrical resistivity of compacted mixtures of polymeric and metallic powders. *Journal of Applied Physics*, *42*(2), 614-618.

[16]   Grunlan, J. C., Gerberich, W. W., & Francis, L. F. (2001). Lowering the percolation threshold of conductive composites using particulate polymer microstructure. *Journal of applied polymer science*, *80*(4), 692-705.

[17] Al-Saleh, M. H., & Sundararaj, U. (2009). Electromagnetic interference shielding mechanisms of CNT/polymer composites. *Carbon*, *47*(7), 1738-1746.

[18] Yang, Y., Gupta, M. C., Dudley, K. L., & Lawrence, R. W. (2005). Novel carbon nanotube− polystyrene foam composites for electromagnetic interference shielding. *Nano letters*, *5*(11), 2131-2134.

[19] D.C Blackley. (1987). Latices in Encyclopedia of Polymer Science, 2nd edn, John Wiley & Sons, New York, Vo1.8. 647

[20] J. d'Auzac, J.L. Jacob, H. Chrestin. (Eds.) J. d'Auzac, J.L. Jacob. (1989). The composition of latex from Hevea brasiliensis as laticiferous cytoplasm, Physiology of the Rubber Tree Latex, CRC Press, Boca Raton, Florida.

[21] Ho, C. C., Subramaniam, A., & Yong, W. M. (1975). Lipids associated with the particles in Hevea latex. In *Proc Int Rubber Conf Kuala Lumpur* (Vol. 2, p. 441).

[22] Hasma, H. (1991). Lipids associated with rubber particles and their possible role in mechanical stability of latex concentrates. *Journal of Natural Rubber Research (Malaysia)*.6 (1991) 105-114.

[23] Cornish, K., Wood, D. F., & Windle, J. J. (1999). Rubber particles from four different species, examined by transmission electron microscopy and electron-paramagnetic-resonance spin labeling, are found to consist of a homogeneous rubber core enclosed by a contiguous, monolayer biomembrane. *Planta*, *210*(1), 85-96.

[24] Nawamawat, K., Sakdapipanich, J. T., Ho, C. C., Ma, Y., Song, J., & Vancso, J. G. (2011). Surface nanostructure of Hevea brasiliensis natural rubber latex particles. *Colloids and Surfaces A: Physicochemical and Engineering Aspects*, *390*(1), 157-166.

[25] Rochette, C. N., Crassous, J. J., Drechsler, M., Gaboriaud, F., Eloy, M., De Gaudemaris, B., & Duval, J. F. (2013). Shell structure of natural rubber particles: evidence of chemical stratification by electrokinetics and cryo-TEM. *Langmuir*, *29*(47), 14655-14665.

[26] X. Wang, M. Shi, X. Lu, R. Ma, C. Wu, A. Guo, M. Peng, W. Tian, A method for protein extraction from different subcellular fractions of laticifer latex in Hevea brasiliensis compatible with 2-DE and MS, *Proteome Sci.* 8 (2010) 35.

[27] Dai, L., Kang, G., Li, Y., Nie, Z., Duan, C., & Zeng, R. (2013). In-depth proteome analysis of the rubber particle of Hevea brasiliensis (para rubber tree). *Plant molecular biology*, *82*(1-2), 155-168.

[28] Ho, C. C. (1989). Changes in electrokinetic properties of natural rubber latex after surface chemical modifications. *Colloid & Polymer Science*, *267*(7), 643-647.

[29] Chen, S. F., & Ng, C. S. (1984). The natural higher fatty acid soaps in natural rubber latex and their effect on the mechanical stability of the latex. *Rubber chemistry and technology*, *57*(2), 243-253.

[30] Tanaka, Y. (2001). Structural characterisation of natural polyisoprenes: solve the mystery of natural rubber based on structural study. *Rubber chemistry and technology*, *74*(3), 355-375.

[31] Mandelkern, L. (1993). The role of elastomers in the study of polymer crystallization. *Rubber chemistry and technology*, *66*(3), G61-G75.

[32] Takahashi, Y., & Kumano, T. (2004). Crystal structure of natural rubber. *Macromolecules*, *37*(13), 4860-4864.

[33] Brown, H. P. (1957). Carboxylic elastomers. *Rubber Chemistry and Technology*, *30*(5), 1347-1386.

[34] Ibarra, L., & Alzorriz, M. (2003). Ionic elastomers based on carboxylated nitrile rubber and calcium oxide. *Journal of applied polymer science*, *87*(5), 805-813.

[35] Sahoo, S., & Bhowmick, A. K. (2007). Influence of ZnO nanoparticles on the cure characteristics and mechanical properties of carboxylated nitrile rubber. *Journal of applied polymer science*, *106*(5), 3077-3083.

[36] Tulyapitak, T. (2006). Cure and mechanical properties of carboxylated nitrile rubber (XNBR) vulcanized by alkaline earth metal compounds, *Doctoral dissertation, University of Akron.*

[37] Iijima, S. (1991). Helical microtubules of graphitic carbon. *nature*, *354*(6348), 56.

[38] Popov, V. N. (2004). Carbon nanotubes: properties and application. *Materials Science and Engineering: R: Reports*, *43*(3), 61-102.

[39] Wong, E. W., Sheehan, P. E., & Lieber, C. M. (1997). Nanobeam mechanics: elasticity, strength, and toughness of nanorods and nanotubes. *Science*, *277*(5334), 1971-1975.

[40] Wang, X., Li, Q., Xie, J., Jin, Z., Wang, J., Li, Y., ... & Fan, S. (2009). Fabrication of ultralong and electrically uniform single-walled carbon nanotubes on clean substrates. *Nano letters*, *9*(9), 3137-3141.

[41]   a) https://www.istockphoto.com/ch/foto/dieses-einlagige-expeditionszelt-carbon-nanotube-gm182207312-10936011(b)   https://dx.eng.uiowa.edu/dave/cnt.php (c) http://vnitmvd.50webs.com/ss/report.htm

[42]   Ebbesen, T. W., & Ajayan P. M. (1992). Large-scale synthesis of carbon. *Nature*, *358*, 16.

[43]   Morales, A. M., & Lieber, C. M. (1998). A laser ablation method for the synthesis of crystalline semiconductor nanowires. *Science*, *279*(5348), 208-211.

[44]   Ren, Z. F., Huang, Z. P., Xu, J. W., Wang, J. H., Bush, P., Siegal, M. P., & Provencio, P. N. (1998). Synthesis of large arrays of well-aligned carbon nanotubes on glass. *Science*, *282*(5391), 1105-1107.

[45]   Song, K. (2014). *Customizing fiber spinning approaches for polymer/nano-carbon composites*. Northeastern university.

[46]   Girifalco, L. A., Hodak, M., & Lee, R. S. (2000). Carbon nanotubes, buckyballs, ropes, and a universal graphitic potential. *Physical Review B*, *62*(19), 13104.

[47]   Pötschke, P., Bhattacharyya, A. R., & Janke, A. (2004). Melt mixing of polycarbonate with multiwalled carbon nanotubes: microscopic studies on the state of dispersion. *European Polymer Journal*, *40*(1), 137-148.

[48]   Kwiatkowska, M., Broza, G., Schulte, K., & Roslaniec, Z. (2006). The in-situ synthesis of polybutylene terephthalate/carbon nanotubes composites. *Reviews on Advanced Materials Science*, *12*(2), 154-159.

[49]   Sandler, J., Broza, G., Nolte, M., Schulte, K., Lam, Y. M., & Shaffer, M. S. P. (2003). Crystallization of carbon nanotube and nanofiber polypropylene composites. *Journal of Macromolecular Science, Part B*, *42*(3-4), 479-488.

[50]   Varadan, V. K., & Xie, J. (2002). Large-scale synthesis of multi-walled carbon nanotubes by microwave CVD. *Smart materials and structures*, *11*(4), 610-616.

[51]   Hyung, H., Fortner, J. D., Hughes, J. B., & Kim, J. H. (2007). Natural organic matter stabilizes carbon nanotubes in the aqueous phase. *Environmental science & technology*, *41*(1), 179-184.

[52]   Liu, J., Rinzler, A. G., Dai, H., Hafner, J. H., Bradley, R. K., Boul, P. J., ... & Rodriguez-Macias, F. (1998). Fullerene pipes. *Science*, *280*(5367), 1253-1256.

[53]   Yudianti, R., Onggo, H., Sudirman, Y. S., Iwata, T., & Azuma, J. I. (2011). Analysis of functional group sited on multi-wall carbon nanotube surface. *Open Materials Science Journal*, *5*, 242-247.

[54] Datsyuk, V., Kalyva, M., Papagelis, K., Parthenios, J., Tasis, D., Siokou, A., ... & Galiotis, C. (2008). Chemical oxidation of multiwalled carbon nanotubes. *Carbon*, *46*(6), 833-840.

[55] Dyke, C. A., & Tour, J. M. (2004). Covalent functionalisation of single-walled carbon nanotubes for materials applications. *The Journal of Physical Chemistry A*, *108*(51), 11151-11159.

[56] Hilding, J., Grulke, E. A., George Zhang, Z., & Lockwood, F. (2003). Dispersion of carbon nanotubes in liquids. *Journal of dispersion science and technology*, *24*(1), 1-41.

[57] Moniruzzaman, M., & Winey, K. I. (2006). Polymer nanocomposites containing carbon nanotubes. *Macromolecules*, *39*(16), 5194-5205.

[58] Vaisman, L., Wagner, H. D., & Marom, G. (2006). The role of surfactants in dispersion of carbon nanotubes. *Advances in colloid and interface science*, *128*, 37-46.

[59] Richard, C., Balavoine, F., Schultz, P., Ebbesen, T. W., & Mioskowski, C. (2003). Supramolecular self-assembly of lipid derivatives on carbon nanotubes. *Science*, *300*(5620), 775-778.

[60] Tkalya, E. E., Ghislandi, M., de With, G., & Koning, C. E. (2012). The use of surfactants for dispersing carbon nanotubes and graphene to make conductive nanocomposites. *Current Opinion in Colloid & Interface Science*, *17*(4), 225-232.

[61] Rastogi, R., Kaushal, R., Tripathi, S. K., Sharma, A. L., Kaur, I., & Bharadwaj, L. M. (2008). Comparative study of carbon nanotube dispersion using surfactants. *Journal of colloid and interface science*, *328*(2), 421-428.

[62] Anand K, A., Jose T, S., Alex, R., & Joseph, R. (2009). Natural rubber-carbon nanotube composites through latex compounding. *International Journal of Polymeric Materials*, *59*(1), 33-44.

[63] Vigolo, B., Penicaud, A., Coulon, C., Sauder, C., Pailler, R., Journet, C., ... & Poulin, P. (2000). Macroscopic fibers and ribbons of oriented carbon nanotubes. *Science*, *290*(5495), 1331-1334.

[64] Smith, R. J., Lotya, M., & Coleman, J. N. (2010). The importance of repulsive potential barriers for the dispersion of graphene using surfactants. *New Journal of Physics*, *12*(12), 125008.

[65] Sun, Z., Nicolosi, V., Rickard, D., Bergin, S. D., Aherne, D., & Coleman, J. N. (2008). Quantitative evaluation of surfactant-stabilized single-walled carbon nanotubes: dispersion quality and its correlation with zeta potential. *The Journal of Physical Chemistry C*, *112*(29), 10692-10699.

[66] Lotya, M., Hernandez, Y., King, P. J., Smith, R. J., Nicolosi, V., Karlsson, L. S., ... & Duesberg, G. S. (2009). Liquid phase production of graphene by exfoliation of graphite in surfactant/water solutions. *Journal of the American Chemical Society*, *131*(10), 3611-3620.

[67] Marsh, D. H., Rance, G. A., Zaka, M. H., Whitby, R. J., & Khlobystov, A. N. (2007). Comparison of the stability of multiwalled carbon nanotube dispersions in water. *Physical Chemistry Chemical Physics*, *9*(40), 5490-5496.

[68] Werner Hofman, In: Rubber Technology Handbook' -Ed. Werner

[69] Rahman, I. A., & Padavettan, V. (2012). Synthesis of silica nanoparticles by sol-gel: size-dependent properties, surface modification, and applications in silica-polymer nanocomposites—a review. *Journal of Nanomaterials*, *2012*, 8.

[70] Young, G. J. (1958). Interaction of water vapor with silica surfaces. *Journal of colloid science*, *13*(1), 67-85.

[71] https://en.wikipedia.org/wiki/Colloidal_silica

[72] Rezende, C. A., Bragança, F. C., Doi, T. R., Lee, L. T., Galembeck, F., & Boué, F. (2010). Natural rubber-clay nanocomposites: Mechanical and structural properties. *Polymer*, *51*(16), 3644-3652.

[73] Wu, Y. P., Jia, Q. X., Yu, D. S., & Zhang, L. Q. (2003). Structure and properties of nitrile rubber (NBR)–clay nanocomposites by co-coagulating NBR latex and clay aqueous suspension. *Journal of Applied Polymer Science*, *89*(14), 3855-3858.

[74] Kim, J. T., Oh, T. S., & Lee, D. H. (2003). Preparation and characteristics of nitrile rubber (NBR) nanocomposites based on organophilic layered clay. *Polymer International*, *52*(7), 1058-1063.

[75] Kader, M. A., Kim, K., Lee, Y. S., & Nah, C. (2006). Preparation and properties of nitrile rubber/montmorillonite nanocomposites via latex blending. *Journal of materials science*, *41*(22), 7341-7352.

[76] Zhang, Y., Liu, Q., Zhang, Q., & Lu, Y. (2010). Gas barrier properties of natural rubber/kaolin composites prepared by melt blending. *Applied Clay Science*, *50*(2), 255-259.

[77] Ruamcharoen, J. Chotisuwan, S. Ruamcharoen, P. (2012). *Advanced Materials Research* Vols., 488,701.

[78] Zhang, L., Wang, Y., Wang, Y., Sui, Y., & Yu, D. (2000). Morphology and mechanical properties of clay/styrene-butadiene rubber nanocomposites. *Journal of Applied Polymer Science*, *78*(11), 1873-1878.

[79] Stephen, R. (2005). Doctoral dissertation, Mahatma Gandhi University, Kottayam, India.

[80] Das, A. Jurk, R. Stöckelhuber, K.W. Majumder, P.S. Engelhardt T. FritzscheJ. Klüppel, M Heinrich, G. (2009). *Journal of Macromolecular Science,* Part A Pure and Applied Chemistry, 46, 7.

[81] Fritzsche, J., Das, A., Jurk, R., Stöckelhuber, K. W., Heinrich, G., & Klüppel, M. (2008). Relaxation dynamics of carboxylated nitrile rubber filled with organomodified nanoclay. *Express Polymer Letters*, *2*, 373-381.

[82] Park, Y. S., Huh, M., Kang, S. J., Yun, S. I., & Ahn, K. H. (2009). Effect of CNT diameter on physical properties of styrene-butadiene rubber nanocomposites. *Carbon letters*, *10*(4), 320-324.

[83] Bauhofer, W., & Kovacs, J. Z. (2009). A review and analysis of electrical percolation in carbon nanotube polymer composites. *Composites Science and Technology*, *69*(10), 1486-1498.

[84] Girun, N., Ahmadun, F. R., Rashid, S. A., & Ali Atieh, M. (2007). Multi-Wall Carbon Nanotubes/Styrene Butadiene Rubber (SBR) Nanocomposite. *Fullerenes, Nanotubes, and Carbon Nanostructures*, *15*(3), 207-214.

[85] Peddini, S. K., Bosnyak, C. P., Henderson, N. M., Ellison, C. J., & Paul, D. R. (2014). Nanocomposites from styrene-butadiene rubber (SBR) and multiwall carbon nanotubes (MWCNT) part 1: Morphology and rheology. *Polymer*, *55*(1), 258-270.

[86] Bokobza, L. (2007). Multiwall carbon nanotube elastomeric composites: a review. *Polymer*, *48*(17), 4907-4920.

[87] Zhou, X., Zhu, Y., Gong, Q., & Liang, J. (2006). Preparation and properties of the powder SBR composites filled with CNTs by spray drying process. *Materials letters*, *60*(29), 3769-3775.

[88] Perez, L. D., Zuluaga, M. A., Kyu, T., Mark, J. E., & Lopez, B. L. (2009). Preparation, characterisation, and physical properties of multiwall carbon nanotube/elastomer composites. *Polymer Engineering and Science*, *49*(5), 866.

[89] Xiao-hong, Chen, & Huai-he, Song. (2004). Multi walled carbon nanotube filled SBR rubber composites. *New carbon materials*, *19*(3), 214-218.

[90] Bhattacharyya, S., Sinturel, C., Bahloul, O., Saboungi, M. L., Thomas, S., & Salvetat, J. P. (2008). Improving reinforcement of natural rubber by networking of activated carbon nanotubes. *Carbon*, *46*(7), 1037-1045.

[91] Atieh, M. A., Girun, N., Ahmadun, F. R., Guan, C. T., Mahdi, E. S., & Baik, D. R. (2005). Multi-wall carbon nanotubes/natural rubber nanocomposites. *AzoNano–Online Journal of Nanotechnology*, *1*, 1-11.

[92] Abdullateef, A. A., Thomas, S. P., Al-Harthi, M. A., De, S. K., Bandyopadhyay, S., Basfar, A. A., & Atieh, M. A. (2012). Natural rubber nanocomposites with functionalised carbon nanotubes: mechanical, dynamic mechanical, and morphology studies. *Journal of Applied Polymer Science*, *125*(S1).

[93] Nakaramontri, Y., Nakason, C., Kummerlöwe, C., & Vennemann, N. (2015). Influence of modified natural rubber on properties of natural rubber-carbon nanotube composites. *Rubber Chemistry and Technology*, *88*(2), 199-218.

[94] Frogley, M. D., Ravich, D., & Wagner, H. D. (2003). Mechanical properties of carbon nanoparticle-reinforced elastomers. *Composites Science and technology*, *63*(11), 1647-1654.

[95] Subramaniam, K., Das, A., & Heinrich, G. (2011). Development of conducting polychloroprene rubber using imidazolium based ionic liquid modified multi-walled carbon nanotubes. *Composites Science and Technology*, *71*(11), 1441-1449.

[96] Zhan, Y., Wu, J., Xia, H., Yan, N., Fei, G., & Yuan, G. (2011). Dispersion and Exfoliation of Graphene in Rubber by an Ultrasonically-Assisted Latex Mixing and In situ Reduction Process. *Macromolecular Materials and Engineering*, *296*(7), 590-602.

[97] Wang, L., Zhang, L., & Tian, M. (2012). Effect of expanded graphite (EG) dispersion on the mechanical and tribological properties of nitrile rubber/EG composites. *Wear*, *276*, 85-93.

[98] Xing, W., Wu, J., Huang, G., Li, H., Tang, M., & Fu, X. (2014). Enhanced mechanical properties of graphene/natural rubber nanocomposites at low content. *Polymer International*, *63*(9), 1674-1681.

[99] Wu, X., Lin, T. F., Tang, Z. H., Guo, B. C., & Huang, G. S. (2015). Natural rubber/graphene oxide composites: Effect of sheet size on mechanical properties and strain-induced crystallization behavior. *Express Polymer Letters*, *9*(8).

[100] Zhou, S., Xiong, M., & Wu, L. (2003). The properties of high solid acrylic based polyurethane and acrylic latex embedded with nano-silica. *Journal of chemical engineering of Japan*, *36*(10), 1263-1269.

[101] Ji, X., Hampsey, J. E., Hu, Q., He, J., Yang, Z., & Lu, Y. (2003). Mesoporous silica-reinforced polymer nanocomposites. *Chemistry of Materials*, *15*(19), 3656-3662.

[102] Wolff, S., & Wang, M. J. (1992). Filler—elastomer interactions. Part IV. The effect of the surface energies of fillers on elastomer reinforcement. *Rubber chemistry and technology*, *65*(2), 329-342.

[103] Kohjiya, S., & Ikeda, Y. (2000). Reinforcement of general-purpose grade rubbers by silica generated in situ. *Rubber chemistry and technology*, *73*(3), 534-550.

[104] Lin, Y., Zhang, A., Sun, J., & Wang, L. (2013). Properties of natural rubber vulcanisates/nanosilica composites prepared based on the method of in-situ generation and coagulation. *Journal of Macromolecular Science, Part B*, *52*(11), 1494-1507.

[105] Gorl, U., Munzenberg, J., Luginsland, D., & Muller, A. (1999). Investigations on the reaction silica/organosilane and organosilane/polymer-Part 4: Studies on the chemistry of the silane sulfur chain. *Kautschuk Gummi Kunststoffe*, *52*(9), 588-597.

[106] George, K. M., Varkey, J. K., Thomas, K. T., & Mathew, N. M. (2002). Epoxidized natural rubber as a reinforcement modifier for silica-filled nitrile rubber. *Journal of applied polymer science*, *85*(2), 292-306.

[107] Cataldo, F. (2002). Preparation of Silica-Based Rubber Compounds without the Use of a Silane Coupling Agent through the Use of Epoxidized Natural Rubber. *Macromolecular Materials and Engineering*, *287*(5), 348-352.

[108] Subramaniam, K., Das, A., Häußler, L., Harnisch, C., Stöckelhuber, K. W., & Heinrich, G. (2012). Enhanced thermal stability of polychloroprene rubber composites with ionic liquid modified MWCNTs. *Polymer degradation and stability*, *97*(5), 776-785.

[109] Khalid, M., Ismail, A. F., Ratnam, C. T., Faridah, Y., Rashmi, W., & Al Khatib, M. F. (2010). Effect of radiation dose on the properties of natural rubber nanocomposite. *Radiation Physics and Chemistry*, *79*(12), 1279-1285.

[110] Fakhru'l-Razi, A., Atieh, M. A., Girun, N., Chuah, T. G., El-Sadig, M., & Biak, D. R. A. (2006). Effect of multi-wall carbon nanotubes on the mechanical properties of natural rubber. *Composite Structures*, *75*(1), 496-500.

[111] Yu, J., Lu, K., Sourty, E., Grossiord, N., Koning, C. E., & Loos, J. (2007). Characterisation of conductive multiwall carbon nanotube/polystyrene composites prepared by latex technology. *Carbon*, *45*(15), 2897-2903.

[112] Das, A., Stöckelhuber, K. W., Jurk, R., Saphiannikova, M., Fritzsche, J., Lorenz, H., ... & Heinrich, G. (2008). Modified and unmodified multiwalled carbon nanotubes in high performance solution-styrene–butadiene and butadiene rubber blends. *Polymer*, *49*(24), 5276-5283.

[113] Verge, P., Peeterbroeck, S., Bonnaud, L., & Dubois, P. (2010). Investigation on the dispersion of carbon nanotubes in nitrile butadiene rubber: Role of polymer-to-filler grafting reaction. *Composites Science and Technology*, *70*(10), 1453-1459.

[114] Wang, D., Li, H., Li, M., Jiang, H., Xia, M., & Zhou, Z. (2013). Stretchable conductive polyurethane elastomer in situ polymerized with multi-walled carbon nanotubes. *Journal of Materials Chemistry C*, *1*(15), 2744-2749.

[115] Mao, Y., Wen, S., Chen, Y., Zhang, F., Panine, P., Chan, T. W., ... & Liu, L. (2013). High performance graphene oxide based rubber composites. *Scientific reports*, *3*, 2508.

[116] Xing, W., Tang, M., Wu, J., Huang, G., Li, H., Lei, Z., ... & Li, H. (2014). Multifunctional properties of graphene/rubber nanocomposites fabricated by a modified latex compounding method. *Composites Science and Technology*, *99*, 67-74.

[117] Varghese, S., & Karger-Kocsis, J. (2003). Natural rubber-based nanocomposites by latex compounding with layered silicates. *Polymer*, *44*(17), 4921-4927.

[118] Kang, H., Zuo, K., Wang, Z., Zhang, L., Liu, L., & Guo, B. (2014). Using a green method to develop graphene oxide/elastomers nanocomposites with combination of high barrier and mechanical performance. *Composites Science and Technology*, *92*, 1-8.

[119] Yang, J., Zhang, L. Q., Shi, J. H., Quan, Y. N., Wang, L. L., & Tian, M. (2010). Mechanical and functional properties of composites based on graphite and carboxylated acrylonitrile butadiene rubber. *Journal of applied polymer science*, *116*(5), 2706-2713.

[120] Aliabadi, M. M., Naderi, G., Shahtaheri, S. J., Forushani, A. R., Mohammadfam, I., & Jahangiri, M. (2014). Transport properties of carboxylated nitrile butadiene rubber (XNBR)-nanoclay composites; a promising material for protective gloves in occupational exposures. *Journal of Environmental Health Science and Engineering*, *12*(1), 51.

[121] Peng, Z., Feng, C., Luo, Y., Li, Y., & Kong, L. X. (2010). Self-assembled natural rubber/multi-walled carbon nanotube composites using latex compounding techniques. *Carbon*, *48*(15), 4497-4503.

[122] Ponnamma, D., Sung, S. H., Hong, J. S., Ahn, K. H., Varughese, K. T., & Thomas, S. (2014). Influence of non-covalent functionalisation of carbon nanotubes on the rheological behavior of natural rubber latex nanocomposites. *European Polymer Journal*, *53*, 147-159.

[123] Poompradub, S., Thirakulrati, M., & Prasassarakich, P. (2014). In situ generated silica in natural rubber latex via the sol–gel technique and properties of the silica rubber composites. *Materials Chemistry and Physics*, *144*(1), 122-131.

[124] Li, S. D., Peng, Z., Kong, L. X., & Zhong, J. P. (2006). Thermal degradation kinetics and morphology of natural rubber/silica nanocomposites. *Journal of nanoscience and nanotechnology*, *6*(2), 541-546.

[125] Arun, K., Francis, P. J., & Joseph, R. (2010). Mechanical properties of nr latex-nano silica composites. *Optoelectronics and Advanced material*, 4(10), 1520 – 1525.

[126] Jose Paul Meleth., K E Geore, G Madhu., Rani Joseph. (2012). Study on the properties of NR latex-Nanosilica composite for surgical gloves. *International Journal of Science and Technology*.

[127] Stankovich, S., Dikin, D. A., Dommett, G. H., Kohlhaas, K. M., Zimney, E. J., Stach, E. A., ... & Ruoff, R. S. (2006). Graphene-based composite materials. *Nature, 442*(7100), 282-286.

[128] Deng, H., Lin, L., Ji, M., Zhang, S., Yang, M., & Fu, Q. (2014). Progress on the morphological control of conductive network in conductive polymer composites and the use as electroactive multifunctional materials. *Progress in Polymer Science*, *39*(4), 627-655.

[129] Ma, P. C., Siddiqui, N. A., Marom, G., & Kim, J. K. (2010). Dispersion and functionalisation of carbon nanotubes for polymer-based nanocomposites: a review. *Composites Part A: Applied Science and Manufacturing*, *41*(10), 1345-1367.

[130] Stauffer, D., & Aharony, A. (1994). *Introduction to percolation theory*. London: Taylor and Francis; CRC press. p. 192.

[131] Gupta, S., Ou, R., & Gerhardt, R. A. (2006). Effect of the fabrication method on the electrical properties of poly (acrylonitrile-co-butadiene-co-styrene)/ carbon black composites. *Journal of electronic materials*, *35*(2), 224-229.

[132] Kusy, R. P., & Turner, D. T. (1973). Electrical conductivity of a polyurethane elastomer containing segregated particles of nickel. *Journal of Applied Polymer Science*, *17*(5), 1631-1633.

[133] Du, J., Zhao, L., Zeng, Y., Zhang, L., Li, F., Liu, P., & Liu, C. (2011). Comparison of electrical properties between multi-walled carbon nanotube and graphene nanosheet/high density polyethylene composites with a segregated network structure. *Carbon*, *49*(4), 1094-1100.

[134] Zhang, C., Ma, C. A., Wang, P., & Sumita, M. (2005). Temperature dependence of electrical resistivity for carbon black filled ultra-high molecular weight polyethylene composites prepared by hot compaction. *Carbon*, *43*(12), 2544-2553.

[135] Wang, B., Li, H., Li, L., Chen, P., Wang, Z., & Gu, Q. (2013). Electrostatic adsorption method for preparing electrically conducting ultrahigh molecular weight polyethylene/graphene nanosheets composites with a segregated network. *Composites Science and Technology*, *89*, 180-185.

[136] Grunlan, J. C., Gerberich, W. W., & Francis, L. F. (2001). Electrical and mechanical behavior of carbon black–filled poly (vinyl acetate) latex–based composites. *Polymer Engineering & Science*, *41*(11), 1947-1962.

[137] Grossiord, N., Loos, J., & Koning, C. E. (2005). Strategies for dispersing carbon nanotubes in highly viscous polymers. *Journal of Materials Chemistry*, *15*(24), 2349-2352.

[138] Mechrez, G., Suckeveriene, R. Y., Zelikman, E., Rosen, J., Ariel-Sternberg, N., Cohen, R., ... & Segal, E. (2012). Highly-tunable polymer/carbon nanotubes systems: Preserving dispersion architecture in solid composites via rapid microfiltration. *ACS Macro Letters*, *1*(7), 848-852.

[139] Zhang, Y. C., Dai, K., Tang, J. H., Ji, X., & Li, Z. M. (2010). Anisotropically conductive polymer composites with a selective distribution of carbon black in an in situ microfibrillar reinforced blend. *Materials Letters*, *64*(13), 1430-1432.

[140] Jurewicz, I., Worajittiphon, P., King, A. A., Sellin, P. J., Keddie, J. L., & Dalton, A. B. (2011). Locking Carbon Nanotubes in Confined Lattice Geometries− A Route to Low Percolation in Conducting Composites. *The Journal of Physical Chemistry B*, *115*(20), 6395-6400.

[141] Regev, O., ElKati, P. N., Loos, J., & Koning, C. E. (2004). Preparation of conductive nanotube–polymer composites using latex technology. *Advanced Materials*, *16*(3), 248-251.

[142] Hermant, M. C., Smeets, N., van Hal, R. C., Meuldijk, J., Heuts, H., Klumperman, B., ... & Koning, C. E. (2009). Influence of the molecular weight distribution on the percolation threshold of carbon nanotube–polystyrene composites. *e-Polymers*, *9*(1), 248-260.

[143] Pang, H., Chen, C., Bao, Y., Chen, J., Ji, X., Lei, J., & Li, Z. M. (2012). Electrically conductive carbon nanotube/ultrahigh molecular weight polyethylene composites with segregated and double percolated structure. *Materials Letters*, *79*, 96-99.

[144] Álvarez, M. P., Poblete, V. H., & Rojas, P. A. (2010). Structural, electrical and percolation threshold of Al/polymethylmethacrylate nanocomposites. *Polymer Composites*, *31*(2), 279-283.

[145] Bao, Y., Xu, L., Pang, H., Yan, D. X., Chen, C., Zhang, W. Q., ... & Li, Z. M. (2013). Preparation and properties of carbon black/polymer composites with segregated and double-percolated network structures. *Journal of Materials Science*, *48*(14), 4892-4898.

[146] Miriyala, S. M., Kim, Y. S., Liu, L., & Grunlan, J. C. (2008). Segregated networks of carbon black in poly (vinyl acetate) latex: influence of clay on the electrical and mechanical behavior. *Macromolecular Chemistry and Physics*, *209*(23), 2399-2409.

[147] Pham, V. H., Dang, T. T., Hur, S. H., Kim, E. J., & Chung, J. S. (2012). Highly conductive poly (methyl methacrylate)(PMMA)-reduced graphene oxide composite prepared by self-assembly of PMMA latex and graphene oxide through electrostatic interaction. *ACS applied materials & interfaces*, *4*(5), 2630-2636.

[148] Wang, D., Zhang, X., Zha, J. W., Zhao, J., Dang, Z. M., & Hu, G. H. (2013). Dielectric properties of reduced graphene oxide/polypropylene composites with ultralow percolation threshold. *Polymer*, *54*(7), 1916-1922.

[149] Yoonessi, M., & Gaier, J. R. (2010). Highly conductive multifunctional graphene polycarbonate nanocomposites. *Acs Nano*, *4*(12), 7211-7220.

[150] Long, G., Tang, C., Wong, K. W., Man, C., Fan, M., Lau, W. M., ... & Wang, B. (2013). Resolving the dilemma of gaining conductivity but losing environmental friendliness in producing polystyrene/graphene composites via optimizing the matrix-filler structure. *Green Chemistry*, *15*(3), 821-828.

[151] Mamunya, Y., Boudenne, A., Lebovka, N., Ibos, L., Candau, Y., & Lisunova, M. (2008). Electrical and thermophysical behaviour of PVC-MWCNT nanocomposites. *Composites Science and Technology*, *68*(9), 1981-1988.

[152] Hao, X., Gai, G., Yang, Y., Zhang, Y., & Nan, C. W. (2008). Development of the conductive polymer matrix composite with low concentration of the conductive filler. *Materials Chemistry and Physics*, *109*(1), 15-19.

[153] Zhao, Z., Zheng, W., Yu, W., & Long, B. (2009). Electrical conductivity of poly (vinylidene fluoride)/carbon nanotube composites with a spherical substructure. *Carbon*, *47*(8), 2118-2120.

[154] Wu, X., Lu, C., Xu, H., Zhang, X., & Zhou, Z. (2014). Biotemplate synthesis of polyaniline@ cellulose nanowhiskers/natural rubber nanocomposites with 3D hierarchical multiscale structure and improved electrical conductivity. *ACS applied materials & interfaces*, *6*(23), 21078-21085.

[155] Potts, J. R., Shankar, O., Du, L., & Ruoff, R. S. (2012). Processing–morphology–property relationships and composite theory analysis of reduced graphene oxide/natural rubber nanocomposites. *Macromolecules*, *45*(15), 6045-6055.

[156] Zhan, Y., Lavorgna, M., Buonocore, G., & Xia, H. (2012). Enhancing electrical conductivity of rubber composites by constructing interconnected network of self-assembled graphene with latex mixing. *Journal of Materials Chemistry*, *22*(21), 10464-10468.

[157] Tian, M., Zhang, J., Zhang, L., Liu, S., Zan, X., Nishi, T., & Ning, N. (2014). Graphene encapsulated rubber latex composites with high dielectric constant, low dielectric loss and low percolation threshold. *Journal of colloid and interface science*, 430, 249-256.

[158] Tian, M., Ma, Q., Li, X., Zhang, L., Nishi, T., & Ning, N. (2014). High performance dielectric composites by latex compounding of graphene oxide-encapsulated carbon nanosphere hybrids with XNBR. *Journal of Materials Chemistry A*, *2*(29), 11144-11154.

[159] Ren, P. G., Di, Y. Y., Zhang, Q., Li, L., Pang, H., & Li, Z. M. (2012). Composites of Ultrahigh-Molecular-Weight Polyethylene with Graphene Sheets and/or MWCNTs with Segregated Network Structure: Preparation and Properties. *Macromolecular Materials and Engineering*, *297*(5), 437-443.

[160] Hu, J. W., Li, M. W., Zhang, M. Q., Xiao, D. S., Cheng, G. S., & Rong, M. Z. (2003). Preparation of binary conductive polymer composites with very low percolation threshold by latex blending. *Macromolecular rapid communications*, *24*(15), 889-893.

[161] Zhou XW, Zhu YF, Liang J. Preparation and properties of powderstyrene–butadiene rubber composites filled with carbon black andcarbon nanotubes. *Mater Res Bull*, 2007;42:456–64.

[162] Chen, J., Shi, Y. Y., Yang, J. H., Zhang, N., Huang, T., Chen, C., ... & Zhou, Z. W. (2012). A simple strategy to achieve very low percolation threshold via the selective distribution of carbon nanotubes at the interface of polymer blends. *Journal of Materials Chemistry*, *22*(42), 22398-22404.

[163] Gubbels, F., Jérôme, R., Teyssie, P., Vanlathem, E., Deltour, R., Calderone, A., ... & Brédas, J. L. (1994). Selective localization of carbon black in immiscible polymer blends: a useful tool to design electrical conductive composites. *Macromolecules*, *27*(7), 1972-1974.

[164] Tian, M., Ma, Q., Li, X., Zhang, L., Nishi, T., & Ning, N. (2014). High performance dielectric composites by latex compounding of graphene oxide-encapsulated carbon nanosphere hybrids with XNBR. *Journal of Materials Chemistry A*, *2*(29), 11144-11154.

[165] Cheng, J., Wang, L., Huo, J., & Yu, H. (2011). A novel polycaprolactone-grafted-carbon black nanocomposite-based sensor for detecting solvent vapors. *Journal of Applied Polymer Science*, *121*(6), 3277-3282.

[166] Al-Saleh MH, Sundararaj U. Electromagnetic interferenceshielding mechanisms of CNT/polymer composites. *Carbon*, 2009;47:1738–46.

[167] Yan DX, Pang H, Xu L, Bao Y, Ren PG, Lei J, Li ZM. Electromagnetic interference shielding of segregated polymer composite with an ultralow loading of in situ thermally reduced graphene oxide. Nanotechnology 2014;25:145705/1–145705.

[168] Goyal RK. Cost-efficient high performance polyetheretherketone/expanded graphite nanocomposites with high conductivity for EMI shielding application. *Mater Chem Phys*, 2013;142:195–8.

[169] Yan, D. X., Pang, H., Li, B., Vajtai, R., Xu, L., Ren, P. G., ... & Li, Z. M. (2015). Structured Reduced Graphene Oxide/Polymer Composites for Ultra-Efficient Electromagnetic Interference Shielding. *Advanced Functional Materials*, *25*(4), 559-566.

.....෩............

Chapter 2

MATERIALS AND METHODS

The materials used and experimental methods adopted in the study are presented in this chapter.

2.1 Materials

2.1.1 Rubbers

2.1.1.1 Natural rubber latex (NR)

NR latex used for the study was centrifuged NR latex, purchased from Njavallil latex, Cochin, India. Specifications are given in Table 2.1.

Table 2.1 Characteristics of NR latex

Dry rubber content (%)	60.04
Total solid content (%)	61.42
Ammonia content (%)	0.70
Specific gravity	0.95

2.1.1.2 Carboxylated nitrile butadiene rubber latex (XNBR)

XNBR latex used was SYNTHOMER 6338, supplied by Synthomer Sdn. Bhd., Malaysia. The latex contains an emulsifier system and is stabilized with an antioxidant. Specifications of the XNBR latex is given in Table 2.2.

Table 2.2 Characteristics of XNBR latex

Total solid content (%)	45
Brookfield viscosity (cP)	64
Surface tension (N/m)	32
Average particle size (nm)	160
Acrylonitrile content (%)	34-38
pH	8.2

2.1.2 Fillers

Fillers used were multiwalled carbon nanotube (MWCNT) and nanosilica.

2.1.2.1 Multiwalled carbon nanotube (MWCNT)

CVD synthesised MWCNT was supplied by Shenzhen Nano Technologies Port Co. Ltd., China. Specifications are given in Table 2.3.

Table 2.3. Characteristics of MWCNT

Purity	> 95 %
Diameter	< 10 nm
Length	1-2 μm
Amorphous Carbon	< 3 %
Ash (Catalyst residue)	< 0.2 %
Thermal conductivity	2000 W/m.k

2.1.2.2 Nanosilica

Colloidal nanosilica of particle size 10 ± 5 nm, total solid content (TSC) 33% and pH around 10 was supplied by Bee Chems, Kanpur.

2.1.3 Chemicals

2.1.3.1 Non-ionic surfactant vulcastab VL (VL)

VL is chemically poly ethylene oxide condensate with the molecular formula $H(C_2H_4O)_nOR$ where R is a hydrocarbon chain having 2 to 20 carbon atoms, and 'n' can vary from 5 to 35. Average molecular weight of

VL ($\bar{M}_n$) is ~600. A 20% aqueous solution of VL supplied by M/s Alkali and Chemical co-operation of India Ltd., Calcutta, was used for the study.

2.1.3.2 Rubber compounding ingredients

Chemicals used in the rubber compounding along with their suppliers are listed in Table 2.4.

Table 2.4 Chemicals and their suppliers

Compounding ingredients	Suppliers
ZnO (activator)	M/s Meta Zinc Ltd. Mumbai
Stearic acid (co- activator)	Godrej soaps pvt. Ltd. Mumbai
Zinc diethyl di thio carbamate (ZDC) (accelerator)	M/s Bayer India Ltd. Mumbai
Morpholino thio benzthiazylsulfenamide (MOR) (accelerator)	Merchem Ltd., Cochin
Tetramethyl thiuram disulphide (TMTD) (accelerator)	
N-cyclo hexyl 2-benzothiazole sulphenamide (CBS) (accelerator)	
Sulphur (crosslinking agent)	M/s Standard Chemicals Co. Pvt. Ltd. Chennai
Styrenated phenol (SP) (antioxidant)	Olympic Chemicals, Maharashtra
TQ (2,2,4-trimethyl-1,2-dihydro quinolone (antioxidant)	M/s Bayer India Ltd. Mumbai

2.1.3.3 Other chemicals

Dispersol F (Sodium methylene bis naphthalene sulphonic acid) (dispersing agent) was supplied by M/S Bayer India Ltd. Mumbai, India. Toluene and Methyl ethyl ketone (MEK) used for swelling studies were supplied by Spectrochem Pvt. Ltd. Mumbai, India. Sodium hydroxide, Potassium hydroxide and Calcium chloride used were of analytical grade. Analytical grade Glacial acetic acid (CH_3COOH), Hydrochloric acid, HCl (35%), Sulphuric acid, H_2SO_4 (98%) and Nitric acid, HNO_3 (69%) were purchased from Merck Specialities Private Ltd., Mumbai, India.

2.2 Experimental Methods

2.2.1 Ball milling

Water insoluble materials were added to the rubber latex in the form of aqueous dispersions. Ball milling was used for the preparation of these aqueous dispersions.

Ball mill comprises of a steel cylindrical container, fed with the slurry and a charge of ceramic balls as grinding elements. The mill is operated by causing the cylindrical container to revolve slowly about its longitudinal axis, which is horizontal. The collision of the balls against each other and also against the walls of the container causes reduction in the particle size of the material[1]. The details of preparation of various dispersions are given below:

a)   **ZnO dispersion (50%)**
     ZnO   -   200g
     Dispersol F -   2 g   (Ball milled for 48 h)
     Water   -   400ml

b)   **ZDC dispersion (50%)**
     ZDC   -   200g
     Dispersal F -   2 g   (Ball milled for 48 h)
     Water   -   400 ml

c)   **Sulphur dispersion (50%)**
     Sulphur   -   200g
     Dispersal F -   2 g   (Ball milled for 72 h)
     Water   -   400 ml

2.2.2 Ultrasonication

In the present study ultrasonication was used to prepare aqueous dispersions of nanofillers. Sonication process was performed using two types of sonicator: one is horn sonicator (Sonics VCX-750 Vibra Cell Ultra Sonic Processor) with a cylindrical tip (13 mm end cap diameter), operating

at 40% of the maximum power, 750W and the other is a bath sonicator (BRANSON 1510E-MT) operating at 70 W power and 42 kHz frequency.

The ultrasonic power supply converts line voltage to high frequency electrical energy which in turn is converted to mechanical vibrations by a piezoelectric transducer within a converter. These vibrations are intensified by a probe thereby causing pressure waves in the liquid. This action produces millions of bubbles or cavities which expand and then collapse causing enormous shock waves in the liquid, along with an increase in temperature and pressure. The extremely high level of energy released during the process leads to the disruption of the interaction forces between the particles causing dispersion of the suspended particles in the solvent. To prevent the rise in temperature the sample container is kept in an ice bath.

2.2.3 Latex compounding and film casting

Compounding ingredients were added to the rubber latex according to their compounding formulations, stirred and ultrasonicated in a bath sonicator to achieve uniformity, kept overnight for maturation, cast on to flat glass trays, dried and cured in an air oven to get the vulcanised films. Compounding formulation for NR and XNBR latex is given in Table 2.5 and 2.6 respectively.

Table 2.5 Compounding formulation for NR latex

Ingredients	Amount (g)
Centrifuged NR latex (60 % DRC)	167
Filler	As per requirement
10 % KOH solution	1.0
10 % Potassium oleate solution	1.0
20 % Vulcastab VL	1.0
50 % ZnO dispersion	1.0
50 % ZDC dispersion	2.0
50 % Sulphur dispersion	3.0

Table 2.6 Compounding formulation for XNBR latex

Ingredients	Amount (g)
XNBR latex (45% DRC)	222
Filler	As per requirement
20% VL solution	1.0
50% ZnO dispersion	4.0
50% ZDC dispersion	2.0
50% Sulphur dispersion	2.0

2.2.4 Compounding in an internal mixer

Nanofiller aqueous suspension was added to the compounded rubber latex at various compositions. These mixtures were stirred well under magnetic stirring for 15 minutes so as to achieve uniform distribution of the filler in the NR latex. After that, the latex mix was poured into tray and coagulated by rapid addition of the coagulant. The coagulum was isolated by vacuum filtration, washed several times with water and dried at 50 °C in an air oven.

Table 2.7 Formulation of NR nanocomposites

Ingredients	Amount (phr[a])
NR	100
Filler	As per requirement
Stearic acid	2.25
ZnO	5.0
Antioxidant SP[b]	1.0
Accelerator MOR[c]	0.75
Accelerator TMTD[d]	0.2
Sulphur	2.5

[a] Parts by weight per hundred parts of rubber
[b] Styrenated phenol
[c] Morpholino thio benzthiazylsulfenamide
[d] Tetramethyl Thiuram Disulfide

Table 2.8 Formulation used in the preparation of XNBR nanocomposites

Ingredients	Amount (phr[a])
XNBR	100
Filler	As per requirement
Sulphur	1.5
Stearic acid	2.0
ZnO	4.5
Antioxidant TQ[b]	1.0
Accelerator CBS[c]	1.0
Accelerator TMTD[d]	0.3

[a] Parts by weight per hundred parts of rubber
[b] 2,2,4-trimethyl-1,2-dihydro quinolone (oligomer)
[c] N-Cyclohexyl-2-benzothiazole sulfenamide
[d] Tetramethyl Thiuram Disulfide

The dried coagulum containing nanofillers was mixed in an internal mixer equipped with Banbury rotors (Thermo Haake Polylab QC Version 1.02) with mixing chamber volume of 69 cc, at 70 °C, for 8 minutes at 60 rpm with compounding ingredients as per formulation given in Table 2.7 for NR and Table 2.8 for XNBR and according to the ASTM D 3184 and ASTM D 3187 respectively. After mixing the batch was passed six times for NR and twice for XNBR through tight nip in a two-roll mill and was finally sheeted out at a nip gap of 3 mm. The samples were kept overnight for maturation.

2.2.5 Moulding

The test specimens were moulded in standard moulds by compression moulding on an electrically heated hydraulic press having 45 cm × 45 cm platen at a pressure of 200 kg/cm^2 at 150 °C for an optimum cure time. After curing the mouldings were cooled by dipping in cold water and conditioned for 24 h before testing.

2.3 Characterisation Techniques

2.3.1 Cure Characteristics

Cure characteristics at 150 °C were determined by using Rubber Process Analyser, RPA 2000 (as per ASTM D 5289). The machine has two directly heated, opposed biconical dies that are designed to achieve a constant shear gradient over the entire sample chamber. The specimen was kept in the lower die, which was oscillating through a small deformation angle (± 0.2°) at a frequency of 50 oscillations per minute. The torque transducer on the upper die senses the force being transmitted through the rubber. The measurements made by the torque transducer are fed into the computer. The selected properties are measured and the results are calculated and displayed. A typical cure curve is shown in Fig. 2.1.
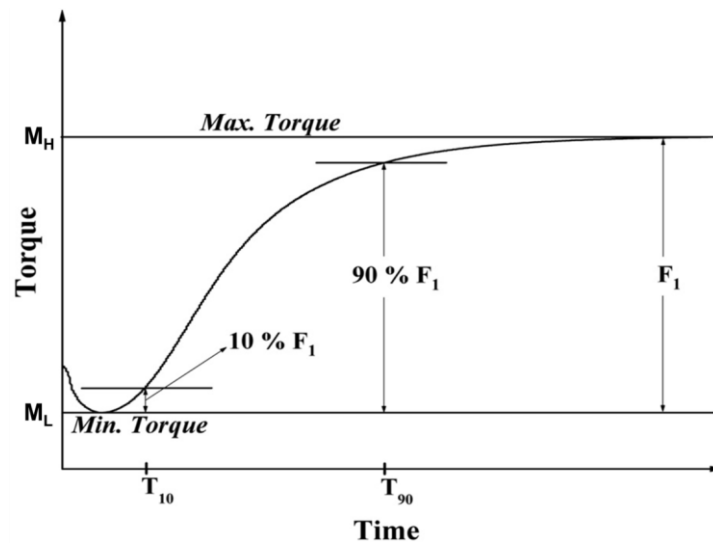
Fig. 2.1 A typical cure curve

Data obtained from a torque-time curve is given below.

a) *Minimum torque (M_L)*: Measure of the stiffness of unvulcanised test specimen. It is the torque shown by the mix at the test temperature before the onset of cure.

b)   *Maximum torque (*M_H*)*: Measure of the stiffness or shear modulus of the fully vulcanised test specimen at the vulcanisation temperature. It is the torque recorded after curing of the mix is completed.

c)   *Scorch time (*T_{10}*)*: It is the time taken for attaining 10% of the maximum torque.

d)   *Optimum cure time (*T_{90}*)*: Time taken for attaining 90% of the maximum torque. It is the time corresponding to a torque equal to $0.9(M_H - M_L) + M_L$.

e)   *Cure rate index (CRI)*: It is a measure of the rate of cure and can be calculated from Eq. 2.1

$$CRI = \frac{100}{T_{90} - T_{10}}$$ ....(2.1)

2.3.2 Physical tests

Tensile properties

Tensile strength is the force per unit area of cross section, which is required to break the test specimen, provided the stress is substantially uniform over whole of the cross section.

Tensile strength=load (N) /area of cross section (mm^2) ....(2.2)

Elongation at break is the maximum value of elongation, expressed as a percentage of the original length.

Elongation at break= $(L-L_0)100/L_0$ ....(2.3)

L_0 and L are the initial and final length of the sample.

The value of tensile stress (force/unit area) required to stretch the test piece from the unstrained condition to a given elongation is called modulus or tensile stress at a given strain. It is expressed in the unit of stress (MPa or N/mm^2)

These tests were done on a Shimadzu Model AGI Universal Testing Machine as per ASTM D 412. Standard dumbbell shaped test specimens were punched out from the moulded sheet using the C-type die, along the mill grain direction. The measurements were carried out at a crosshead speed of 500 mm/min.

Tear strength

Tear strength or tear resistance is, how well a material resists the growth of any cut when under tension. It is expressed in N/mm.

Tear strength = Load (N) / Thickness (mm) ....(2.4)

Tear strength of the samples were tested on Shimadzu Model AGI Universal Testing Machine according to ASTM D 624, using unnicked 90° angle test specimens that were punched out from the moulded sheets, along the mill grain direction. The measurements were carried out at a crosshead speed of 500 mm per minute.

Hardness

The hardness of the sample (Shore A) was determined using Mitutoyo Hardmatic hardness tester according to ASTM D 2240–86. Samples having dimensions of 12 mm diameter and minimum 6 mm thickness were used. Readings were taken 10 seconds after the indenter had made a firm contact with the specimen.

Abrasion Resistance

The abrasion resistance of the samples were measured on a DIN Abrader (DIN 53516). Moulded samples of 12 ± 0.2 mm diameter and 16-20 mm thickness were prepared as per ASTM D 3183 and abrasion loss was measured as per ASTM D 5963-04. Initially a pre run was given for all samples and its weight was taken. The weight after final run was also noted. Abrasion loss was calculated using Eq. 2.5.

$$Abrasion\ loss = \frac{loss\ of\ weight}{specific\ gravity} \dots\dots\dots(2.5)$$

Abrasion loss for a standard reference compound was also measured using the same procedure and the abrasion resistance index was calculated using Eq. 2.6.

$$Abrasion\ resistance\ index = \frac{Abrasion\ loss\ of\ reference}{Abrasion\ loss\ of\ sample} \times 100 \dots(2.6)$$

Rebound Resilience

Rebound resilience was measured using a vertical rebound resilience tester as per ASTM D 2632-01. A plunger weighing 28 ± 0.5 g is dropped from a height of 40 cm to the sample of thickness 12.5 mm and the rebound height is measured. The resilience scale was marked in 100 equally spaced divisions and hence the rebound height is equal to the resilience (%).

Compression Set

Circular samples (1.25 cm thick and 2.8 cm diameter) compressed to a constant strain (25 %) were kept in an air oven for 22 h, at 70 °C and 100 °C respectively for NR and XNBR (ASTM D 395-1998 method B). The samples were taken out, cooled to room temperature for half an hour and the final thickness measured. The compression set was calculated using the equation

$$Compression\ set\ (\%) = \frac{T_0 - T_1}{T_0 - T_S} \times 100 \dots(2.7)$$

where T_0 and T_1 are the initial and final thickness of the specimen and T_S is the thickness of the spacer bar used.

2.3.3 Density

The densities of the samples were estimated by the method of displacement of liquid (ASTM D 792).

2.3.4 Ultraviolet-visible spectroscopy (UV-vis)

UV-vis absorption spectra were recorded with Thermo Scientific Evolution 201 UV-Visible Spectrophotometer operating between 200 and 900 nm.

2.3.5 Brunauer-Emmett-Teller (BET) method

Surface area, pore volume, and pore diameter of the samples were measured at 77 K by a Micromeritics (TriStar 3000 V6.07 A) using nitrogen adsorption.

2.3.6 X- ray diffraction (XRD)

X-ray diffraction study was done using a Bruker AXS D8 Advance X-ray powder diffractometer equipped with Cu Kα radiation at the operating voltage of 40 kV and current of 35 mA. The diffraction intensities were recorded between 3 and 80º (2θ angle range) at increments of 0.02º at a wavelength of 1.541Å.

2.3.7 Fourier transform infrared spectroscopy (FTIR)

FTIR is a good analytical tool used to determine the structure and functional groups in a molecule. FTIR is useful in detecting the characteristic vibrational frequencies of molecules. FTIR analysis was conducted using Thermo Nicolet, Avatar 370 model IR spectrometer, in 4000-400 cm^{-1} spectral range with a resolution of 4 cm^{-1}. Here transmittance % is presented as the function of wave number (cm^{-1}).

2.3.8 Raman spectra

Raman spectra of MWCNT and MWCNTR were recorded with Horiba Jobin Yvon Lab Ram HR system at a resolution of 2 mm by using excitation of 514.5 nm by Argon ion laser.

2.3.9 XPS analysis

X-ray photoelectron spectroscopy (XPS) analysis was carried out on a Kratos Axis Ultra X-ray photoelectron spectroscope (UK) with Al Ka radiation of 1486.6 eV.

2.3.10 Particle size analysis

Particle size of nanofillers was recorded by dynamic light scattering (DLS) system using Nanotrac equipment from Microtrac. The technique is also referred as photon correlation spectroscopy (PCS) in which particle size is determined by measuring the random changes in the intensity of light scattered from a suspension or solution. The sample is illuminated by a laser beam followed by detection of the resultant fluctuations of the scattered light at a known scattering angle θ by a fast photon detector. Aqueous dispersions of the nanofillers were used for the study.

2.3.11 High resolution transmission electron microscopy (HRTEM)

Transmission electron microscopy (TEM) is a microscopy technique in which a high energy beam of electrons is transmitted through an ultra-thin specimen, interacting with the specimen as it passes through. An image is formed from the interaction of the electrons transmitted through the specimen.

High resolution transmission electron microscopy (HRTEM) was performed using high resolution transmission electron microscope (HRTEM, JEOL model JEM-2100). For TEM observation aqueous suspensions of nanofillers were sonicated for 15 min to disperse the aggregated particles. The well dispersed suspensions were directly dropped on a copper microgrid and dried before observation. In the case of nanocomposite samples prepared by film casting, the rubber latex compound containing nano fillers was diluted and put on the copper grids and the water was evaporated before TEM observation.

The micrographs of the composite samples prepared by Haake mixing were taken using JEOL JEM-2100 transmission electron microscope with an accelerating voltage of 200 keV. Ultrathin sections of bulk specimens (about 100 nm in thickness) were obtained by cryocutting with an ultramicrotome fitted with a diamond knife.

2.3.12 Scanning electron microscopy (SEM)

Scanning electron microscopy is a method for high-resolution imaging of surfaces. The method uses a focused beam of high-energy electrons to generate a variety of signals at the surface of solid specimens. These signals include secondary electrons, back scattered electrons, diffracted backscattered electrons, photons, visible light, and heat. Of these, the signals produced by secondary electrons are the most important for studying the morphology and topography of the samples.

The morphology of nanofillers and fractured surface of rubber nanocomposites were examined using a scanning electron microscope JEOL Model JSM 6390 LV. In the case of nanofillers, dispersion of the filler in a suitable solvent was sonicated and placed on carbon tapes. After evaporating the solvent all the specimens were sputtered with gold before imaging.

2.3.13 Energy dispersive X-ray spectroscopy (EDS)

Qualitative elemental analysis, standardless quantitative analysis, X-ray line scans and mapping are performed with SEM-EDS combination. EDS has the specification JEOL Model, JED-2300.

2.3.14 Dynamic mechanical analysis (DMA)

The strain-amplitude dependent dynamic mechanical properties of the vulcanisates were measured at room temperature by means of a dynamic mechanical analyser (Model Q 800, TA instruments). For this experiment

tension mode was selected for the variation of the strain amplitude from 0.01% to 40% at 1 Hz frequency.

2.3.15 Thermal analysis

Thermogravimetric analyses (TGA) were done using a TGA-Q 50 Thermal Analyser (TA Instruments). In all cases the sample weights were between 5 and 10 mg. All the measurements were conducted under a high-purity nitrogen flow over a temperature range of 40-700 ºC with a ramp rate of 20 ºC/min.

2.3.16 Swelling studies

Sorption behavior and cross-link density of the samples were determined by equilibrium swelling method. For NR, toluene and for XNBR, methyl ethyl ketone (MEK) was used as the solvent. Circular samples were punched out from vulcanised sheets using a sharp-edged steel die. The samples were weighed and dipped in 30 ml solvent in diffusion bottles. Samples were taken out at regular intervals of time, wiped of the excess solvent and weighed. Each time after weighing they were immediately immersed into the bottles and weighing continued until they reached equilibrium swelling. Finally deswollen weight of the samples was taken after drying.

Mol% uptake (Qt %) of solvent for the samples were calculated using Eq. 2.8.

$$Q_t\ mol\% = \left(\frac{Mass\ of\ solvent\ sorbed/Molar\ mass\ of\ solvent}{Mass\ of\ polymer}\right) \times 100 \quad ...(2.8)$$

Swelling index was computed according to the following equation.

$$Swelling\ index = \frac{W_s - W_i}{W_i} \times 100 \quad \cdots\cdots\cdots\cdots\cdots\cdots\cdots\cdots(2.9)$$

where W_s is the weight of the swollen sample and W_i is the initial weight of the sample i.e. the weight of the sample before swelling.

Crosslink density was calculated according to Eq. 2.10

$$\nu = \frac{1}{2M_c} \quad \dots\dots\dots\dots\dots\dots\dots\dots\dots\dots\dots\dots\dots\dots(2.10)$$

where M_c is the molecular mass between successive crosslinks. M_c is given by the Flory-Rehner equation (Eq. 2.11)[2].

$$M_c = \frac{-\rho_r V_s V_r^{1/3}}{\ln(1 - V_r) + V_r + \chi V_r^2} \quad \dots\dots\dots\dots\dots\dots\dots\dots\dots\dots(2.11)$$

where ρ_r is the density of rubber, V_s is the molar volume of the solvent, χ is the rubber solvent interaction parameter and V_r is the volume fraction of swollen rubber which was calculated using Ellis and Welding equation (Eq. 2.12)[3].

$$V_r = \frac{(d - fw)\rho_r^{-1}}{(d - fw)\rho_r^{-1} + A_s\rho_s^{-1}} \quad \dots\dots\dots\dots\dots\dots\dots\dots\dots\dots(2.12)$$

where d is the deswollen weight of the polymer, f is the volume fraction of insoluble components, w is the initial weight of the polymer, A_s is the amount of solvent absorbed and ρ_s is density of the solvent. χ is determined using Hildebrand Equation (Eq. 2.13)[4].

$$\chi = \beta + \frac{V_s(\delta_s - \delta_p)^2}{RT} \quad \dots\dots\dots\dots\dots\dots\dots\dots\dots\dots\dots\dots(2.13)$$

where β is the lattice constant, R is the universal gas constant, T is the absolute temperature, δ_s and δ_p are solubility parameters of the solvent and polymer respectively.

2.3.17 Conductivity studies

2.3.17.1 DC electrical conductivity

DC electrical conductivity measurements were done using a Keithley 2400 source-measure unit in dry air at room temperature. Disc shaped rubber

samples having diameter 10 mm and thickness of about 1 mm were used for the measurements. The sample was mounted between two parallel copper electrodes and conductivity was calculated using the formula

$$\sigma = (I/V) \times l/A \quad \text{..(2.14)}$$

where σ is the electrical conductivity (S/m), I is the current (amperes), V is the voltage (volts), l is the thickness of the sample (m) and A is the area of contact of electrodes with sample (m^2) which is given by

$$A = \pi \times (5 \times 10^{-3})^2 \quad \text{...(2.15)}$$

2.3.17.2 Dielectric studies

Permittivity describes the interaction of a material with an electric field. The major use of dielectrics is in fabricating capacitors. These have many uses including storage of energy in the electric field between the plates, filtering out noise from signals as part of a resonant circuit and supplying a burst of power to another component.

The large the dielectric constant, the more charge the capacitor can store in a given field. Dielectric constant (k) is equivalent to the complex relative permittivity ($\mathcal{E}_r$) which is given by

$$\mathcal{E}_r = \mathcal{E}/\mathcal{E}_0 \quad \text{...(2.16)}$$

where $\mathcal{E}$ = Permittivity of the material (F/m)

$\mathcal{E}_0$= Permittivity of free space = 8.854 x 10^{-12} (F/m)

$\mathcal{E}_r$ = Relative permittivity (dielectric constant) of the test material.

From Eq. 2.16, $\qquad \mathcal{E} = \mathcal{E}_0 \mathcal{E}_r = \dfrac{t}{A} \times C_p$

$$\mathcal{E}_r = \frac{t}{A} \times \frac{C_P}{\mathcal{E}_0} \quad \text{...(2.17)}$$

where t = Thickness of test material

A = Area of the electrode

C_p= Capacitance

Dielectric and AC conductivity studies in the frequency range 40Hz to 30MHz were done using Precision Impedance Analyser (Agilent 4294A) with dielectric text fixture 16451B (Fig. 2.2). Parallel plate method was employed to measure the permittivity. Here permittivity was measured from capacitance value. Circular specimens of 10 mm diameter and about 1 mm thickness were used for the study.

AC conductivity was calculated using the formula

$$\sigma = 2\pi f \varepsilon_0\, \varepsilon^{''}$$ ....(2.18)

where, f is the frequency in Hz, ε_0 is the permittivity of free space and ε'' is the imaginary part of permittivity.
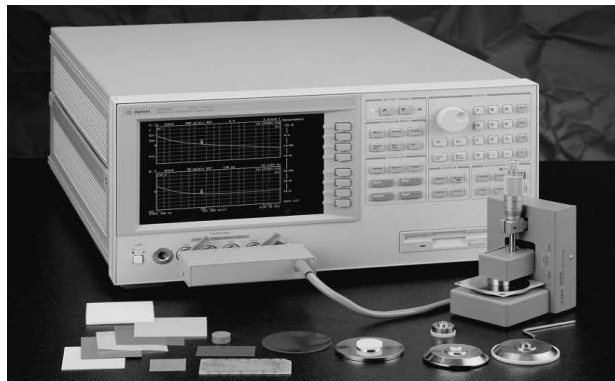
**Fig. 2.2 Precision Impedance Analyser (Agilent 4294A)
with dielectric text fixture (16451B)**

2.3.18 EMI shielding measurements

EMI shielding measurements were performed using a wave-guide coupled to an Agilent Performance Network Analyser E8362 B in the X

band. The test port cables of the network analyser were connected, to wave-guide via coaxial adapters. The network analyser was calibrated in the X band frequency range (8-12) GHz for the through response. The samples used were rectangular slices of dimensions 2.3×1×0.18 cm and was placed between the two sections of the wave-guide for measurement. The set-up is shown in Fig. 2.3. The magnitude of complex scattering parameters that correspond to the reflection (S11 or S22) and transmission (S21 or S12) in the sample were measured and from the measured scattering parameters, the EMI shielding effectiveness was calculated[5,6].

Reflection shielding effectiveness (SE_R) and the absorption shielding effectiveness (SE_A) can be expressed as

$$SE_R = -10 \log(1 - S11^2)$$ .... (2.19)

$$SE_A = -10 \log\left(\frac{S21^2}{1 - S11^2}\right)$$ .... (2.20)

The total shielding effectiveness (SE) is given as

$$SE = SE_R + SE_A$$ .... (2.21)

$$= -10 \log (S21^2)$$ .... (2.22)

Fig. 2.3 Set-up for EMI shielding measurement

References

[1]   Blackley, D.C. Polymer Latices Science and Technology, Chapman and Hall, London, UK. 1997,3,12.

[2]   P.J. Flory, J. Rehner Jr, Statistical Mechanics of Cross-Linked Polymer Networks I. Rubberlike Elasticity, J. Chem. Phys. 11 (1943) 512–520.

[3]   B. Ellis, G.N. Welding, Estimation, from Swelling, of the Structural Contribution of Chemical Reactions to the Vulcanisation of Natural Rubber. Part I, Rubber Chem. Technol. 37 (1964) 563–570.

[4]   C.H.M. Jacques, H.B. Hopfenberg, Vapor and liquid equilibria in glassy polyblends of polystyrene and poly (2, 6-dimethyl-1, 4-phenylene oxide) Part I, Polym. Eng. Sci. 14 (1974) 441–448.

[5]   Bao WL, Yang S, Zhen XY, Ce WN. Enhanced microwave absorption in nickel/hexagonal-ferrite/polymer composites. Appl Phys Lett 2006;89: 132504–6.

[6]   Joseph, N., & Sebastian, M. T. (2013). Electromagnetic interference shielding nature of PVDF-carbonyl iron composites. Materials Letters, 90, 64-67.

.....ജ്ഞ.....

NATURAL RUBBER/MULTIWALLED CARBON NANOTUBE COMPOSITES WITH SEGREGATED NETWORK

Contents	
	Part A *Modification of MWCNTs by Surfactant Treatment*
	Part B *NR/MWCNT Composites with Segregated Structure through Latex Stage Processing*

Vulcastab VL (polyethylene oxide condensate) has been used as a non-ionic surfactant to get stable aqueous dispersions of multiwalled carbon nanotubes (MWCNTs). Sonication time and surfactant concentration were optimised with the aid of UV-visible spectroscopy and Dynamic light scattering technique. Homogeneously dispersed, surfactant coated individual MWCNTs in water were clearly evident from Transmission electron microscopy (TEM). Natural rubber–Multiwalled carbon nanotube (NR-MWCNT) nanocomposites were prepared by latex stage mixing method. Instead of being randomly dispersed, MWCNTs were found to be retained at the boundary of rubber particles. This resulted in a segregated network which was clearly evident from TEM. Addition of very small amount of MWCNT showed remarkable improvement in mechanical, electrical and barrier properties of NR. Segregated network of CNTs resulted in a very low electrical percolation threshold (0.043 vol%) for the composite with enhanced dielectric properties[*].

MODIFICATION OF MWCNTs BY SURFACTANT TREATMENT

3.A.1 Introduction

A great deal of interest has been given to the use of carbon nanotubes (CNTs), in composite materials to harness their exceptional mechanical[1] and electrical properties[2]. The main challenge in processing carbon nanotubes is to exfoliate them into individual entities since they always remain as bundles or ropes due to strong van der Waals force of attraction[3]. Various methods have been used to obtain good dispersion of carbon nanotubes in the polymer matrix. Mechanical and chemical methods are the two commonly used methods. Mechanical method involves ultrasonication and high shear mixing. But there are reports that both can adversely affect the inherent properties of CNTs as they lead to fragmentation of tubes[4]. Chemical methods involve both covalent and non-covalent functionalisation of CNTs[5]. The non-covalent method is preferred over the covalent method since the π system in graphene sheets remains undisturbed and inherent properties of the nanotubes are preserved[6]. In non-covalent approach a number of surfactants have been reported to be useful in getting good aqueous dispersions of nanotubes[7-11].

Sonication is the most commonly used and so far reported technique for exfoliation of CNTs in order to get stable aqueous dispersions of Carbon nanotubes (CNT) by using surfactants. But the sonication procedure has to be controlled in terms of sonication energy, CNT to surfactant ratio etc. Because prolonged sonication process not only results in energy loss but also damages the nanotubes and thereby adversely affect the inherent properties of the nanotubes[12]. Higher surfactant concentration will lead to reduction in electrical properties since it can form an insulating layer around the tubes.

Different methods have been reported so far to evaluate the state of dispersion of CNTs in any solvent or polymer; which includes optical microscopy, AFM, SEM, TEM, cryo-TEM, Raman spectroscopy etc.[13-18]. Particle size analyser based on dynamic light scattering technique is also reported to be useful in characterising MWCNT suspensions[19]. An interesting work has been reported by Junrong et al.[20] in which they report the use of UV-vis spectroscopy to understand the sonication driven dispersion mechanism and factors that optimise its efficiency in SDS surfactant stabilised aqueous dispersion of MWCNT. Present study deals with the use of a non-ionic surfactant VL (polyethylene oxide condensate) in the preparation of aqueous dispersions of multiwalled carbon nanotubes. Dispersion of CNTs using this surfactant has not been studied earlier. This is a novel, environment friendly method since water is used as the only solvent throughout. UV-vis spectroscopy is used as the main tool in optimising the sonication energy and nanotube to surfactant ratio. HRTEM studies have been performed to understand the morphology of separated tubesin the dispersion. The possible mechanism involved in the preparation of stable aqueous dispersion of individually separated carbon nanotubes using VL has been proposed.

3.A.2 Experimental

3.A.2.1 Optimisation of surfactant concentration and sonication time

MWCNT dispersions were prepared by mixing 0.1 g of MWCNT in 100 ml distilled water with varying amounts of VL in order to get the CNT to VL weight ratio of 1:0.5, 1:1 and 1:2. The resulting mixture was sonicated for different times noting the sonication energy. Sonication process was performed with horn sonicator. The output power was fixed at 30 W thus delivering energy of 1700-1800 J/min. The beaker containing dispersion was placed in an ice bath during sonication in order to reduce heat development during sonication.

3.A.2.2 Characterisation

Fourier transform infrared spectra (FTIR) of MWCNT, VL and VL coated MWCNT; and UV-vis absorption spectra of aqueous dispersions of MWCNTs were recorded. Samples were taken regularly during sonication and diluted 100 times with water for UV-vis measurements. The blank used was the original VL solution diluted by the same factor as the samples.

To understand the dispersive power of the surfactant VL at different concentrations, particle size of MWCNT dispersion in water was recorded by dynamic light scattering (DLS) system using Microtrac Nanotrac Wave.

SEM of the pristine MWCNTs and TEM of both MWCNT and MWCNT dispersions were analysed. TEM samples were prepared by placing one drop of the MWCNT aqueous dispersion on the carbon coated copper grid followed by drying. More detailed description of materials and methods is given in Chapter 2.

3.A.3 Results and discussion

Fig. 3.A.1 shows the SEM and TEM images of the MWCNTs used in the present work. The SEM image clearly shows that the nanotubes are highly bundled in nature. High aspect ratio and flexibility of the nanotubes along with strong van der Waals interaction make the nanotubes highly entangled and closely packed[21].
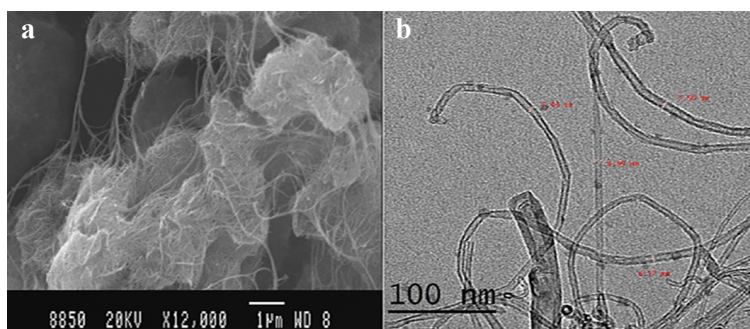
Fig. 3.A.1 (a) SEM and (b) TEM images of the MWCNTs

3.A.3.1 Fourier transform infrared spectroscopy (FTIR)
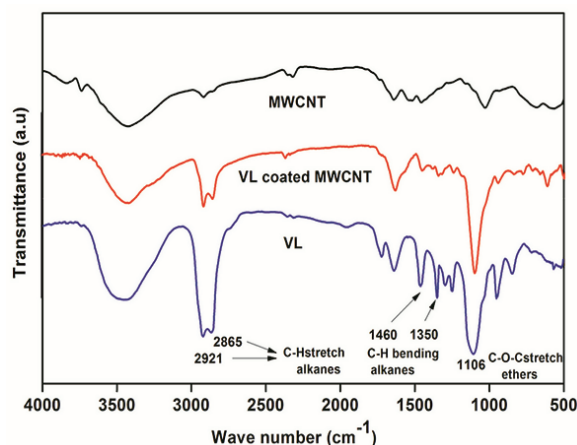
Fig. 3.A.2 FTIR spectra of MWCNT,VL coated MWCNT and VL

FTIR spectrum of MWCNT, VL and VL coated MWCNT is given in Fig. 3.A.2. VL shows intense peaks of C-O-C stretching in ethers (1106 cm^{-1}) and C-H stretching and bending in alkanes (C-H stretch; 2865, 2921cm^{-1} and C-H bend; 1350, 1460 cm^{-1}). The same peaks are observed in the VL coated MWCNT indicating the presence of polyethylene oxide based surfactant coating over the MWCNT.

3.A.3.2 UV-visible spectroscopy

UV-visible spectra have been proved to be an important tool in monitoring the dispersion efficiency of different surfactants in producing stable aqueous dispersions of carbon nanotubes. The nanotube-surfactant ratio and sonication energy can be optimised by using UV-visible spectroscopy [22]. The principle behind the practice is that only individual nanotubes show characteristic absorption bands due to 1D van Hove singularities [23,24]. In bundled CNTs, tunnelling of the carriers between the nanotubes causes quenching of photoluminescence and as a result nanotubes cannot absorb in the UV-vis region[25]. The area under the spectrum or the maximum absorbance can be taken as a measurement of the degree of CNT dispersion.
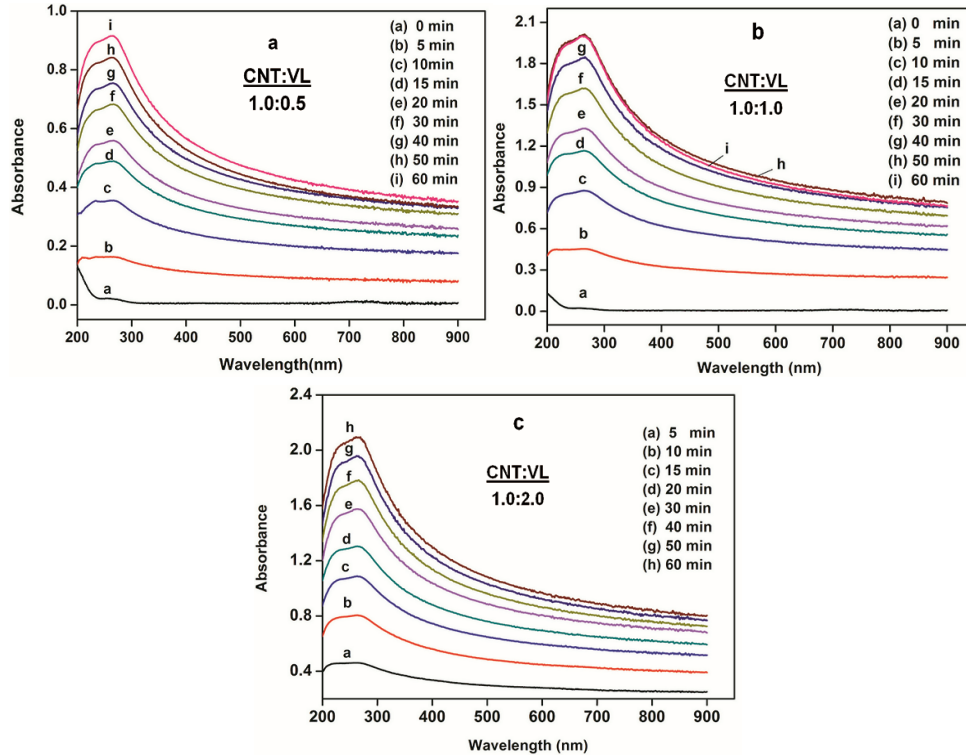
Fig. 3.A.3 (a), (b) and (c) UV-vis spectra of 0.1 wt %MWCNT in aqueous VL solutions of different concentrations at different sonication times

Fig. 3.A.3(a), (b) and (c) shows the UV-vis spectra of 0.1 wt % MWCNT in aqueous VL solutions of different concentrations at different sonication times. Before sonication i.e. at 0 min there is no absorbance peak but as the sonication time increases the absorbance around 260 nm increases. This clearly indicates that nanotubes remain highly bundled in the beginning leading to quenching of photoluminescence with no absorption. On sonication more individual nanotubes are produced in the solution since the high sonication energy helps in breaking the strong van der Waals' force of attraction between the tubes. With increase in sonication time total energy supplied to the solution increases and hence more and more CNTs go into the solution as individual tubes. This enhances absorbance value of the solution. Similar results have been reported earlier[20,26].

Fig. 3.A.4(a) and (b) show the plot of maximum absorbance against total sonication energy supplied for making aqueous dispersions containing 0.1 wt% of MWCNT with varying concentrations of VL. In all cases absorbance increases with sonication energy and reaches a plateau. The plateau corresponds to the maximum achievable degree of dispersion of MWCNTs for the given concentration of VL. As the concentration of VL increases, the plateau value also increase which indicates enhanced degree of dispersion of MWCNTs. Absorbance values are almost the same for the surfactant concentrations of 0.1 and 0.2 wt% (ie. 1:1 and 1:2 CNT to VL weight ratio) with the latter being slightly lower. This clearly indicates that maximum dispersibility of nanotubes has been achieved at 1:1 CNT/VL weight ratio and addition of further surfactant does not alter the dispersibility of MWCNT and may even cause destabilisation of the suspension.
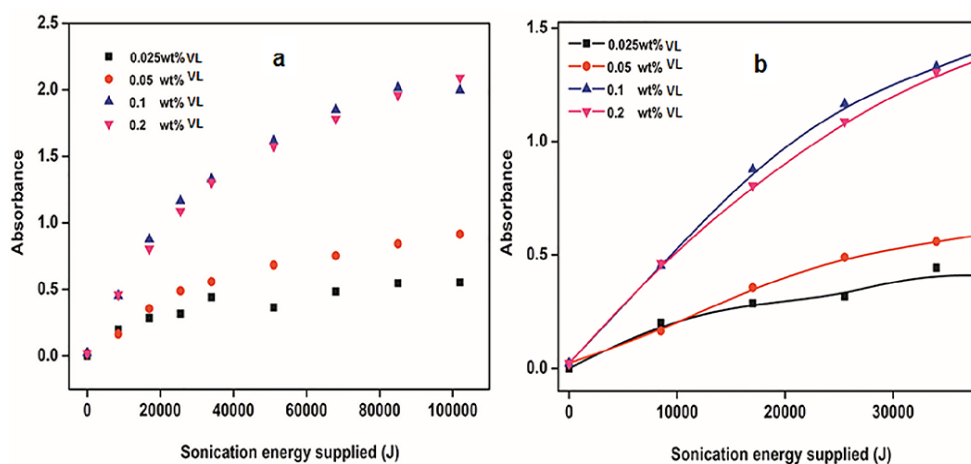
Fig. 3.A.4 **(a) Maximum absorbance as a function of total sonication energy supplied, of 0.1 wt% MWCNTs in aqueous solution for different VL concentrations; (b) zoom-in of the curve at the beginning of the sonication process to show the dispersion rates for different VL concentrations**

3.A.3.3 Particle size analysis by DLS

Efficiency of VL as MWCNT dispersant was confirmed by particle size analyser. Table 3.A.1 shows the number of MWCNT particles (in

percentile) and their corresponding size in aqueous suspension at different VL concentrations after 50 min of sonication. The particles were found to be in micrometre range instead of nanometres. Dynamic light scattering technique is based on the assumption that the particles under measurement are spherical in shape. But nanotubes are rod like particles with diameter in nanometre range while their length falls in micrometre range.

Table 3.A.1 Particle size distribution of MWCNT suspended in water at different concentration of VL after 50 min sonication (equivalent to sonication energy of 85000J)

MWCNT particles (%)	Particle size (μm) for CNT/VL ratio		
	1:0.5	1:1	1:2
10	0.0836	0.0843	0.073
20	0.1051	0.0928	0.099
30	0.1261	0.0998	0.122
40	0.1485	0.1064	0.1431
50	0.1729	0.113	0.1633
60	0.1992	0.1202	0.1844
70	0.2284	0.1288	0.2085
80	0.264	0.1399	0.2407
90	0.318	0.1579	0.2965
95	0.368	0.1757	0.354

So the average size of nanotubes obtained through DLS technique ends up in micrometres. Particle size distribution is broad for 1:0.5 (Fig. 3.A.5a) and 1:2 (Fig. 3.A.5c) CNT/VL dispersions, whereas very narrow size distribution of particles is observed for 1:1 CNT/VL dispersion (Fig. 3.A.5b). Here almost 90 % of the particles are below 0.16 μm in size. A narrow size distribution of MWCNTs had been expected in the case of 1:2 CNT/VL, since higher surfactant concentration should have resulted in more nanotubes being separated from bundles. However the broad peak in Fig. 3.A.5c reveals that the particles are larger and aggregated. This behaviour is in accordance with the results of UV-vis measurements. This may be due to the formation of too large amount of surfactant micelles in the aqueous solution as reported by

J. Yu et al.[20]. The osmotic pressure of micelles around the MWCNT bundles creates an effective attraction, resulting in the depletion-induced aggregation of MWCNTs. This confirms that almost all the nanotubes are evenly coated with VL at 1:1 CNT/VL ratio, eliminatig the possibility of further improvement in dispersibility on increased addition of surfactant.
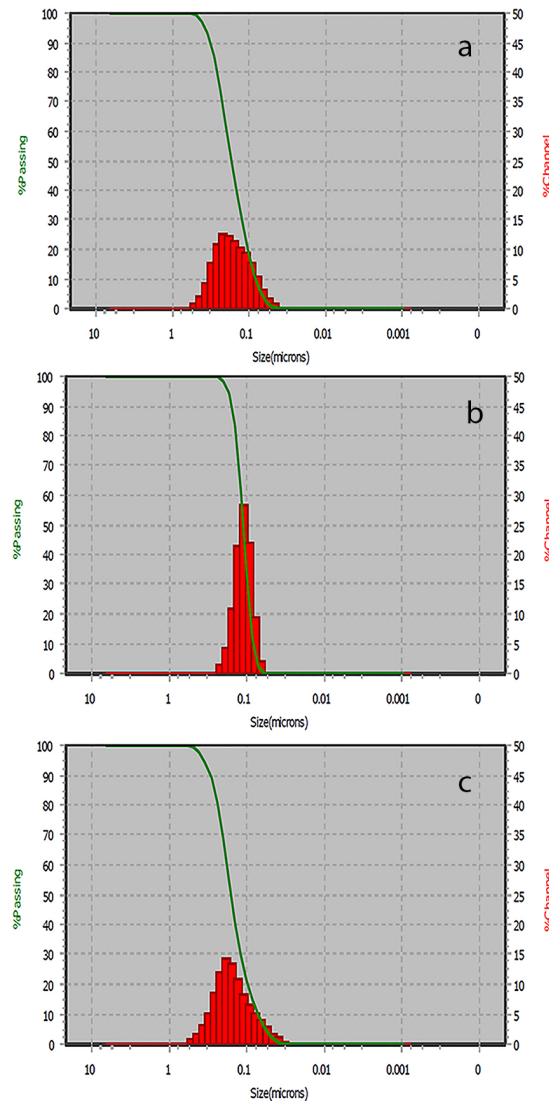
Fig. 3.A.5. Particle size distribution of 0.1 wt % CNT aqueous suspension at different concentrations of VL (a) 0.05 wt% (b) 0.1 wt% and (c) 0.2 wt%

3.A.3.4 Mechanism of VL adsorption on the surface of CNT

The exact mechanism of surfactant assisted dispersion of carbon nanotubes has not yet been clearly understood. Strano et al.[17] have proposed an unzipping mechanism according to which sonication power helps in unzipping the ends of carbon nanotube bundles, allowing the surfactant to be seeped into the bundle and adsorbed on the nanotube surface pushing apart the nanotubes. The process goes on resulting in the separation of surfactant coated individual nanotubes. There are several models proposed for explaining the adsorption of surfactant molecules on the CNT surface. For the ionic surfactants coloumbic attraction is the driving force whereas in the case of non-ionic surfactants adsorption results from strong hydrophobic attraction between the nanotube surface and hydrophobic tail of the surfactant. Surfactant molecules adsorbed on the nanotube surface self-organise to form micelles above a critical micelle concentration (CMC). Different orientations are possible for the surfactants on the nanotube surface viz. cylindrical micelle around the nanotube axis, half-cylinder structures oriented parallel or perpendicular to the tube axis and random physical adsorption on the tube surface without any structural organisation. According to Richard et al.[27] ionic surfactants like sodium dodecyl sulphate (SDS) and octadecyltrimethylammonium bromide (OTAB), exhibit different structural organisations on the CNT surface whereas non-ionic surfactants get randomly adsorbed over the entire tube surface leading to a full coating of the tube without any organization.

In the case of ionic surfactants coloumbic repulsion between the likely charged head groups stabilise the dispersion whereas in the case of non-ionic surfactants steric repulsion between hydrophilic parts help in debundling of tubes and gives stabilisation of the CNT dispersion. VL used in the present study has a hydrophobic hydrocarbon tail that adsorbs to the nanotube surface and a long hydrophilic polyethylene oxide head part that interacts with water

and offers the advantage of enhanced steric stabilisation as suggested by Moore et al.[14]. The unzipping mechanism possible in the present case is depicted in Fig. (3.A.6a-c). The proposed model of VL adsorption in this study is given in Fig 3.A.6d. VL, being a non-ionic surfactant forms a coating over the entire tube by random adsorption without any orientation. Hydrocarbon tail groups are attached onto the CNT surface and poly ethylene oxide head portion is extended towards the aqueous environment.
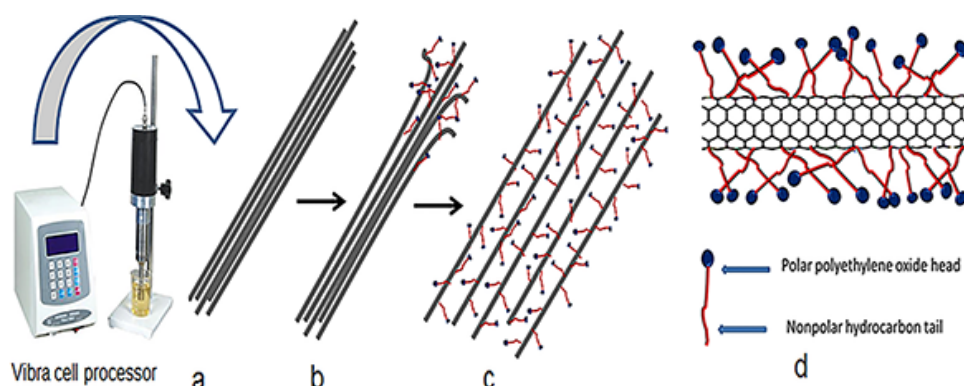
Fig. 3.A.6 **Mechanism of debundling of nanotubes using surfactants with the aid of sonication (a) ultrasonication separates the nanotube ends from bundles (b) surfactant adsorbs on to the nanotube ends and the process continues in an "unzipping" fashion, (c) individual nanotubes coated with surfactant (d) proposed model of VL adsorption on the surface of CNT**

3.A.3.5 High resolution transmission electron microscopy (HRTEM)

Fig. 3.A.7 shows the TEM images of MWCNT dispersions (MWCNT to VL weight ratio 1:1). Fig. 3.A.7a shows the TEM image of MWCNT dispersion after 10 min of sonication (17000J) and Fig. 3.A.7(b-d) show the images after 50 min (85000J) of sonication. From the highly bundled state of MWCNTs in Fig. 3.A.7a it can be inferred that the sonication energy supplied for 10 min (17000J) is insufficient for the exfoliation of the nanotube bundles. This is in agreement with the low absorbance peak value observed in UV-vis studies as given in Fig. 3.A.4. TEM images of dispersion

after 50 min of sonication show individual tubes separated from bundles with a thin uniform layer of surfactant coating over the surface. This indicates that the total energy supplied to the dispersion medium by 50 min of sonication (85000J) is sufficient to exfoliate the highly aggregated and bundled MWCNTs into individual tubes. This is again supported by the absorbance plateau in the corresponding UV-vis spectrum (Fig. 3.A.4).
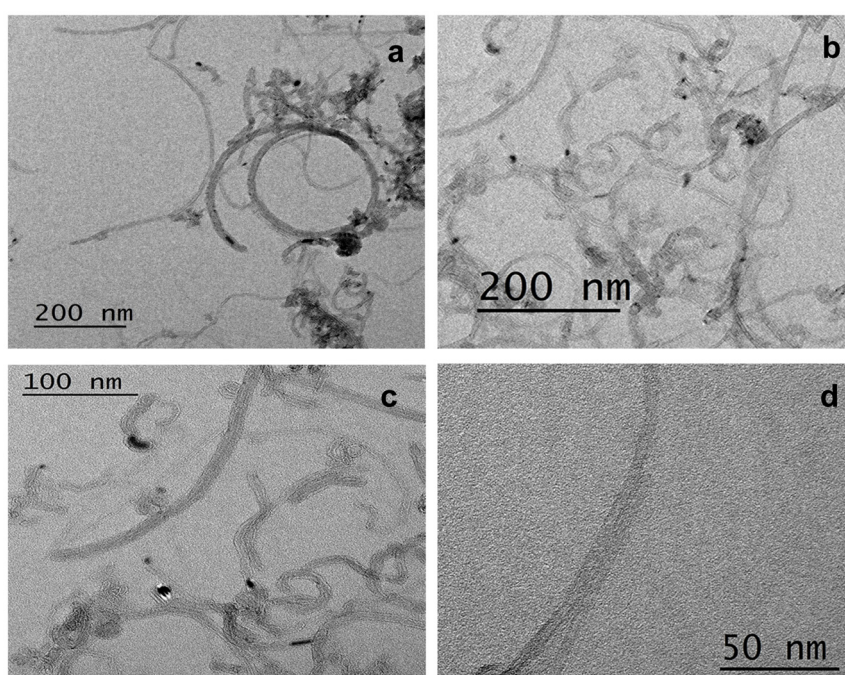
Fig. 3.A.7 TEM images of VL-coated MWCNT (a) after 10 min sonication showing bundled nanotubes (b), (c) and (d) after 50 min sonication at different magnifications. The weight ratio of VL to MWCNTs in the solution was 1:1

3.A.3.6 Stability of aqueous dispersions of VL coated MWCNTs

The aqueous suspensions of nanotubes with 0.1 and 0.2 wt% VL did not phase separate macroscopically after several weeks, indicating its stability. Fig. 3.A.8 shows darkening of the MWCNT dispersions with 0.1% VL on increasing sonication energy. As the sonication proceeds, more and

more nanotubes get separated from bundles and dispersed in water. Fig. 3.A.9 shows the photographs of CNT films formed after evaporating aqueous suspensions of nanotubes sonicated for 50 min with different concentrations of VL. Fig. 3.A.9a and 3.A.9c shows rough textures indicating the presence of coarse particles or nanotube bundles whereas in Fig. 3.A.9b a smooth pattern is visible for the CNT film. At lower surfactant concentration van der Waals' forces resist exfoliation of tubes during sonication and the tubes remainin in an aggregated/bundled state. At higher concentration, surfactant micelles cannot fit in between two bundles that are close to each other and osmotic pressure of the micelles around bundles creates an effective attraction known as depletion attraction[28]. This leads to the formation of small clusters along with dispersed nanotubes. There is an intermediate VL concentration at which the steric repulsion between the adsorbed surfactants balances the van der Waals' attraction between the tubes and stabilises the dispersion. At this optimum concentration of the surfactant, MWCNTs get homogeneously dispersed and form a single phase. In the present study the optimum concentration is found to be 0.1 wt% VL for 0.1wt % of MWCNT in aqueous media, ie a 1:1 ratio of CNT to VL.
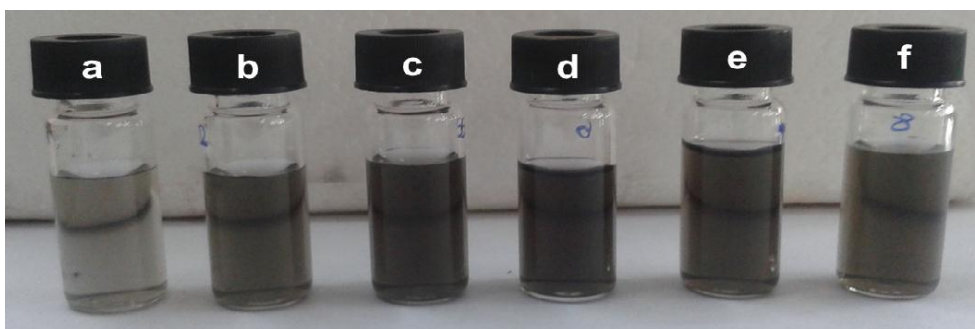
Fig. 3.A.8 Evolution of the colour of the 0.1 wt% MWCNT solutions as a function of the sonication energy/time of sonication: Sample (a) after 10min of sonication, which corresponds to energy input of about 17000 J; (b) 20 min; (c) 30 min; (d) 40 min; (e) 50 min; (f) 60min. (all samples are 100 times diluted)

Fig. 3.A.9 Photographs of MWCNT film formed after drying the aqueous suspensions having MWCNT and VL in different ratios (a) 1: 0.5 (b) 1:1 (c) 1:2

3.A.4 Conclusions

Non-ionic surfactant, vulcastab VL (VL) has been successfully used as a dispersant of MWCNT in water. Concentration of VL and sonication energy required for stable nanotube dispersion have been optimised by UV-vis spectral studies and particle size analysis based on dynamic light scattering. CNT to VL ratio was optimised to be 1:1 for getting stable aqueous dispersions of MWCNTs. At this concentration steric repulsion between the adsorbed surfactants balances the van der Waals' attraction between the tubes and stabilises the dispersion. Minimum sonication energy required was 85000 J. Morphological studies using TEM confirmed the formation of surfactant wrapped exfoliated MWCNTs. VL, which is chemically poly ethylene oxide condensate are expected to get adsorbed on the MWCNTs with their hydrocarbon tail attached to the nanotube surface and polyethylene oxide part extended towards the aqueous environment. The aqueous dispersions of MWCNTs obtained were found to be stable without any phase separation even after several weeks. Aqueous dispersion of MWCNTs can be mixed with water based latex systems which will ensure uniform dispersion of nanotubes in the composite resulting in enhanced properties.

References

[1] Treacy, M. J., Ebbesen, T. W., & Gibson, J. M. (1996). Exceptionally high Young's modulus observed for individual carbon nanotubes. *Nature*, *381*(6584), 678.

[2] Wilder, J. W., Venema, L. C., Rinzler, A. G., Smalley, R. E., & Dekker, C. (1998). Electronic structure of atomically resolved carbon nanotubes. *Nature*, *391*(6662), 59-62.

[3] Girifalco, L. A., Hodak, M., & Lee, R. S. (2000). Carbon nanotubes, buckyballs, ropes, and a universal graphitic potential. *Physical Review B*, *62*(19), 13104.

[4] Lu, K. L., Lago, R. M., Chen, Y. K., Green, M. L. H., Harris, P. J. F., & Tsang, S. C. (1996). Mechanical damage of carbon nanotubes by ultrasound. *Carbon*, *34*(6), 814-816.

[5] Bose, S., Khare, R. A., & Moldenaers, P. (2010). Assessing the strengths and weaknesses of various types of pre-treatments of carbon nanotubes on the properties of polymer/carbon nanotubes composites: A critical review. *Polymer*, *51*(5), 975-993.

[6] Hilding, J., Grulke, E. A., George Zhang, Z., & Lockwood, F. (2003). Dispersion of carbon nanotubes in liquids. *Journal of dispersion science and technology*, *24*(1), 1-41.

[7] Rastogi, R., Kaushal, R., Tripathi, S. K., Sharma, A. L., Kaur, I., & Bharadwaj, L. M. (2008). Comparative study of carbon nanotube dispersion using surfactants. *Journal of colloid and interface science*, *328*(2), 421-428.

[8] Vigolo, B., Penicaud, A., Coulon, C., Sauder, C., Pailler, R., Journet, C., ... & Poulin, P. (2000). Macroscopic fibers and ribbons of oriented carbon nanotubes. *Science*, *290*(5495), 1331-1334.

[9] Tkalya, E. E., Ghislandi, M., de With, G., & Koning, C. E. (2012). The use of surfactants for dispersing carbon nanotubes and graphene to make conductive nanocomposites. *Current Opinion in Colloid & Interface Science*, *17*(4), 225-232.

[10] Ponnamma, D., Sung, S. H., Hong, J. S., Ahn, K. H., Varughese, K. T., & Thomas, S. (2014). Influence of non-covalent functionalisation of carbon nanotubes on the rheological behavior of natural rubber latex nanocomposites. *European Polymer Journal*, *53*, 147-159.

[11] Vaisman, L., Wagner, H. D., & Marom, G. (2006). The role of surfactants in dispersion of carbon nanotubes. *Advances in colloid and interface science*, *128*, 37-46.

[12] Vichchulada, P., Cauble, M. A., Abdi, E. A., Obi, E. I., Zhang, Q., & Lay, M. D. (2010). Sonication power for length control of single-walled carbon nanotubes in aqueous suspensions used for 2-dimensional network formation. *The Journal of Physical Chemistry C*, *114*(29), 12490-12495.

[13] Islam, M. F., Rojas, E., Bergey, D. M., Johnson, A. T., & Yodh, A. G. (2003). High weight fraction surfactant solubilization of single-wall carbon nanotubes in water. *Nano letters*, *3*(2), 269-273.

[14] Moore, V. C., Strano, M. S., Haroz, E. H., Hauge, R. H., Smalley, R. E., Schmidt, J., & Talmon, Y. (2003). Individually suspended single-walled carbon nanotubes in various surfactants. *Nano letters*, *3*(10), 1379-1382.

[15] Kedem, S., Schmidt, J., Paz, Y., & Cohen, Y. (2005). Composite polymer nanofibers with carbon nanotubes and titanium dioxide particles. *Langmuir*, *21*(12), 5600-5604.

[16] Dror, Y., Pyckhout-Hintzen, W., & Cohen, Y. (2005). Conformation of polymers dispersing single-walled carbon nanotubes in water: a small-angle neutron scattering study. *Macromolecules*, *38*(18), 7828-7836.

[17] Strano, M. S., Moore, V. C., Miller, M. K., Allen, M. J., Haroz, E. H., Kittrell, C., ... & Smalley, R. E. (2003). The role of surfactant adsorption during ultrasonication in the dispersion of single-walled carbon nanotubes. *Journal of Nanoscience and Nanotechnology*, *3*(1-1), 81-86.

[18] Shen, K., Curran, S., Xu, H., Rogelj, S., Jiang, Y., Dewald, J., & Pietrass, T. (2005). Single-walled carbon nanotube purification, pelletization, and surfactant -assisted dispersion: a combined TEM and resonant micro-Raman spectroscopy study. *The Journal of Physical Chemistry B*, *109*(10), 4455-4463.

[19] Vaisman, L., Marom, G., & Wagner, H. D. (2006). Dispersions of surface-modified carbon nanotubes in water-soluble and water-insoluble polymers. *Advanced Functional Materials*, *16*(3), 357-363.

[20] Yu, J., Grossiord, N., Koning, C. E., & Loos, J. (2007). Controlling the dispersion of multi-wall carbon nanotubes in aqueous surfactant solution. *Carbon*, *45*(3), 618-623.

[21] Thess, A., Lee, R., Nikolaev, P., Dai, H., Petit, P., Robert, J., ... & Colbert, D. T. (1996). Crystalline ropes of metallic carbon nanotubes. *Science*, 483-487.

[22] Grossiord, N., Regev, O., Loos, J., Meuldijk, J., & Koning, C. E. (2005). Time-dependent study of the exfoliation process of carbon nanotubes in aqueous dispersions by using UV− visible spectroscopy. *Analytical chemistry*, *77*(16), 5135-5139.

[23] Kataura, H., Kumazawa, Y., Maniwa, Y., Umezu, I., Suzuki, S., Ohtsuka, Y., & Achiba, Y. (1999). Optical properties of single-wall carbon nanotubes. *Synthetic metals*, *103*(1-3), 2555-2558.

[24] Saito, R., Fujita, M., Dresselhaus, G., & Dresselhaus, U. M. (1992). Electronic structure of chiral graphene tubules. *Applied physics letters*, *60*(18), 2204-2206.

[25] Lauret, J. S., Voisin, C., Cassabois, G., Delalande, C., Roussignol, P., Jost, O., & Capes, L. (2003). Ultrafast carrier dynamics in single-wall carbon nanotubes. *Physical review letters*, *90*(5), 057404.

[26] Jiang, L., Gao, L., & Sun, J. (2003). Production of aqueous colloidal dispersions of carbon nanotubes. *Journal of Colloid and Interface Science*, *260*(1), 89-94.

[27] Richard, C., Balavoine, F., Schultz, P., Ebbesen, T. W., & Mioskowski, C. (2003). Supramolecular self-assembly of lipid derivatives on carbon nanotubes. *Science*, *300*(5620), 775-778.

[28] Bonard, J. M., Stora, T., Salvetat, J. P., Maier, F., Stöckli, T., Duschl, C., ... & Châtelain, A. (1997). Purification and size-selection of carbon nanotubes. *Advanced Materials*, *9*(10), 827-831.

NR/MWCNT COMPOSITES WITH SEGREGATED STRUCTURE THROUGH LATEX STAGE PROCESSING

3.B.1 Introduction

Electrically conductive polymer composites (CPCs) have attracted immense interest among researchers due to their wide range of applications as antistatic materials, electromagnetic interference (EMI) shields, sensors and conductors[1-3]. Conventional CPCs have conductive fillers randomly dispersed in the polymer matrix resulting in high electrical percolation threshold 'ϕ_c'. For achieving a low 'ϕ_c' in CPCs one promising method is to form a segregated structure in the CPC material. Segregated CPC(s-CPC) materials contain conductive fillers located at the interfaces of the polymeric particles instead of being randomly dispersed in the polymer matrix[4,5]. Segregated network of conductive fillers (especially of high aspect ratio) results in composites with ultralow ϕ_c[6-8].

Latex technology is one of the fabrication method employed in the preparation of s-CPCs in which conductive fillers dispersed in the polymer latex emulsion gets retained within the interstitial spaces of the latex particles on drying[4]. Along with the advantage in processing, homogeneity and uniformity of filler dispersion plays an important role in getting superior mechanical and electrical properties. A great deal of interest has been given to the use of carbon nanotubes (CNTs), in composite materials to harness their exceptional mechanical[9] and electrical properties[10]. They are being actively investigated for their uses as reinforcing components to deliver outstanding properties to the polymeric matrices[11-13] and many research works are going on in the field of Carbon nanotube-Rubber composites[14-19]. Most of the studies reveal the difficulty in obtaining a homogeneous dispersion of carbon nanotubes in the polymer matrix on account of their tendency to bundle together due to strong van der Waals force of attraction.

Efforts are made to reinforce rubber with carbon nanotubes by conventional mill mixing method and were found to be ineffective. The main reason they have reported is the severe agglomeration of carbon nanotubes in the rubber matrix[20,21]. But the reports on surfactant assisted dispersion of carbon nanotubes in water reveal the possibility of getting good aqueous dispersions of carbon nanotubes[22-25]. These aqueous dispersions can be used for the preparation for natural rubber–carbon nanotube composites through latex compounding. Latex stage incorporation of MWCNTs could be expected to result in better dispersion of the nanofiller in the polymer matrix.

In the present part of the chapter, development of a simple, environmental friendly method for the preparation of the NR-MWCNT composite with segregated network of MWCNTs is reported. Optimum concentration of the surfactant VL (CNT to VL ratio of 1:1 as obtained from previous study) was used for the preparation of aqueous dispersions of MWCNTs. To ensure segregated network formation of nanotubes which is beneficial in getting low percolation threshold, latex stage mixing of the nanotube dispersion was adopted in the preparation of natural rubber–MWCNT composites. This is a novel, environment friendly method since water is used as the only solvent throughout. HRTEM studies have been performed to confirm the formation of MWCNT network in the composite film. Mechanical properties, fracture surface morphology and electrical conductivity measurements were done and electrical percolation threshold and critical exponent were determined using linear power law equation. A detailed study on the dielectric properties and AC conductivity of the composites was carried out to understand the influence of the segregated network on these properties. Effect of segregated structure on the solvent swelling behaviour and thermal properties of the elastomer were studied and the relationship between microstructure of the composites and their properties were discussed.

3.B.2 Experimental

3.B.2.1 Preparation of NR-MWCNT composites

The aqueous dispersions of MWCNTs were prepared by adding optimum concentration of VL (1:1 CNT/VL weight ratio) followed by sonication for optimum time (50 min at 30 W). These dispersions were mixed with the NR latex so as to get MWCNT concentrations ranging from 0 - 5.0 phr in NR. The mix was compounded as per formulation given in Table 3.B.1 and sonicated again for 30 minutes using a bath sonicator to achieve uniformity. The samples were kept overnight for maturation and then cast onto flat glass trays. They were dried at 50 °C for 24 h and then cured at 100 ºC for 30 min in an air oven.

Table 3.B.1 Formulation of NR-MWCNT composites

Ingredients	Amount (g)
Centrifuged NR latex (60 % DRC)	167.0
MWCNT	0, 0.05, 0.1, 0.3, 0.5, 1.0, 3.0, 5.0
10 % KOH solution	1.0
10 % Potassium oleate solution	1.0
20 % Vulcastab VL	1.0
50 % ZnO dispersion	1.0
50 % ZDC dispersion	2.0
50 % Sulphur dispersion	3.0

3.B.2.2 Characterisation

SEM and TEM analysis of NR–MWCNT composites were performed to understand the microstructure. The tensile and tear strength was determined using UTM. The strain-amplitude dependent dynamic mechanical properties of the vulcanisates were measured using DMA. Sorption behavior and cross-link density values of the samples were determined by equilibrium swelling method using toluene as the solvent. Thermogravimetric analysis (TGA) was done using a TGA-Q 50 Thermal Analyser. DC electrical conductivity measurements

were carried out using a Keithley 2400 source-measure unit. Dielectric and AC conductivity studies of the samples were conducted using Precision Impedance Analyser. EMI shielding measurements were performed using a wave-guide coupled to an Agilent Performance Network Analyser in the X band frequency range (8-12) GHz.

Detailed description of the characterisation methods is given in Chapter 2.

3.B.3 Results and discussion

3.B.3.1 Segregated network formation in NR-MWCNT composite

Film formation from rubber latex can be divided into 3 stages (1) water evaporation from the latex resulting in close packing of rubber particles (2) deformation of the rubber spheres induced by interfacial and capillary forces and (3) further coalescence by inter-diffusion of polymer chains of adjacent rubber particles[26,27]. One of the production methods in getting segregated conductive polymer composites (s-CPCs) is latex technology. The schematic representation of the segregated network formation proposed in the present study is given in Fig. 3.B.1.
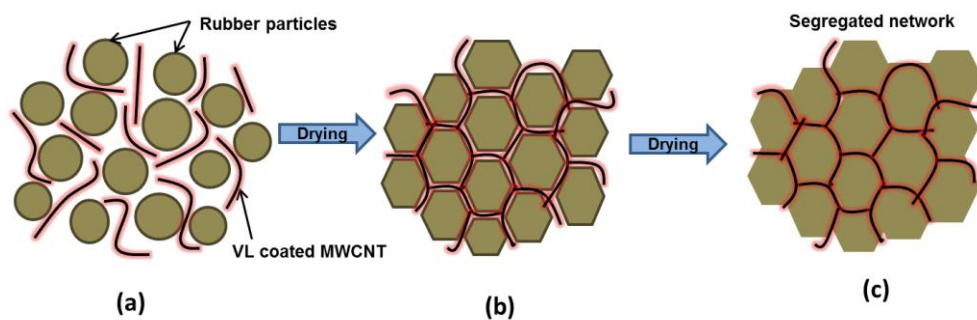
Fig. 3.B.1 Schematic representation of the segregated nanotube network formation in the NR-MWCNT composite preparation (a) Separated nanotubes with VL coating in the aqueous dispersion are uniformly distributed in the compounded NR latex (b) Nanotubes are retained at the boundary of rubber spheres on evaporation of water (c) Segregated network of MWCNT in the continuous rubber phase after curing

Aqueous dispersion of MWCNTs with CNT/VL in the ratio 1:1, mix very well with the compounded NR latex since about 40% of the latex is water. On drying, the VL coated nanotubes are pushed to the periphery of the rubber spheres and retained at the boundaries. High viscosity of the rubber phase prevents the penetration of CNTs inside the rubber. The deformation of latex particles into polyhedra followed by inter-diffusion of rubber chains results in segregated MWCNT network in the continuous rubber phase.

The segregated network of MWCNT throughout the NR phase is evident from the TEM images of the thin composite film formed on the TEM grid (Fig. 3.B.2). The tubes unbundled due to steric stabilisation by VL coating on the surface form a beautiful network throughout the rubber matrix as depicted in the schematic. The network conforms to the shape of a number of polyhedra joined together; the size of which range from 150-450 nm. The findings supports the hypothesis that the nanotube dispersion prepared using an optimum concentration of VL, get mixed uniformly throughout the rubber latex and CNTs wrap the individual rubber spheres during latex film formation forming a beautiful segregated network.
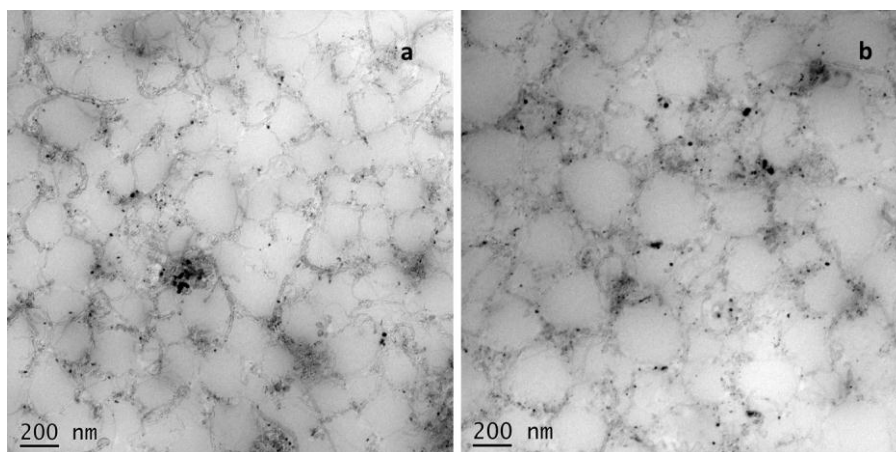
Fig. 3.B.2 TEM images of the NR-MWCNT composite film showing segregated network of MWCNTs in the NR matrix

3.B.3.2 Mechanical properties

Mechanical properties of NR-MCWNT nanocomposites prepared through latex stage mixing are given in Table 3.B.2. It is evident from the results, that incorporation of MWCNTs significantly increases the tensile strength and modulus of natural rubber vulcanisate.

Table 3.B.2 Mechanical properties of NR and NR-MWCNT composites

MWCNT (phr)	Tensile strength(MPa)	Elongation at break (%)	Tensile Modulus at 300 % elongation (MPa)	Tear strength (N/mm)
0	21.0±0.5	1691±10	1.06±0.08	34.8±0.2
0.05	30.0±0.5	1812±61	1.68±0.05	45.6±0.9
0.1	35.2±0.7	1788±43	1.91±0.03	53.9±1.1
0.3	33.7±0.6	1780±58	1.86±0.05	49.6±1.1
0.5	32.2±0.3	1769±78	1.71±0.02	47.6±1.1
1.0	29.6±0.6	1728±63	1.44±0.03	46.9±1.4

The tensile strength of NR has been improved by almost 68 %, tensile modulus (300% elongation) by 80%, and tear strength by 55% on addition of 0.1phr of MWCNT. Beyond the loading of 0.1 phr further improvement in properties does not occur, which may be due to the aggregation of nanotubes in the network structure or may be due to the influence of surfactant. It has been reported by Aguilar-Bolados et al.[28] that high SDS concentration can adversely affect the strength of NR since SDS at high concentration forms aggregates and promote the formation of defects in the interstices of NR particles. The elongation at break is higher than NR for all the CNT composites indicating plasticizing effect of the added surfactant and strong bridging between the NR polyhedra by interaction with MWCNTs arranged in the interstices which prevents premature failure at the polyhedral interface. Uniform distribution of the individualized nanotubes in the matrix, accomplished through surfactant assisted sonication and their interaction with the rubber matrix account for the superior mechanical properties of CNT composites compared to neat NR. The

MWCNT network formed through the interfaces can bear the applied stress resulting in enhanced mechanical properties.

Stress-strain graph for NR and NR-MWCNT composite is given in Fig. 3.B.3. There is a marginal increase in the onset of strain induced crystallization. The strengthening of interfaces by the uniformly distributed nanotubes and the interior of polyhedra devoid of nanotubes, allow the formation of crystallites inside the NR polyhedra without interference from filler particles, thus improving tensile strength and modulus avoiding premature tearing at the interface.
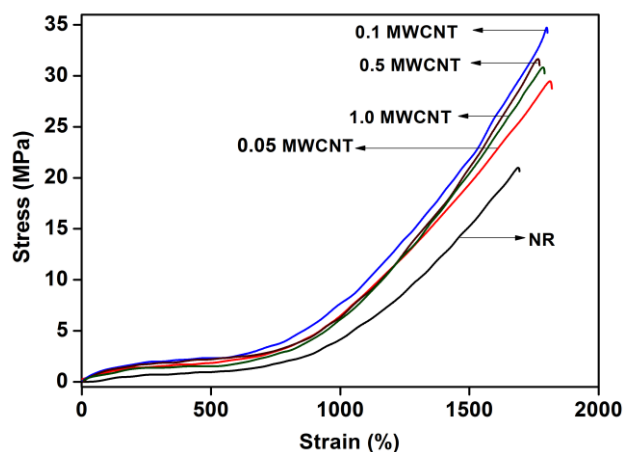
Fig. 3.B.3 Stress-strain graph of NR and NR-MWCNT composites

Reinforcement of NR by the MWCNT in the composite can also be explained in terms of the large aspect ratio and physical entanglement of CNTs with rubber. The nanotube network formed around the rubber particles divides the NR matrix into small units and gives a cellular structure. The cellular structure and occluded rubber (due to the confinement of rubber within the networks) in the NR-MWCNT composite provides tremendous reinforcement.

3.B.3.3 Fracture surface morphology

Morphology of tensile and tear fractured surfaces of NR and NR-MWCNT composites for 0.1 and 0.5 phr of nanotube concentration are given in

Fig.3.B.4. For neat NR, fractured surfaces are smooth whereas rough surfaces are visible in the composite images. Spherical granular shapes with craters and special patterns in the composite fracture surfaces can be due the highly ordered segregated network of nanotubes in the rubber. Gao et al.[29] have reported special fracture patterns for ultrahigh molecular weight polyethylene-MWCNT composite with conductive segregated network. Latex stage mixing adopted in the present study distributes nanotubes at the interfaces of rubber particles resulting in a microstructure having well-ordered segregated network. In tensile fracture surfaces rough texture and special patterns are more pronounced for composites with 0.1 phr of MWCNTs (Fig. 3.B.4b) compared to 0.5 phr composites (Fig. 3.B.4c), conforming to the higher reinforcement experienced in the former case.
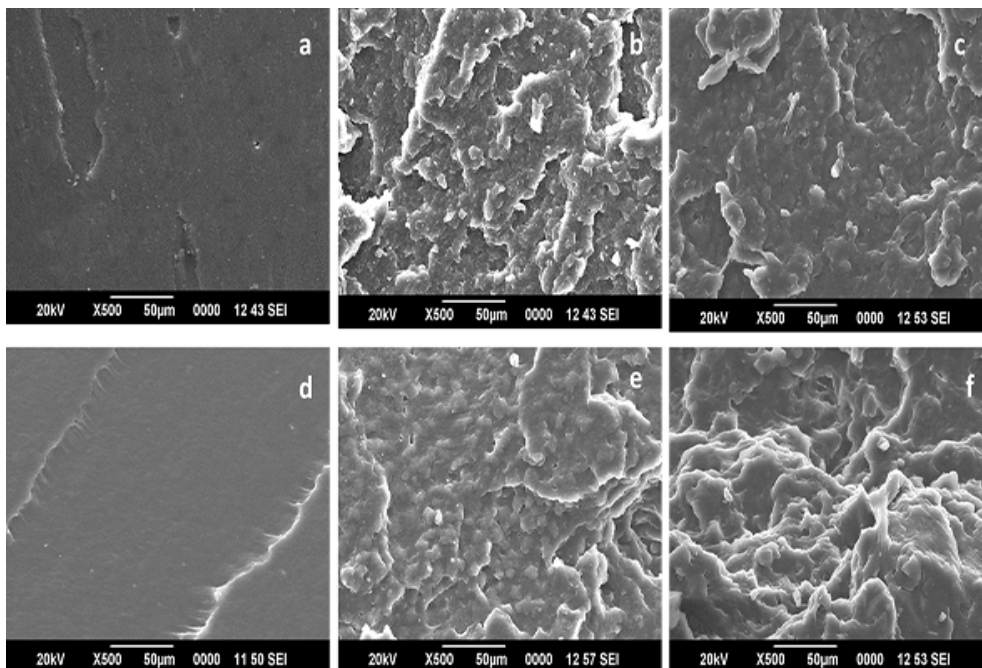
Fig. 3.B.4 SEM micrographs of NR and NR-MWCNT composites: (a-c) Tensile fractured surface of (a) NR (b) NR-0.1 MWCNT (c) NR-0.5 MWCNT; (d-f) Tear fractured surface of (d) NR (e) NR-0.1 MWCNT (f) NR-0.5 MWCNT

3.B.3.4 Strain sweep studies

Strain dependence of storage modulus (E') for NR and NR-MWCNT composites is depicted in Fig. 3.B.5. Dynamic properties are usually independent of strain for neat rubber. Filled rubbers show Payne effect which is dependence of storage modulus on strain amplitude especially at low strains and the most commonly accepted reason is the breakdown of filler-filler networks on increasing strain[30]. From the figure it is clear that Payne effect becomes more pronounced as MWCNT concentration increases with a high E'_0-E'_∞ where E'_0 and E'_∞ are low and high strain moduli respectively. This observation is supported by the non-linear viscoelastic behaviour reported for MWCNT filled chloroprene rubber by Subramaniam et al.[31].
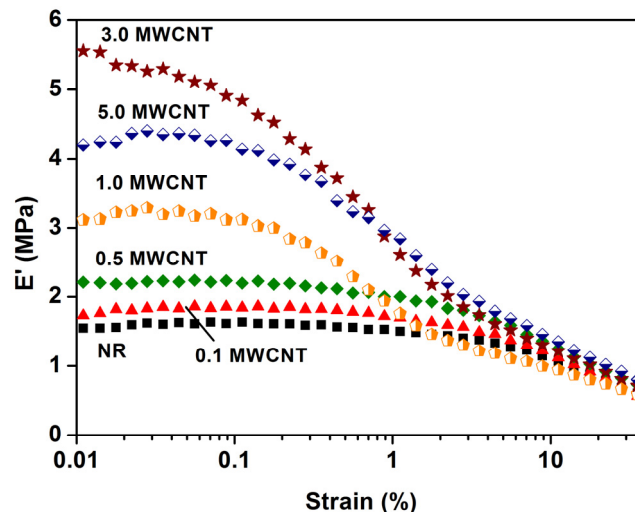
Fig. 3.B.5 Strain dependence of storage modulus for NR and NR-MWCNT composite

They have observed an increase in E'_0 with increase in concentration of nanotubes as well as with addition of ionic liquid that assists in dispersing nanotubes. They have suggested that the stronger Payne effect observed at very low filler loading can be attributed to the enhanced nanotube dispersion caused by the debundling of nanotubes by the ionic liquid and thereby

improved filler-filler network. The same trend is observed here with increasing amount of VL coated MWCNTs. In our study the role of ionic liquid is played by the surfactant VL which effectively disperses the nanotubes and facilitates the formation of network along the periphery of rubber particles even at very low concentration.

3.B.3.5 Swelling studies

Mol% uptake (Qt %) of toluene for NR and NR-MWCNT composites is plotted against square root of time ($\sqrt{t}$) (Fig.3.B.6).
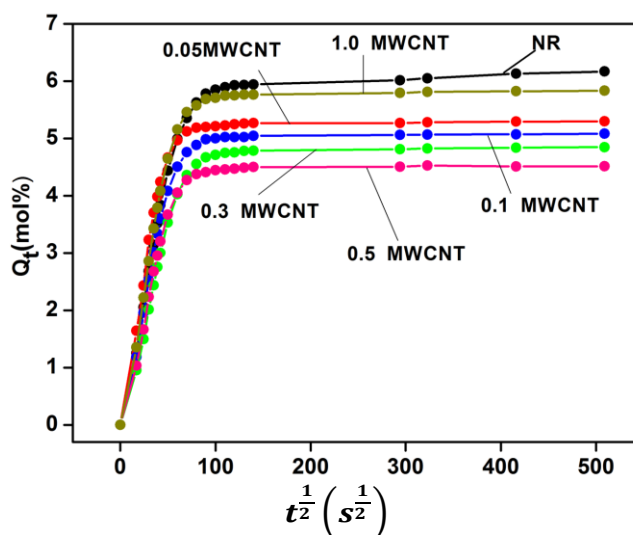
Fig. 3.B.6 Sorption curves of NR and NR-MWCNT composites

Rate of solvent uptake is high initially and reaches a plateau (equilibrium solvent uptake) with time. Equilibrium solvent uptake decreases with addition of MWCNT upto 0.5 phr and increases beyond that concentration. Segregated network of nanotubes play an important role in improving the solvent barrier properties of NR. Rubber particles are wrapped by the nanotubes creating a tortuous path that slow down the solvent penetration through the rubber. As the nanotube concentration increases, the network extends

throughout the rubber matrix and the penetration of solvent molecules is hindered more. Increase in solvent uptake after 0.5 phr of CNT can be due to the aggregation of CNTs in the network. The aggregation can create micro voids in the segregated structure through which solvents can easily penetrate[32,33].

Table 3.B.3 represents variation of crosslink density and swelling index of NR with MWCNT concentration. Crosslink density increases with filler loading, reaches maximum for 0.5 phr MWCNT and decreases beyond that concentration whereas swelling index variation follows an exactly reverse order. Crosslink density can be taken as an index of reinforcement of the rubber by the added filler. Improvement in the crosslink density on adding nanotubes indicates better rubber–nanotube interaction and ensuing reinforcement. Rubber chains are constrained or immobilized on the segregated nanotube network and the penetration of solvent molecules are hindered due to the restricted motion of rubber chains. At high CNT concentration aggregation occurs that lead to porosity in the sample resulting in easy penetration of solvent molecules leading to high swelling index.

Table 3.B.3 Crosslink density and swelling index of NR and NR-MWCNT composites

MWCNT (phr)	Crosslink density (x 10^{-5}mol/g)	Swelling Index (%)
0	3.1	569
0.05	3.9	493
0.1	4.1	494
0.3	4.8	438
0.5	5.1	423
1.0	3.5	514

3.B.3.6 Thermal studies

Fig. 3.B.7 shows the thermograms and Table 3.B.4 shows the TGA data of NR and NR-MWCNT composites.
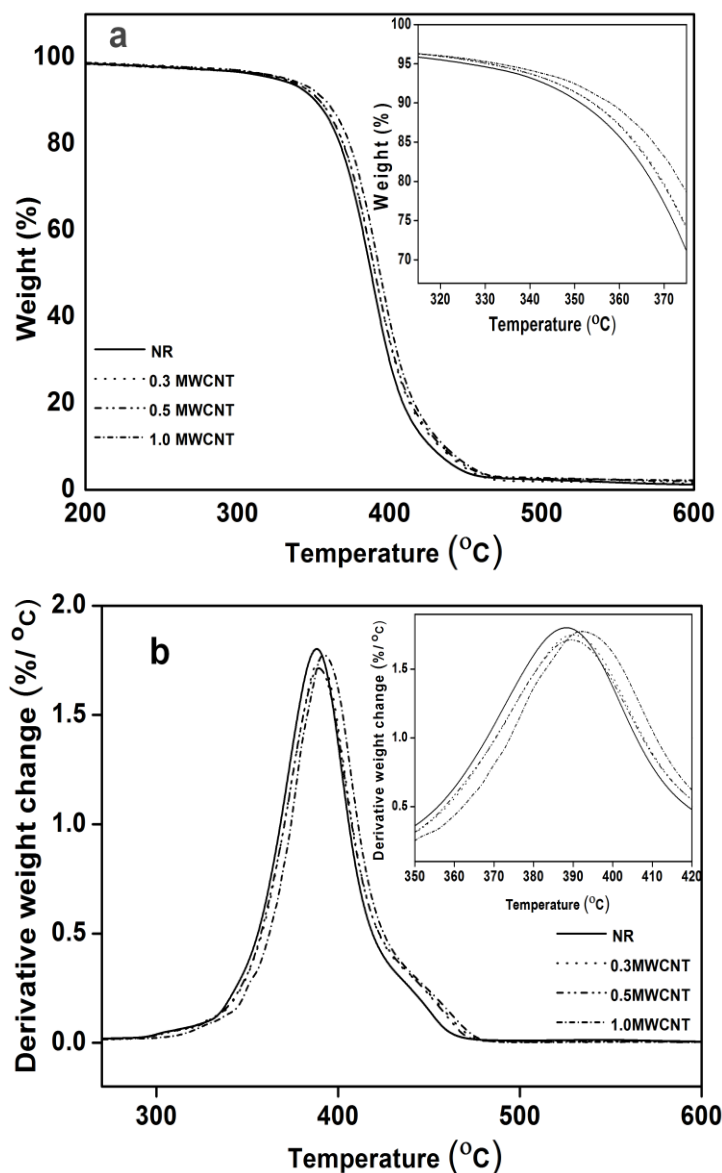
Fig. 3.B.7 (a) TGA and (b) DTG curves of NR and NR-MWCNT nanocomposites

Table 3.B.4 TGA data for NR and NR-MWCNT nanocomposites

Property	NR	NR-0.3MWCNT	NR-0.5MWCNT	NR-1.0MWCNT
Onset degradation temperature (T_0,°C)	316	323	324	329
End set degradation temperature	461	471	471	476
Maximum degradation temperature (T_{max},°C)	388	390	390	392
Temperature at 50% degradation (T_{50},°C)	388	390	390	394
Residue at 600 °C (%)	1.22	1.48	1.98	2.19

There is marginal increase in the onset, endset, maximum degradation temperature and temperature at which 50 % decomposition occurs (T_{50}), with MWCNT concentration. Improved physical and chemical interactions between thermally stable MWCNTs and the polymer, is reported to slow down the thermal degradation of the composites[34]. Apart from this, the formation of segregated network achieved by good dispersion of MWCNTs can act as a barrier to the escape of degradation products from the bulk of the polymer, the efficiency of which depends on the perfection of the network as evidenced by the comparatively higher thermal stability of composites containing 1 phr MWCNTs. High thermal conductivity of the CNTs ($3000 Wm^{-1}K^{-1}$) also play a part in enhancing thermal stability by dissipating heat more quickly from the composites[35,36].

3.B.3.7 DC electrical conductivity

Electrical properties are usually explained in terms of vol% of the fillers rather than phr. For better understanding, the concentration of MWCNT in NR-MWCNT composites in both phr and vol% is given in Table 3.B.5.

Table 3.B.5 Concentration of MWCNT in NR-MWCNT composites

Concentration of MWCNT	
phr	**vol%**
0.05	0.022
0.1	0.043
0.3	0.129
0.5	0.215
1.0	0.430
3.0	1.28
5.0	2.11

Electrical percolation threshold and nature of conductive network present in the system were analysed using classical percolation theory. The power law equation is given by

$$\sigma = \sigma_0 \, (\phi - \phi_c)^t \qquad \dots\dots\dots\dots\dots\dots\dots\dots\dots\dots\dots\dots\dots\dots\dots\dots\dots\dots (3.B.1)$$

Where 'σ' is the conductivity of the composite, σ_0 is the proportionality constant depending on the intrinsic conductivity of the filler, ϕ is the filler volume fraction, ϕ_c is the percolation volume fraction and t is the critical exponent in the conducting region.

Variation of DC electrical conductivity of NR-MWCNT composites is given in Fig. 3.B.8. Straight line plot in the inset shows the least square fitted log-log plot of conductivity versus ϕ-ϕ_c which gives the values of the percolation concentration ϕ_c and the critical exponent, t of the composites. ϕ_c in the present work is 0.043 vol% (0.1 phr) which is lower than previously reported values for composites with segregated structure[4]. The very low percolation threshold obtained points to the efficiency of VL in dispersing MWCNTs individually and the segregated conductive network structure in the composite. Though the critical exponent (t~1.39) in the present system is close to that for a 2D network as per Stauffer et al.[37], TEM images clearly show that rubber spheres are wrapped by thin layer of MWCNTs suggesting a 3D segregated network. Moreover the reported experimental t values vary widely from 0.37 to 6.92 depending on the complexity of the network[4].
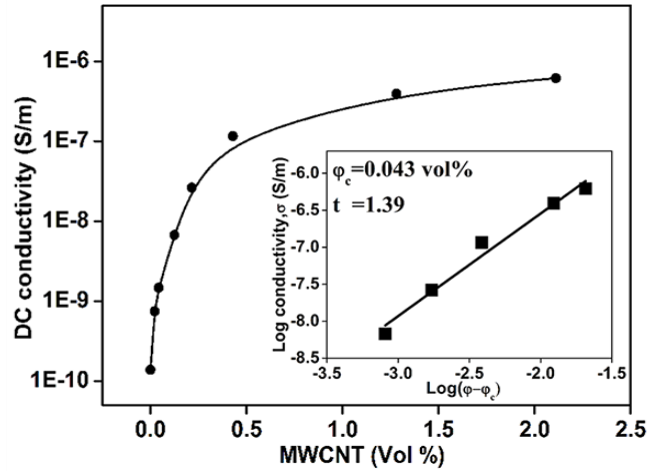
Fig. 3.B.8 Conductivity versus concentration of MWCNT for the NR-MWCNT composite. Inset is the log-log plot of conductivity as a function of φ-φ$_c$ with least square fitting of the experimental data

Systems with segregated structure should possess high electrical conductivity as suggested in the previous reports[38-40]. The lower than expected DC conductivity values in the present study can be credited to the presence of non-ionic VL coating over MWCNTs. Though the amount of VL used was minimum for the efficient dispersion of nanotubes in water, long hydrophilic tails and bulky character of non-ionic surfactant can create large distance between the tubes and can result in lack of contact between the tubes[41]. Aguilar-Bolados et al.[28] cited insufficient dispersion by the non-ionic surfactant as the reason for lower conductivity of thermally reduced graphene oxide/ natural rubber composites compared to composites prepared using ionic surfactant. The results of the study clearly reveal the high efficiency of VL as a good dispersant for MWCNTs. So the only possibility for low conductivity of the NR-MWCNT composites is the presence of an insulating surfactant coating over the nanotube surface. With increase in MWCNT concentration there is increase in the concentration of VL and a corresponding decrease in conductivity. Instead of insulating stabilizers conducting polymer based surfactants such as poly(3,4-ethylenedioxythiophene):poly(styrene sulfonate)

(PEDOT:PSS) have been employed by Hermant and Kim et al. to disperse conductive fillers which can solve the problem and can be used in the preparation of highly conducting composites[42,43].

3.B.3.8 Dielectric studies

Frequency dependency of dielectric permittivity, dielectric loss and AC conductivity of NR-MWCNT nanocomposites with different nanotube concentration measured at room temperature is shown in Fig. 3.B.9(a-c). An exponential decrease in dielectric permittivity is observed with increase in frequency (Fig.3.B.9a). There is increase in dielectric permittivity of NR with MWCNT addition which is more pronounced at low frequencies.
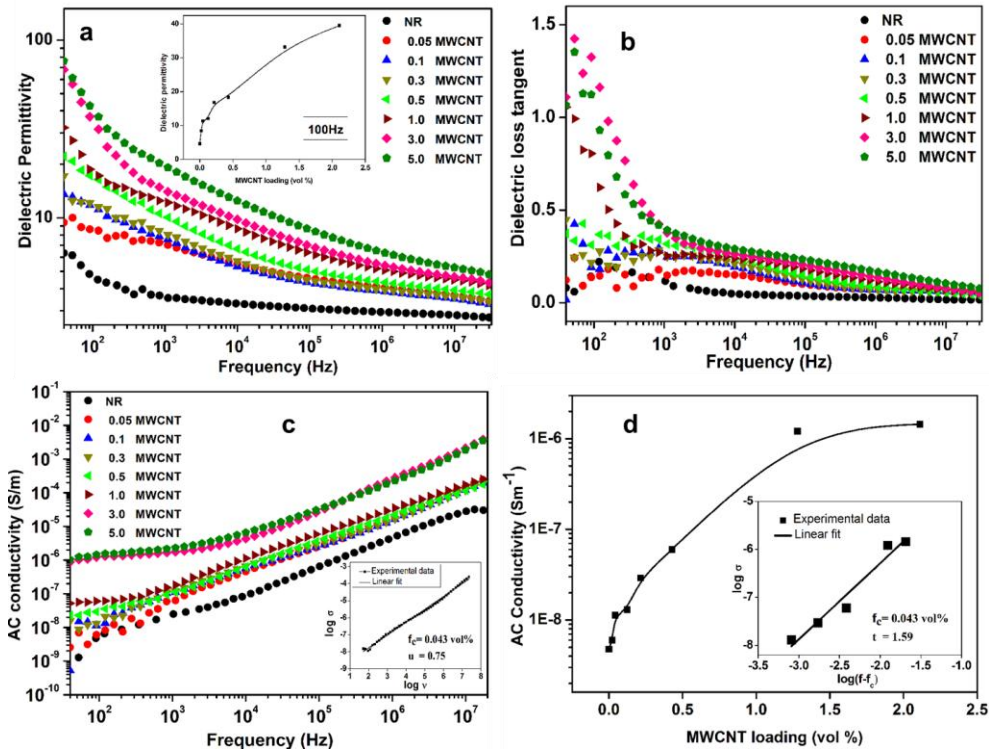
Fig. 3.B.9 Dielectric properties as a function of frequency (a) dielectric constant (b) dielectric loss tangent (c) AC conductivity and (d) effect of MWCNTR on AC conductivity of NR at 1 kHz. Inset of (c) shows the best fit of the ac conductivity of the NRMWCNT composite with 0.043 vol% of MWCNT to Eq. (3.B.3). Inset of (d) shows linear fit of the power law Eq. (3.B.2)

Fig. 3.B.9a inset shows the dielectric permittivity of NR-MWCNT composites as a function of MWCNT vol% measured at room temperature and 100 Hz. Dielectric permittivity at 100 Hz increases from 4.7 for pure NR to 41 for 5phr MWCNT. Improved dielectric properties and frequency dependency of the dielectric constant can be explained in terms of the interfacial polarisation effect or Maxwell-Wagner-Sillars (MWS) polarisation effect[44]. According to this effect the dielectric permittivity improvement in heterogeneous systems is attributed to the accumulation of free charges at the interfaces between conducting fillers and insulating polymer layers. NR-MWCNT composites with segregated structure has a lot of interfaces between the nanotube and rubber particles and as the nanotube concentration increases accumulation of free charges at these interfaces increases leading to an increase in dielectric permittivity. At higher frequencies the interfacial polarisation cannot cope up with the change in electric field and as a result the dielectric permittivity decreases.

Similar to dielectric permittivity, dielectric loss values also decrease with frequency and the frequency dependence becomes notable after the percolation threshold (0.1 phr). Dielectric loss value for the composite with 5 phr MWCNTs is < 1.5. The dielectric loss can be due to three factors: direct current (DC) conductance, interfacial polarization and the usual dipole orientation. There are previous reports suggesting that high DC conductivity can increase dielectric loss by current leakage and thereby decrease the overall dielectric performance of the composite[45]. In the present study NR-MWCNT composites possess low DC conductivity (~10^{-7} Sm^{-1} for 5 phr MWCNT) (Fig. 3.B.8) because the surfactant coating over nanotubes prevents the direct tube-tube contact and prevents the leakage of current. This leads to low dielectric loss of the NR-MWCNT composites.

An opposite effect is observed in the AC conductivity (σ) of the material, in which σ increases with increase in frequency. σ attained a value

of 5.9×10^{-8} S/m at 100 Hz and 1.7×10^{-4} S/m at 10 MHz for 1 phr MWCNT. The conductivity values obtained in the present study which used VL as non-ionic surfactant for dispersing CNT are very close to the values reported by Aguilar-Bolados et al.[28].

Fig. 3.B.9d shows the ac conductivity of NR-MWCNT composites as a function of MWCNT vol%, measured at room temperature and 100 Hz. The conductivity was analysed with the critical MWCNT concentration f_c by the following power law[46].

$$\sigma \,\alpha\, (f - f_c)^t \; for \; f > f_c \quad\text{...(3.B.2)}$$

Where σ is the conductivity of the composite, f is the MWCNT volume fraction, f_c is the percolation threshold, and t is the critical exponent in the conducting region. Inset of Fig. 3.B.9d, gives best linear fit of the conductivity data to the log–log plots of the power law and the calculated percolation threshold is 0.043 vol%. The critical exponent (t =1.59) obtained from the data fitting, is very close to the universal value (t_{un}~1.6-2) suggesting that the high aspect ratio MWCNTs have been efficiently utilised in forming segregated network making the electrical percolation possible at very low concentration of the conductive filler.

When f reaches f_c, the percolation threshold power law can be written as

$$\sigma \,\alpha\, \omega^\mu, \qquad as \; f \to f_c \quad\text{..(3.B.3)}$$

In equation 3.B.3, $\omega = 2\pi\nu$, where ν and μ are the frequency and corresponding critical exponent, respectively. Best linear fit of the log-log plot of equation 3.B.3 using experimental data for f = 0.043 vol% (f_c) give $\mu = 0.75$, which is very close to the normal value ($\mu_{uni} = 0.70$)[44]. Very low percolation threshold ($f_c = 0.043$ vol%) obtained in the present study is indicative of the efficiency of VL in dispersing MWCNTs and also the segregated network structure of the composite. MWCNTs suspended in VL

are distributed uniformly in the rubber matrix and form a percolating segregated network at very low nanotube content and create a lot of interfaces in the matrix and enhance dielectric properties of the NR. The low frequency conductivities are inferior which can be due to the presence of insulating sheath of VL around the nanotubes. The primary transport mechanism in CNT/polymer composites is tunneling conduction. After the surfaces of MWCNTs get coated with VL, the tunneling current between the MWCNTs might become smaller than that between the pristine MWCNTs thereby lowering conductivity of the composites[47].

3.B.3.9 EMI shielding effectiveness

Carbon based composites are light weight and their flexibility and easy processability make them attractive compared to conventional metal based EMI shielding materials[48,49]. Among carbon based conducting fillers CNTs are noted for their light weight, high aspect ratio, conductivity and excellent mechanical strength and have attracted interest among researchers for making high performance EMI shielding materials.

EMI shielding effectiveness (SE) of the NR-MWCNT composites in the frequency range 8-12 GHz is shown in Fig.3.B.10. SE of neat NR is very poor which is due to the electrically insulating nature of NR. SE increases with increase in concentration of MWCNT in the composites.

The s-CPC has a "special foam structure" with dense conductive filler layers that act as highly conductive "struts" and polymer domain that act as "microcells", forming numerous interactive interfaces[50]. The incident electromagnetic microwaves that enter the s-CPCs are attenuated by reflecting and scattering many times between these "strut-cell" interfaces and conductive filler surfaces, hindering the escape of the waves from the s-CPC material before being dissipated as heat; therefore, s-CPCs have great potential as high performance EMI shielding materials. The results of EMI shielding for NR-

MWCNT composites show that, the concept of "struts" mentioned can be attained at very low concentration in the case of graphene sheets leading to high SE, but the same may need high concentration of MWCNTs.
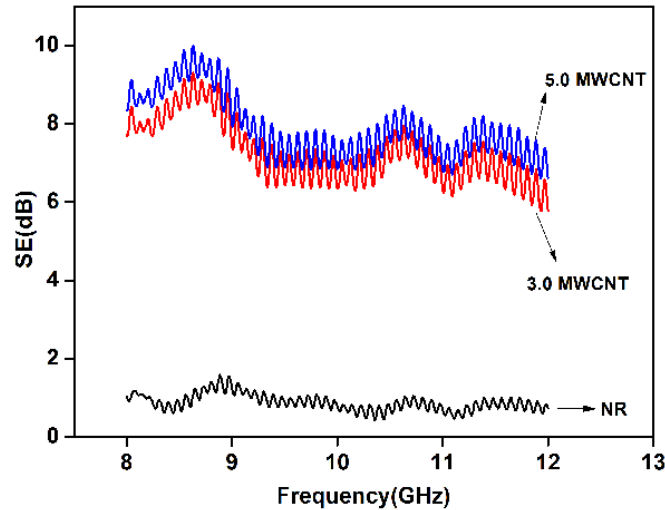
Fig. 3.B.10 Variation of SE with frequency of NR-MWCNT composites

For 3 phr MWCNT loading, SE is above 6 dB. SE increases with further addition of MWCNT and reaches a maximum SE of 10 dB at 8.6 GHz for 5phr MWCNT. Though practical applications require minimum acceptable SE of 20dB, composites with low SE can be used for dissipation of static charges[51,52]. It is also noted from the figure that SE of the NR-MWCNT composites decreases with increase in frequency.

SE of a conductive polymer composite depends on factors like conductivity, resistance loss and interfacial polarisation loss. The NR-MWCNT composites exhibit frequency dependent dielectric behaviour which has been discussed in the previous section. With increase in nanotube content in NR there is increase in the interfacial polarisation due to the accumulation of more and more charge carriers at the interfaces in the segregated structure. Strong interfacial polarisation results in large loss leading to high shielding

efficiency[53]. Interfacial polarisation decreases with increase in frequency and this explains the decrease in SE observed at high frequency.

3.B.4 Conclusions

NR-MWCNT composites prepared by the latex stage mixing of the surfactant treated nanotube dispersions showed a segregated network of nanotubes throughout the rubber matrix as evident from TEM images. The composites exhibited very good mechanical properties with 68% increase in tensile strength, 80% increase in tensile modulus and 55% increase in tear strength at 0.1phr MWCNT loading. Fracture surface morphology and strain sweep studies supported the presence of segregated network in the composite. Network of MWCNTs around the rubber particles created tortuous path and slowed down the solvent penetration through the rubber. Thermogravimetric analysis showed that thermal stability of NR was unaffected by the addition of MWCNTs. Very low percolation threshold of 0.043 vol% obtained from electrical conductivity studies revealed the segregated network structure. High dielectric permittivity and low DC conductivity of the nanocomposites were found to be suitable for making low loss materials. The low DC conductivity observed for the NR/MWCNT composites can be attributed to the presence of insulating sheath of VL around the nanotubes.

References

[1] Ma, P. C., Siddiqui, N. A., Marom, G., & Kim, J. K. (2010). Dispersion and functionalisation of carbon nanotubes for polymer-based nanocomposites: a review. *Composites Part A: Applied Science and Manufacturing*, *41*(10), 1345-1367.

[2] Dang, Z. M., Yuan, J. K., Zha, J. W., Zhou, T., Li, S. T., & Hu, G. H. (2012). Fundamentals, processes and applications of high-permittivity polymer–matrix composites. *Progress in Materials Science*, *57*(4), 660-723.

[3] Villmow, T., Pegel, S., John, A., Rentenberger, R., & Pötschke, P. (2011). Liquid sensing: smart polymer/CNT composites. *Materials Today*, *14*(7), 340-345.

[4]   Pang, H., Xu, L., Yan, D. X., & Li, Z. M. (2014). Conductive polymer composites with segregated structures. *Progress in Polymer Science*, *39*(11), 1908-1933.

[5]   Deng, H., Lin, L., Ji, M., Zhang, S., Yang, M., & Fu, Q. (2014). Progress on the morphological control of conductive network in conductive polymer composites and the use as electroactive multifunctional materials. *Progress in Polymer Science*, *39*(4), 627-655.

[6]   Grunlan, J. C., Mehrabi, A. R., Bannon, M. V., & Bahr, J. L. (2004). Water-Based Single-Walled-Nanotube-Filled Polymer Composite with an Exceptionally Low Percolation Threshold. *Advanced Materials*, *16*(2), 150-153.

[7]   Long, G., Tang, C., Wong, K. W., Man, C., Fan, M., Lau, W. M., ... & Wang, B. (2013). Resolving the dilemma of gaining conductivity but losing environmental friendliness in producing polystyrene/graphene composites via optimizing the matrix-filler structure. *Green Chemistry*, *15*(3), 821-828.

[8]   George, N., Chandra, J., Mathiazhagan, A., & Joseph, R. (2015). High performance natural rubber composites with conductive segregated network of multiwalled carbon nanotubes. *Composites Science and Technology*, *116*, 33-40.

[9]   Treacy, M. J., Ebbesen, T. W., & Gibson, J. M. (1996). Exceptionally high Young's modulus observed for individual carbon nanotubes. *Nature*, *381*(6584), 678.

[10]   Wilder, J. W., Venema, L. C., Rinzler, A. G., Smalley, R. E., & Dekker, C. (1998). Electronic structure of atomically resolved carbon nanotubes. *Nature*, *391*(6662), 59-62.

[11]   Moniruzzaman, M., & Winey, K. I. (2006). Polymer nanocomposites containing carbon nanotubes. *Macromolecules*, *39*(16), 5194-5205.

[12]   Andrews, R., & Weisenberger, M. C. (2004). Carbon nanotube polymer composites. *Current Opinion in Solid State and Materials Science*, *8*(1), 31-37.

[13]   Coleman, J. N., Khan, U., Blau, W. J., & Gun'ko, Y. K. (2006). Small but strong: a review of the mechanical properties of carbon nanotube–polymer composites. *Carbon*, *44*(9), 1624-1652.

[14]   Zhou, X., Zhu, Y., Gong, Q., & Liang, J. (2006). Preparation and properties of the powder SBR composites filled with CNTs by spray drying process. *Materials letters*, *60*(29), 3769-3775.

[15] Bokobza, L., & Kolodziej, M. (2006). On the use of carbon nanotubes as reinforcing fillers for elastomeric materials. *Polymer International*, *55*(9), 1090-1098.

[16] Frogley, M. D., Ravich, D., & Wagner, H. D. (2003). Mechanical properties of carbon nanoparticle-reinforced elastomers. *Composites Science and technology*, *63*(11), 1647-1654.

[17] Fakhru'l-Razi, A., Atieh, M. A., Girun, N., Chuah, T. G., El-Sadig, M., & Biak, D. R. A. (2006). Effect of multi-wall carbon nanotubes on the mechanical properties of natural rubber. *Composite Structures*, *75*(1), 496-500.

[18] Yue, D., Liu, Y., Shen, Z., & Zhang, L. (2006). Study on preparation and properties of carbon nanotubes/rubber composites. *Journal of materials science*, *41*(8), 2541-2544.

[19] Kueseng, K., & Jacob, K. I. (2006). Natural rubber nanocomposites with SiC nanoparticles and carbon nanotubes. *European Polymer Journal*, *42*(1), 220-227.

[20] Thomas, S., & Maria, H. J. (2016). Progress in Rubber Nanocomposites. *Woodhead: Sawston, Cambridge, UK*.

[21] Ponnamma, Deepalekshmi, Sang Hoon Sung, Joung Sook Hong, Kyung Hyun Ahn, K. T. Varughese, and Sabu Thomas. "Influence of non-covalent functionalization of carbon nanotubes on the rheological behavior of natural rubber latex nanocomposites." *European Polymer Journal* 53 (2014): 147-159.

[22] Islam, M. F., Rojas, E., Bergey, D. M., Johnson, A. T., & Yodh, A. G. (2003). High weight fraction surfactant solubilization of single-wall carbon nanotubes in water. *Nano letters*, *3*(2), 269-273.

[23] Valerie C. Moore, Michael S. Strano, Erik H. Haroz, Robert H. Hauge, and Richard E. Smalley. (2003). Individually Suspended Single-Walled Carbon Nanotubes in Various Surfactants, *Nanoletters*, 3(10), 1379-1382.

[24] Gong, X., Liu, J., Baskaran, S., Voise, R. D., & Young, J. S. (2000). Surfactant-assisted processing of carbon nanotube/polymer composites. *Chemistry of materials*, *12*(4), 1049-1052.

[25] Christopher A. Dyke and James M. Tour. (2003). Unbundled and Highly Functionalized Carbon Nanotubes from Aqueous Reactions. *Nanoletters*, 3(9), 1215-1218.

[26] Vanderhoff, J. W. (1970). Mechanism of film formation of latices. *British Polymer Journal*, *2*(3), 161-173.

[27] Daniels, E. S., & Klein, A. (1991). Development of cohesive strength in polymer films from latices: effect of polymer chain interdiffusion and crosslinking. *Progress in Organic Coatings*, *19*(4), 359-378.

[28] Aguilar-Bolados, H., Brasero, J., López-Manchado, M. A., & Yazdani-Pedram, M. (2014). High performance natural rubber/thermally reduced graphite oxide nanocomposites by latex technology. *Composites Part B: Engineering*, *67*, 449-454.

[29] Gao, J. F., Li, Z. M., Meng, Q. J., & Yang, Q. (2008). CNTs/UHMWPE composites with a two-dimensional conductive network. *Materials Letters*, *62*(20), 3530-3532.

[30] Payne, A. R., & Whittaker, R. E. (1971). Low strain dynamic properties of filled rubbers. *Rubber chemistry and technology*, *44*(2), 440-478.

[31] Subramaniam, K., Das, A., & Heinrich, G. (2011). Development of conducting polychloroprene rubber using imidazolium based ionic liquid modified multi-walled carbon nanotubes. *Composites Science and Technology*, *71*(11), 1441-1449.

[32] Galimberti, M., Cipolletti, V., Musto, S., Cioppa, S., Peli, G., Mauro, M., ... & Kumar, V. (2014). Recent advancements in rubber nanocomposites. *Rubber Chemistry and Technology*, *87*(3), 417-442.

[33] Abraham, J., Maria, H. J., George, S. C., Kalarikkal, N., & Thomas, S. (2015). Transport characteristics of organic solvents through carbon nanotube filled styrene butadiene rubber nanocomposites: the influence of rubber–filler interaction, the degree of reinforcement and morphology. *Physical Chemistry Chemical Physics*, *17*(17), 11217-11228.

[34] Pham, T. T., Sridhar, V., & Kim, J. K. (2009). Fluoroelastomer-MWNT nanocomposites-1: Dispersion, morphology, physico-mechanical, and thermal properties. *Polymer Composites*, *30*(2), 121-130.

[35] Kim, P., Shi, L., Majumdar, A., & McEuen, P. L. (2001). Thermal transport measurements of individual multiwalled nanotubes. *Physical review letters*, *87*(21), 215502.

[36] Huxtable, S. T., Cahill, D. G., Shenogin, S., Xue, L., Ozisik, R., Barone, P., ... & Keblinski, P. (2003). Interfacial heat flow in carbon nanotube suspensions. *Nature materials*, *2*(11), 731-734.

[37]   Aharony, A., & Stauffer, D. (2003). *Introduction to percolation theory*. Taylor & Francis.

[38]   Grunlan, J. C., Gerberich, W. W., & Francis, L. F. (2001). Lowering the percolation threshold of conductive composites using particulate polymer microstructure. *Journal of applied polymer science*, *80*(4), 692-705.

[39]   Pang, H., Chen, C., Bao, Y., Chen, J., Ji, X., Lei, J., & Li, Z. M. (2012). Electrically conductive carbon nanotube/ultrahigh molecular weight polyethylene composites with segregated and double percolated structure. *Materials Letters*, *79*, 96-99.

[40]   Gupta, S., Ou, R., & Gerhardt, R. A. (2006). Effect of the fabrication method on the electrical properties of poly (acrylonitrile-co-butadiene-co-styrene)/carbon black composites. *Journal of electronic materials*, *35*(2), 224-229.

[41]   Tkalya, E. E., Ghislandi, M., de With, G., & Koning, C. E. (2012). The use of surfactants for dispersing carbon nanotubes and graphene to make conductive nanocomposites. *Current Opinion in Colloid & Interface Science*, *17*(4), 225-232.

[42]   Hermant, M. C., van der Schoot, P., Klumperman, B., & Koning, C. E. (2010). Probing the cooperative nature of the conductive components in polystyrene/poly (3, 4-ethylenedioxythiophene): poly (styrene sulfonate)− single-walled carbon nanotube composites. *Acs nano*, *4*(4), 2242-2248..

[43]   Kim, D., Kim, Y., Choi, K., Grunlan, J. C., & Yu, C. (2009). Improved thermoelectric behavior of nanotube-filled polymer composites with poly (3, 4-ethylenedioxythiophene) poly (styrenesulfonate). *ACS nano*, *4*(1), 513-523.

[44]   Z.M. Dang, L. Wang, Y. Yin, Q. Zhang, Q.Q. Lei, Giant dielectric permittivities in functionalised carbon-nanotube/electroactive-polymer nanocomposites, Adv. Mater 19 (2007) 852e857.

[45]   Wu, C., Huang, X., Wang, G., Wu, X., Yang, K., Li, S., & Jiang, P. (2012). Hyperbranched-polymer functionalisation of graphene sheets for enhanced mechanical and dielectric properties of polyurethane composites. *Journal of Materials Chemistry*, *22*(14), 7010-7019.

[46]   Li, Q., Xue, Q., Zheng, Q., Hao, L., & Gao, X. (2008). Large dielectric constant of the chemically purified carbon nanotube/polymer composites. *Materials Letters*, *62*(26), 4229-4231.

[47] Yang, Y., Sun, H., Zhu, B., Wang, Z., Wei, J., Xiong, R., ... & Lei, Q. (2015). Enhanced dielectric performance of three phase percolative composites based on thermoplastic-ceramic composites and surface modified carbon nanotube. *Applied Physics Letters*, *106*(1), 012902.

[48] Liu, Z., Bai, G., Huang, Y., Ma, Y., Du, F., Li, F., ... & Chen, Y. (2007). Reflection and absorption contributions to the electromagnetic interference shielding of single-walled carbon nanotube/polyurethane composites. *Carbon*, *45*(4), 821-827.

[49] Chung, D. D. L. (2001). Electromagnetic interference shielding effectiveness of carbon materials. *carbon*, *39*(2), 279-285.

[50] Yan, D. X., Pang, H., Li, B., Vajtai, R., Xu, L., Ren, P. G., ... & Li, Z. M. (2015). Structured Reduced Graphene Oxide/Polymer Composites for Ultra-Efficient Electromagnetic Interference Shielding. *Advanced Functional Materials*, *25*(4), 559-566.

[51] Koul, S., Chandra, R., & Dhawan, S. K. (2000). Conducting polyaniline composite for ESD and EMI at 101GHz. *Polymer*, *41*(26), 9305-9310.

[52] Dhawan, S. K., Singh, N., & Rodrigues, D. (2003). Electromagnetic shielding behaviour of conducting polyaniline composites. *Science and Technology of Advanced Materials*, *4*(2), 105-113.

[53] Yuping, D., Shunhua, L., & Hongtao, G. (2005). Investigation of electrical conductivity and electromagnetic shielding effectiveness of polyaniline composite. *Science and Technology of Advanced Materials*, *6*(5), 513-518.

…..�ణ…..

Chapter 4

NATURAL RUBBER/CARBOXYLATED MULTIWALLED CARBON NANOTUBE COMPOSITES WITH SEGREGATED NETWORK

The previous chapter results revealed that NR-MWCNT composites prepared by the latex stage mixing of the surfactant VL based nanotube dispersions exhibited inferior electrical properties than expected. Hence an alternative method to disperse MWCNTs in water and subsequent preparation of NR based composites with better electrical properties is discussed in this chapter. Here multiwalled carbon nanotubes (MWCNTs) were covalently functionalised by H₂SO₄/HNO₃ treatment to produce carboxylated multiwalled carbon nanotubes (MWCNTR). Presence of carboxyl moieties on MWCNT were confirmed by Raman spectroscopy, X-ray photoelectron spectroscopy (XPS), Fourier transform infrared spectroscopy (FTIR) and Thermogravimetric analysis (TGA). These hydrophilic polar groups helped in getting stable aqueous dispersion of nanotubes. High performance composite with good mechanical and electrical properties was prepared by ultrasonication assisted mixing of aqueous dispersions of MWCNTR with natural rubber (NR) latex followed by film casting and curing. A segregated network of nanotubes was formed along the boundary of the latex spheres even at low concentration which is evident from very low percolation threshold (0.086 vol%), high conductivity and dielectric constant exhibited by the composite. The network formation was confirmed by Transmission electron microscopy (TEM), Scanning electron microscopy (SEM) and supported by strain sweep studies[*].

COVALENT MODIFICATION OF MWCNTS BY H_2SO_4/HNO_3 TREATMENT

4.A.1 Introduction

Carbon nanotubes (CNTs) have been extensively used as reinforcing and electrically conductive nanofillers in the preparation of polymer nanocomposites. Effective and uniform distribution of CNTs in the polymer matrix plays a major role in the achievement of percolative network formation at low filler loadings. If the entire volume of fillers can participate in a conductive network, percolation can be achieved at very low filler loading. Carbon nanotubes[1-3] and graphite nanoplates[4] have been dispersed in the polymer matrix to obtain percolative composites with high dielectric constant (k). High k elastomeric composites are promising materials for the fabrication of flexible electronics. According to the percolation theory, the effective dielectric constant of the composites can be dramatically increased when the concentration of conductive fillers approaches percolation threshold. According to the microcapacitor model principle, the dispersion of conductive fillers in the nonconductive polymer matrix can improve the dielectric constant of the polymer matrix by forming plenty of microcapacitors[5].

The NR/MWCNT composites with segregated network of VL coated MWCNTs showed better mechanical and solvent barrier properties. But electrical properties were found to be inferior as evident from the results of Chapter 3. Literature also supports the fact that surfactants especially the non-ionic surfactants adversely affect the conductivity of CNTs by forming an insulating layer over the tube surface[6,7]. So an alternative method of MWCNT modification has been adopted in the first part (Part A) of this chapter. CNTs are more reactive than flat graphene sheets because of the local strain in carbon nanotubes, which arises from pyramidalization and misalignment of the π-orbitals of the sp^2- hybridized carbon atoms. This paves

the way to covalent attachment of suitable chemical species to nanotubes to improve their dispersion in solvents and polymers[8]. It has been reported that an acid treatment of CNT could improve the processability and performance of composites by introducing carboxylic acid groups on the surface of CNT, for its stabilization in polar solvents and to covalently link with polymers which in turn will lead to a composite with improved properties[9].

The present part of the chapter discusses acid treatment of MWCNT to introduce carboxyl moieties on CNT in order to get a stable aqueous dispersion. The presence of carboxyl groups on the MWCNTR surface were analysed using different characterisation methods such as Raman spectroscopy, X-ray photoelectron spectroscopy (XPS), Fourier transform infrared spectroscopy (FTIR) and Thermogravimetric analysis (TGA). Morphological studies of MWCNTR were done using Scanning electron microscopy (SEM) and Transmission electron microscopy (TEM).

4.A.2 Experimental

4.A.2.1 Acid modification of MWCNT

1 g of the as received MWCNT was mixed with 200 ml of H_2SO_4/ HNO_3 mixture (3:1 v/v) in a 500 ml round bottom flask. The mixture was ultrasonicated in a bath sonicator for 1 h and refluxed under magnetic stirring at 100 ºC for 30 min. The mixture was cooled and diluted with distilled water five times by volume, allowed to stand overnight. The resulting solid was filtered through PTFE membrane filter (0.2 µm pore size) and washed with excess of water until no residual acid was present. The solid was dried under vacuum for 12 h at 60 ºC and labeled as MWCNTR.

4.A.2.2 Qualitative and quantitative analysis of carboxyl groups on MWCNTR

Solubility of modified CNTs in water was determined by first sonicating them in water followed by filtering through a tightly wadded glass wool plug

to remove any insoluble particulates and the weight of nanotubes in known volume of water was measured.

The modified MWCNT was quantitatively analysed by titration to determine the carboxyl group concentrations on the surface of the treated CNTs. In a typical experiment, 0.05 g of MWCNTR was added into a 25 ml 0.01 N NaOH solution and stirred overnight. The dispersion was then filtered and washed with water. The filtrate was titrated with a 0.01 N HCl solution to determine the NaOH in the filtrate and from that to assess the amount of NaOH molecules that were attached to the carboxylated nanotubes.

MWCNTRs were characterised by FTIR, Raman spectra, XPS and TGA. The surface morphology of MWCNTRs was examined using SEM and HRTEM. Detailed discussion on the characterisation methods is given in Chapter 2.

4.A.2.3 Preparation of MWCNTR aqueous dispersions

MWCNTR dispersions were prepared using a mechanical probe sonicator by sonicating aqueous suspension of modified nanotubes for 30 min.

4.A.3 Results and discussion
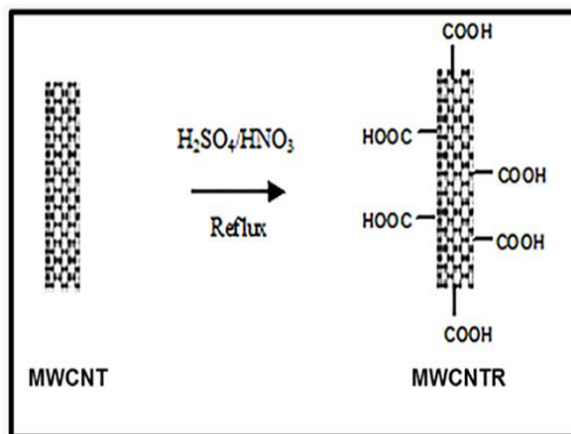
Fig. 4.A.1. Schematic representation of carboxylation of MWCNTs

Fig. 4.A.1 shows the schematic representation of the carboxylation of MWCNTs by acidic treatment with 3:1 conc.H_2SO_4/HNO_3. The polar - COOH groups introduced on the nanotube surface facilitated their dispersion in water.

4.A.3.1 Titration analysis

A direct acid–base titration technique using NaOH was performed to determine the concentration of carboxylic groups on the nanotube surface[10]. In Table 4.A.1, the amount of carboxylic groups per gram of MWCNT material is given.

Table 4.A.1 Quantitative Analysis of carboxylic groups on oxidized nanotubes

Weight of MWCNTR (mg)	NaOH added (mol)	HCl used for the titration (mol)	Carboxyl groups on nanotubes (mol/g)
50	2.50×10^{-4}	1.14×10^{-4}	2.72×10^{-3}

4.A.3.2 Dispersion stability and solubility of MWCNTR in water

The distribution of carboxylated MWCNT in the NR latex is largely influenced by their dispersion state in water. CNTs have an innate strong tendency to agglomerate due to their nano size and high surface energy. However introduced polar hydroxylic and carboxylic groups on oxidised CNTs can favourably interact with water and create the electrostatic stability required for a colloidal dispersion. The good dispersion stability of the MWCNTR in water in comparison with the pristine MWCNTs is clearly evident from the photographic images in Fig. 4.A.2, taken 6 months after the ultrasonic dispersion. The solution had no visible particulates. Solubility of MWCNTR in water was found to be 600 mg/L.
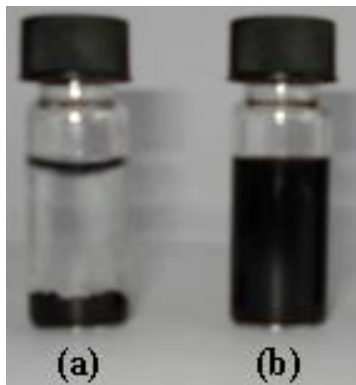
Fig. 4.A.2 Aqueous dispersions of (a) pristine MWCNTs (b) MWCNTRs

4.A.3.3 Fourier transform infrared spectroscopy (FTIR)

Fig. 4.A.3 shows the FTIR spectra of MWCNT and MWCNTR. The IR peak observed at 1566 cm^{-1} in MWCNTs can be assigned to aromatic C=C stretching. The acid treated MWCNTs displayed a broad band at 3462 cm^{-1} due to the O-H stretching frequency of the carboxyl groups. Peak at 1710 cm^{-1} corresponded to C=O stretching in carboxylic group while the peak at 1505 cm^{-1} can be associated with the stretching of the carbon nanotube backbone. The FTIR results clearly indicated the successful attachment of carboxyl groups to the MWCNTs as a result of the acid treatment.
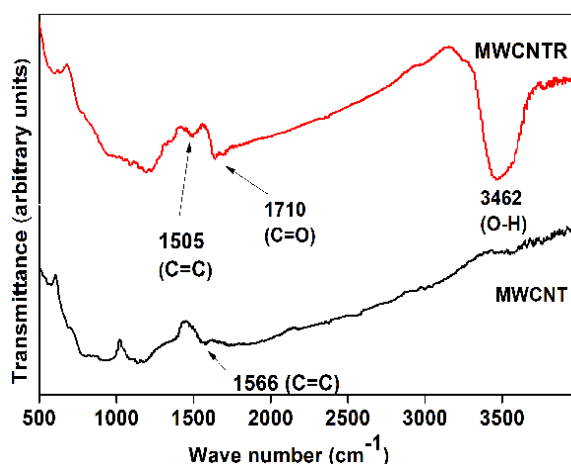
Fig. 4.A.3 FTIR spectra of MWCNT and MWCNTR

4.A.3.4 Raman spectroscopy

Raman spectroscopy is a very valuable tool for the characterisation of carbon-based nanostructures. Raman spectra of both MWCNT and MWCNTR (Fig. 4.A.4) consist of three characteristic bands, namely the D-band at 1320 cm⁻¹, the G-band at 1572 cm⁻¹ and the D′ band (shoulder in G) at 1602 cm⁻¹. The D-band is a disorder induced feature arising from double resonance Raman scattering process from a non-zero-center phonon mode[11]. The D band is usually attributed to the presence of amorphous or disordered carbon in the CNT samples. The carbon structural disorders are due to the finite or nanosized graphitic planes and other forms of carbon such as rings, along with defects on the nanotube walls, vacancies, heptagon-pentagon pairs, kinks and heteroatoms. The G band originates from in-plane tangential stretching of the carbon-carbon bonds in graphene sheets. The D′ band which is a weak shoulder of the G-band at higher frequencies is also a double resonance feature induced by disorder and defects. D* band which is second order overtone band occurs at 2688cm⁻¹.
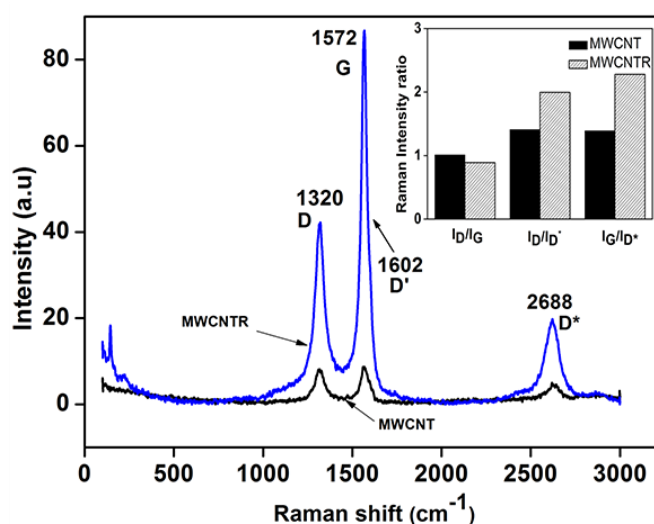
**Fig. 4.A.4 Raman spectra of MWCNT and MWCNTR.
Inset shows the intensity ratio**

Usually the intensity ratio of D to G (I_D/I_G) is taken as a measure of defect concentration. The introduction of functional groups has resulted in an enhancement in the intensity of disorder induced D band. It is based on the assumption that G band is unaffected by defects in the nanotubes. But it has been argued that the G mode in the Raman spectra of carbon nanotubes originates from a defect induced double resonance scattering process[12]. According to Murphy et al.[13] in order to get reliable information about the defect density it is necessary to include the intensity of the second order overtone mode D*, which is due to two phonon processes and hence to first approximation independent of defect concentration.

In this study I_D/I_G value decreased from 1.01 to 0.89 after acid treatment which is controversy to earlier reports in which the ratio increases upon covalent functionalisation of nanotubes[14,15]. This may be due to the presence of impurities in the form of amorphous carbon and nano graphitic particles in pristine CNTs. Fig. 4.A.4 inset shows the variation of I_D/I_G, I_D/I_{D*} and I_G/I_{D*} for MWCNT and MWCNTR. I_D/I_{D*} and I_G/I_{D*} ratio increases significantly for MWCNTR compared to MWCNT, which confirms the presence of increased number of sp^3 hybridized carbons (disorder due to carboxylation) in the nanotube framework due to acid treatment.

4.A.3.5 XPS analysis

XPS provide useful information about the functional groups and presence of structural defects on the nanotube surface. Fig. 4.A.5 shows deconvoluted C1s peak of MWCNTR from XPS. The main peak at 284.1 eV confirms the graphitic structure of MWCNTR[16]. Peak at 285.1 eV shows the presence of defects on the nanotube surface, whereas the peaks at 287 and 288.6 eV, represent carbon atoms bonded to different oxygen-containing moieties[17].
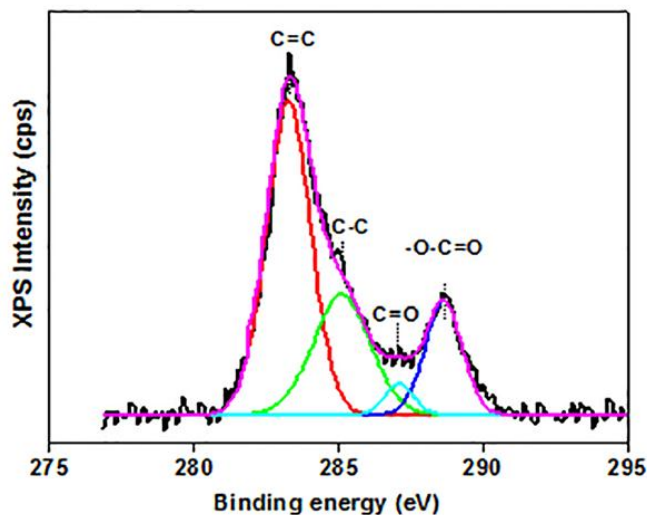
Fig. 4.A.5 Deconvoluted C1s X-ray photoelectron spectroscopy of MWCNTR

4.A.3.6 Thermogravimetric analysis

The thermograms of MWCNTs and MWCNTRs are presented in Fig. 4.A.6. The thermogram of MWCNTR shows clear evidence for the covalent functionalisation of MWCNTs. From the graph it is understood that the thermal degradation of MWCNTRs is a multi-stage process. In the first stage, up to a temperature of 150 ℃, a weight loss of approximately 2% is detected, which corresponds to the evaporation of the adsorbed water. The second stage from 150 to 350 ℃ is attributed to the decarboxylation of the carboxylic groups present on the MWCNT walls. Thermal degradation in the range between the 350 ℃ and 500 ℃ can be explained in terms of the elimination of hydroxyl functionalities, attached to the MWCNT walls. Finally, at the temperatures higher than 500 ℃, the observed degradation corresponds to the thermal oxidation of the remaining disordered carbon. TGA can be used to roughly calculate the amount of carboxyl groups that are introduced on the surface of MWCNT. Calculations show that about 6.7 wt% of carboxyl groups are introduced on the nanotube surface as a result of oxidation.
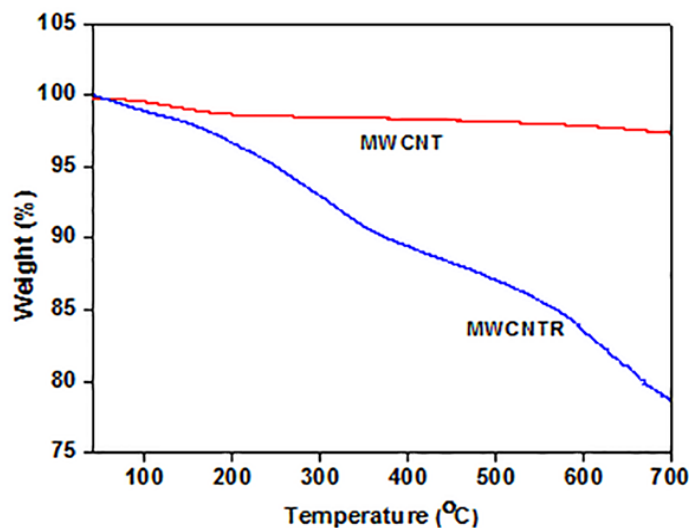
Fig. 4.A.6 TG curves of MWCNT and MWCNTR

4.A.3.7 Morphology and microstructure

Fig. 4.A.7(a) and (b) show the SEM images and (c) and (d), show the TEM images of MWCNT and MWCNTR respectively. MWCNTR is shorter and debundled than that of pristine MWCNT. The amorphous carbon materials in MWCNTR are less than that in pristine MWCNTs. Shortening and debundling of MWCNTs may have occurred during the sonication step of MWCNTs in the oxidizing acid medium. According to Smalley et al.[18] sonication in the presence of strong acid mixture can damage the sides of MWCNTs with subsequent attack by the acid at the point of damage resulting in shortening of the nanotubes. The shortened tube will get separated from other tubes in the rope. The presence of a large amount of oxygen containing functionalities at the cut ends enhances the colloidal stability of the acid treated MWCNTs in water.
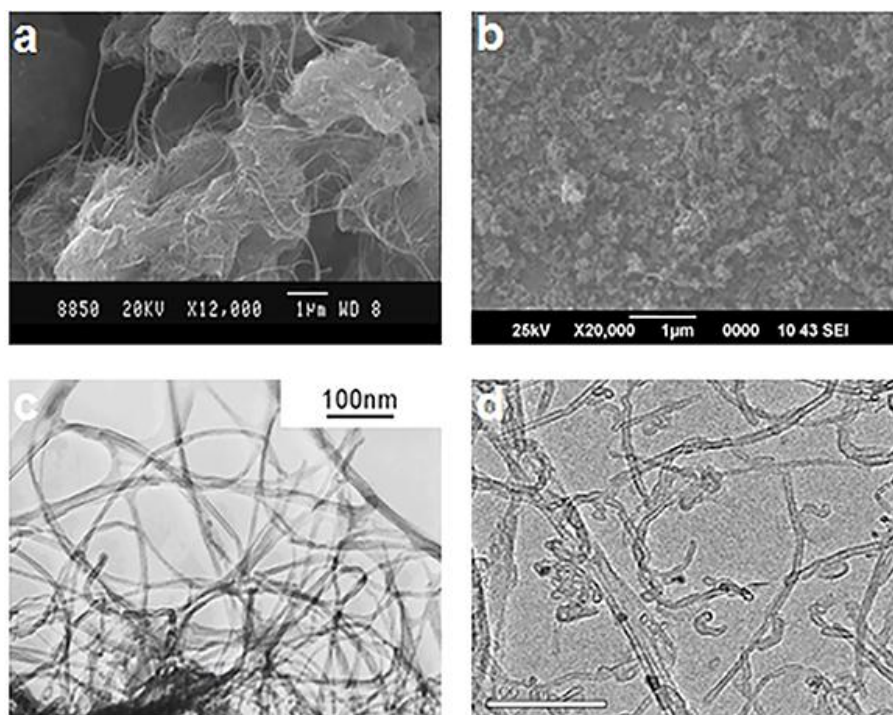
**Fig. 4.A.7 (a) and (b) SEM images of MWCNT and MWCNTR
(c) and (d) TEM images of MWCNT and MWCNTR**

4.A.4 Conclusions

MWCNTs were functionalised with carboxyl moieties by the reaction with H_2SO_4/HNO_3 mixture. The solubility of the resulting samples in water provided visual indication for the functionalisation of the carbon nanotubes. The aqueous dispersions prepared by ultrasonication of MWCNTR in water were found to be stable over months and gave a dispersibility of 600 mg of MWCNTR per lire of water. Strong evidence for the functionalisation was provided by the FTIR spectroscopy, Raman spectroscopy, XPS and TGA. Morphological studies of MWCNTR using SEM and TEM showed that the acid treatment shortens and purifies the nanotubes and helps in debundling of the tubes into individual tubes. The polar groups introduced over the MWCNT surface can improve water-affinity of MWCNTs and thus would be

beneficial for the preparation of the MWCNT–NR latex suspension. Moreover, the functional groups loaded on the surfaces of MWCNTs could be favorable for improving the interfacial bonding between MWCNTs and the rubber matrix, thereby improving the mechanical properties of the composites.

References

[1]   Li, Q., Xue, Q., Hao, L., Gao, X., & Zheng, Q. (2008). Large dielectric constant of the chemically functionalised carbon nanotube/polymer composites. *Composites Science and Technology*, *68*(10), 2290-2296.

[2]   Zhang, S., Wang, H., Wang, G., & Jiang, Z. (2012). Material with high dielectric constant, low dielectric loss, and good mechanical and thermal properties produced using multi-wall carbon nanotubes wrapped with poly (ether sulphone) in a poly (ether ether ketone) matrix. *Applied Physics Letters*, *101*(1), 012904.

[3]   Yadav, S. K., Mahapatra, S. S., & Cho, J. W. (2013). Tailored dielectric and mechanical properties of noncovalently functionalised carbon nanotube/poly (styrene-b-(ethylene-co-butylene)-b-styrene) nanocomposites. *Journal of Applied Polymer Science*, *129*(4), 2305-2312.

[4]   He, F., Lau, S., Chan, H. L., & Fan, J. (2009). High dielectric permittivity and low percolation threshold in nanocomposites based on poly (vinylidene fluoride) and exfoliated graphite nanoplates. *Advanced Materials*, *21*(6), 710-715.

[5]   Song, Y., Noh, T. W., Lee, S. I., & Gaines, J. R. (1986). Experimental study of the three-dimensional ac conductivity and dielectric constant of a conductor-insulator composite near the percolation threshold. *Physical Review B*, *33*(2), 904.

[6]   Aguilar-Bolados, H., Brasero, J., López-Manchado, M. A., & Yazdani-Pedram, M. (2014). High performance natural rubber/thermally reduced graphite oxide nanocomposites by latex technology. *Composites Part B: Engineering*, *67*, 449-454.

[7]   Li, Q., Xue, Q., Zheng, Q., Hao, L., & Gao, X. (2008). Large dielectric constant of the chemically purified carbon nanotube/polymer composites. *Materials Letters*, *62*(26), 4229-4231.

[8]   Niyogi, S., Hamon, M. A., Hu, H., Zhao, B., Bhowmik, P., Sen, R., ... & Haddon, R. C. (2002). Chemistry of single-walled carbon nanotubes. *Accounts of Chemical Research*, *35*(12), 1105-1113.

[9]   Yuen, S. M., Ma, C. C. M., Lin, Y. Y., & Kuan, H. C. (2007). Preparation, morphology and properties of acid and amine modified multiwalled carbon nanotube/polyimide composite. *Composites Science and Technology*, *67*(11), 2564-2573.

[10]   Shieh, Y. T., Liu, G. L., Wu, H. H., & Lee, C. C. (2007). Effects of polarity and pH on the solubility of acid-treated carbon nanotubes in different media. *Carbon*, *45*(9), 1880-1890.

[11]   Dresselhaus, M. S., Dresselhaus, G., Saito, R., & Jorio, A. (2005). Raman spectroscopy of carbon nanotubes. *Physics reports*, *409*(2), 47-99.

[12]   Maultzsch, J., Reich, S., Thomsen, C., Webster, S., Czerw, R., Carroll, D. L., ... & Rego, C. A. (2002). Raman characterisation of boron-doped multiwalled carbon nanotubes. *Applied physics letters*, *81*(14), 2647-2649.

[13]   Murphy, H., Papakonstantinou, P., & Okpalugo, T. T. (2006). Raman study of multiwalled carbon nanotubes functionalised with oxygen groups. *Journal of Vacuum Science & Technology B: Microelectronics and Nanometer Structures Processing, Measurement, and Phenomena*, *24*(2), 715-720.

[14]   Yudianti, R., Onggo, H., Sudirman, Y. S., Iwata, T., & Azuma, J. I. (2011). Analysis of functional group sited on multi-wall carbon nanotube surface. *Open Materials Science Journal*, *5*, 242-247.

[15]   Datsyuk, V., Kalyva, M., Papagelis, K., Parthenios, J., Tasis, D., Siokou, A., ... & Galiotis, C. (2008). Chemical oxidation of multiwalled carbon nanotubes. *Carbon*, *46*(6), 833-840.

[16]   Ago, H., Kugler, T., Cacialli, F., Salaneck, W. R., Shaffer, M. S., Windle, A. H., & Friend, R. H. (1999). Work functions and surface functional groups of multiwall carbon nanotubes. *The Journal of Physical Chemistry B*, *103*(38), 8116-8121.

[17]   Beamson, G., & Briggs, D. (1992). *High resolution XPS of organic polymers*. Wiley.

[18]   Liu, J., Rinzler, A. G., Dai, H., Hafner, J. H., Bradley, R. K., Boul, P. J., ... & Rodriguez-Macias, F. (1998). Fullerene pipes. *Science*, *280*(5367), 1253-1256.

NR/CARBOXYLATED MWCNT COMPOSITES THROUGH LATEX STAGE PROCESSING

4.B.1 Introduction

The acid treatment of carbon nanotubes has been reported by many researchers but there are only few reports on composites with natural rubber (NR). Bhattacharyya et al.[1] studied the reinforcement of natural rubber by activated multiwalled carbon nanotubes (MWCNT) dispersed with the assistance of sodium dodecyl sulphate. As a result mechanical properties and electrical conductivity of NR dramatically increased. They have reported a percolation threshold of 0.4 vol% of MWCNTs, which is associated with the formation of interconnected nanotube network. The previous chapter clearly revealed that the surfactant assisted solubilisation of MWCNTs followed by the preparation of NR/MWCNT composites resulted in better mechanical properties but poor electrical properties due to formation of an insulating sheath around the nanotubes. So in the present part of the study we aim at the preparation of natural rubber composite with a segregated MWCNT network, having good mechanical and electrical properties at very low percolation threshold avoiding the usage of any surfactant.

NR latex is a stable colloidal dispersion of cis-1,4-polyisoprene in an aqueous medium. It is an industrially and economically important polymer because of their excellent mechanical properties and elasticity[2]. The carbon nanotubes can be well dispersed in the NR latex when they are added as their aqueous dispersions. In the present study, carboxylated MWCNTs (MWCNTR) were used instead of surfactant modified MWCNTs. To ensure lower electrical percolation threshold with segregated nanotube network, composites were prepared by mixing the MWCNTR aqueous dispersion with compounded NR latex under ultrasonication followed by film casting.

Mechanical properties, fracture surface morphology and microstructure of the composites were studied. Thermal properties and solvent barrier properties of the composites were investigated. Frequency dependence of dielectric properties and electrical conductivity were examined. Electrical percolation threshold was determined using linear power law and the relationship between the microstructure and properties were analysed.

4.B.2 Experimental

4.B.2.1 Preparation of NR-MWCNTR nanocomposites

The NR-MWCNTR composite with segregated network of nanotubes was prepared by ultrasonication assisted latex mixing and film casting method. The MWCNTR aqueous dispersion was prepared by sonicating aqueous suspension of modified nanotubes for 30 min and the dispersion was then mixed with the NR latex. Various concentrations of MWCNTR aqueous dispersions (0.05 to 1.0 phr) were prepared and added separately to NR latex. The resulting mixes were compounded as per the formulation given in Table 4.B.1 and sonicated again for 30 minutes to achieve uniformity. The samples were kept overnight for maturation and then cast onto flat glass trays to get films. These films were dried at room temperature and then cured at 100 ºC for 1 h in an air oven.

Table 4.B.1 Formulation of NR-MWCNTR composites

Ingredients	Amount (g)
Centrifuged NR latex (60 % DRC)	167.0
MWCNTR	0, 0.05, 0.1, 0.3, 0.5, 1.0
10 % KOH solution	1.0
10 % Potassium oleate solution	1.0
20 % Vulcastab VL	1.0
50 % ZnO dispersion	1.0
50 % ZDC dispersion	2.0
50 % Sulphur dispersion	3.0

4.B.2.2 Characterisation

The surface morphology of NR-MWCNTR composites were examined using SEM and microstructure was analysed using TEM. The tensile and tear strength was determined using Universal Testing Machine (10 kN). The strain-amplitude dependent dynamic mechanical properties of the vulcanisates were measured at room temperature by means of a dynamic mechanical analyzer (Model Q 800, TA instruments). Sorption behaviour and cross-link density of the samples were determined by equilibrium swelling method using toluene as the solvent. Thermogravimetric analysis (TGA) was done using a TGA-Q 50 Thermal Analyser (TA Instruments). DC electrical conductivity measurements were carried out by a standard two-probe electrode using a Keithley 2400 source-measure unit in dry air at room temperature. Dielectric and AC conductivity studies of the samples were conducted using Precision Impedance Analyser (Agilent 4294A) over the frequency range of 40 Hz to 30 MHz at room temperature. EMI shielding measurements were performed using a wave-guide coupled to an Agilent Performance Network Analyzer E8362 B in the X band frequency range (8-12) GHz.

Detailed description of the characterisation methods is given in Chapter 2.

4.B.3 Results and discussion
4.B.3.1 Segregated carbon nanotube network formation

Latex stage incorporation of MWCNT dispersion in NR can lead to segregated network formation since the MWCNTs have a tendency to get adhered around the NR latex spheres forming a rigid network during the composite film formation. The proposed schematic representation of the preparation of NR-MWCNTR composites with segregated network is shown in Fig. 4.B.1. Oxygen containing functional groups in MWCNTR

helps them to uniformly disperse in the NR latex and these conductive tubes are forced to occupy the spaces between the compacting latex particles during drying. The segregated rigid network along the boundary of latex spheres is retained even after curing since the high viscosity of the rubber particles restrict the diffusion of the nanotubes.

The formation of segregated network of MWCNTRs in NR was confirmed by the TEM analysis. Alignment of MWCNTRs at the periphery of the latex spheres is clearly evident from the TEM images (Fig. 4.B.2) of NR-MWCNTR composite film formed on the TEM microgrid.
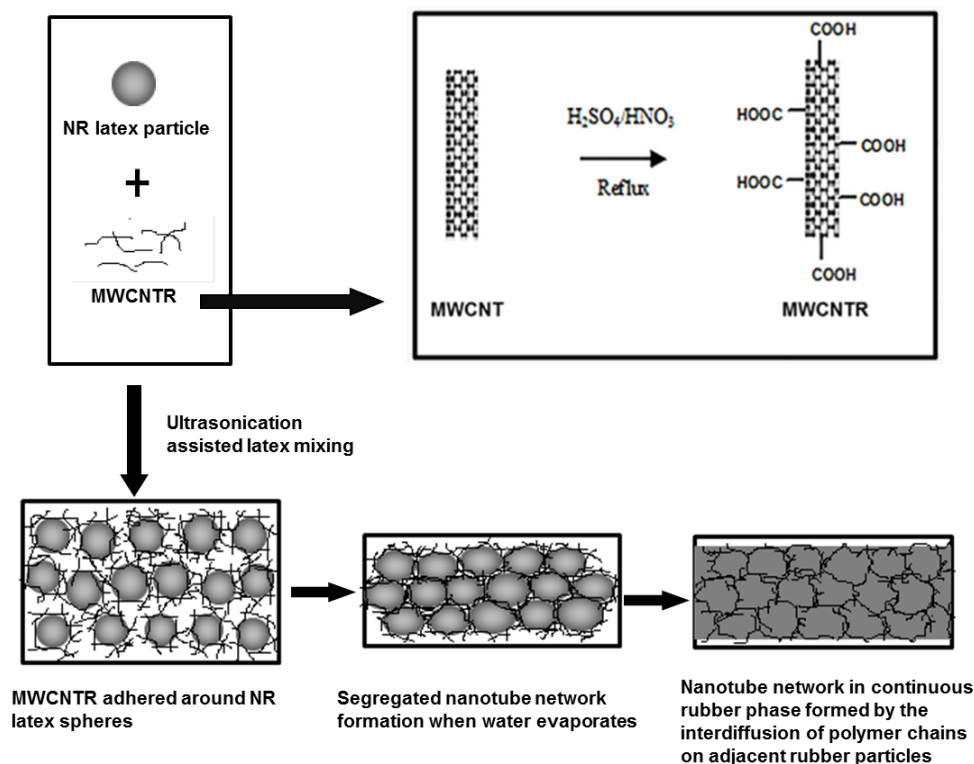
Fig. 4.B.1 Schematic representation of the preparation of NR-MWCNTR composites with segregated network
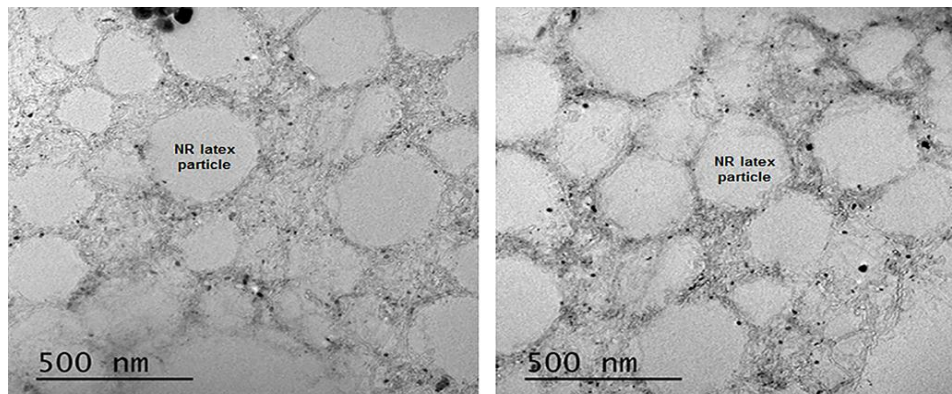
Fig. 4.B.2 TEM images of NR-MWCNTR composite film formed on the grid

4.B.3.2 Morphology and microstructure

The fracture surface morphologies of pure NR and NR-MWCNTR composites witht 0.1 and 0.5 phr MWCNTR loading are shown in Fig. 4.B.3. The tensile and tear fractured surfaces of NR and its composites with MWCNTR shows significant differences in their fracture pathways which can be explained in terms of the network formation. For neat NR both tensile and tear fractured surfaces appear to be relatively smooth. On the contrary the fractured surface of NR-MWCNTR nanocomposites shows specific patterns (as reported by Gao et al.[3]) which can be explained based on the processing method adopted in our work. As already mentioned, latex stage mixing and subsequent film casting distributes the CNTs along specific paths at the polymer-particle interfaces which results in a microstructure with an ordered segregated network of CNTs. Tensile fracture surface for 0.5 phr MWCNTR (Fig. 4.B.3c) is more rough with craters compared to 0.1 phr MWCNTR (Fig. 4.B.3b) suggesting more completed 3D network and strong interaction between the network and NR. For neat NR the tear fracture surface exhibits a smooth and straight tear path in the direction of tear (Fig. 4.B.3d). On the other hand, the fracture surfaces of the nanocomposites (Fig. 4.B.3e and f) exhibit a rough surface with curved tear paths which again confirms the possibility of the alignment of nanotubes

along specific path in the composite. The tear paths show a pattern because the tear lines are deviated by the network formed in the rubber matrix. The fine patterning of the ridges present in the tear fractured surface indicate better bonding between the rubber chains and the network, predicting an improvement in mechanical properties of the nanocomposites[4].
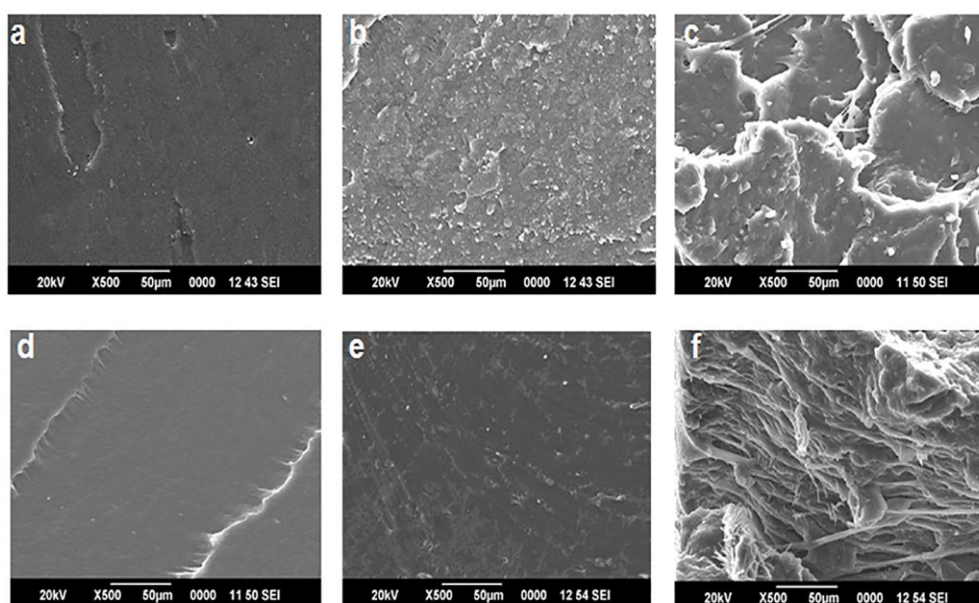
Fig. 4.B.3 SEM images of the nanocomposites: (a-c) Fractured surfaces of tensile test specimens of (a) NR (b) NR-MWCNTR0.1 (c) NR-MWCNTR0.5 (d-f) Fractured surfaces of tear test specimens of (d) NR (e) NR-MWCNTR0.1 (f) NR-MWCNTR0.5

4.B.3.3 Mechanical properties

Fig. 4.B.4 shows the stress−strain curves of the nanocomposites. The figure clearly shows that the stress increases slowly upto a particular strain and after that the stress increases very rapidly and reaches a maximum value. This change in behaviour is known as the strain induced crystallisation of NR, which becomes more pronounced as the concentration of MWCNTR increases.
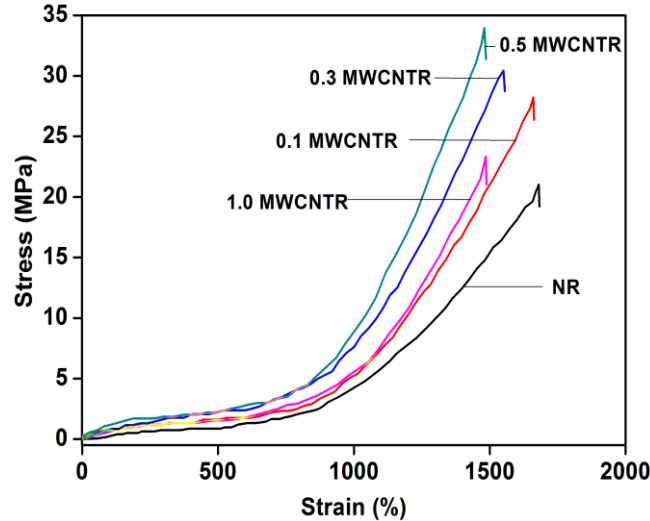
Fig. 4.B.4 Stress-strain curves of NR-MWCNTR nanocomposites

The mechanical properties of the nanocomposites are presented in Table 4.B.2. The tensile strength, modulus and tear strength of the nanocomposites increase with nanotube concentration, whereas elongation at break value decreases. NR with 0.5 phr MWCNTR shows best properties with 61% increase in tensile strength, 75 % in modulus and 59% in tear strength. The tensile strength, tear strength and tensile modulus increase with the addition of MWCNTR upto 0.5 phr loading and decrease on further addition. Segregated MWCNTR network in the NR matrix plays a significant role in improving the mechanical properties. This well distributed rigid network can bear most of the stress applied, thus enhancing the mechanical properties of the nanocomposite.

Reinforcement of NR by the MWCNTR in the composite can be explained in terms of the large aspect ratio and physical entanglement of CNTs with rubber. The nanotube network formed around the rubber particles divides the NR matrix into small units and gives a cellular structure. The cellular structure and occluded rubber (due to the confinement of rubber within the networks) in the NR-MWCNTR composite provides tremendous reinforcement[5].

When the MWCNTR content is high, nanotube aggregation in the network increases, which gives better electrical conductivity with a concomitant reduction in the mechanical properties as suggested by Francis et al.[6]. It is believed that the enhancement of tensile strength is a consequence of polymer diffusion across the particle-particle interface in the film. For higher concentration of nanofillers, the network becomes more aggregated and the interpenetration of polymer becomes difficult which leads to poor mechanical properties. The film casting method along with poor dispersion of filler at higher concentration may also result in the porosity of sample, thus reducing the mechanical properties[7].

Table 4.B.2 Mechanical Properties of NR-MWCNTR nanocomposites

MWCNTR (phr)	Tensile strength(MPa)	Elongation at break (%)	Modulus 300 % (MPa)	Tear strength (N/mm)
0	21.0±0.5	1691±10	1.06±0.08	34.8±0.2
0.05	23.0±0.3	1638±41	1.24±0.02	35.5±0.9
0.1	28.2±0.6	1660±40	1.32±0.03	42.5±1.1
0.3	30.4±0.5	1550±38	1.74±0.01	43.4±1.2
0.5	33.9±0.6	1480±63	1.86±0.03	55.4±1.0
1.0	23.3±0.8	1485±86	1.21±0.11	30.3±0.6

4.B.3.4 Strain-amplitude dependent dynamic mechanical properties

Fig. 4.B.5 shows the strain dependence of the storage modulus of NR and MWCNTR filled composites. Usually for neat rubber dynamic properties are independent of strain amplitude but for filled rubber it is found to vary with strain, especially under small deformations. This phenomenon, known as the Payne effect, is responsible for the decrease in the storage modulus with increasing strain amplitude in filled rubbers. The most commonly accepted model to explain Payne effect arises from the breakdown of a filler network formed by filler–filler interactions via a model of immobilized elastomeric layers on the filler surface[8,9]. Fig. 4.B.5 shows that

the Payne effect is not observable below 0.3 phr MWCNTR, and above that, the effect increases with increase in the amount of MWCNTR. This confirms the formation of MWCNTR network at 0.3 phr in the nanocomposite.
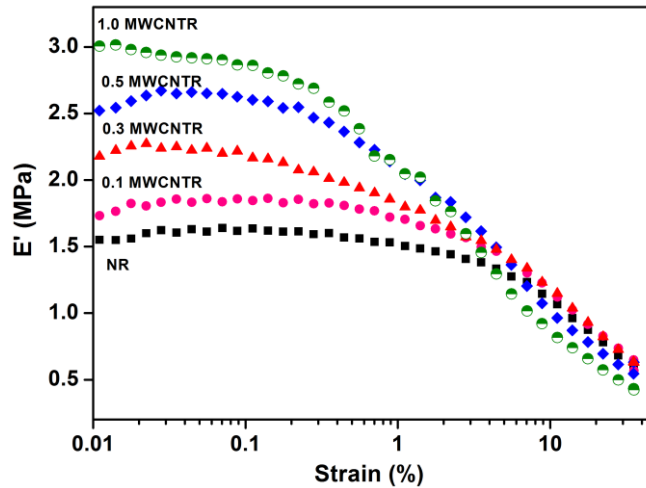
Fig. 4.B.5 Strain dependence of the storage modulus of NR and NR-MWCNTR

4.B.3.5 Swelling studies

Sorption curves of NR and NR-MWCNTR composites are given in Fig.4.B.6. The rate of solvent uptake of the composite is high initially and reaches a plateau (equilibrium solvent uptake) with time. Equilibrium solvent uptake decreases with addition of MWCNTR upto 0.5 phr and increases beyond that concentration. Thus segregated network of nanotubes play an important role in improving the solvent barrier properties of NR. Rubber particles are wrapped by the nanotubes creating a tortuous path that slow down the solvent penetration through the rubber. As the nanotube concentration increases the network extends throughout the rubber matrix and the penetration of solvent molecules is hindered. Increase in solvent uptake after 0.5 phr of MWCNTR can be due to the aggregation of CNTs in the network. The aggregation can create micro voids in the segregated structure through which solvents can easily penetrate[10,11].
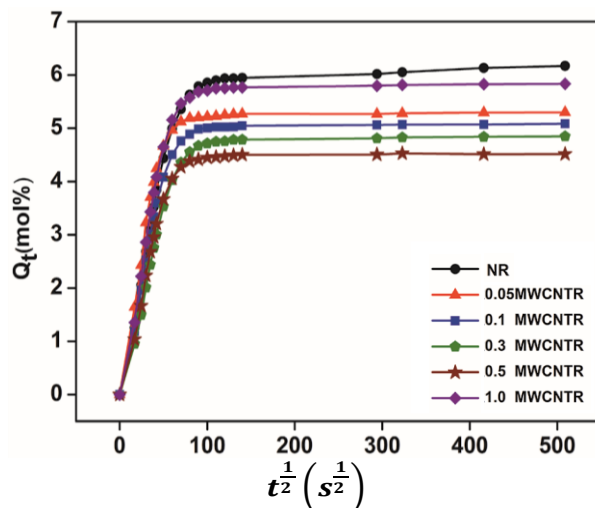
Fig. 4.B.6 Sorption curves of NR and NR-MWCNTR composites

The crosslink density of the NR-MWCNTR composites increase while the swelling index decrease with addition of MWCNTR up to 0.5 phr loading. Lower swelling in the presence of nanofillers is apparently due to the increased crosslink density restricting the polymer chain mobility. The increase in crosslink density and decrease in swelling index of rubber nanocomposites with the addition of 0.5phr of MWCNTR show the reinforcement of rubber and MWCNTR (Table 4.B.3).

Table 4.B.3 Crosslink density and Swelling index of NR and NR-MWCNTR composites

MWCNTR (phr)	Crosslink density (x 10^{-5} mol/g)	Swelling Index (%)
0	3.1	569
0.05	3.1	561
0.1	3.2	546
0.3	3.6	497
0.5	4.0	470
1.0	3.2	567

The higher crosslink density values indicate more strain on the network due to restricted chain mobility and thus results in lower swelling. Crosslink density value for the composite with 1phr MWCNTR is low which may be due to some

porosity developed in the film due to the agglomeration and poor dispersion of the nanotubes at high concentration.

4.B.3.6 Thermal studies

TGA and DTG curves of NR and its nanocomposites with MWCNTR are shown in Fig. 4.B.7(a) and (b) respectively. Both NR and NR-MWCNTR nanocomposites have almost the same thermal stability. The major degradation peak in the 330–470 °C range can be assigned to the thermal decomposition of natural rubber into oligomers in inert atmosphere.
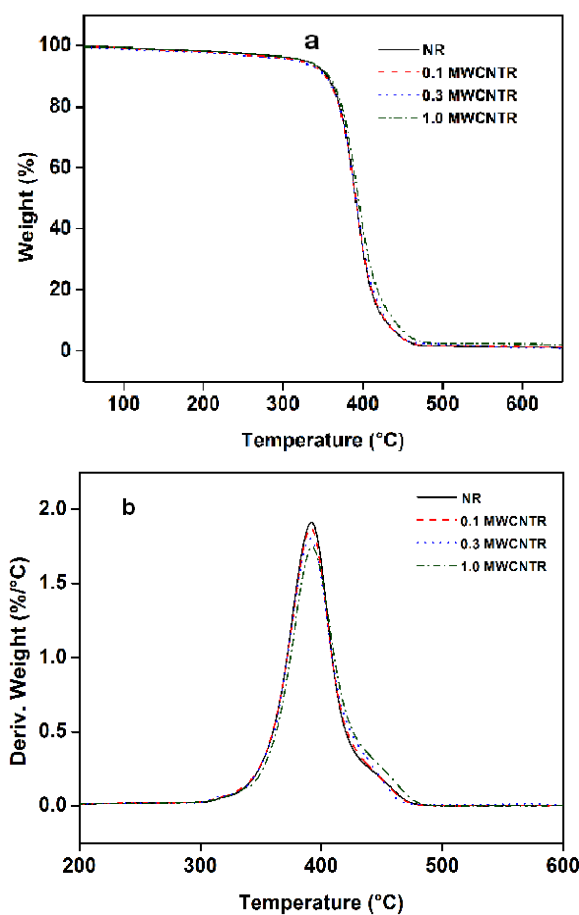
Fig. 4.B.7 (a) TGA and (b) DTG curves of NR and NR-MWCNTR nanocomposites

Table 4.B.4 shows the analysed TGA data for NR and NR-MWCNTR nanocomposites. There is only marginal increase in the onset degradation temperature with addition of MWCNTR. Maximum degradation temperature (T_{max}) is comparable for NR and nanocomposites. The temperature at which 50% decomposition occurs (T_{50}) is generally considered as an index of thermal stability. T_{50} remains unaffected with the addition of MWCNTRs which again confirms that both NR and NR-MWCNTR composites have almost similar thermal stability.

Table 4.B.4 TGA data for NR and NR-MWCNTR nanocomposites

Property	NR	0.1 MWCNTR	0.3 MWCNTR	1.0 MWCNTR
Onset degradation temperature (T_0,°C)	335	336	338	338
Maximum degradation temperature (T_{max},°C)	391	391	391	392
Temperature at 50% degradation (T_{50},°C)	391	391	391	394
Temperature at 75% degradation (T_{75},°C)	405	406	407	412
Residue at 550 °C	1.60	1.71	1.74	2.48

4.B.3.7 Dielectric properties

Electrical properties are usually explained in terms of vol% of the fillers rather than phr. For better understanding, the concentration of MWCNTR in NR-MWCNTR composites in both phr and vol% is given in Table 4.B.5.

Table 4.B.5 Concentration of MWCNTR in NR-MWCNTR composites

Concentration of MWCNTR	
phr	**vol%**
0.05	0.022
0.1	0.043
0.3	0.129
0.5	0.215
1.0	0.430

Fig. 4.B.8(a) and (b) shows the frequency dependence of dielectric constant and dielectric loss of the NR-MWCNTR composites at room temperature. Both dielectric constant and dielectric loss values are high at low frequencies and then decrease exponentially with increase in frequency.

There is a remarkable increase in the dielectric constant from 4.7 for pure NR to approximately 1000 at 100 Hz for 1 phr MWCNTR composites (about 200 times higher than for pure NR). If this material is exposed to electromagnetic plane waves, the electric dipole moments created per unit volume will be higher. This will result in a high dielectric constant and dielectric loss at lower frequencies. As the frequency increases the induced dielectric polarisability will decrease, which can result in a reduction in both properties. An opposite effect is observed in the conductivity (σ) of the material; that is σ increases with increase in frequency (Fig. 4.B.9a). σ reached a value of 1.7×10^{-5} S/m at 1 kHz and 4.5×10^{-4} S/m at 10 MHz for 1phr MWCNTR. This observation can be explained by the fact that at higher frequencies the external electromagnetic field will induce surface currents within the material and the conduction will be dominated by the conduction current, whereas at lower frequencies conduction will be enabled by the displacement currents associated with the dipole moments created. But the ohmic losses (I^2R loss) associated with the conduction current will be lower as compared to the losses offered by the electric dipole moments and hence the dielectric loss is higher at low frequencies.
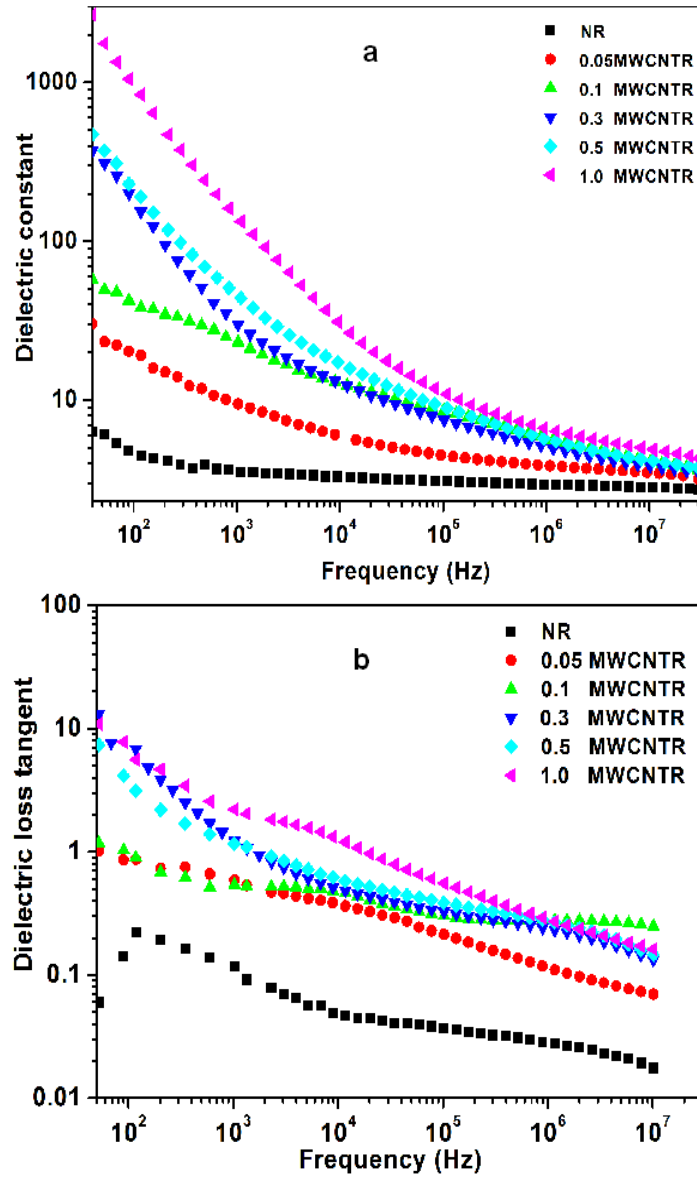
Fig. 4.B.8   Dielectric properties as a function of frequency
(a) Dielectric constant (b) Dielectric loss tangent
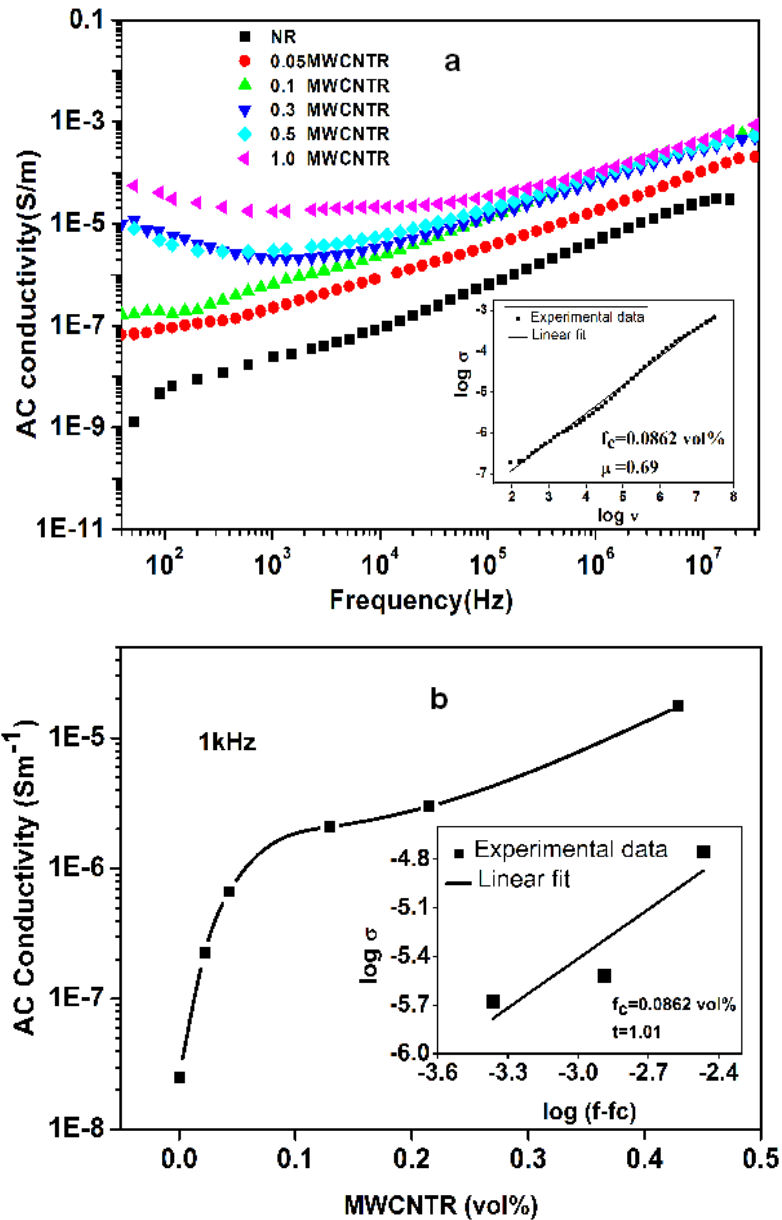
Fig. 4.B.9 **(a) AC conductivity as a function of frequency. The inset shows the best fit of the ac conductivity of the composite with 0.086 vol% of MWCNTR to Eq. (4.B.2). (b) AC conductivity of the NR-MWCNTR composites as a function of MWCNTR concentration measured at 1 kHz and room temperature. Inset shows the best fit of the conductivity to Eq. (4.B.1)**

The dielectric properties of the composites can be understood by the percolation theory and interfacial polarization effect. In these composites, the conducting MWCNTRs are segregated around the insulating rubber particles and can form a lot of interfaces. The large π-orbital of the MWCNTs can provide large domains for free electrons. These electrons can be orientated under electric field, and interfacial polarization can take place. As the MWCNTR concentration increases, the number of interfaces also increases as more and more CNTs get distributed in the interfacial region forming a completed network throughout the matrix. So dielectric constant increases with increasing MWCNTR concentration. High dielectric constant of the composites can also be attributed to the electron-withdrawing nature of carboxylic groups present in MWCNTR which can strengthen interfacial polarization[12].

Fig. 4.B.9b shows AC conductivity (σ) values at 1 kHz for the nanocomposites as a function of MWCNTR volume fraction at room temperature. In order to estimate electrical percolation threshold, the experimental conductivity (σ) was fitted to the well-known power law equation for conductivity[13].

$$\sigma \propto (f - f_c)^t \ for \ f > f_c$$ ....(4.B.1)

where f is the volume fraction of the filler, f_c is the volume fraction at percolation threshold and t is the critical exponent in the conducting region. The best linear fits of the conductivity data to the log–log plots of the power law Eq.4.B.1 gives $f_c = 0.0862$vol% (0.2 phr), t = 1.01 (inset in Fig. 4.B.9b).

The critical exponent 't' obtained for the NR-MWCNTR composites deviates from the universal value (t_{un}~1.6-2). The deviation can be ascribed to the complexity of the segregated network in NR-MWCNTR composites. A similar result has been reported by Zhi-Min Dang et al.[14].

When f reaches f_c, the relation between conductivity and frequency can be related through percolation threshold power law as given in Equation 4.B.2.

$$\sigma \propto \omega^\mu, \text{ as } f \rightarrow f_c \quad ....(4.B.2)$$

where $\omega = 2\pi v$, v is the frequency and μ is the corresponding critical exponent. The value of μ obtained ($\mu = 0.69$) from the linear fit of the log-log plot of Eq.4.B.2 using experimental data for f=0.086 vol% (near f_c) is found to be close to the normal value ($\mu_{uni} = 0.70$) (4.B.9a inset).

Percolation threshold obtained for segregated NR-MWCNTR composite is found to be very low compared to the traditional non-segregated CNT filled rubber composites[15-17]. The conventional mill mixing usually makes the CNTs randomly distribute in the composites and a large amount of CNTs are needed to form the conductive network resulting in high percolation threshold. In the present work, CNTs are aligned in the interfacial regions of the composite, so as to make a conductive network with minimum amount of filler.

Near the percolation threshold, the electrical conductivity and dielectric permittivity of the composites increased tremendously similar to other reports[18,19]. From figures 4.B.8(a) and 4.B.9(a) it is clear that both the dielectric permittivity and conductivity increased significantly as the MWCNTR volume fraction increased particularly near the percolation threshold. When $f < f_c$, the conductivity increases almost linearly with the increase of frequency; when $f > f_c$, the conductivity values are much higher than those for $f < f_c$, and are almost independent of the change of frequency within a low-frequency range. Very low dielectric percolation threshold (0.086 vol%) and high dielectric constant obtained for the composites confirms the nanotube 3D network formation in the polymer matrix at very low filler loading. These, nanoscale, flexible, polymer-based composites with

giant dielectric permittivity and dielectric loss can be used as electromagnetic wave absorbers in the low frequency region.

4.B.3.8 DC electrical conductivity

As already mentioned the percolation threshold is characterised by a sudden increase in the conductivity of the composite due to the formation of conductive network of the fillers in the polymer matrix. The variation of the DC conductivity of NR composites with MWCNTR loading is shown in Fig. 4.B.10. The conductivity increases from 1.7×10^{-12} to 5.65×10^{-7} Sm^{-1} at 0.3 phr MWCNTR (0.1293 vol%) loading. The tremendous increase in DC conductivity at this low concentration give credence to the formation of nanotube network within the polymer matrix.
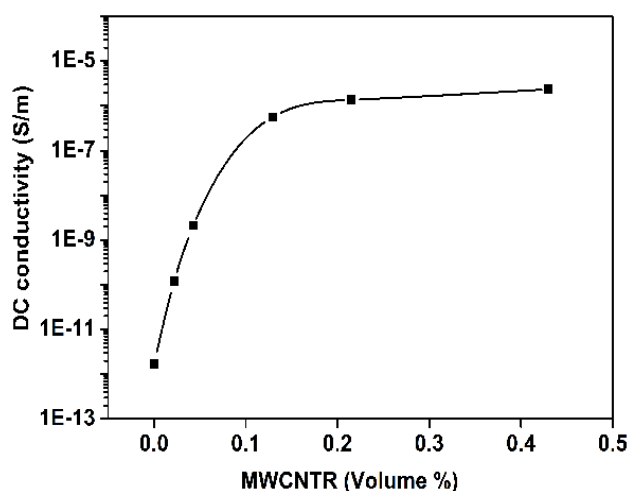
Fig. 4.B.10 Variation of dc conductivity of NR composite with MWCNTR

4.B.3.9 EMI shielding effectiveness

EMI shielding effectiveness (SE) of the NR-MWCNTR composites in the frequency range 8-12 GHz is shown in Fig.4.B.11. Conductivity and dielectric properties of NR-MWCNTR composites are high compared to NR-MWCNT composites. But there is only marginal increase in shielding

efficiency for NR-MWCNR composites with MWCNTR addition. This may be due to the low concentration of MWCNTR used in the present work (maximum concentration of MWCNTR used is only 1 phr). Even literature reports show appreciable increase in SE at loadings higher than 5 wt %[20,21]. Aspect ratio of nanotubes also plays an important role in EMI shielding and long nanotubes are reported to have more SE compared to short ones[22,20]. MWCNTRs used in the present study are shorter than pure MWCNTs used in NR-MWCNT composites because oxidation treatment shortens the nanotubes and decreases the aspect ratio. This lowering in the aspect ratio may be the reason for the poor SE obtained in the present case.
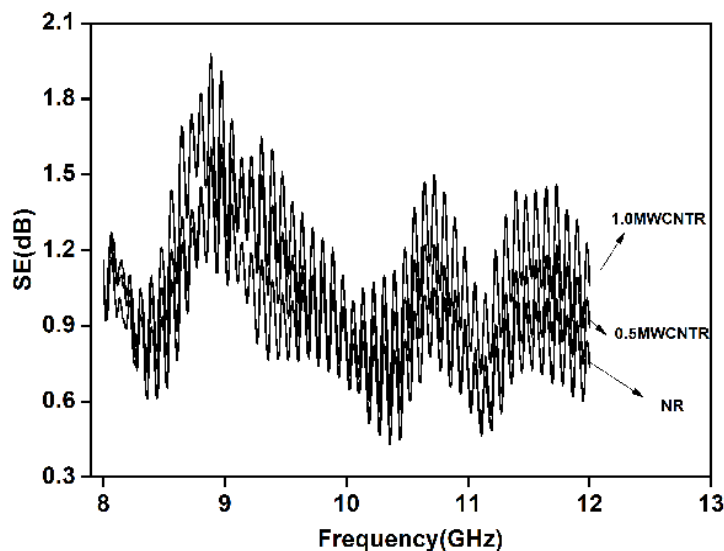
Fig. 4.B.11 Variation of SE with frequency of NR-MWCNTR composites

4.B.4 Conclusions

NR-MWCNTR composite with segregated nanotube network has been prepared by the latex stage incorporation of aqueous dispersion of MWCNTR in NR. Instead of random dispersion, the oxidised nanotubes are found to adhere around NR latex spheres resulting in segregated nanotube network. Very low electrical percolation threshold (0.086 vol%), high

electrical conductivity and dielectric constant exhibited by the composite reveals the presence of segregated structure of MWCNTR within NR matrix with nanotubes distributed at the boundaries between the polymer grains. The network model has been confirmed by TEM and supported by strain sweep studies. These flexible composites exhibit improved mechanical properties with 61%, 75 % and 59 % enhancement in tensile strength, tensile modulus and tear strength respectively even at 0.5 phr loading of MWCNTR. The inclusion of 1.0 phr MWCNTR in the NR matrix increases the dielectric constant from 4.7 (for pure NR) to 918 at 100 Hz. The AC conductivity of NR reaches a value of 10^{-4} S/m for 1phr MWCNTR. The composites exhibit good solvent barrier properties along with a marginal improvement in thermal stability. This nanoscale, flexible, reinforced natural rubber based composites with high dielectric constant and conductivity can find application as electromagnetic wave absorbers in the low frequency region.

References

[1]   Bhattacharyya, S., Sinturel, C., Bahloul, O., Saboungi, M. L., Thomas, S., & Salvetat, J. P. (2008). Improving reinforcement of natural rubber by networking of activated carbon nanotubes. *Carbon*, *46*(7), 1037-1045.

[2]   D.C Blackley, Latices in Encyclopedia of Polymer Science, Vol.8, 647 2nd edn., John Wiley & Sons, New York, 1987.

[3]   Gao, J. F., Li, Z. M., Meng, Q. J., & Yang, Q. (2008). CNTs/UHMWPE composites with a two-dimensional conductive network. *Materials Letters*, *62*(20), 3530-3532.

[4]   Gong, X., Liu, J., Baskaran, S., Voise, R. D., & Young, J. S. (2000). Surfactant-assisted processing of carbon nanotube/polymer composites. *Chemistry of materials*, *12*(4), 1049-1052.

[5]   Nah, C., Lim, J. Y., Cho, B. H., Hong, C. K., & Gent, A. N. (2010). Reinforcing rubber with carbon nanotubes. *Journal of applied polymer science*, 118(3), 1574-1581.

[6]   Francis, L. F., Grunlan, J. C., Sun, J., & Gerberich, W. W. (2007). Conductive coatings and composites from latex-based dispersions. *Colloids and Surfaces A: Physicochemical and Engineering Aspects*, *311*(1), 48-54.

[7]   Jin, S. H., Park, Y. B., & Yoon, K. H. (2007). Rheological and mechanical properties of surface modified multi-walled carbon nanotube-filled PET composite. *Composites Science and Technology*, *67*(15), 3434-3441.

[8]   Payne, A. R., & Whittaker, R. E. (1971). Low strain dynamic properties of filled rubbers. *Rubber chemistry and technology*, *44*(2), 440-478.

[9]   Bokobza, L., & Kolodziej, M. (2006). On the use of carbon nanotubes as reinforcing fillers for elastomeric materials. *Polymer International*, *55*(9), 1090-1098.

[10]   Galimberti, M., Cipolletti, V., Musto, S., Cioppa, S., Peli, G., Mauro, M., ... & Kumar, V. (2014). Recent advancements in rubber nanocomposites. *Rubber Chemistry and Technology*, *87*(3), 417-442.

[11]   Abraham, J., Maria, H. J., George, S. C., Kalarikkal, N., & Thomas, S. (2015). Transport characteristics of organic solvents through carbon nanotube filled styrene butadiene rubber nanocomposites: the influence of rubber–filler interaction, the degree of reinforcement and morphology. *Physical Chemistry Chemical Physics*, *17*(17), 11217-11228.

[12]   Li, Q., Xue, Q., Gao, X. L., & Zheng, Q. B. (2009). Temperature dependence of the electrical properties of the carbon nanotube/polymer composites. *Express Polym Lett*, *3*(12), 769-77.

[13]   Nan, C. W. (1993). Physics of inhomogeneous inorganic materials. *Progress in Materials Science*, *37*(1), 1-116.

[14]   Dang, Z. M., Wang, L., Yin, Y. I., Zhang, Q., & Lei, Q. Q. (2007). Giant dielectric permittivities in functionalised carbon-nanotube/electroactive-polymer nanocomposites. *Advanced Materials*, *19*(6), 852-857.

[15]   Tsuchiya, K., Sakai, A., Nagaoka, T., Uchida, K., Furukawa, T., & Yajima, H. (2011). High electrical performance of carbon nanotubes/rubber composites with low percolation threshold prepared with a rotation–revolution mixing technique. *Composites Science and Technology*, *71*(8), 1098-1104.

[16]   Das, A., Kasaliwal, G. R., Jurk, R., Boldt, R., Fischer, D., Stöckelhuber, K. W., & Heinrich, G. (2012). Rubber composites based on graphene nanoplatelets, expanded graphite, carbon nanotubes and their combination: a comparative study. *Composites Science and Technology*, *72*(16), 1961-1967.

[17]   Bokobza, L. (2012). Enhanced electrical and mechanical properties of multiwall carbon nanotube rubber composites. *Polymers for Advanced Technologies*, *23*(12), 1543-1549.

[18] Dang, Z. M., Fan, L. Z., Shen, Y., & Nan, C. W. (2003). Dielectric behavior of novel three-phase MWNTs/BaTiO 3/PVDF composites. *Materials Science and Engineering: B*, *103*(2), 140-144.

[19] Pötschke, P., Abdel-Goad, M., Alig, I., Dudkin, S., & Lellinger, D. (2004). Rheological and dielectrical characterisation of melt mixed polycarbonate-multiwalled carbon nanotube composites. *Polymer*, *45*(26), 8863-8870.

[20] Li, N., Huang, Y., Du, F., He, X., Lin, X., Gao, H., ... & Eklund, P. C. (2006). Electromagnetic interference (EMI) shielding of single-walled carbon nanotube epoxy composites. *Nano letters*, *6*(6), 1141-1145.

[21] Yang, Y., Gupta, M. C., Dudley, K. L., & Lawrence, R. W. (2005). Novel carbon nanotube– polystyrene foam composites for electromagnetic interference shielding. *Nano letters*, *5*(11), 2131-2134.

[22] Bryning, M. B., Islam, M. F., Kikkawa, J. M., & Yodh, A. G. (2005). Very Low Conductivity Threshold in Bulk Isotropic Single-Walled Carbon Nanotube–Epoxy Composites. *Advanced materials*, *17*(9), 1186-1191.

.....ഊരു.....

Chapter 5

NANOSILICA AS REINFORCING FILLER IN NATURAL RUBBER LATEX

Colloidal nanosilica has been incorporated in NR latex and the nanocomposites were prepared by two different processes. NR-nanosilica composites prepared by the latex stage mixing of the colloidal nanosilica with NR followed by film casting and curing resulted in segregated filler network due to the alignment of nanosilica along the periphery of the rubber latex spheres on drying. But the composites prepared by co-coagulating the nanosilica dispersion with NR latex followed by drying and mixing in an internal mixer destroyed the segregated network structure and yielded a random dispersion of fillers in the matrix. Comparison of the properties of both vulcanisates revealed that incorporation of nanosilica in the natural rubber (NR) significantly improved the mechanical and solvent barrier properties in both cases without affecting the thermal stability.

NR/NANOSILICA COMPOSITES WITH SEGREGATED NETWORK

5.A.1 Introduction

Silica plays an important role in the rubber industry as a reinforcing mineral filler owing to its ability to impart high tensile strength, tear strength, abrasion resistance, low heat build-up, rolling resistance etc. to the rubber composite[1,2]. Conventional mixing of silica with rubber usually results in non-uniform distribution of silica in the rubber matrix. Moreover the polar hydroxyl groups residing on the surface of silica facilitates hydrogen bonding between the silica particles and results in large aggregates of silica, leading to enhanced filler-filler interaction and poor mechanical properties of rubber composites[3-5].

To overcome the difficulties with the incorporation of silica in rubber many researchers have tried the in situ precipitation of silica in natural rubber latex and such composites are reported to have superior mechanical properties[6-8]. Prasertsri et al. obtained improved mechanical and dynamic properties for the NR composites reinforced with fumed and precipitated silica. They have prepared natural rubber masterbatches by adding the aqueous suspensions of fumed and precipitated silica into the NR latex and obtained good distribution of silica particles in the rubber matrix[9]. Prasertsri et al. have also reported the preparation of NR-composites from NR/silica masterbatches, in which silica suspensions were prepared using laboratory agitator bead mill that resulted in good silica dispersion in NR latex[10]. The composites prepared were compared with those prepared by a conventional method, with and without silane-coupling agent (Si-69) and their results revealed that the NR/silica masterbatches having more than 10 phr of silica exhibited superior mechanical properties.

The NR-MWCNTR composites discussed in the previous chapter were of high dielectric constant and dielectric loss. Keeping in mind that the incorporation of insulating nanosilica particles along with carboxylated MWCNTs could reduce the dielectric loss, the influence of colloidal nanosilica on the properties of NR has been studied in this chapter and the concentration of nanosilica has been optimised for further studies. In the present study latex stage incorporation of colloidal nanosilica to the NR has been done. The chapter has been divided into two parts. First part deals with the film casting and curing of the nanosilica/natural rubber latex compound. Second part deals with the co-coagulation of the colloidal nanosilica with NR latex followed by mixing in an internal mixer. The dependence of processing method on nanocomposite morphology is investigated and differences in the properties of the two types of nanocomposites with respect to filler distribution is also analysed.

5.A.2 Experimental

5.A.2.1 Preparation of natural rubber/ nanosilica (NRSF) composites

Nanosilica colloid was diluted with distilled water and sonicated for 15 minutes using horn type sonicator (13mm, Vibracell Processor VC 750, operating at 40% of the maximum power 750W) in order to separate agglomerated nano silica particles using high energy.

Nanosilica suspensions were added to the NR latex (60% DRC) at various compositions so as to get nanosilica concentration of 1, 2, 3, 4 and 5 phr in the dry NR. These mixtures were sonicated again for 15 minutes using a bath sonicator to achieve uniform distribution of the filler in the NR matrix. After that, latex containing silica was compounded as per formulation given in Table 5.A.1 and stirred well to achieve uniformity. The compounded latex was kept overnight for maturation and then it was cast on flat glass tray in order to get films. The films were dried at 50 °C for 24 h and cured at 100 °C for 20 minutes in an air oven to get NRSF composite films.

Table 5.A.1 Formulation of NRSF composites

Ingredients	Amount (g)
Centrifuged NR latex (60 % DRC)	167
Nanosilica	0, 1, 2, 3, 4, 5
10 % KOH solution	1.0
10 % Potassium oleate solution	1.0
20 % Vulcastab VL	1.0
50 % ZnO dispersion	1.0
50 % ZDC dispersion	2.0
50 % Sulphur dispersion	3.0

NRSF1, NRSF2, NRSF3, NRSF4 and NRSF5 are the notations used for NR/nanosilica composites (prepared by latex stage mixing method), with 1, 2, 3, 4 and 5 phr of nanosilica.

5.A.2.2 Characterisation

Nanosilica was characterised using FTIR, BET, SEM, HRTEM, EDX, XRD and Particle size analyser. Colloidal nanosilica was dried at 70 °C under vacuum for the characterisations except for particle size analysis. For particle size analysis using DLS system the colloidal nanosilica was used as such. Surface morphology of the fractured NRSF composites were examined using SEM and the formation of segregated nanosilica network inside the rubber matrix was confirmed by HRTEM studies.

The tensile test was done on a UTM. Strain-amplitude dependent dynamic mechanical properties of the vulcanisates were measured at room temperature by means of DMA.

Sorption behavior and cross-link density values of the samples were determined by equilibrium swelling method using toluene as the solvent. Thermogravimetric analysis (TGA) was done using a TGA-Q 50 Thermal Analyser.

Further details on the Characterisation are discussed in Chapter 2.

5.A.3 Results and discussion
5.A.3.1 Characterisation of nanosilica
5.A.3.1.1 Fourier transform infrared spectroscopy (FTIR)

Fig. 5.A.1 illustrates the FTIR spectral peaks obtained for nanosilica. Nanosilica particles show a broad peak at 3455 cm^{-1} due to adsorbed water and H-bonded silanol (OH) groups. The peaks at 790 cm^{-1} and 1100 cm^{-1} corresponds to the Si-O-Si and Si-O symmetric stretching respectively and the peak at 1630 cm^{-1} is attributed to the bending vibration of H$_2$O molecules confirming the structure of silica[11,12].
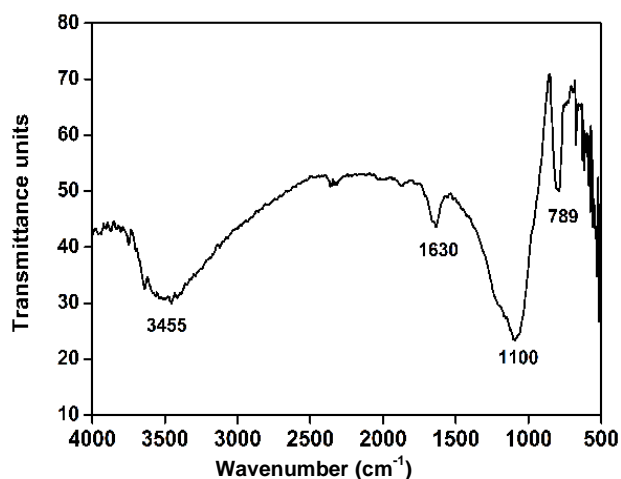
Fig. 5.A.1 FTIR spectrum of nanosilica

5.A.3.1.2 BET surface area analysis

The BET surface area, pore volume and pore size of the silica obtained after charring of the NR/nanosilica masterbatch in muffle furnace at 550 °C is given in Table 5.A.2. The results clearly indicate that the nanosized silica particles have large surface area which is beneficial in reinforcement and the large pore volume provides enough space for the rubber chains to enter into the pores[13].

Table 5.A.2 BET analysis of nanosilica

BET surface area (m²/g)	Pore volume (cm³/g)	Pore size (Å)
235.7	1.14	180.3

5.A.3.1.3 Particle size analysis by DLS

Colloidal silica consists of dense, amorphous particles of SiO_2. Most colloidal silicas are monodisperse suspensions with particle sizes ranging from 2 to 100 nm in diameter. Particle size distribution of nanosilica in the colloidal nanosilica suspension after sonication is clear from the Fig. 5.A.2, which shows broad peak with 90% of the particles having size less than 0.085 µm.
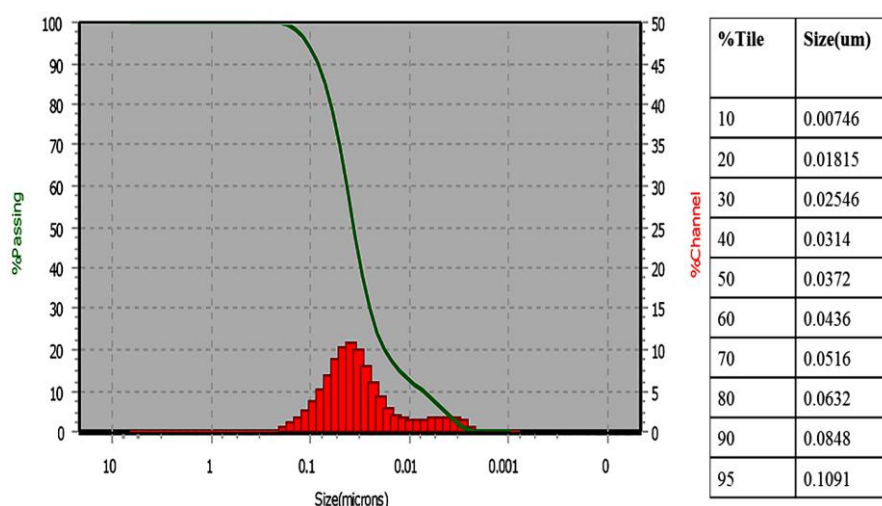
Fig. 5.A.2 Particle size distribution of nanosilica

5.A.3.1.4 Morphological studies of nanosilica

SEM and TEM images of nanosilica give a clear picture of the particles at the microscopic level. SEM analysis supports (Fig. 5.A.3a) the highly agglomerated nature of nanosilica with particles around 140 nm diameter. Individual particles are not clear from the SEM image whereas TEM (Fig. 5.A.3b) clearly shows spherical nanosilica particles in the colloid with diameter less than about 10 nm.
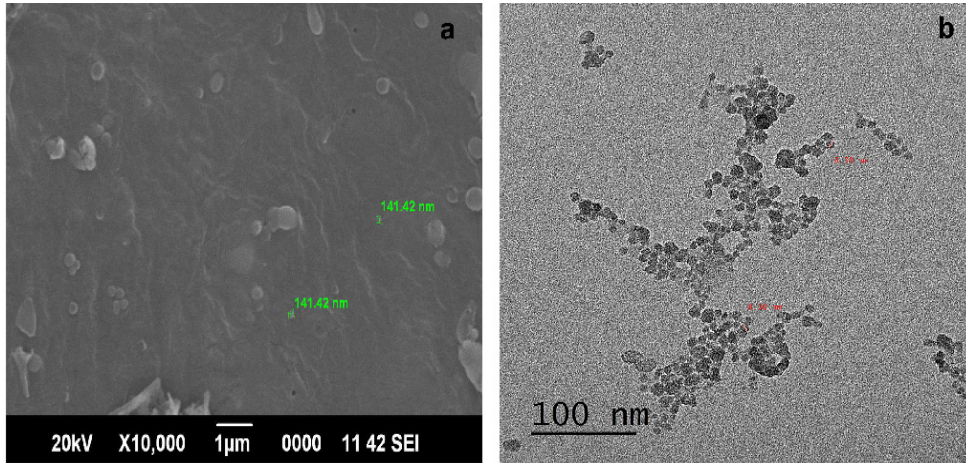
Fig. 5.A.3 Microscopic images of nanosilica using (a) SEM and (b) TEM

5.A.3.1.5 Energy dispersive X-ray spectroscopy (EDS)

Fig 5.A.4 shows the EDS spectrum of nanosilica. The spectrum shows sharp peaks for Si and O atoms only, confirming that the nanosilica has high chemical purity.
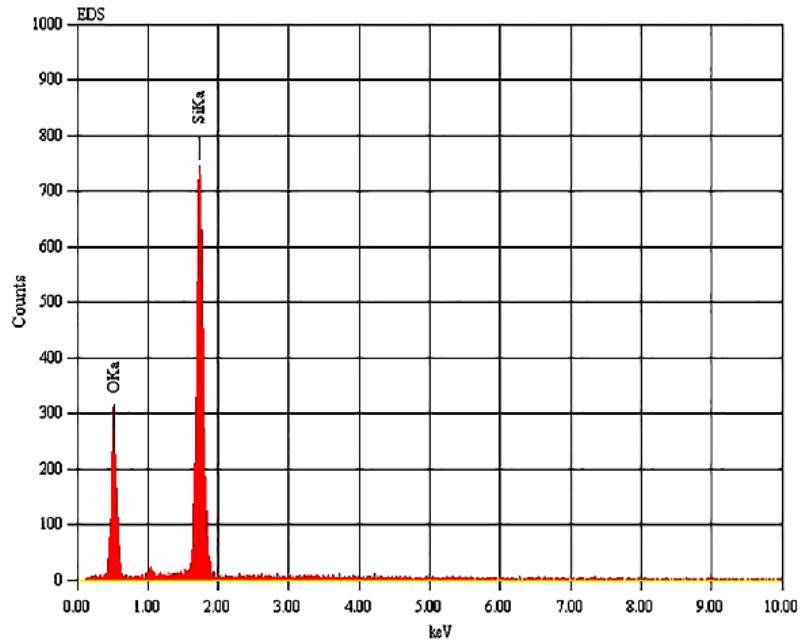
Fig. 5.A.4 EDS spectrum of nanosilica

5.A.3.1.6 X- ray diffraction analysis (XRD)

Fig. 5.A.5 represents the powder X-ray diffraction patterns of nanosilica. The spectrum appears as a broad band with the equivalent Bragg angle at $2\theta = 19.2°$, which indicates that the material is amorphous silica[14].
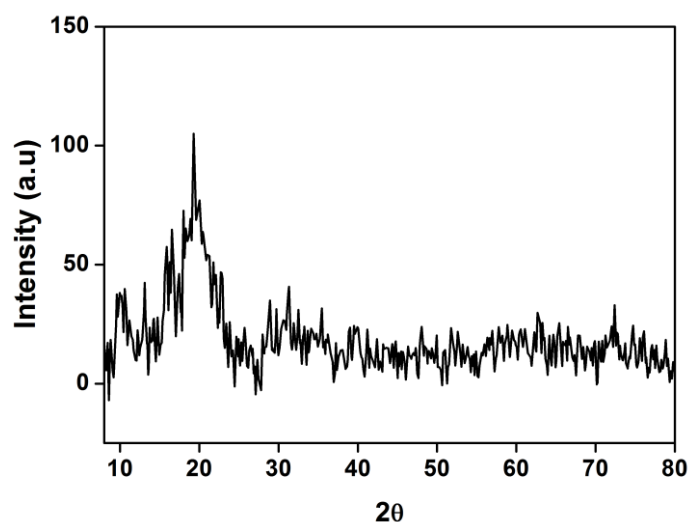
Fig. 5.A.5 XRD patterns of nanosilica

5.A.3.2 Formation of segregated nanosilica network

Latex stage incorporation of nanofillers into rubber followed by film formation or hot pressing favours segregated filler network formation as per the previous reports[15,16]. Fig. 5.A.6 illustrates schematic of segregated network formation of nanosilica in the NRSF nanocomposite. Colloidal nanosilica mix uniformly with the compounded NR latex and are pushed to the periphery of rubber spheres on drying and are located at the interfaces of the rubber particles. The segregated nanosilica structure is retained even after curing since the highly viscous nature of crosslinked rubber prevents the nanofillers from getting inside the rubber.
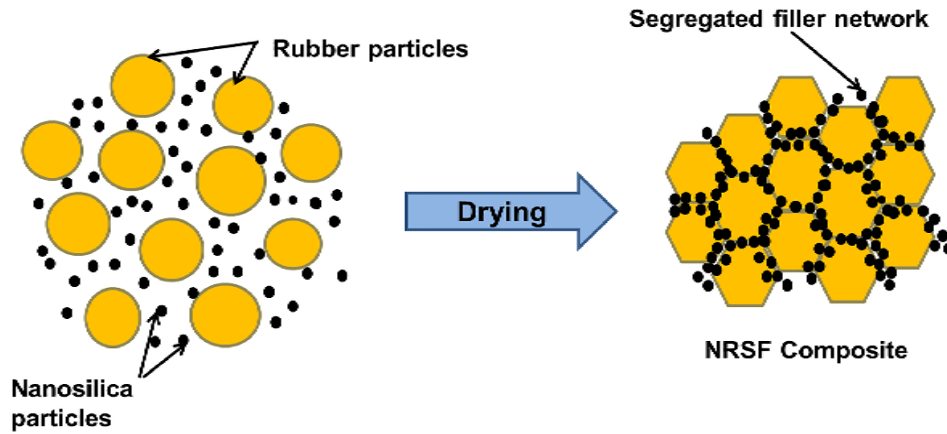
Fig. 5.A.6 Schematic representation of the segregated network formation of nanosilica in NRSF nanocomposite
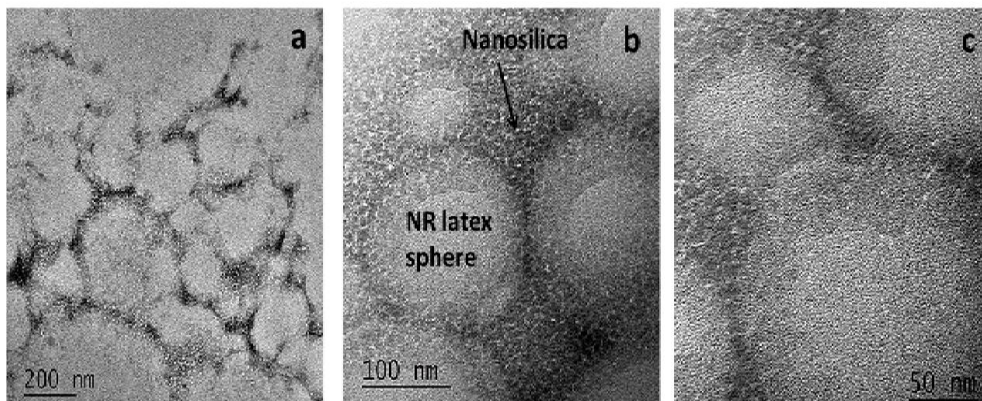
Fig. 5.A.7 TEM images of NRSF4 composite film formed on the TEM grid showing the segregated structure of nanosilica particles in the NR matrix

The proposed scheme has been supported by the TEM images obtained for NRSF4 nanocomposites (Fig. 5.A.7). The nanosilica particles are uniformly dispersed around the spherical rubber latex particles and form a segregated structure.

5.A.3.3 Fracture surface morphology

The tensile and tear fracture surface morphologies of NR and NRSF nanocomposite are shown in Fig. 5.A.8a-f. Tensile and tear fracture surfaces (Fig. 5.A.8a and d respectively) of neat rubber shows smooth patterns where as those of nanosilica filled rubber are very rough with special fracture patterns. The special fracture patterns for segregated structured composites are reported elsewhere[17]. The craters and granular patterns of the fracture surfaces can be explained on the basis of the rigid nanosilica network present throughout the rubber matrix. The surface roughness results from the deviation in tensile and tear paths caused by the presence of segregated nanosilica network.
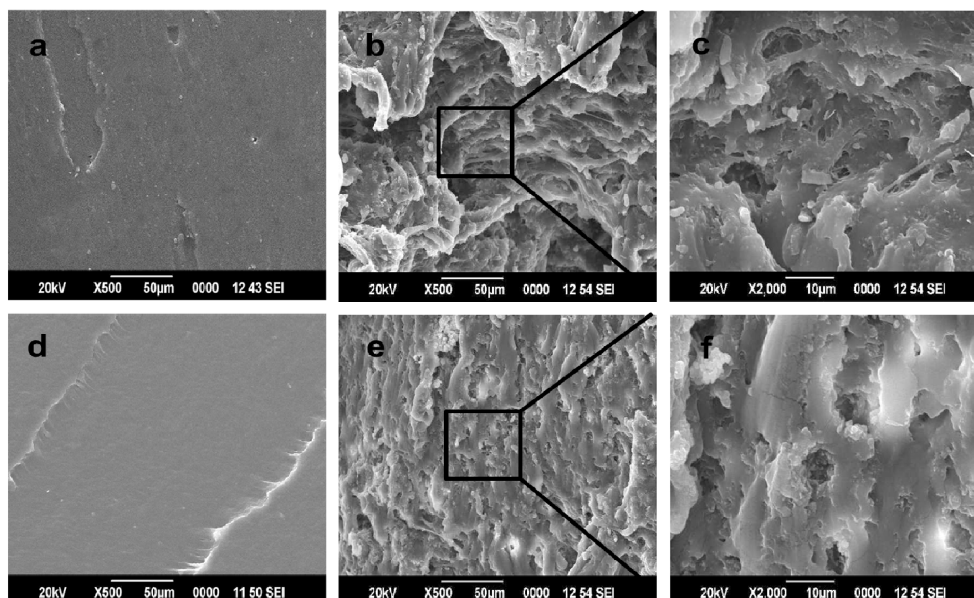
Fig. 5.A.8 SEM micrographs of NR and NRSF composites: (a-c) Tensile fractured surface of (a) NR, (b) and (c) NRSF4; (d-f) Tear fractured surface of (a) NR, (b) and (c) NRSF5

5.A.3.4 Mechanical properties
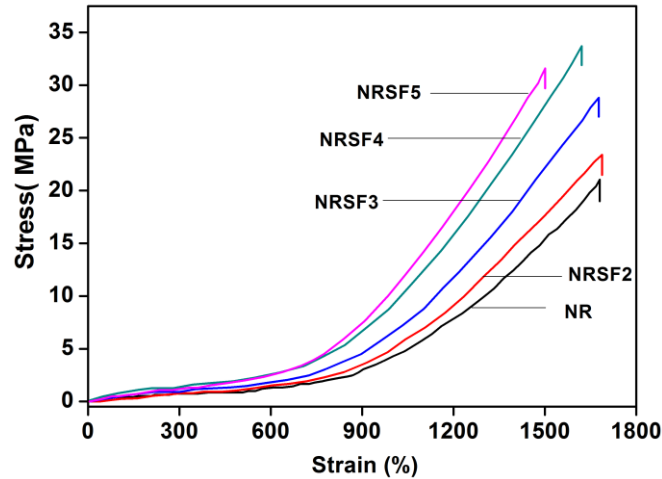
Fig. 5.A.9 Stress-strain graph of NR and NRSF composites

Stress-strain behaviour of NR and NRSF composites is depicted in Fig. 5.A.9. Both NR and NRSF composites exhibit sigmoidal shaped stress-strain curves indicating strain induced crystallisation at high strain values. Strain induced crystallisation becomes more pronounced as the filler concentration increases indicating reinforcing nature of nanosilica.

Fig. 5.A.10 shows the Mooney-Rivlin plots of NR and NRSF nanocomposites and gives clear picture of the reinforcing effect of nanosilica. The plots are based on the following equation

$$\sigma^* = \frac{\sigma}{\alpha - \alpha^{-2}} = 2C_1 + 2C_2\alpha^{-1} \quad ....(5.A.1)$$

where σ^* is the reduced stress, σ is the nominal stress, α is the extension ratio and $2C_1$ and $2C_2$ are constants independent of α. σ^* is equal to the elastic modulus E as per James and Guth approach[18]. Mooney-Rivlin plots show an enhancement in σ^* with nanosilica addition at all deformations. Strain induced crystallisation is characterised by an upturn in the curve and this shifts to

higher α^{-1} (lower extension ratio) as the filler concentration increases. The modulus (the reduced stress) enhancement in the present case can be ascribed to the factors viz. the rigid segregated network of the nanofillers causing mechanical restrain of the rubber chains, enhanced strain induced crystallisation and alignment of filler particles during stretching[19,20].
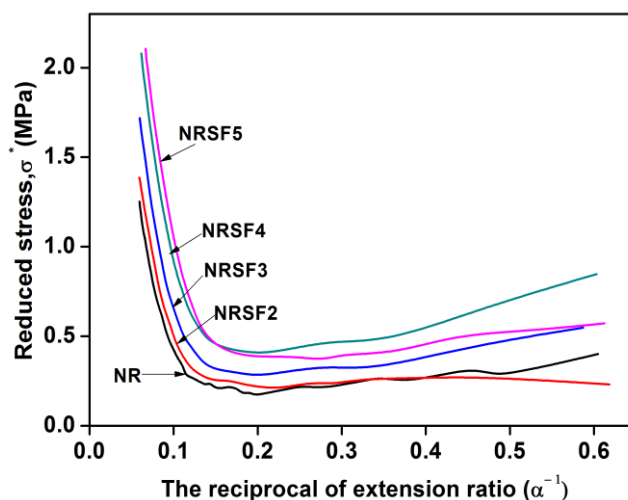
Fig. 5.A.10 Mooney-Rivlin plots of NR and NRSF nanocomposites

Mechanical properties of pure NR and NRSF nanocomposites at different nanosilica loadings are given in Fig. 5.A.11. There is significant improvement in tensile strength on incorporation of nanosilica into the rubber. The tensile strength shows an improvement by 60% by the addition of only 4 phr of nanosilica. Further addition of silica causes a decrease in tensile strength which can be due to the silica-silica particle aggregation.

One of the problems for natural rubber latex products is their poor tear resistance. However it is evident from the figure that tear strength has improved significantly by the incorporation of silica. At 5 phr of nanosilica the tear strength shows almost 157 % enhancement compared to neat NR. This significant improvement in tear strength can be better explained with the help of segregated network of nanosilica around the rubber latex

spheres. The network restricts the polymer chain mobility and increases the mechanical properties of the polymer including tear resistance.[21] The network also prevents the easy propagation of crack though the rubber matrix and imparts improved tear resistance for the composite.
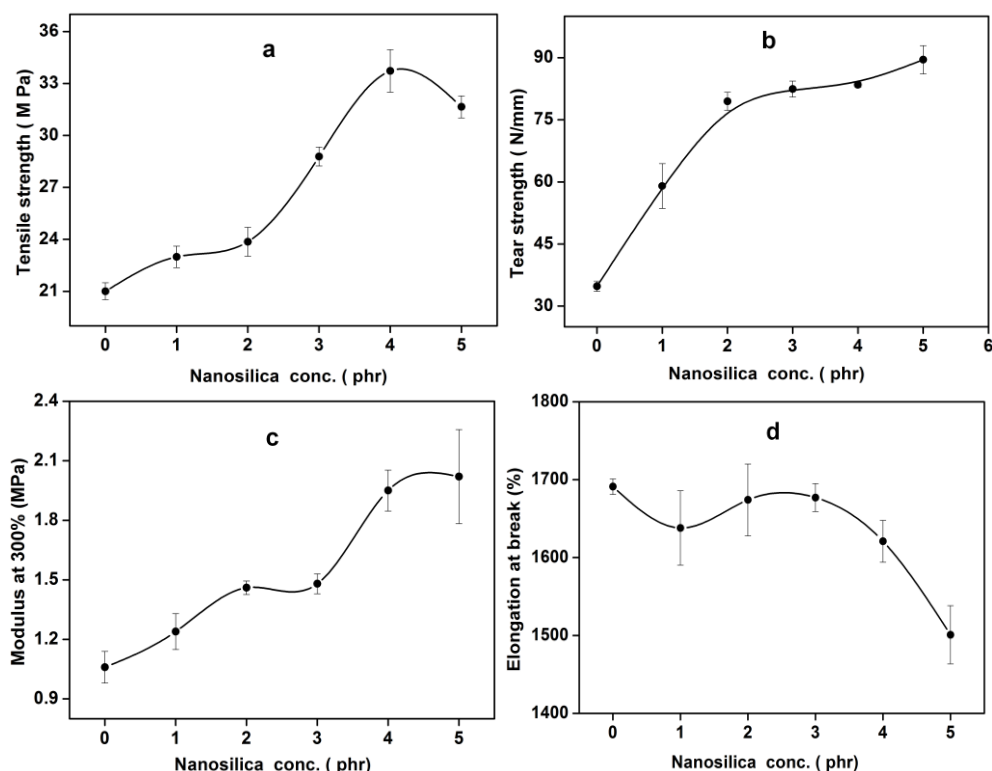
Fig. 5.A.11 **Effect of nanosilica concentration on (a) tensile strength (b) tear strength (c) modulus at 300% elongation and (d) elongation at break of NRSF composites**

Modulus at 300% elongation shows 90 % improvement compared to neat NR by the incorporation of 5 phr of silica. Elongation at break decreases with filler loading due to the reduction in NR chain flexibility caused by the presence of the silica network throughout the matrix.

Significant improvement in mechanical properties of the NRSF nanocomposites can be attributed to the rigid network of the nanosilica located

in the interstitial spaces between the latex spheres which help in dissipating a large amount of energy through the interface, thus bringing better ability to bear loading[22]. Reduction in the mechanical properties after a particular filler concentration can be explained as follows. At low concentrations the nanosilica particles are almost fully separated and well dispersed in the rubber latex leading to the formation of thin filler network around the latex particles. Crosslinks between rubber chains along with diffusion across the latex particles leads to reinforcement whereas at higher filler concentration; especially in the case of silica filler; severe aggregation occurs due to the filler-filler interaction in the segregated network that prevents molecular diffusion between the rubber domains[23]. The film casting method along with poor filler dispersion at higher concentration leads to micro-void formation in the segregated filler path, resulting in inferior mechanical properties[24,25].

5.A.3.5 Strain dependence of viscoelastic properties

Strain dependence of storage modulus (E') at various silica concentrations for NRSF nanocomposites is shown in Fig. 5.A.12. The plots show typical characteristics of the Payne effect[26]. Figure clearly shows that the magnitude of Payne effect ($E'_0 - E'_\infty$) increases with the nanosilica concentration, where E'_0 and E'_∞ are storage modulus at low and high strain amplitudes respectively. The most commonly accepted reason for this behaviour is the breakdown of the filler-filler networks at high strains. The NRSF composite under study has segregated silica network as evident from TEM and further supports the strain dependent behaviour of the storage modulus, because the Payne effect is strongly influenced by the state of dispersion and aggregation of the filler particles in the rubber matrix[27]. As the silica content increases the silica particles tend to agglomerate and this is favoured by the small particle size (10 ± 5 nm) and high specific surface area (236 ± 2 m^2/g) of the colloidal nanosilica particles used in the present study. As the silica concentration increases the segregated network becomes

more extensive and aggregated with large filler-filler interaction resulting in high storage modulus at low strains and a large decrease at high strains. Amplitude of Payne effect observed in the case of rubber composites with segregated filler structure is larger than that with randomly distributed fillers at same loading level, since the filler network formation occurs at very low filler content in the former.
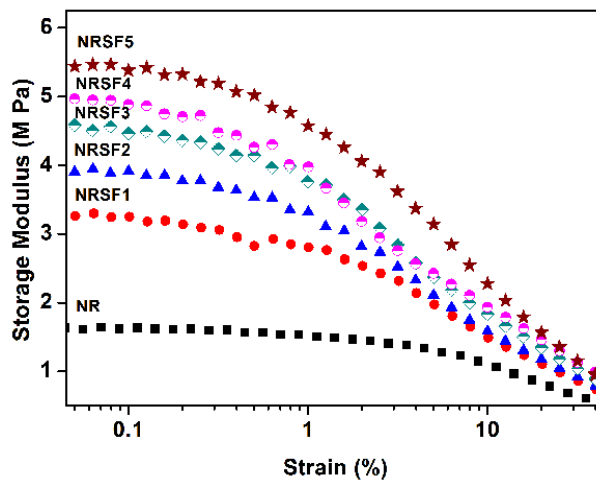
Fig. 5.A.12   Strain dependence of the storage modulus for NR and NRSF nanocomposites

Fig. 5.A.13 shows the variation of loss modulus (E″) with strain amplitude in which all the composites show a maximum in the curve. As the filler loading increases maxima also increases indicating that the dissipated energy increases with silica content. Many factors contribute towards the dissipated energy viz. contribution from the rubbery matrix, contribution from the shearing of the glassy layers around the silica particles and another contribution to the energy dissipation can be from the friction between the nanosilica particles. For bound rubber the friction can be of the rubber chains either on the surface of the filler particles or within the glassy layer during softening when stress is applied. When the filler content increases total surface area of the filler part increases and more will be the amount of

dissipated energy. There is a competition between the breaking and making of filler-filler network, entanglement, glassy bridges etc. As the strain increases the rate of network breakdown exceeds the rate of reconstruction of the network. This explains the loss modulus maxima in the figure[27].
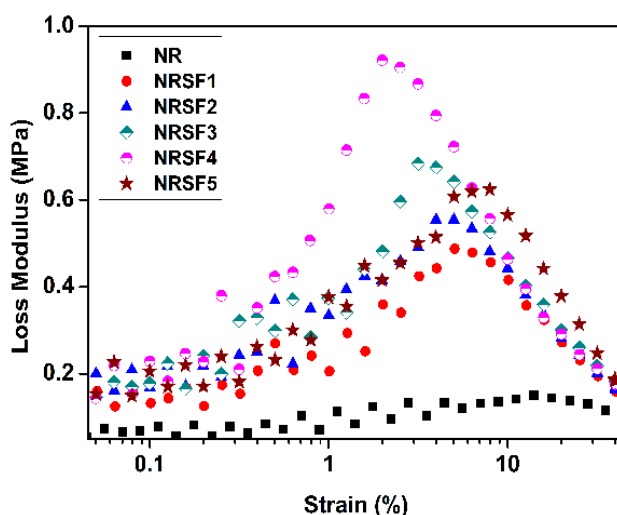
Fig. 5.A.13 Strain dependence of loss modulus for NR and NRSF nanocomposites

Generally accepted principle of Payne effect is that the storage modulus is independent of strain amplitude for unfilled rubber whereas in the present case the neat NR shows a little contradictory behaviour with some variation of storage modulus with strain. Pan and Kelley also reported an enhanced Payne effect near the glass transition region for gum vulcanisates prepared from oil extended styrene-butadiene rubber (SBR)[28]. According to Meera et al.[27], this can be due to the existence of an entanglement network in the unfilled rubber which breaks on increasing the strain causing a decrease in storage modulus.

5.A.3.6 Cross-link density and solvent swelling behaviour

Fig. 5.A.14 illustrates the variation of mol% uptake of toluene (Q_t) versus square root of time ($\sqrt{t}$). Rate of toluene uptake is high in the

beginning, then gradually decreases and reaches a steady value. This steady value known as the equilibrium solvent uptake decreases with increase in nanosilica content in NRSF nanocomposite. Significant reduction in the solvent uptake is observed in the present study. 67 % reduction in Q_t of NR is observed by the incorporation of only 5 phr of nanosilica. Segregated silica structure present in the composite successfully explains this behaviour. Rubber particles are surrounded by the nanosilica network which creates a tortuous path and prevents the easy penetration of solvent through them[29]. As the silica concentration increases the bound rubber also increases which reduces flexibility of the polymer chains thereby reducing the solvent penetration into the rubber[30]. At low concentrations nanosilica particles are homogenously dispersed throughout the rubber matrix causing the passage of solvent molecules very easy. When the filler concentration increases to a level capable of forming an extensive network the transport of solvent molecules through the polymer is hindered[31].
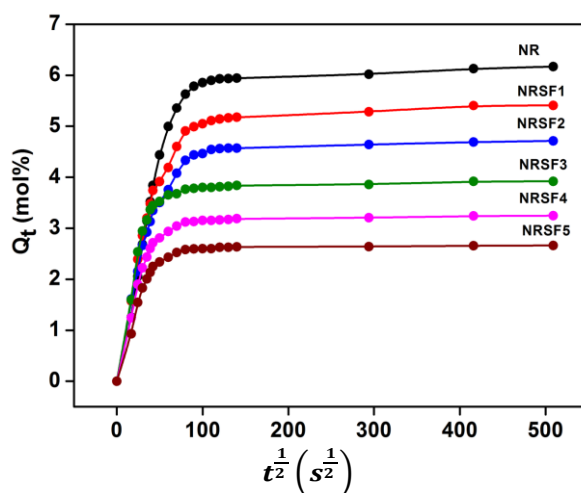
Fig. 5.A.14   Sorption curves of NR and NRSF composites

Fig. 5.A.15 shows the crosslink density and swelling index values of NR with varying nanosilica content. Silica addition improves rubber-filler interaction and hence swelling index shows a decreasing trend indicating

reduction in the solvent uptake since rubber chains are constrained or immobilized on the segregated nanosilica network. As the silica concentration increases network becomes more extended and flexibility of rubber chains are retarded more, slowing down the solvent permeation.
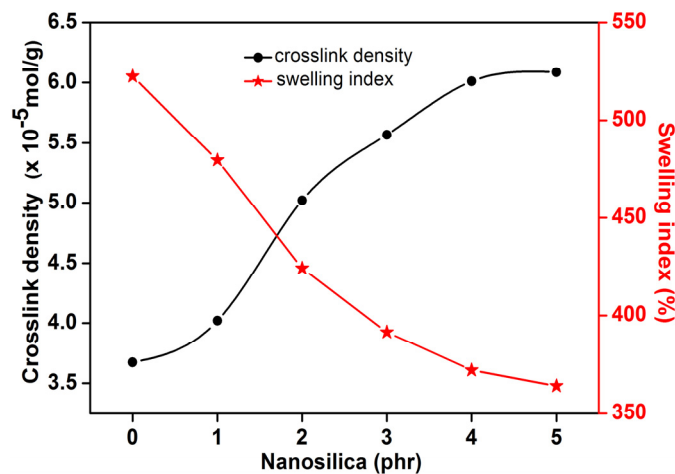
Fig. 5.A.15 Variation of Crosslink density and Swelling index of NR and NRSF composites with nanosilica loading

5.A.3.7 Thermogravimetric Analysis
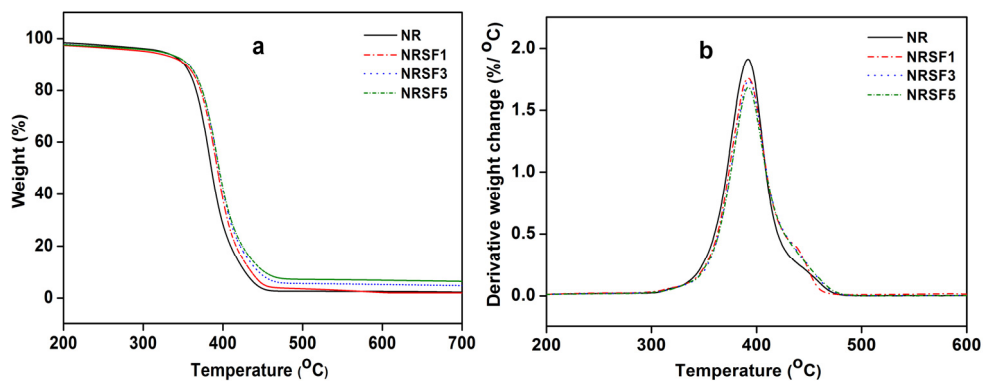
Fig. 5.A.16 TGA (a) and DTG (b) curves of NR and NRSF nanocomposites

Influence of nanosilica on the thermal stability of NR in the present study is clear from the TGA results. Fig 5.A.16 shows the TGA and DTG

curves and Table 5.A.3 shows the relevant data. A nominal increase is observed in the case of the onset, maximum degradation and 50% degradation temperature whereas the degradation rate is decreased with silica loading. This indicates that the thermal stability of the NRSF nanocomposites is slightly improved by the nanosilica segregated structure. The network can act as thermal barrier and reduce the pyrolysis rate by reducing the polymer chain mobility[32].

Table 5.A.3 TGA data for NR and NR-MWCNT nanocomposites

Property	NR	NRSF1	NRSF3	NRSF5
Onset degradation temperature (T_0,ºC)	335	336	337	339
Maximum degradation temperature (T_{max},ºC)	391	392	392	392
Degradation rate at T_{max} (%/ ºC)	1.91	1.76	1.74	1.68
Temperature at 50% degradation (T_{50},ºC)	391	393	394	395
Temperature at 75% degradation (T_{75},ºC)	405	410	414	416
Residue at 600 ºC	1.46	2.14	5.22	6.87

5.A.4 Conclusions

NRSF composites prepared by adding colloidal nanosilica to the NR latex ensure the effective distribution of the nanofillers. The composite microstructure and morphology clearly reveal the segregated structure of nanosilica within the NR matrix. The rigid nano network imparts significant improvement in tear strength (157%) and tensile modulus (90%) even at 5 phr of silica loading. Almost 60% improvement in tensile strength is observed at 4 phr nanosilica indicating better rubber-filler interaction. The network structure of nanosilica is further confirmed from the increasing Payne effect observed with nanosilica loading. 67% reduction in mol% uptake of toluene with 5 phr of nanosilica and improvement in crosslink density indicate the efficiency of nanosilica rigid network in improving the solvent barrier properties.

References

[1] Heinrich, G., Klüppel, M., & Vilgis, T. A. (2002). Reinforcement of elastomers. *Current opinion in solid state and materials science*, *6*(3), 195-203.

[2] Mark, J. E., Erman, B., & Roland, M. (Eds.). (2013). *The science and technology of rubber*. (Chap 9) Academic press.

[3] Wolff, S., & Wang, M. J. (Mark, J. E., Erman, B., & Roland, M. (Eds.). (2013). *The science and technology of rubber*. Academic press. (Chap 9)1992). Filler-elastomer interactions. Part IV. The effect of the surface energies of fillers on elastomer reinforcement. *Rubber chemistry and technology*, *65*(2), 329-342.

[4] Dierkes, W. K. (2005). *Economic mixing of silica-rubber compounds: interaction between the chemistry of the silica-silane reaction and the physics of mixing*. University of Twente.

[5] Sahakaro, K., & Beraheng, S. (2008). Reinforcement of maleated natural rubber by precipitated silica. *Journal of applied polymer science*, *109*(6), 3839-3848.

[6] Kohjiya, S., & Ikeda, Y. (2003). In situ formation of particulate silica in natural rubber matrix by the sol-gel reaction. *Journal of sol-gel science and technology*, *26*(1), 495-498.

[7] Poompradub, S., Thirakulrati, M., & Prasassarakich, P. (2014). In situ generated silica in natural rubber latex via the sol–gel technique and properties of the silica rubber composites. *Materials Chemistry and Physics*, *144*(1), 122-131.

[8] Lin, Y., Zhang, A., Sun, J., & Wang, L. (2013). Properties of natural rubber vulcanisates/nanosilica composites prepared based on the method of in-situ generation and coagulation. *Journal of Macromolecular Science, Part B*, *52*(11), 1494-1507.

[9] Prasertsri, S., & Rattanasom, N. (2012). Fumed and precipitated silica reinforced natural rubber composites prepared from latex system: Mechanical and dynamic properties. *Polymer Testing*, *31*(5), 593-605.

[10] Prasertsri, S., & Rattanasom, N. (2011). Mechanical and damping properties of silica/natural rubber composites prepared from latex system. *Polymer Testing*, *30*(5), 515-526.

[11] Tai, X., hong Ma, J., Du, Z., Wang, W., & Wu, J. (2013). A simple method for synthesis of thermal responsive silica nanoparticle/PNIPAAm hybrids. *Powder technology*, *233*, 47-51.

[12] Pérez-Quintanilla, D., del Hierro, I., Fajardo, M., & Sierra, I. (2006). Adsorption of cadmium (II) from aqueous media onto a mesoporous silica chemically modified with 2-mercaptopyrimidine. *Journal of Materials Chemistry*, *16*(18), 1757-1764.

[13] Wei, L., Hu, N., & Zhang, Y. (2010). Synthesis of polymer—mesoporous silica nanocomposites. *Materials*, *3*(7), 4066-4079.

[14] Singh, D., Kumar, R., Kumar, A., & Rai, K. N. (2008). Synthesis and characterisation of rice husk silica, silica-carbon composite and H3PO4 activated silica. *Cerâmica*, *54*(330), 203-212.

[15] Grunlan, J. C., Kim, Y. S., Ziaee, S., Wei, X., Abdel-Magid, B., & Tao, K. (2006). Thermal and Mechanical Behavior of Carbon-Nanotube-Filled Latex. *Macromolecular Materials and Engineering*, *291*(9), 1035-1043.

[16] Tian, M., Zhang, J., Zhang, L., Liu, S., Zan, X., Nishi, T., & Ning, N. (2014). Graphene encapsulated rubber latex composites with high dielectric constant, low dielectric loss and low percolation threshold. *Journal of colloid and interface science*, *430*, 249-256.

[17] Gao, J. F., Li, Z. M., Meng, Q. J., & Yang, Q. (2008). CNTs/UHMWPE composites with a two-dimensional conductive network. *Materials Letters*, *62*(20), 3530-3532.

[18] James, H. M., & Guth, E. (1943). Theory of the elastic properties of rubber. *The Journal of Chemical Physics*, *11*(10), 455-481.

[19] Fornes, T. D., & Paul, D. R. (2003). Modeling properties of nylon 6/clay nanocomposites using composite theories. *polymer*, *44*(17), 4993-5013.

[20] Mullins, L., & Tobin, N. R. (1965). Stress softening in rubber vulcanisates. Part I. Use of a strain amplification factor to describe the elastic behavior of filler-reinforced vulcanised rubber. *Journal of Applied Polymer Science*, *9*(9), 2993-3009.

[21] Peng, Z., Kong, L. X., Li, S. D., Chen, Y., & Huang, M. F. (2007). Self-assembled natural rubber/silica nanocomposites: its preparation and characterisation. *Composites Science and Technology*, *67*(15), 3130-3139.

[22] Pang, H., Yan, D. X., Bao, Y., Chen, J. B., Chen, C., & Li, Z. M. (2012). Super-tough conducting carbon nanotube/ultrahigh-molecular-weight polyethylene composites with segregated and double-percolated structure. *Journal of Materials Chemistry*, *22*(44), 23568-23575.

[23] Francis, L. F., Grunlan, J. C., Sun, J., & Gerberich, W. W. (2007). Conductive coatings and composites from latex-based dispersions. *Colloids and Surfaces A: Physicochemical and Engineering Aspects*, *311*(1), 48-54.

[24] Zhan, Y., Lavorgna, M., Buonocore, G., & Xia, H. (2012). Enhancing electrical conductivity of rubber composites by constructing interconnected network of self-assembled graphene with latex mixing. *Journal of Materials Chemistry*, *22*(21), 10464-10468.

[25] Jin, S. H., Park, Y. B., & Yoon, K. H. (2007). Rheological and mechanical properties of surface modified multi-walled carbon nanotube-filled PET composite. *Composites Science and Technology*, *67*(15), 3434-3441.

[26] Payne, A. R. (1964). Strainwork dependence of filler-loaded vulcanisates. *Journal of Applied Polymer Science*, *8*(6), 2661-2686.

[27] Meera, A. P., Said, S., Grohens, Y., & Thomas, S. (2009). Nonlinear viscoelastic behavior of silica-filled natural rubber nanocomposites. *The Journal of Physical Chemistry C*, *113*(42), 17997-18002.

[28] Pan, X. D., & Kelley, E. D. (2003). Enhanced apparent Payne effect in a gum vulcanisate at low temperature approaching glass transition. *Polymer Engineering & Science*, *43*(8), 1512-1521.

[29] Galimberti, M., Cipolletti, V., Musto, S., Cioppa, S., Peli, G., Mauro, M., ... & Kumar, V. (2014). Recent advancements in rubber nanocomposites. *Rubber Chemistry and Technology*, *87*(3), 417-442.

[30] F. W. Billmeyer. (1994). Text book of polymer science, Wiley Interscience, A Wiley-lnterscience Publication, John Wiley & Sons, Singapore.

[31] Abraham, J., Maria, H. J., George, S. C., Kalarikkal, N., & Thomas, S. (2015). Transport characteristics of organic solvents through carbon nanotube filled styrene butadiene rubber nanocomposites: the influence of rubber–filler interaction, the degree of reinforcement and morphology. *Physical Chemistry Chemical Physics*, *17*(17), 11217-11228.

[32] Perez, L. D., Zuluaga, M. A., Kyu, T., Mark, J. E., & Lopez, B. L. (2009). Preparation, characterisation, and physical properties of multiwall carbon nanotube/elastomer composites. *Polymer Engineering and Science*, *49*(5), 866.

NR/NANOSILICA COMPOSITES WITH RANDOM NETWORK

5.B.1 Introduction

Conventional method of preparation of silica reinforced rubber involves mechanical mixing followed by compression moulding for vulcanisation. But the large surface area of silica gives rise to high viscosity during mixing. It can also retard the curing and crosslinking of rubber by deactivating the curatives and accelerators. Incompatibility of inorganic silica with organic rubber also prevents the uniform dispersion of the filler inside rubber. In situ precipitation of silica has been reported to be one of the methods to solve these problems and can give more uniform silica distribution and enhanced properties[1-5]. This can be done by sol gel process in which tetraethyl orthosilicate (TEOS) polymerises to produce silica inside the rubber matrix. Here the silica production reaction involves two steps; hydrolysis and condensation. But this method involves the use a large quantity of solvent and takes a long reaction time. This difficulty can be overcome by latex stage precipitation methods which involve the latex stage addition of sodium silicate with subsequent precipitation of silica using ammonia or sulphuric acid[6-8]. The latex stage incorporation of silica is reported to provide uniform distribution leading to better mechanical properties of the resulting composites.

Instead of precipitation, if aqueous silica dispersion can be mixed at the latex stage, the process becomes easier. The present study involves the latex stage mixing of the colloidal nanosilica followed by coagulation. The dried coagulum was then compounded in an internal mixer and cured by compression moulding. From the chapter 5A it is known that latex stage incorporation of colloidal nanosilica in rubber results in segregated network structure. The rigid structure is retained on film formation since the filler

cannot penetrate inside the highly viscous rubber spheres. Similar network can be expected in the dried coagulum of the latex containing filler. But the intense shear forces in an internal mixer during mixing can affect the filler morphology and hence the properties of the composites. So in the present part of study, effect of mixing process in an internal mixer on the morphology and properties of the NRSH nanocomposites prepared by latex coagulation method is proposed to be investigated. Comparative study of both NRSF and NRSH composites is also proposed to be done to understand how the difference in filler morphology influences the overall properties of the composite.

5.B.2 Experimental
5.B.2.1 Preparation of natural rubber/ nanosilica (NRSH) nanocomposites

Nanosilica colloid was diluted with distilled water and sonicated for 15 minutes using horn type sonicator in order to separate agglomerated nano silica particles.

Nanosilica dispersions were added to the NR latex at various compositions so as to get nanosilica concentration of 1, 3, 5 and 7 phr in the dry NR. These mixtures were stirred well using a magnetic stirrer for 15 minutes to achieve uniform distribution of filler in the NR matrix. After that the latex mixes were poured into trays and coagulated by rapid addition of 2% v/v acetic acid solution. The coagula were isolated by vacuum filtration, washed several times with water and dried at 50 °C in an air oven. The dried coagulum containing nanosilica was mixed in an internal mixer (Thermo Haake, at 70 °C, 8 min, 60 rpm) with compounding ingredients as per formulation given in Table 5.B.1 and procedure outlined in the ASTM D 3182. After mixing the batch was passed six times through tight nip in a two-roll mill and was finally sheeted out. The samples were kept overnight for maturation.

Table 5.B.1 Formulation of NRSH composites

Ingredients	Amount (phr)
NR	100
Nanosilica	0, 1, 3, 5, 7
Stearic acid	2.25
ZnO	5.0
Antioxidant SP	1.0
Accelerator MOR	0.75
Accelerator TMTD	0.2
Sulphur	2.5

The cure characteristics of the mixes were determined using Rubber Process Analyser. The optimum cure time, scorch time, maximum torque, minimum torque etc. were determined from the rheograph. The rubber compounds were compression moulded as per procedure outlined in chapter 2 (section 2.2.6) to get NRSH nanocomposites.

5.B.2.2 Characterisation

Microstructure analysis of the samples was done using SEM and TEM. Mechanical properties of the samples were tested according to the relevant ASTM standards. Strain dependent dynamic mechanical properties were evaluated using DMA. TGA and swelling studies were done to understand the thermal and solvent resistance properties.

Detailed description on each characterisation method is given in Chapter 2.

5.B.3 Results and discussion

5.B.3.1 Morphology and microstructure

Schematic representation proposed for the preparation of NRSH nanocomposites is shown in Fig. 5.B.1. Colloidal nanosilica contains nanosilica particles in the aqueous medium and can homogeneously mix with the NR latex. On coagulation, nanosilica particles are pushed to the periphery of the

rubber spheres to give a segregated filler structure. When the dried coagulum is subjected to mixing in an internal mixer, the structure is destroyed and a composite with well-dispersed nanosilica particles is obtained.
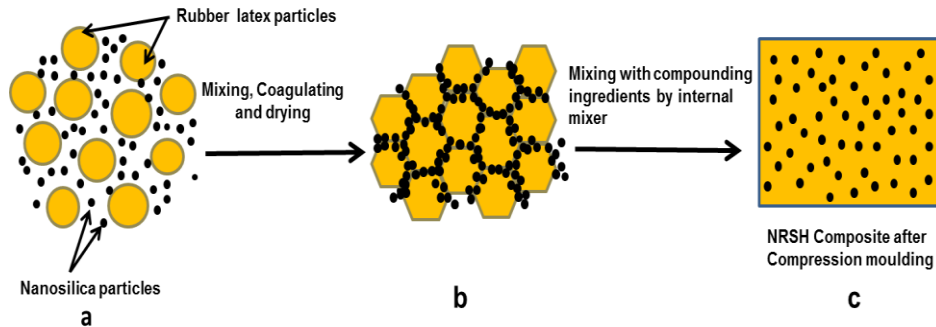
Fig. 5.B.1 **Schematic representation of the preparation of NRSH nanocomposites by latex coagulation followed by Haake mixing (a) colloidal nanosilica particles uniformly distributed in the NR latex (b) nanosilica form segregated structure in the rubber matrix on coagulation and drying (c) Mixing in an internal mixer with compounding ingredients breaks the segregated network and homogeneously distributes the silica particles in the NR matrix**
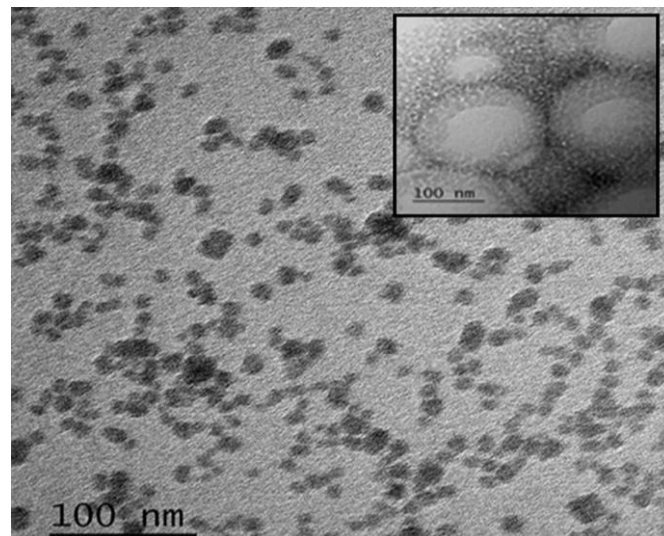
Fig. 5.B.2 **TEM image of NRSH composite containing 5 phr of nanosilica. Inset shows TEM image of the NRSF nanocomposite at 4 phr of nanosilica**

TEM photograph (Fig. 5.B.2) clearly differentiates the microstructure of the NRSH and NRSF nanocomposite. The images provide clear supporting evidence for the suggestion that the processing method has a major role in determining the filler morphology in the polymer matrix[9]. Nanosilica particles are uniformly distributed in the NRSH nanocomposite whereas in the NRSF composite they form a segregated structure. In NRSF composite during film formation, nanosilica particles which are uniformly dispersed in the NR latex are pushed to the interstitial sites between the rubber particles, giving web-like nanosilica network inside the rubber. The processing method adopted for the NRSH composite is different which involves co-coagulation of the NR latex and colloidal nanosilica followed by mixing the dry coagulum in Haake mixer as mentioned before. The web-like nanosilica network present in the coagulum is broken by the intense shear forces in the internal mixer and the final sample has uniformly distributed nanosilica particles in NR matrix.
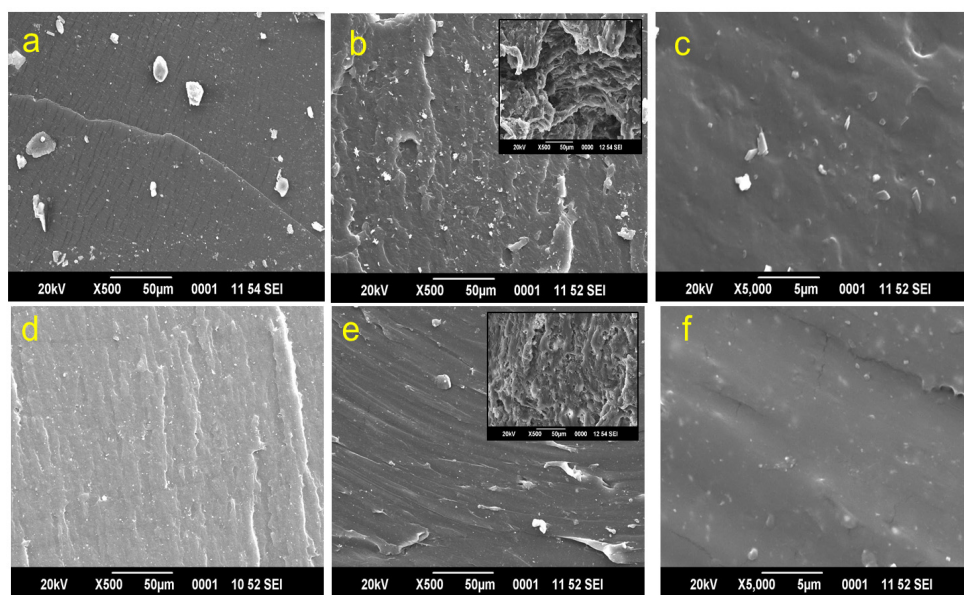
Fig. 5.B.3 SEM images of the fracture surfaces of NRSH composites: tensile fracture surfaces of (a) NR, (b) and (c) NRSH5; tear fracture surfaces of (d) NR, (e) and (f) NRSH5. (b) and (e) insets show the tensile and tear fracture surface images of NRSF5

SEM images of the tensile and tear fracture surfaces shown in Fig. 5.B.3 again supports the difference in filler morphology of the NRSF and NRSH composites. The fracture surfaces in NRSF composites (Fig. 5.B.3b and e inset) show special patterns whereas the surface seems to be smooth in the NRSH composites which can be attributed to the assembly of nanosilica particles around the spherical rubber particles in the NRSF and even distribution of nanosilica in NRSH. Tear lines are more rough in NRSH nanocomposites compared to neat NR indicating that the incorporated nanosilica particles allow better stress transfer and hence promotes the tensile and tear properties.

5.B.3.2 Cure characteristics of NRSH composites

The cure graphs of NR and NRSH nanocomposites at 150 ºC are given in Fig.5.B.4. The initial decrease in torque is due to the softening of the rubber matrix, which is followed by a sharp increase in torque due to the crosslinking between the rubber chains and finally reaches a steady value on completion of curing.
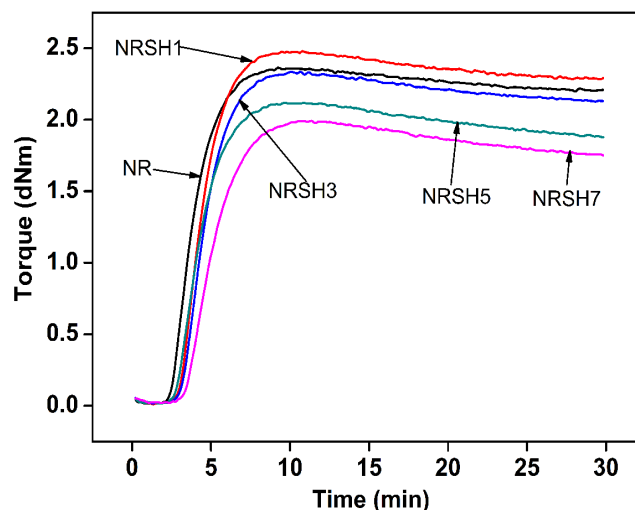
Fig. 5.B.4 Cure curves of the NRSH nanocomposites

The cure characteristics of the NRSH nanocomposites are summarized in Table 5.B.2. The scorch time (T_{10}) and cure time (T_{90}) of the NR compounds increase while cure rate index decreases with increasing silica content. Increase in scorch time ensures scorch safety of the compound[10]. Silanol groups on the surface of silica particles are acidic and can retard the curing efficiency by reacting with basic accelerators and activators leading to an increased cure time[11].

Table 5.B.2 Cure characteristics of NRSH nanocomposites

PROPERTIES	NR	NRSH1	NRSH3	NRSH5	NRSH7
Min. torque. M_L (dN.m)	0.001	0.006	0.010	0.016	0.016
Max. torque, M_H (dN.m)	2.37	2.48	2.35	2.25	2.0
$\Delta M = M_H - M_L$ (dNm)	2.37	2.48	2.34	2.23	1.98
Scorch time, T_{10} (min)	2.67	3.24	3.32	3.33	3.63
Opt. cure time, T_{90} (min)	5.90	6.39	6.72	7.02	7.42
Cure rate index (min^{-1})	30.96	31.75	29.41	27.10	26.39

The decrease in maximum torque (M_H) with silica loading can be related to the high thermal history of these compounds during mixing, resulting from the high viscosity of compounds on adding silica, leading to the breakdown of NR molecular chains.

5.B.3.3 Mechanical properties

Stress-strain curves given in Fig. 5.B.5 show the reinforcing nature of nanosilica. Strain induced crystallisation in NR becomes more pronounced as the silica content increases. Homogeneous filling of the colloidal nanosilica in NR can enhance the stress at a given strain. Mooney-Rivlin plots in Fig. 5.B.6 as per equation 5.B.1 further supports the reinforcing nature of added colloidal nanosilica in NR.

$$\sigma^* = \frac{\sigma}{\alpha - \alpha^{-2}} = 2C_1 + 2C_2\alpha^{-1} \quad\text{...(5.B.1)}$$

where σ^* is the reduced stress, σ is the nominal stress, α is the extension ratio and $2C_1$ and $2C_2$ are constants independent of α. σ^* can be equated to

the elastic modulus E as per James and Guth approach[12]. An increase in elastic modulus is observed for all the composites. Strain induced crystallisation is indicated by an upturn in the curve and this upturn shifts to higher α^{-1} as the silica content in NR increases. The large surface area of the nanosilica particles can favour the early onset of strain induced crystallization and thus restrict the mobility of rubber chains which enhances the modulus of the NRSH composites.
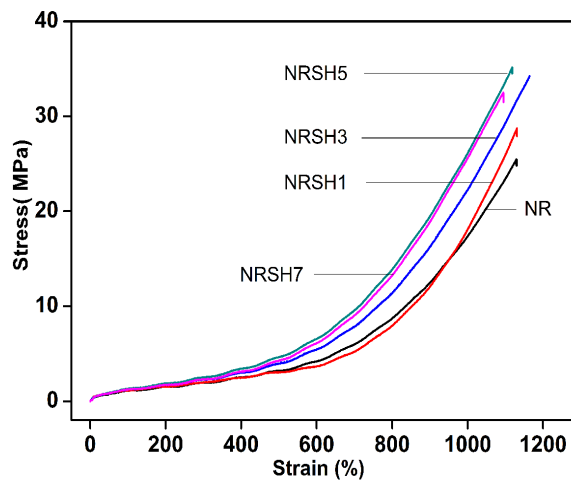
Fig. 5.B.5 Stress-strain curves of NR and NRSH nanocomposites
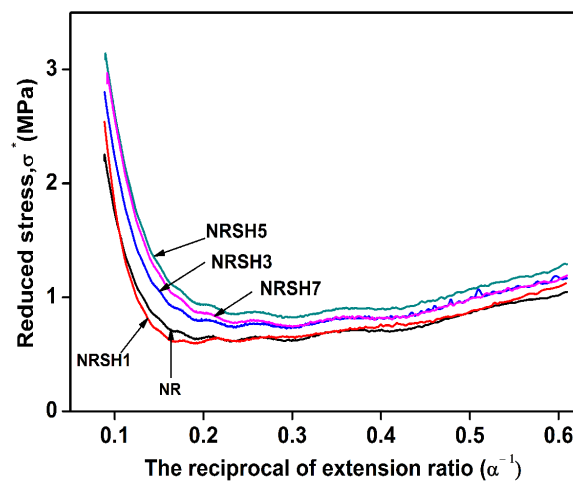
Fig. 5.B.6 Mooney-Rivlin plots for NRSH nanocomposites

Mechanical properties of the NRSH nanocomposites are summarized in Table 5.B.3. The tensile strength, tear strength and modulus (300%) of NR have been improved by nanosilica addition. The elongation at break of the NRSH composites remains almost the same compared to neat NR. NRSH5 nanocomposite exhibits best properties with 28% enhancement in modulus, 38% in tensile strength and 29% in tear strength. The results suggest that latex stage mixing and coagulation causes homogeneous filling of nanosilica in rubber which increases the rubber-filler interaction and produces good reinforcement effect[13]. The uniform filler distribution and improved rubber-filler interaction permits the dissipation of external energy by viscoelastic processes[14]. The well distributed nanosilica particles also play a major role in delaying the onset of failure by deflecting or arresting the growing cracks. Enhancement in the degree of strain induced crystallisation of NR with nanosilica loading as evident from Fig. 5.B.5 has major role in improving mechanical properties of NR vulcanisates[15]. The upward trend in properties is halted after NRSH5 which can be due to the replacement of the silica-rubber interactions by silica-silica interactions leading to aggregation of the filler particles and poor mechanical properties[16].

Table 5.B.3 Mechanical properties of NR and NRSH nanocomposites

Sample Name	Tensile strength(MPa)	Elongation at break (%)	Modulus 300 % (MPa)	Tear strength (N/mm)
NR	25.4±0.4	1154±52	1.96±0.09	36.7±0.5
NRSH1	28.7±1.1	1131±42	1.96±0.08	38.5±0.9
NRSH3	34.2±0.6	1164±64	2.27±0.10	45.4±1.1
NRSH5	35.1±0.9	1118±55	2.50±0.06	47.3±0.4
NRSH7	32.5±1.4	1094±88	2.28±0.04	32.7±0.7

Other mechanical properties like abrasion resistance index, compression set, hardness and rebound resilience of NR and NRSH composites are given in Fig. 5.B.7. Abrasion resistance of a material is the ability to resist mechanical

rubbing or erosion[17]. Compared to neat rubber, NRSH nanocomposites exhibit greater abrasion resistance and almost 70 % improvement is observed in the case of NRSH5 composite. Improved wear resistance has been reported for composites with good distribution of silica due to the improvement in interfacial rubber-filler interaction[18,19]. Compression set is found to decrease with silica loading, with 36% reduction exhibited by NRSH5. Rebound resilience measures the elasticity of the material and is found to increase marginally by the nanosilica addition which is in agreement with the elongation at break observed for the NRSH composites compared to NR.
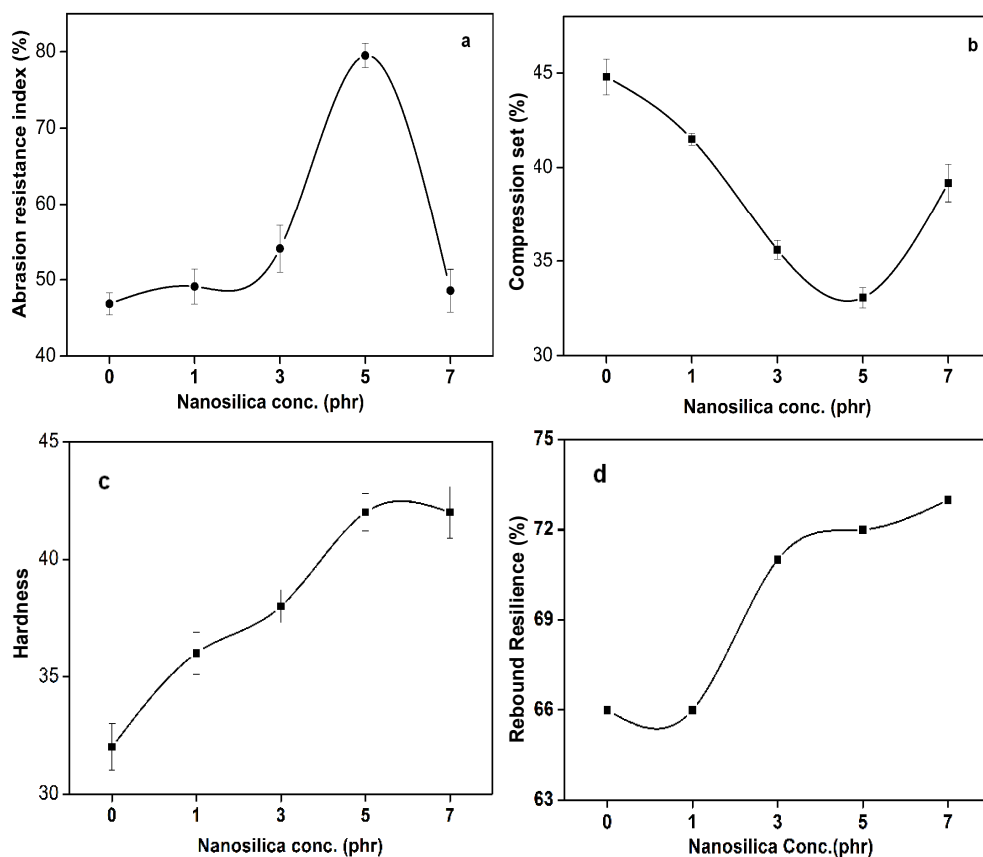
Fig. 5.B.7 Variation of (a) Abrasion resistance index (b) Compression set (c) Hardness and (d) Rebound resilience of NR and NRSH composites with nanosilica loading

Hardness of the nanocomposites increased with silica loading which can be due to the restriction in the rubber chain flexibility on incorporation of rigid silica filler into the matrix. Moreover the well distributed nanosilica fillers provide larger surface area which enhances the rubber-filler interaction and increase the hardness.

5.B.3.4 Comparison of mechanical properties of latex film cast samples with Haake mixed samples

Mechanical properties of the latex film cast (NRSF) and Haake mixed (NRSH) samples are compared in Fig. 5.B.8. Regardless of the processing conditions the mechanical properties of both NRSF and NRSH composites are enhanced with silica loading. Tensile strength of the Haake mixed samples are found to be higher compared to the film cast samples which can be explained in terms of higher cross-link density exhibited by the Haake mixed sample compared to film cast one. Relative increase in tensile strength compared to neat rubber is the same for both. Modulus at 300% elongation of all the Haake mixed samples is higher than that of film cast samples. Elongation at break for both NRSF and NRSH samples remains the same for all the compositions with a slight decrease observed for the NRSF composite with 5 phr silica. The observation is contradictory to earlier reports suggesting that segregated network causes abrupt increase in modulus and hence sharp reduction in elongation at break[20,21]. However relative increase in modulus with silica loading is high for the NRSF composites which can be credited to the segregated silica network. Slight decrease in elongation at break observed for 5phr nanosilica loading in NRSF suggests that as the concentration of the filler increases more fillers are accommodated in the interstitial regions between the rubber particles, preventing inter-particle diffusion of rubber chains thereby resulting in increased stiffness causing failure at lower strain compared to neat rubber[22]. There is significant improvement in tear strength for the NRSF nanocomposites

compared to NRSH which again supports the reinforcing nature of the segregated structure. These structures can deviate the tear lines and increase resistance to crack propagation in the matrix resulting in very high tear strength.
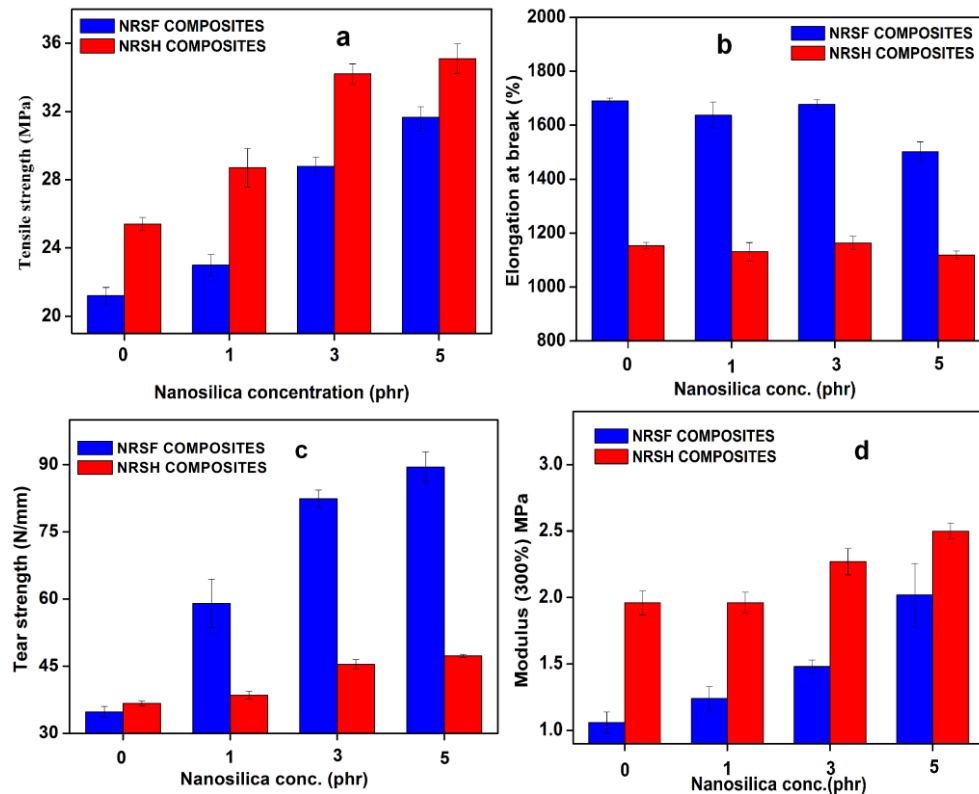
Fig. 5.B.8 Comparison of mechanical properties of NRSF and NRSH composites

5.B.3.5 Strain dependence of storage modulus

Payne effect is the dependence of storage modulus (E') on strain especially in the low strain region and this behaviour is exhibited by filled rubbers. Here the filler-filler network breakage occurs at high strains and causes decrease in storage modulus. Variation of storage modulus with strain for the NRSH composites is given in Fig. 5.B.9 and that of NRSF is shown as the inset. In NRSH samples, Payne effect is not so prominent compared to NRSF which shows the absence of filler network in the former

because NRSF contains segregated nanosilica network whereas NRSH contains randomly distributed nanosilica. This is a clear evidence for the difference in the distribution of nanosilica particles in both samples. The silica-silica network and hence the interaction is more pronounced in NRSF and hence exhibit large decrease in E' with strain. In NRSH composites with random distribution of silica, the amount of filler-filler interaction is less and hence there is a reduction in the amplitude of Payne effect compared to NRSF. In both samples neat rubber also shows strain dependent variation of storage modulus which can be explained in terms of the entanglement network present in neat rubber as suggested by Meera et al.[23].
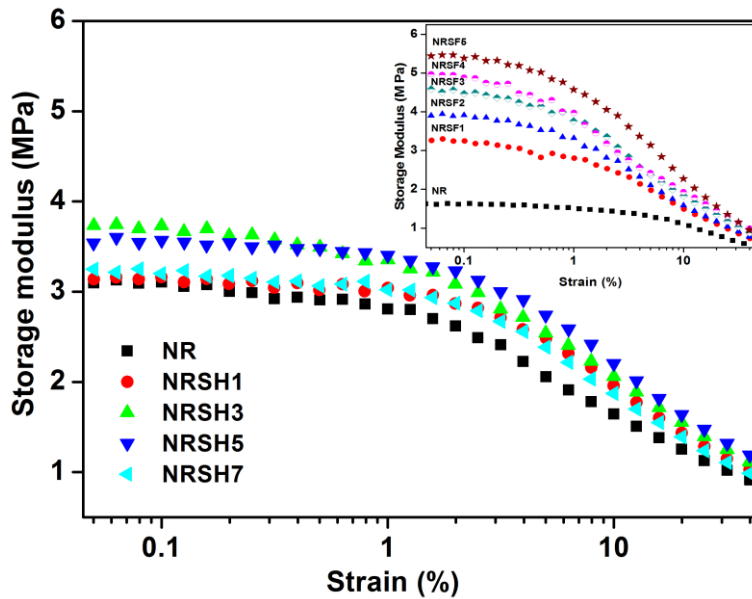
Fig. 5.B.9 Variation of storage modulus with strain of NRSH and NRSF (inset) nanocomposites

5.B.3.6 Swelling studies

Swelling index and cross-link density of the NRSH composites with different silica contents is given in Table 5.B.4. As can be seen, the swelling index tends to decrease with increasing nanosilica loading. This can be

either due to the dilution effect or improved cross-link density, or both. Increase in silica-rubber interaction due to the homogenous distribution of nanosilica particles achieved by the latex stage mixing can also impart improved solvent resistance in the case of NRSH composites. Crosslink density improvement with silica loading is clear from the data and successfully explains the reinforcing nature and hence improvement in mechanical properties of the nanocomposites.

Table 5.B.4 Crosslink density and Swelling index of NR and NRSH composites

Sample name	Crosslink density (x 10^{-5} mol/g)	Swelling Index (%)
NR	5.0	407
NRSH1	5.4	386
NRSH3	5.7	369
NRSH5	6.7	326
NRSH7	4.7	396
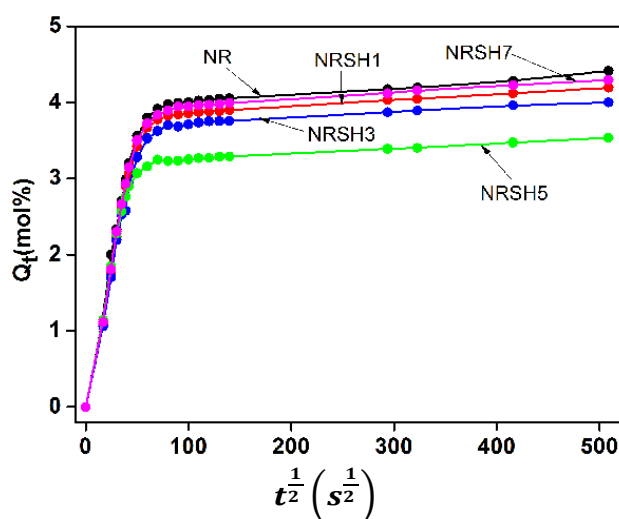
Fig. 5.B.10 Sorption curves of NR and NRSH composites

Fig. 5.B.10 shows the sorption behaviour of NRSH composites. Equilibrium solvent uptake decreases with nanosilica content with least solvent uptake observed at 5 phr loading and beyond that an increase in the

solvent uptake is observed. NRSH composites have more evenly distributed nanosilica and these filler particles can create tortuous path and can slow down the solvent penetration inside rubber. The increase in solvent uptake beyond 5 phr can be due to the presence of aggregates of silica at high concentration which creates free spaces though which the solvents can easily penetrate[24,25].

5.B.3.7 Thermal studies

Fig. 5.B.11(a) and (b) respectively shows the TGA and DTG curves of NRSH nanocomposites whereas Table 5.B.5 shows the relevant data.
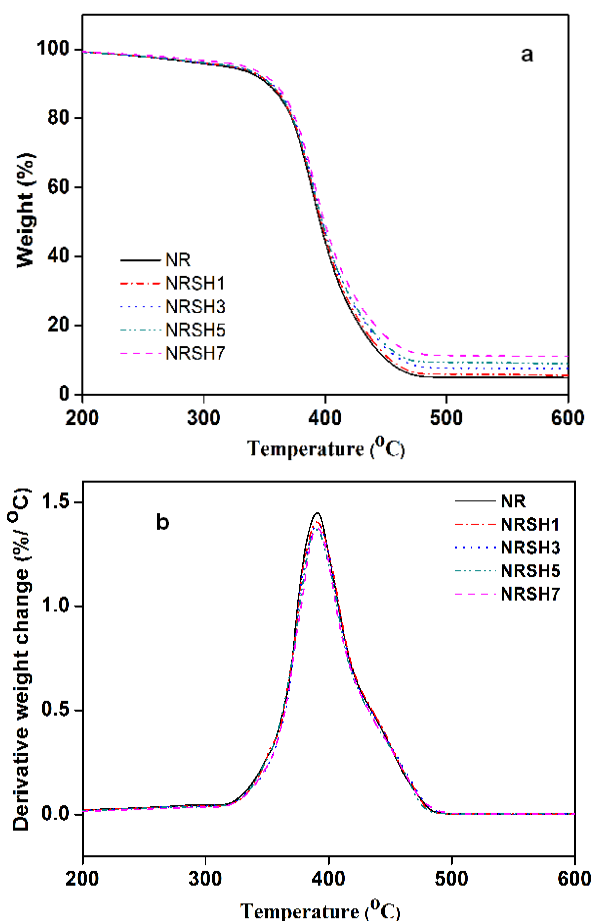
Fig. 5.B.11 (a) TGA and (b) DTG curves of NR and NRSH nanocomposites

Thermogravimetric results clearly reveal that the thermal stability has not been affected by the presence of colloidal nanosilica and there is a marginal increase in the thermal stability of NRSH composites compared to NR. The slight improvement in the thermal stability of the composites can be explained in terms of the homogenous distribution of silica nanoparticles causing strong interaction between the filler and matrix by the combination of nucleation effect, size effect and surface effect. This slows down the thermal degradation of the composites[26]. Another reason can be the migration of inorganic particles to the surface of the polymer due to their relatively low surface potential energy and the NR/SiO_2 char formed can act as a barrier preventing the thermal degradation of the rubber inside[27,28].

Table 5.B.5 TGA data for NR and NRSH nanocomposites

Property	NR	NRSH 1	NRSH 3	NRSH 5	NRSH 7
Onset degradation temperature (T_0,°C)	331	336	333	331	329
Maximum degradation temperature (T_{max},°C)	390	390	391	391	391
Degradation rate at T_{max} (%/ °C)	1.45	1.41	1.39	1.37	1.37
Temperature at 50% degradation (T_{50},°C)	395	397	397	398	399
Residue at 600 °C (%)	4.98	5.70	7.56	9.00	11.18

5.B.4 Conclusions

NRSH composites prepared by latex stage incorporation of nanosilica followed by coagulation, drying and mixing in Haake internal mixer have random distribution of nanosilica inside NR. The random network has been confirmed by TEM, SEM and strain sweep studies. The composites exhibit

significant improvement in mechanical properties at 5phr silica loading. Improved solvent resistance and crosslink density observed for the NRSH composites indicate good rubber filler interaction. On comparing NRSF and NRSH composites it is found that regardless of the processing conditions the mechanical properties of both NRSF and NRSH composites enhance with silica loading. Tensile strength of the Haake mixed samples are found to be higher compared to the film cast samples which can be explained in terms of higher cross-link density exhibited by the Haake mixed sample. Relative increase in tensile strength compared to neat rubber is the same for both. Modulus at 300% elongation of all the Haake mixed samples is higher than that of film cast samples. Tremendous improvement in tear strength for the NRSF nanocomposites compared to NRSH is attributed to the rigid segregated structure. These results suggest that processing method influences the filler morphology inside a polymer which in turn affects the properties of the composite. Higher mechanical properties are obtained at 5 phr nanosilica loading in both NRSF and NRSH composites.

References

[1]   Ikeda, Y., & Kohjiya, S. (1997). In situ formed silica particles in rubber vulcanisate by the sol-gel method. *Polymer*, *38*(17), 4417-4423.

[2]   Sunada, K., Takenaka, K., & Shiomi, T. (2005). Synthesis of polychloroprene – silica composites by sol-gel method in the presence of modified polychloroprene containing triethoxysilyl group. *Journal of applied polymer science*, *97*(4), 1545-1552.

[3]   Hashim, A. S., Kawabata, N., & Kohjiya, S. (1995). Silica reinforcement of epoxidized natural rubber by the sol-gel method. *Journal of Sol-Gel Science and Technology*, *5*(3), 211-218.

[4]   Ikeda, Y., Tanaka, A., & Kohjiya, S. (1997). Effect of catalyst on in situ silica reinforcement of styrene–butadiene rubber vulcanisate by the sol–gel reaction of tetraethoxysilane. *Journal of Materials Chemistry*, *7*(3), 455-458.

[5] Ikeda, Y., Tanaka, A., & Kohjiya, S. (1997). Reinforcement of styrene–butadiene rubber vulcanisatebyin situsilica prepared by the sol–gel reaction oftetraethoxysilane. *Journal of Materials Chemistry*, *7*(8), 1497-1503.

[6] Maya, K. S., & Rani, J. (2007). Preparation of in situ Precipitated Silica Filled Acrylonitrile Butadiene Rubber Composites. *Progress in Rubber, Plastics and Recycling Technology*, *23*(4), 259.

[7] Raman, V. S., Das, A., Stöckelhuber, K. W., Eshwaran, S. B., Chanda, J., Malanin, M., ... & Heinrich, G. (2016). Improvement of mechanical performance of solution styrene butadiene rubber by controlling the concentration and the size of in situ derived sol–gel silica particles. *RSC Advances*, *6*(40), 33643-33655.

[8] Maya, K. S., Joseph, R., Varkey, J. K., & George, B. (2006). Epoxidised natural rubber as a coupling agent in in situ precipitated silica-natural rubber composites. *Journal of Rubber Research*, *9*(4), 204-216.

[9] Zhan, Y., Lavorgna, M., Buonocore, G., & Xia, H. (2012). Enhancing electrical conductivity of rubber composites by constructing interconnected network of self-assembled graphene with latex mixing. *Journal of Materials Chemistry*, *22*(21), 10464-10468.

[10] Okel, T. A., & Waddell, W. H. (1994). Silica properties/rubber performance correlation. Carbon black-filled rubber compounds. *Rubber chemistry and technology*, *67*(2), 217-236.

[11] Sae-Oui, P., Sirisinha, C., Hatthapanit, K., & Thepsuwan, U. (2005). Comparison of reinforcing efficiency between Si-69 and Si-264 in an efficient vulcanisation system. *Polymer testing*, *24*(4), 439-446.

[12] James, H. M., & Guth, E. (1943). Theory of the elastic properties of rubber. *The Journal of Chemical Physics*, *11*(10), 455-481.

[13] S. Blow, Ed.. S. Blow (1998). In: "Handbook of Rubber Technology", Galgotia Publication Ltd, New Delhi, Chapter. 23, 483.

[14] CM. Blow, Ed. CM Blow. (1971). In: "Rubber Teclmology and Manufacture" Published for the Institution of Rubber industry- Butterworths, London, Chapter. 7, 227.

[15] Ikeda, Y., & Kameda, Y. (2004). Preparation of "green" composites by the sol-gel process: in situ silica filled natural rubber. *Journal of sol-gel science and technology*, *31*(1), 137-142.

[16] Sae-oui, P., Sirisinha, C., Wantana, T., & Hatthapanit, K. (2007). Influence of silica loading on the mechanical properties and resistance to oil and thermal aging of CR/NR blends. *Journal of applied polymer science*, *104*(5), 3478-3483.

[17] Wanvimon Arayapranee, Ed. Dr. Marcin Adamiak. (2012). Rubber Abrasion Resistance, Abrasion Resistance of Materials, Chapter 8, ISBN 978-953-51-0300-4.

[18] Arayapranee, W., Na-Ranong, N., & Rempel, G. L. (2005). Application of rice husk ash as fillers in the natural rubber industry. *Journal of applied polymer science*, *98*(1), 34-41.

[19] Choi, S. S. (2002). Improvement of properties of silica-filled natural rubber compounds using polychloroprene. *Journal of applied polymer science*, *83*(12), 2609-2616.

[20] Potts, J. R., Shankar, O., Du, L., & Ruoff, R. S. (2012). Processing–morphology– property relationships and composite theory analysis of reduced graphene oxide/natural rubber nanocomposites. *Macromolecules*, *45*(15), 6045-6055.

[21] Potts, J. R., Shankar, O., Murali, S., Du, L., & Ruoff, R. S. (2013). Latex and two-roll mill processing of thermally-exfoliated graphite oxide/natural rubber nanocomposites. *Composites Science and Technology*, *74*, 166-172.

[22] Steward, P. A., Hearn, J., & Wilkinson, M. C. (2000). An overview of polymer latex film formation and properties. *Advances in colloid and interface science*, *86*(3), 195-267.

[23] Meera, A. P., Said, S., Grohens, Y., & Thomas, S. (2009). Nonlinear viscoelastic behavior of silica-filled natural rubber nanocomposites. *The Journal of Physical Chemistry C*, *113*(42), 17997-18002.

[24] Galimberti, M., Cipolletti, V., Musto, S., Cioppa, S., Peli, G., Mauro, M., ... & Kumar, V. (2014). Recent advancements in rubber nanocomposites. *Rubber Chemistry and Technology*, *87*(3), 417-442.

[25] Abraham, J., Maria, H. J., George, S. C., Kalarikkal, N., & Thomas, S. (2015). Transport characteristics of organic solvents through carbon nanotube filled styrene butadiene rubber nanocomposites: the influence of rubber–filler interaction, the degree of reinforcement and morphology. *Physical Chemistry Chemical Physics*, *17*(17), 11217-11228.

[26] Peng, Z., Kong, L. X., Li, S. D., Chen, Y., & Huang, M. F. (2007). Self-assembled natural rubber/silica nanocomposites: its preparation and characterisation. *Composites Science and Technology*, *67*(15), 3130-3139.

[27] Marosi, G., Marton, A., Szep, A., Csontos, I., Keszei, S., Zimonyi, E., ...& Le Bras, M. (2003). Fire retardancy effect of migration in polypropylene nanocomposites induced by modified interlayer. *Polymer Degradation and Stability*, *82*(2), 379-385.

[28] Gilman, J. W., Jackson, C. L., Morgan, A. B., Harris, R., Manias, E., Giannelis, E. P., ... & Phillips, S. H. (2000). Flammability properties of polymer− layered-silicate nanocomposites. Polypropylene and polystyrene nanocomposites. *Chemistry of materials*, *12*(7), 1866-1873.

…..൭ൿ…..

Chapter 6

NANOSILICA DECORATED MULTIWALLED CARBON NANOTUBES (CS HYBRIDS) IN NATURAL RUBBER LATEX

Multiwalled carbon nanotubes decorated with nanosilica particles (CS hybrids) were prepared for the first time by ultrasonication assisted mixing of the aqueous dispersions of carboxylated multiwalled carbon nanotubes (MWCNTRs) and colloidal nanosilica. Carboxyl groups introduced on the surface of MWCNT by the H_2SO_4/HNO_3 (3:1) treatment enhanced the hydrogen bonding interaction with silanol groups on nanosilica and favoured in getting stable aqueous dispersion of the CS nanofiller hybrids. NR-CS composites were prepared by adopting two different processing methods. NRCSF composites prepared by latex stage mixing method exhibited segregated structure in which nanosilica decorated MWCNTs are aligned along the periphery of the NR latex spheres, whereas NRCSH composites prepared by the Haake mixing method exhibited random filler network. Good dispersion of the nanohybrid fillers in both cases resulted in improved mechanical properties and also enabled the heat dissipation more effective in the composites which is evident from improved thermal stability. Both exhibited good solvent barrier properties. Segregated structure in NRCSF was found to be beneficial in getting good dielectric properties at very low percolation threshold (f_c=0.80 vol% MWCNTR) whereas the random filler structure in NRCSH had a detrimental effect on the electrical properties. The NRCSF composite exhibited low dielectric loss (<1.6 at 10^3 Hz) because of the presence of insulating nanosilica particles around conducting carbon nanotubes, thus preventing the leakage of current by direct contact of MWCNTR.

NR/CS HYBRID COMPOSITES WITH SEGREGATED NETWORK

6.A.1 Introduction

The preparation of percolative composites by dispersing conducting fillers like metal particles[1], carbon black[2], carbon fibers[3], carbon nanotubes[4] and graphite nanoplates[5] in polymer matrix is one of the effective methods to get highly flexible composites with high dielectric constant. Recently carbon nanomaterials are used as conductive fillers in the nonconductive polymer matrix for improving the dielectric constant of the composite which make them a promising material for microcapacitor applications. Normally carbon nanotubes form conductive networks in the polymer matrix which will increase the dielectric constant along with the increase in dielectric loss. Therefore the main challenge is maximising the dielectric constant while minimising the dielectric loss. One of the ways to overcome the drawback of high dielectric loss is to develop a thin insulating layer around the conducting particles thereby preventing the formation of conductive network and thus avoiding direct charge transfer between the conducting particles. Kohlmayer et al.[6] developed high dielectric constant and low dielectric loss polymer nanocomposites using hydroxylated MWCNT as filler. The outer graphene layer is made into nonconducting by covalent functionalisation while keeping the inner graphene layers as unfunctionalised.

In order to get high dielectic property without affecting the polymer flexibility, the dielectric percolation threshold must be achieved at low volume fraction of filler. Preparation of segregated MWCNTR network in natural rubber matrix[7] and its excellent mechanical properties, high dielectric constant and low percolation threshold (0.086 vol%) has been discussed in chapter 4. But the dielectric loss is also high for that composite. Inspired from the works reported in literature, dealing with low dielectric

loss composites, we developed a NR nanocomposite based on conducting MWCNTs decorated with nanosilica particles having high dielectric constant, low dielectric loss and low percolation threshold.

Ultrasonication assisted co-dispersion of carboxylated MWCNT (MWCNTR) and colloidal silica has been done to create an insulating cover of nanosilica over the nanotubes (CS hybrid). Latex stage mixing of CS hybrids with natural rubber latex (NR) was adopted to ensure the segregated network formation at low percolation threshold. Mechanical properties, microstructure, solvent resistance, thermal and electrical properties were studied and the correlation between the properties and microstructure of the composite was explored.

6.A.2 Experimental

6.A.2.1 Preparation of carboxylated multiwalled carbon nanotube-nanosilica hybrid (CS hybrid) dispersions

MWCNT was oxidized using concentrated H_2SO_4/HNO_3 mixture as per procedure given in 4.A.2.1 of Chapter 4 and labeled as MWCNTR. MWCNTRs were separately weighed in calculated amounts so as to get concentrations of 0.5, 1.0, 2.0, 3.0 and 5.0 parts by weight per hundred parts of rubber (phr) in the final composites. To this distilled water was added and the suspension was sonicated for 15 minutes in a bath sonicator and ultrasonicated for 10 minutes using horn type sonicator to get black homogeneous CNT dispersions. Nanosilica dispersion of 5 phr was added to the MWCNTR aqueous dispersions separately and sonicated again for 10 minutes using horn type sonicator. The resulting carboxylated multiwalled carbon nanotube/nanosilica hybrid dispersion was denoted as CS hybrid. The hybrid fillers containing 0.5, 1.0, 2.0, 3.0 and 5.0 phr of MWCNTR along with 5 phr nanosilica were labeled as 0.5C5S, 1C5S, 2C5S, 3C5S and 5C5S respectively.

6.A.2.2 Preparation of natural rubber/carboxylated multiwalled carbon nanotube-nanosilica hybrid (NRCSF) composites

The CS hybrid aqueous dispersion was mixed with NR latex and stirred for 30 minutes. The resulting mix was compounded as per the formulation given in Table 6.A.1 and stirred well to achieve uniformity. After 12 hours of maturation, the latex compound was cast on a flat glass plate, dried at 50 °C for 24 h and cured at 100 °C for 45 minutes in an air oven to get NRCSF composite films. Concentration of nanofillers in each nanocomposite is given in Table 6.A.2.

Table 6.A.1 Compounding formulation of NR latex

Ingredients	Amount (g)
Centrifuged NR latex (60 % DRC)	167.0
Nanosilica	5.0
MWCNTR	0.5, 1.0 ,2.0, 3.0, 5.0
10 % KOH solution	1.0
10 % Potassium oleate solution	1.0
20 % Vulcastab VL	1.0
50 % ZnO dispersion	1.0
50 % ZDC dispersion	2.0
50 % Sulphur dispersion	3.0

Table 6.A.2 Concentrations of the nanofillers in the NRCSF nanocomposites

Composite	Nanosilica (phr)	MWCNTR	
		phr	vol%
NRCSF0.5	5	0.5	0.21
NRCSF1.0	5	1	0.42
NRCSF2.0	5	2	0.84
NRCSF3.0	5	3	1.25
NRCSF5.0	5	5	2.07

6.A.2.3 Characterisation

MWCNTR, nanosilica and CS nanohybrids were characterised using FTIR, TGA, XRD, SEM, HRTEM and UV-vis spectroscopy. Colloidal nanosilica and CS hybrid filler aqueous dispersions were dried in an air

oven at 100 °C to evaporate water and dried samples were used for the analysis. For TEM observation MWCNTR, nanosilica and CS nanohybrids were suspended in water and sonicated for 15 min. The well dispersed suspensions were directly dropped on a TEM grid and dried before observation.

Morphology and microstructure of the NRCSF composites were studied using SEM and HRTEM. The NR latex compound containing CS hybrid filler was diluted and dropped on the copper grids and water was evaporated before TEM observation. The tensile tests were done using Universal Testing Machine as per ASTM D 412 and tear strength was determined by ASTM D 624. The strain-amplitude dependent dynamic mechanical properties of the vulcanisates were measured at room temperature by means of DMA.

Sorption behavior and cross-link density values of the samples were determined by equilibrium swelling method using toluene as the solvent. TGA was done to study the thermal stability of the composites. Dielectric studies were done using Precision Impedance Analyser. DC electrical conductivity measurements were done using a Keithley 2400 source-measure unit. EMI shielding measurements were performed using an Agilent Performance Network Analyser in the X band frequency range.

Detailed description on each characterisation is given in chapter 2.

6.A.3 Results and discussion
6.A.3.1 Characterisation of CS nanohybrid fillers

FTIR spectra of MWCNTR, silica nanoparticles and CS nanohybrid fillers are given in Fig. 6.A.1a. Spectra of nanosilica particles show a broad peak at 3496 cm^{-1} due to adsorbed water and H-bonded silanol (OH) groups. The peaks at 790 cm^{-1} and 1100 cm^{-1} corresponds to the Si-O-Si and Si-O

symmetric stretching respectively and the peak at 1630 cm^{-1} is attributed to the bending vibration of H_2O molecules[8,9]. MWCNTR shows characteristic peaks at 3460 cm^{-1} (-OH stretching), 1742 cm^{-1} (C=O stretch) and 1520 cm^{-1} (C=C stretch in CNT backbone).

The –OH peak in CS hybrid filler is at 3461cm^{-1} for 3C5S, and 3440 cm^{-1} for 1C5S. Broadening of –OH peak due to H-bonding between MWCNTR and silica is not clear from the IR spectra since the silanol groups on silica are H-bonded among themselves and the O-H peak is already shifted to lower wave number. But the broadening of the -OH peak in the CS hybrid and the lowering of intensity when compared to the corresponding peak in MWCNTR confirms the formation of H-bonding between silanol groups on nanosilica and oxygen containing groups on MWCNTR. The peak at 1742 cm^{-1} due to C=O stretch[10] weakens in the hybrid filler confirming the formation of H-bonding. The generation of peak at 1520 cm^{-1} due to aromatic C=C stretch in the CS hybrid fillers suggest that carboxylated carbon nanotubes are embedded in the silica particles with their oxygen containing groups H-bonded to silanol groups on silica.
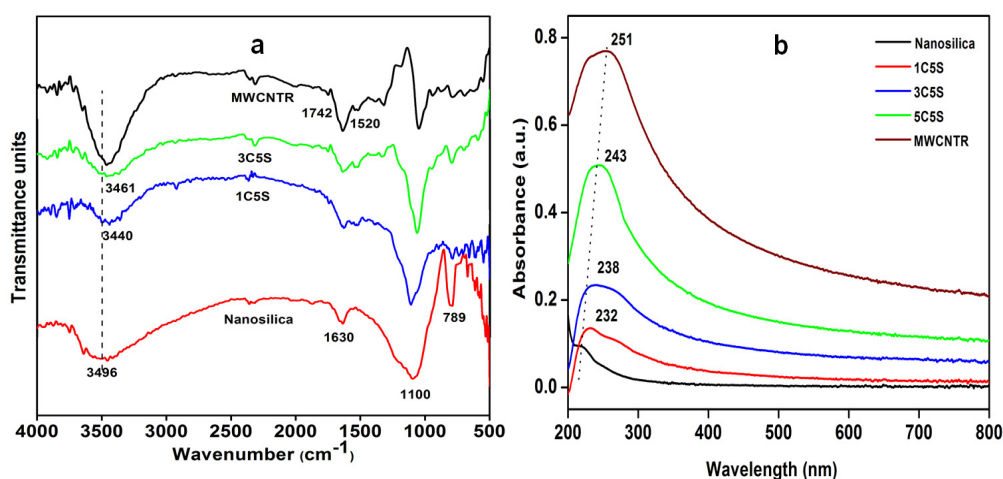
Fig. 6.A.1 (a) FTIR spectra and (b) UV-Visible spectra of MWCNTR, silica nanoparticles and the nanohybrid fillers

UV-visible spectra of dilute aqueous solution of nanohybrid filler, MWCNTR and colloidal silica are shown in Fig. 6.A.1b. The characteristic absorption band of MWCNTR at 251 nm is blue shifted to 243 nm, 238 nm, and 232 nm, respectively for CS hybrid fillers 5C5S, 3C5S and 1C5S. The ultrasonication of MWCNTR with silica helps in the uniform distribution of silica particles over CNT and it leads to a strong interaction between nanosilica and carbon nanotubes through H-bonding. When silica is H-bonded to MWCNTR, >C=O bond in carboxyl group becomes more stabilised making the π-π^{*} transition of high energy causing blue shift of UV absorption wavelength. The broadening of spectra of the nanohybrid compared to nanosilica and MWCNTR also confirms the inter-particle interactions due to H-bonding of silica particles on the sidewall of the nanotubes[11].

The TEM micrographs of CS nanohybrid (5C5S) at different magnifications are shown in Fig. 6.A.2. The images are clear evidence for the presence of silica nano particles on MWCNTR. It is clear from the figure that the MWCNTs are beautifully decorated with nanosilica particles without any aggregation. Strong hydrogen bonding between the oxygen containing groups on MWCNTR and hydroxyl groups on nanosilica helps in the adsorption of nanosilica on the walls of the carbon nanotubes. It is very interesting to note that the attachment of silica on MWCNTR has been achieved by simple ultrasonication assisted mixing of MWCNTR aqueous dispersion and colloidal nanosilica.

Based on the spectroscopic and microscopic analysis, the schematic of hydrogen bond formation in CS nanohybrid is proposed and it is shown in Fig. 6.A.3.
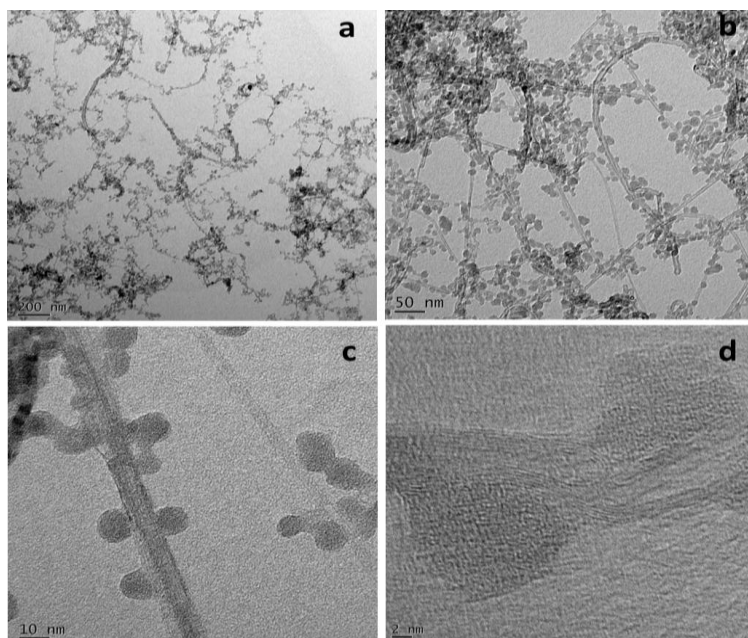
Fig. 6.A.2   High-resolution TEM (HRTEM) images of CS nanohybrid (5C5S) at different magnifications
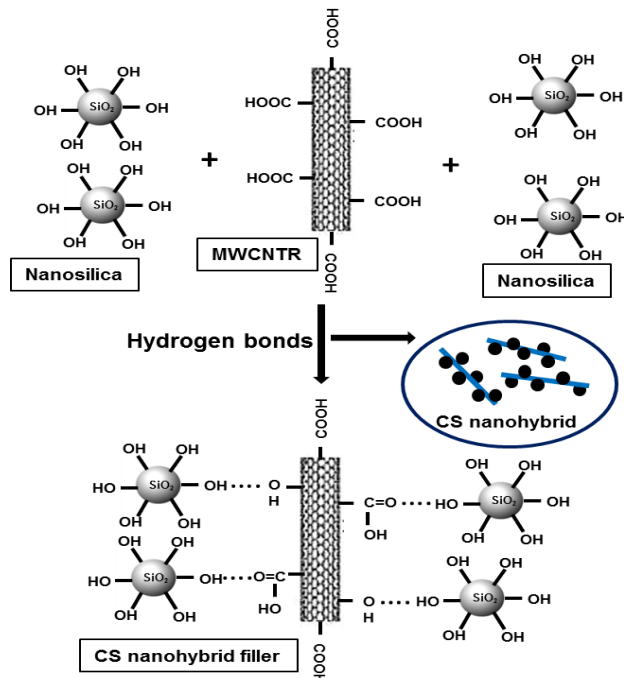
Fig. 6.A.3 Schematic of hydrogen bonding possible in the CS nanohybrid

TGA curves of MWCNTR, nanosilica and nanohybrid fillers are given in Fig. 6.A.4. The initial weight loss starting at 35 ºC and continuing up to around 100 ºC is due to the evaporation of loosely bound water molecules on the surface and the intermolecular hydrogen bonded chemisorbed water[12]. The FTIR spectrum has confirmed the presence of the chemisorbed water. As the MWCNTR to nanosilica weight ratio increases from 1C5S to 5C5S, number of intermolecular hydrogen bonds between silica and MWCNTR increases due to the increase in the oxygen containing groups on the surface of MWCNTR. Intermolecular hydrogen bonding occurs through water molecules which are adsorbed by silica and on heating these molecules escape from the molecules due to the rupturing of H-bonds[13]. Thus TGA curves confirm the presence of intermolecular H-bonding between nanosilica and carboxylated MWCNTs.
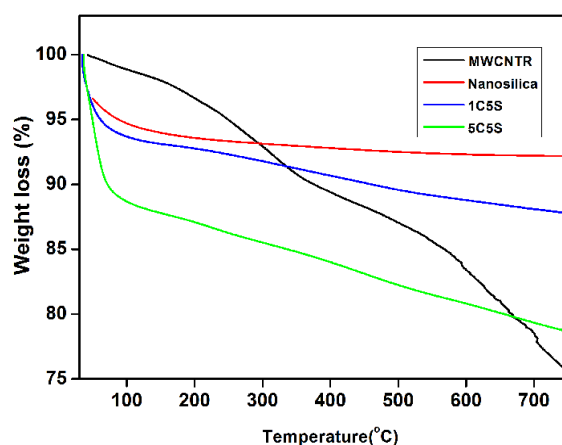
Fig. 6.A.4 TGA curves of MWCNTR, nanosilica and CS hybidfillers

6.A.3.2 NRCSF composites with segregated structure

Schematic representation of the formation of NRCSF composite is given in Fig.6.A.5. The aqueous dispersion of CS hybrid filler (Fig.6.A.5a) is uniformly dispersed in the compounded NR latex (Fig. 6.A.5b) and the hybrid fillers are pushed to the spaces between the compacting latex spheres during drying of rubber latex (Fig. 6.A.5c)[14]. The TEM images of NRCSF2 composite containing 2C5S hybrid are shown in Fig. 6.A.6. The CS hybrid

fillers are uniformly distributed and connected to form a beautiful segregated network structure around the NR particles. Fig. 6.A.6c clearly shows that the silica decorated conducting carbon nanotubes are well dispersed which is beneficial in reducing the electrical percolation threshold. Good distribution of CS hybrid fillers in the NR matrix also guarantees the reinforcement of the rubber at low filler loading.
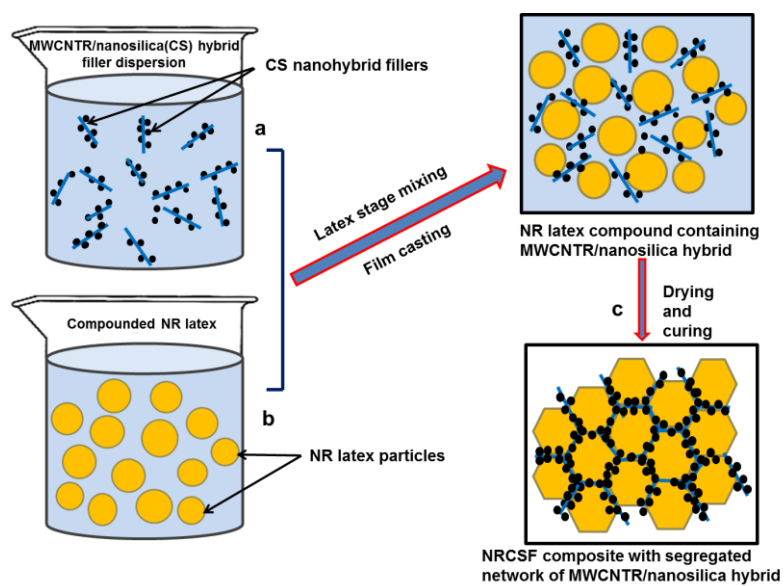
Fig. 6.A.5 Schematic for the preparation of NRCSF composites with segregated network of MWCNTR/nanosilica hybrid
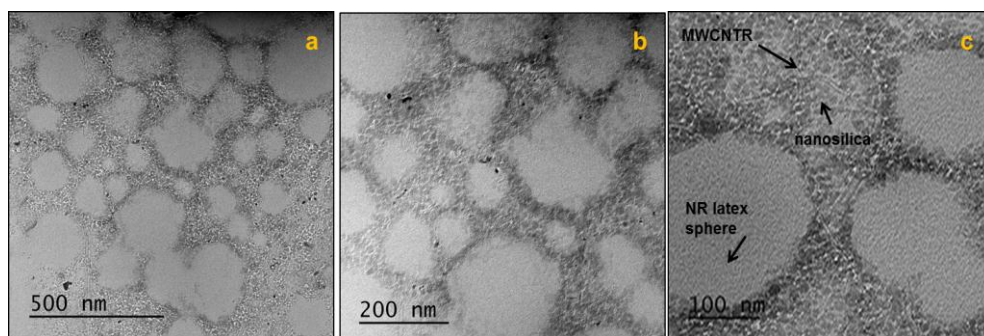
Fig. 6.A.6 (a-c) TEM images of NRCSF2 composite film formed on the TEM grid which shows that the CS nanohybrid fillers form a segregated network in NR matrix

6.A.3.3 Morphology and microstructure

SEM images of the tensile and tear fractured surface of NRCSF composite show significant difference from that of NR as shown in Fig. 6.A.7, but no direct evidence for the presence of fractured CNTs. SEM images of elastomeric polymer nanocomposites with CNTs as fillers do not give clear picture of CNTs on the fractured surfaces of the polymers due to the nanosize of the CNTs or the mismatch in elongation between polymers and CNTs during rupture. The broken ends of CNTs tend to be embedded deeply into the bulk of polymers[15]. But compared to neat NR, the surface of the nanocomposite is very rough and shows special fracture patterns as reported elsewhere[16].
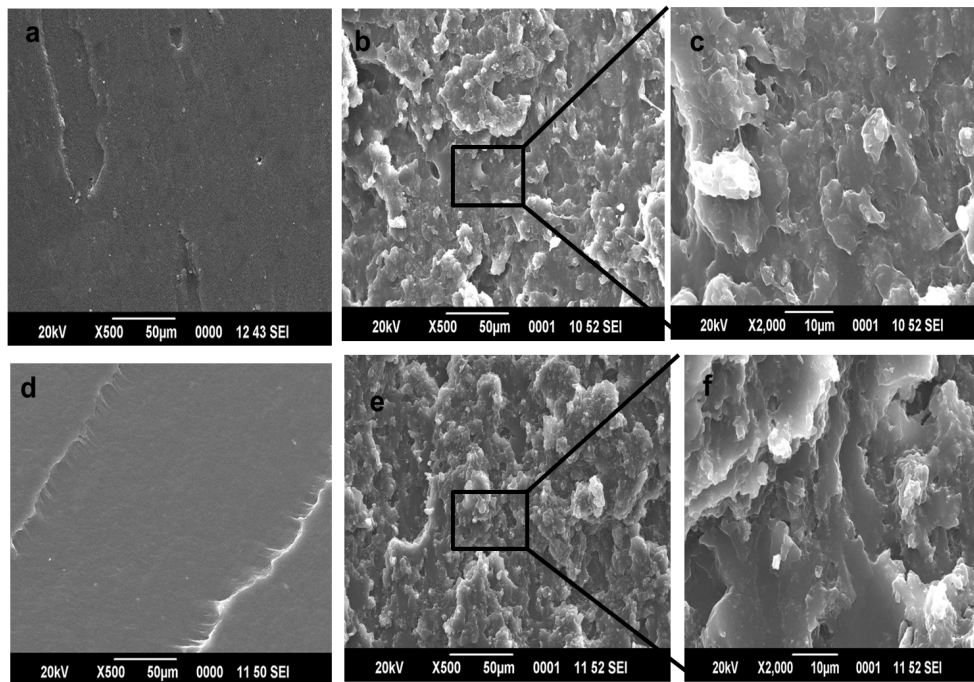
Fig. 6.A.7 SEM images of the nanocomposites: (a–c) Fractured surfaces of tensile test specimens of (a) NR, (b and c) NRCSF2 at different magnifications; (d–f) Fractured surfaces of tear test specimens of (d) NR, (e and f) NRCSF2 at different magnifications

The latex stage mixing method followed by film casting and drying distributes the nanohybrid fillers along the periphery of the rubber latex spheres as evident from TEM micrograph of the composite (Fig. 6.A.6), which results in well-ordered segregated filler network in the rubber matrix. The fracture surface shows granular shapes with craters and special patterns due to the highly ordered segregated network of silica decorated functionalised nanotubes in the rubber. Roughness of the fracture surface of the composite indicates strong adhesion between the network and NR[17]. The tear lines of the NRCSF composite are not straight as in the case of neat NR because of the presence of rigid filler network in the rubber matrix which makes the crack propagation difficult.

6.A.3.4 Mechanical properties

Previous studies on composites with segregated structure of conducting fillers reported inferior mechanical properties which are credited to the weak interfacial interaction between polymer matrix and segregated structure. Moreover the interfacial segregation of the filler largely prevents molecular diffusion between the polymer domains that harm the mechanical behaviours of the composites[18,19]. In this context maintaining or improving the mechanical properties of the neat polymer in these composites is highly beneficial for practical applications.

Stress-strain curves of NRCSF composites (Fig. 6.A.8a) exhibit typical sigmoidal shape, characteristic of neat and filled NR indicating strain induced crystallization at high elongation. The composites exhibit excellent mechanical properties which is clear from the Table 6.A.3. NRCSF2 composite shows best properties with 65% increase in tensile strength, 122% in tensile modulus and 86% in tear strength compared to neat NR and further addition of the nanohybrid filler decreases the properties. Strain at break was found to decrease with the hybrid filler loading, but without any drastic reduction which is contradictory to the findings by Jeffrey et al[18]. According to

them reinforcement of NR with segregated structure of reduced graphene oxide occurs with significant reduction in elongation at break. Significant improvement in the mechanical properties of the NRCSF composites is due to the presence of a rigid network of the hybrid fillers located in the interstitial spaces between the latex spheres which helps in dissipating a large amount of energy through the interface, thus bringing better ability to bear loading[20]. Enhancement in the strain induced crystallization by the addition of high aspect ratio nanohybrid fillers also results in better mechanical properties. Synergetic effect of well dispersed MWCNTs and nanosilica particles also plays an important role in improving the mechanical properties[21].
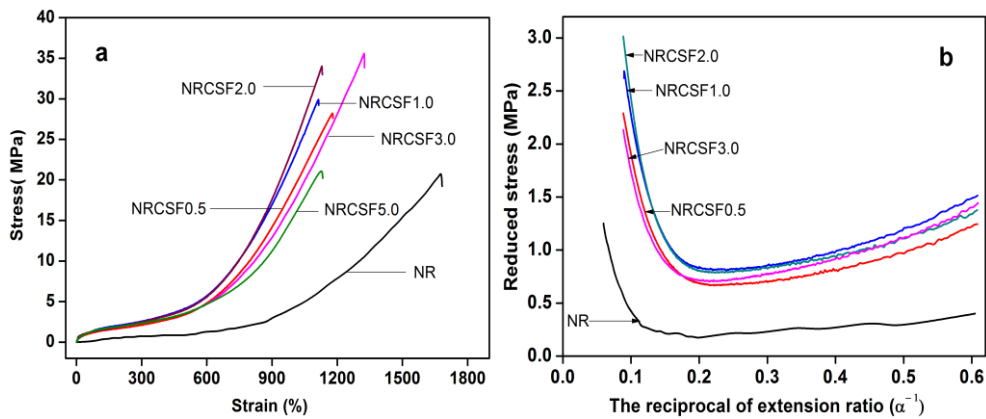
Fig. 6.A.8 (a) Stress-strain curves (b) Mooney-Rivlin plots of NRCSF composites

Fig. 6.A.8b shows the Mooney-Rivlin plots of NR and NRCSF nanocomposites and gives clear picture of the reinforcing effect of the hybrid filler. The plots are based on the following equation

$$\sigma^* = \frac{\sigma}{\alpha - \alpha^{-2}} = 2C_1 + 2C_2\alpha^{-1} \quad ....(6.A.1)$$

where σ^* is the reduced stress, σ is the nominal stress, α is the extension ratio and $2C_1$ and $2C_2$ are constants independent of α. σ^* is equal to the

elastic modulus E as per James and Guth approach[22]. Mooney-Rivlin plots show an enhancement in σ^* with nanofiller addition at all deformations. Strain induced crystallisation is characterised by an upturn in the curve and this shifts to higher α^{-1} (lower extension ratio) as the filler concentration increases. The modulus (the reduced stress) enhancement in the present case can be ascribed to the factors viz. the rigid segregated network of the CS nanofillers causing mechanical restrain of the rubber chains, enhanced strain induced crystallisation and alignment of filler particles during stretching[23,24].

The reason for decrease in mechanical properties after a particular filler concentration can be explained as follows. At low concentrations the fillers are almost fully separated and well dispersed in the rubber latex leading to the formation of thin filler network around the latex particles. Crosslinks between rubber chains along with polymer diffusion across the latex particles leads to reinforcement whereas higher filler concentration can lead to agglomeration of fillers in the segregated network that prevents molecular diffusion between the rubber domains[25]. The film casting method along with poor filler dispersion at higher concentration adds the chance of micro-void formation in the segregated filler path, which leads to inferior mechanical properties[26,27].

Table 6.A.3 Mechanical Properties of NRCSF nanocomposites

Sample Name	MWCNTR (phr)	Nanosilica (phr)	Tensile strength (MPa)	Elongation at break (%)	Modulus 300 % (MPa)	Tear strength (N/mm)
NR	0	5.0	21.2±0.5	1691±10	1.13±0.08	34.8±1.2
NRCSF0.5	0.5	5.0	28.2±0.2	1197±19	2.04±0.07	46.8±0.9
NRCSF1.0	1.0	5.0	29.3±0.6	1194±80	2.41±0.11	55.8±2.2
NRCSF2.0	2.0	5.0	34.0±0.2	1152±22	2.51±0.03	64.7±1.1
NRCSF3.0	3.0	5.0	35±0.6	1306±19	2.35±0.01	47.0±2.6
NRCSF5.0	5.0	5.0	21.3±1.6	1133±73	2.37±0.23	42.1±2.8

6.A.3.5 Strain-amplitude dependent dynamic mechanical properties

Strain dependence of storage modulus (E') for NR and NRCSF composites is depicted in Fig. 6.A.9. Variation of E' at low strain can give information on the filler-filler networks present in the composite. Usually, dynamic properties are independent of strain for neat rubber. Here also neat NR shows strain independent behaviour whereas storage modulus of the composites decreases with strain. This decrease is due to the Payne effect[28] and the effect increases with hybrid filler loading. The most commonly accepted reason for Payne effect is the breakdown of filler-filler networks on increasing strain[29]. This observation also confirms the presence of network of nanohybrid filler in all the nanocomposites.

The modulus values (E′) of all the composites are higher than the unfilled compound. This is due to the hydrodynamic effect of the rigid fillers. Increase in filler concentration leads to increase in bound rubber or trapped rubber in the matrix. This causes increase in the effective volume of the filler causing enhancement in modulus of the rubber[30].
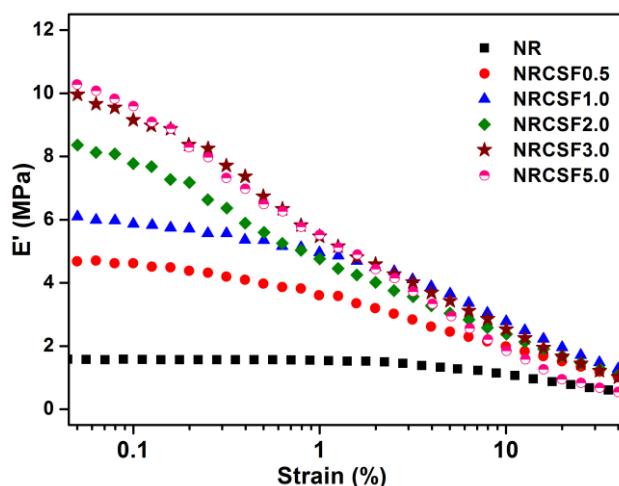
Fig. 6.A.9 **Strain dependence of the storage modulus of NR and NRCSF nanocomposites**

6.A.3.6 Swelling studies

Sorption curves for the NRCSF composites are given in Fig. 6.A.10, in which mol % uptake (Qt %) of toluene is plotted against square root of time ($\sqrt{t}$). It is observed that rate of solvent uptake is high in the beginning due to the large concentration gradient of the penetrant in the composites. Gradually the rate decreases and reaches a plateau indicating the equilibrium solvent uptake. Significant reduction in equilibrium solvent uptake upon addition of the nanohybrid filler can be well explained using the segregated network structure. Here rubber particles are wrapped by the nanohybrid filler network and creates tortuous path that slow down the penetration of solvent through the rubber[31].
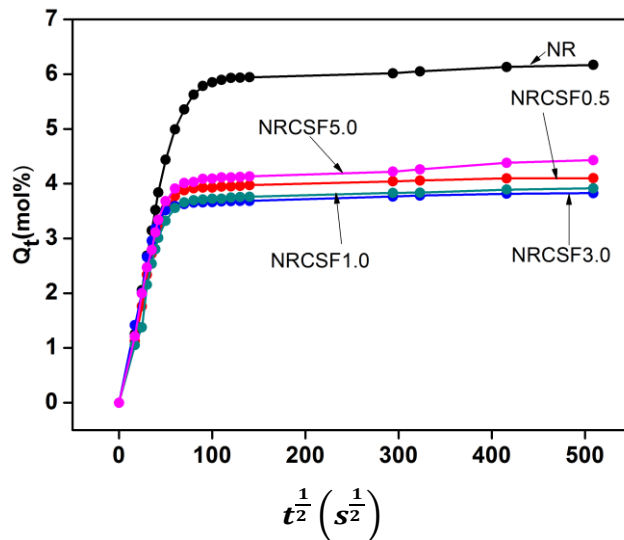
Fig. 6.A.10 Sorption curves of NR and NRCSF composites

Moreover strong interfacial adhesion restricts the chain mobility[32] making the polymer chains less flexible which increases the tortuosity and restricts the entrance of solvent molecules into the interfacial regions. At low concentrations nanohybrid fillers are homogenously dispersed throughout the rubber matrix causing the passage of solvent molecules very easy. When

the filler concentration increases enough to form an extensive network the transport of solvent molecules through the polymer is hindered[33]. There is increase in the solvent uptake for the NRCSF5 composite which may be due to the agglomeration of the fillers in the segregated structure. This agglomeration can lead to micro voids or free volume in the segregated path which allows penetration of solvent into the rubber.

Variation of crosslink density and swelling index of NR and NRCSF composites with addition of the nanohybrid filler is given in Table 6.A.4. Crosslink density slightly increases and reaches maximum for the NRCSF2 composite which indicates increasing rubber-filler interaction on addition of the filler. Swelling index of NR and the nanocomposites shows reverse trend due to the reduction in solvent uptake since rubber chains are constrained or immobilized on the segregated hybrid filler network. 58 % reduction in swelling index was observed for NRCSF2 composite. With addition of filler, extensive networks are formed and segmental motion of rubber chains are more retarded, which slows down the solvent permeation. As the amount of nanohybrid filler further increases agglomeration of nanoparticles occurs leading to porosity and poor rubber filler interaction resulting in slight reduction in crosslink density.

Table 6.A.4 Crosslink density and swelling index of NR and NRCSF composites

Samples	Crosslink density (x 10^{-5} mol/g)	Swelling Index (%)
NR	3.1	568.5
NRCSF0.5	5.8	377.8
NRCSF1.0	6.5	352.7
NRCSF3.0	6.1	360.9
NRCSF5.0	4.9	408.2

6.A.3.7 Thermal studies
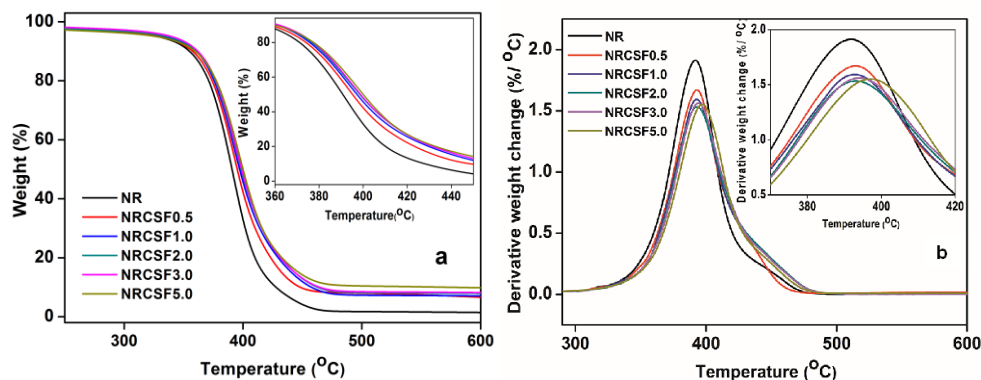
Fig. 6.A.11 (a) TGA and (b) DTG curves of NR and NRCSF nanocomposites

Fig.6.A.11a and 6.A.11b respectively shows the TGA and DTG curves of NR and NRCSF nanocomposites. Thermal stability of NR is slightly improved by the addition of nanohybrid filler as shown in Table 6.A.5.

Table 6.A.5 TGA data for NR and NRCSF nanocomposites

Property	NR	NRCSF0.5	NRCSF1.0	NRCSF2.0	NRCSF3.0	NRCSF5.0
Onset degradation temperature (T_0,°C)	334	334	336	337	336	334
Maximum degradation temperature (T_{max},°C)	391	393	393	393	394	397
Degradation rate at T_{max} (%/°C)	1.91	1.67	1.59	1.53	1.56	1.55
Temperature at 50% degradation (T_{50},°C)	391	395	397	398	399	400
Temperature at 75% degradation (T_{75},°C)	406	416	421	423	423	423
Residue at 600°C	1.46	6.63	7.06	7.95	8.23	9.85

The increase in degradation temperature (T_{max}) while reduction in degradation rate at T_{max}, with addition of nanofillers, suggest improvement in thermal stability. The temperature at which 50% decomposition occurs (T_{50}) is

generally considered as an index of thermal stability and the increase in T_{50} with the addition of the nanohybrid filler again confirms the enhancement in thermal stability of the polymer upon addition of the hybrid filler. The dispersed CS hybrid filler in the rubber matrix helps to dissipate the heat more quickly because of their high thermal conductivity[34,35] and hence the thermal stability of the composite is increased. Good dispersion of nanotubes along with segregated network formation enables the heat dissipation more effective in the composites.

6.A.3.8 Dielectric properties

Fig.6.A.12 shows the room temperature AC conductivity of NRCSF composites as a function of MWCNTR concentration measured at 1 kHz. Increase in conductivity with filler loading is clear from the figure.

Fig. 6.A.12 AC conductivity of the NRCSF composites as a function of MWCNTR concentration measured at 1 kHz and room temperature. Insets show the best fit of the conductivity to Eq. 6.A.2(a) and (b)

The conductivity of a polymer composite containing conductive fillers can be explained in terms of two mechanisms: 1) Ohmic conduction due to direct contact of fillers and 2) non-Ohmic conduction due to the tunnelling

effect between conductive fillers when it is separated by a thin polymer layer. When the concentration of conductive filler reaches percolation threshold there is a transition from non-Ohmic to Ohmic conduction (insulator to conductor transition) which is characterised by an abrupt increase in conductivity of the composite.

According to the percolation theory conductivity (σ) of the composite follows the power law as follows

$\sigma \propto (f_c - f)^{-s}$ for $f < f_c$ ....(6.A.2a) (for insulating region)

$\sigma \propto (f - f_c)^{t}$ for $f > f_c$ ....(6.A.2b) (for conducting region)

where f is the volume fraction of the filler, f_c is the volume fraction at percolation threshold and s and t are the critical exponents in the insulating and conducting regions respectively. The log–log plots of the power laws based on Equations 1(a) and (b) (Fig. 6.A.12 insets) show that volume fraction at percolation threshold (f_c) is 0.80 vol% (~2 phr of MWCNTR in the composite), and the critical exponents in the insulating and conducting regions, 's' and 't' are 2.06 and 0.93 respectively (see the insets in Fig.6.12). The percolation threshold of the as prepared NRCSF composite is found to be very low (f_c=0.80 vol%) due to the segregated network of the nanohybrid filler in the rubber matrix and high aspect ratio of the filler[36,37]. This value is less than that of many CNT/polymer composites with random network as reported in the literature[38,39]. The Low percolation threshold for the nanocomposite is beneficial for maintaining flexibility and low modulus of the polymeric materials.

But the percolation threshold of this composite is high compared to the NR-MWCNTR composite with segregated structure (Chapter 4B). This can be attributed to the presence of insulating nanosilica particles around the conducting nanotubes in NRCSF composite. Both critical exponents obtained from the data fitting (s and t from Fig.6.A.12) are deviating from their

corresponding universal values (s_{un}~0.8-1, t_{un}~1.6-2). The deviation can be due to the complexity of segregated conductive network, filler morphology, distribution and dispersion of conductive fillers as reported elsewhere[40,41].

The dielectric permittivity of the NRCSF composites at 1 kHz against filler loading is given in Fig. 6.A.13. The graph shows a sudden increase in the dielectric constant near the percolation threshold (f_c=0.80 vol %). The dielectric constant of the NRCSF composite at 0.838 vol% of MWCNTR is found to be 40 which is 11 times higher than that of pure NR (3.5). The dielectric constant is sharply increased to 417 after percolation threshold (2.07 vol % of MWCNTR). The percolation theory related to the dielectric constant of the composite can be denoted by power law as shown in Eq. 6.A.3.

$$\varepsilon \propto (f_c - f)^{-s} \text{ for } f < f_c \quad ....(6.A.3)$$

The best linear fit of the law gives f_c=0.80 vol% and s=1.34 (see the inset in Fig. 6.A.13) which is very close to the universal value (s_{un}~0.8-1).
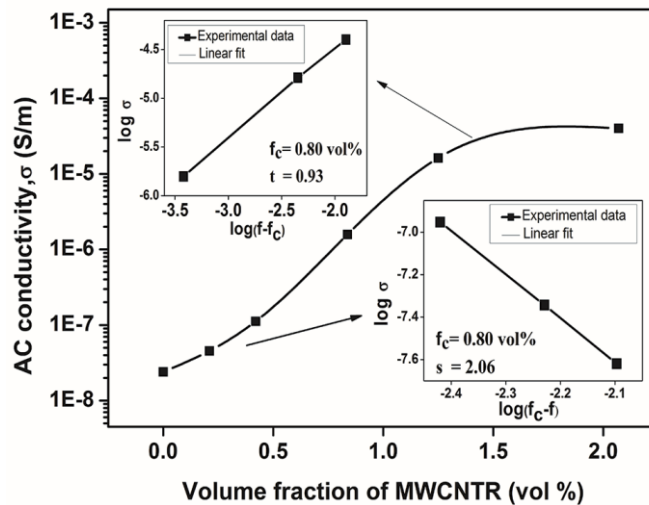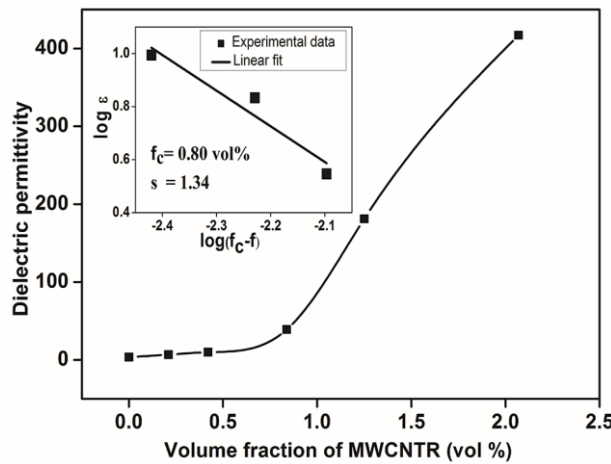

Fig.6.A.13 Dielectric permittivity of the NRCSF composites as a function of MWCNTR concentration measured at 1 kHz and room temperature. Inset shows the best fit of the dielectric permittivity to Eq. (6.A.3)

Dielectric constant versus frequency graph for the NRCSF composite with nanohybrid filler loading (Fig. 6.A.14a) clearly distinguishes the

variation of dielectric constant below and after fc. Below fc the dielectric constant increases slightly on addition of the filler. But after fc there is sharp increase in the dielectric constant at low frequency region on addition of filler. Dielectric constant of all the NRCSF composites decreases with increase in frequency indicating a strong frequency dependence of the dielectric constant of all the composites. The high dielectric constant of the NRCSF composite cannot be explained using microcapacitor model as the parallel microcapacitors are not possible in this case because of the coating of the CS hybrid fillers on spherical or ellipsoidal NR latex particles.
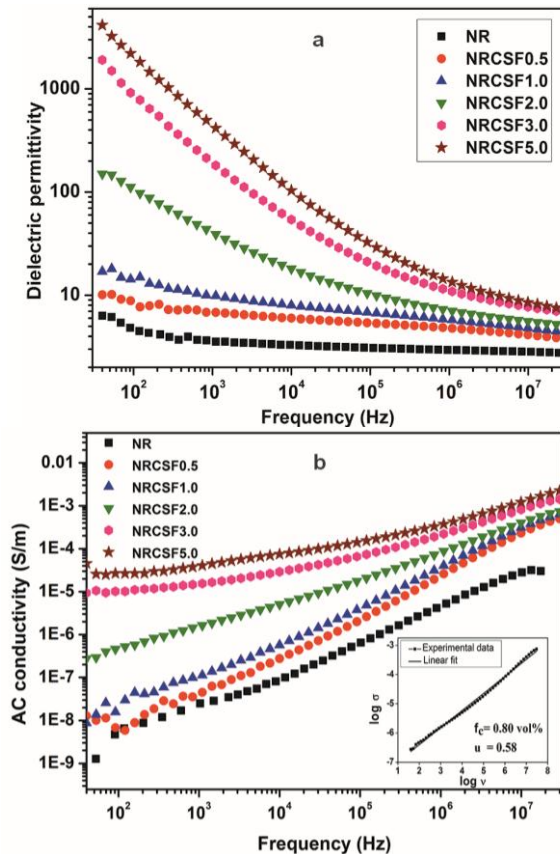
Fig. 6.A.14 Variation of (a) dielectric constant (b) ac conductivity of NR and NRCSF composites with frequency at room temperature. The (b) inset shows the best fit of the ac conductivity of the NRCSF composite with 0.84 vol% of MWCNTR to Eq. (6.A.4)

For a heterogeneous system the frequency dependence of dielectric constant is due to the interfacial polarisation effect called as Maxwell-Wagner-Sillars (MWS) polarisation effect[39]. According to this effect the dielectric constant improvement in heterogeneous systems is attributed to the accumulation of free charges at the interfaces between conducting fillers and insulating polymer layers. When $f < f_c$, the conducting filler concentration is too small to cause accumulation of charges at the interfaces and hence the dielectric constant is almost independent of frequency. When f reaches f_c the available interfaces increase due to the availability of large number of conducting MWCNTs. This in turn leads to an increase in accumulation of free charges at the conductor-insulator interfaces and causes a sharp increase in the dielectric constant value in the low frequency range. As the frequency increases the interfacial polarisation cannot cope up with electric filed frequency and hence the MWS effect decreases.

Conductivity versus frequency graph for NRCSF composites with different nanohybrid filler loadings (Fig. 6.A.14b) shows that the conductivity increases linearly with frequency below the percolation threshold whereas it is almost independent of frequency beyond f_c, especially in the low frequency range. When f reaches f_c, the relation between conductivity and frequency can be related through percolation threshold power law as given in Eq. 6.A.4.

$$\sigma \propto \omega^{\mu}, \text{ as } f{\rightarrow}f_c \dots\dots\dots\dots\dots\dots\dots\dots\dots\dots\dots\dots\dots\dots\dots\dots(6.A.4)$$

where $\omega=2\pi\nu$, ν is the frequency and μ is the corresponding critical exponent. The value of μ obtained ($\mu=0.58$) from the linear fit of the log-log plot of equation 3 using experimental data for f=0.838 vol% (near f_c) is found to be slightly less than the normal value ($\mu_{uni}=0.70$). This deviation may be due to the complexity of segregated network of three phase system as reported elsewhere[42].

The frequency dependence of dielectric loss value is given in Fig. 6.A.15. The dielectric loss is independent of frequency for f < fc and it becomes frequency dependent when f reaches f_c. The three phase NRCSF composite contains more number of conducting nanotubes when f > fc and hence possibility of tube-tube interaction increases. This leads to the leakage of current and causes higher dielectric loss. The dielectric loss behaviours for this three phase composite is very low compared to the NR-MWCNTR composite discussed in chapter 4[7].
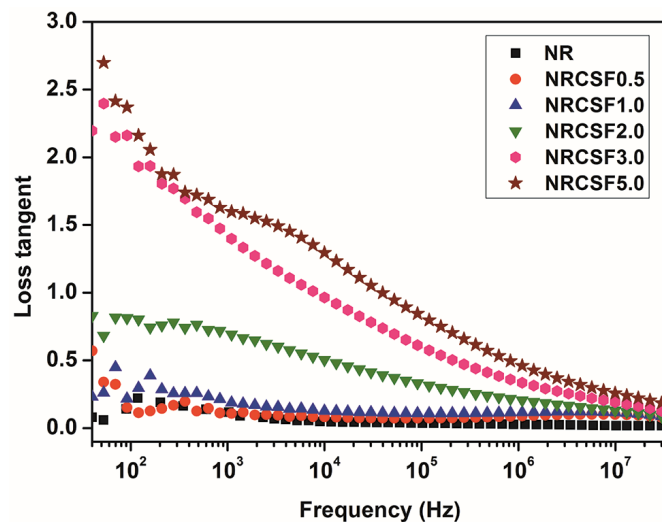
Fig. 6.A.15 Dependence of dielectric loss tangent of the NRCSF composites on frequency at room temperature

To evaluate the competence of the NRCSF segregated filler network composite for microcapacitor applications, the dielectric constant and dielectric loss values of NRCSF is compared with NRMWCNTR at 1 KHz and 1 MHz frequencies in Fig.6.A.16. At 1 kHz frequency the NRCSF composite possess a dielectric constant of 181 and 417 for 1.25 vol% and 2.07 vol% of MWCNTR respectively (Fig. 6.A.16a). The dielectric loss value at the same frequency for 2.07 vol% MWCNTR in NRCSF is 1.6 (Fig. 6.A.16b). Figure also reveals that the dielectric constant value of NRMWCNTR composite is

133 and dielectric loss is 2.2 at 0.43 vol% of MWCNTR which is higher than NRCSF. The Figure clearly shows that at a dielectric constant value of 417 for 2.07 vol% MWCNTR, the dielectric loss value is low (1.6) for the NRCSF composite. But the dielectric loss of NRMWCNTR composite is very high (2.2) at a dielectric constant value of 133.
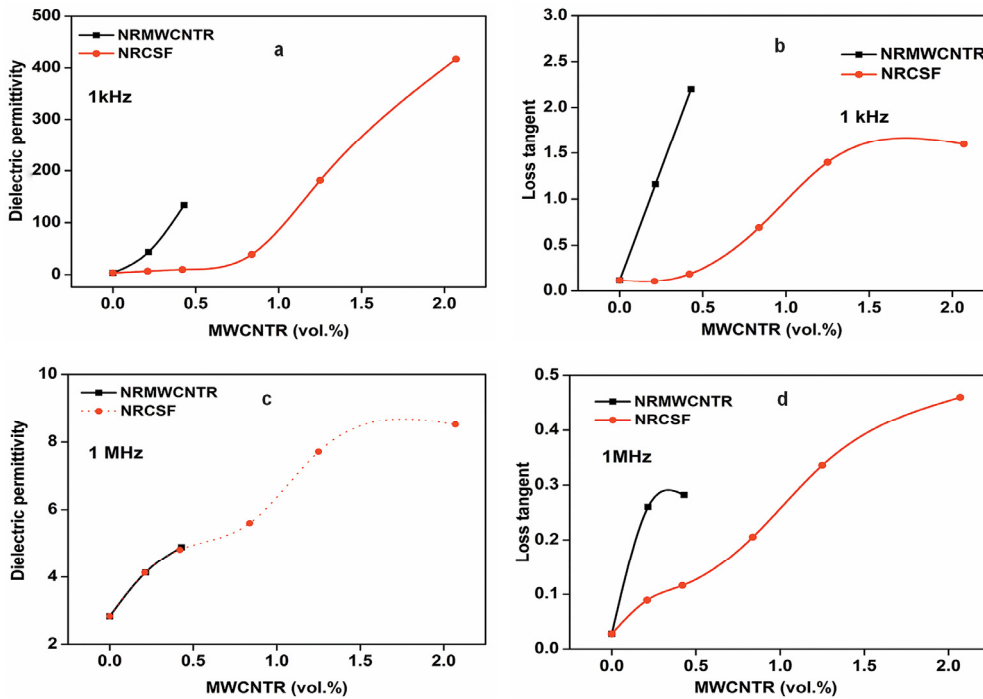
Fig. 6.A.16 Variation of dielectric constant (a and c) and dielectric loss tangent (b and d) as a function of MWCNTR concentration for NRMWCNTR and NRCS composites at different frequencies

At 1MHz frequency both NRMWCNTR and NRCSF have same dielectric permittivity (Fig.6.A.16c), but the dielectric loss tangents are quite low for the NRCSF composite compared to NRMWCNTR (Fig.6.A.16d). In NRCSF the direct contact between the conducting nanotubes is reduced by the presence of nanosilica particles that form an insulating sheath around the nanotubes. This actually reduces the leakage of current and thereby the composite shows low dielectric loss.

6.A.3.9 Advantages of using CS nanohybrids as the dielectric filler

Preparation of CS hybrid fillers involves very simple and environment friendly method that uses water as the solvent and ultrasonication as the processing tool. Rebundling of MWCNTs is prevented by the self-assembly of nanosilica on CNTs. The CS hybrid filler in the NR matrix resulted in composite having high dielectric permittivity and low dielectric loss. Data given in Table 6.A.6 confirms that the NRCSF composite has better dielectric performance than the other reported NR based composites.

Table 6.A.6 Dielectric constant and dielectric loss tangent values of different NR based composites

Composites	f (vol.%)	ε	tan δ
NRCSF	5phr (2.07 vol%) MWCNTR	417 (1 kHz) 8.5 (1 MHz)	1.6 (1kHz) 0.46 (1 MHz)
NR/MWCNTR[7]	1 phr (0.43 vol%)	133 (1k Hz) 4.89 (1MHz)	2.2 0.28
NR/Al$_2$O$_3$[43]	60 wt%	171.575 (500Hz)	-
NR/Barium ferrite[44]	30 phr	7 (100kHz) 6 (1MHz)	0.7 0.5
NR/conductive carbon black[45]	10 vol%	500 (1 kHz)	3
NR/Graphene [22]	3 wt%	8 (1kHz)	1.5
NR/Graphene [22]	10wt%	4.5(10GHz)	2.5

6.A.3.10 EMI shielding effectiveness

EMI shielding effectiveness (SE) of the NRCSF composites in the frequency range 8-12 GHz is shown in Fig. 6.A.17. SE increases with hybrid filler loading and reaches a maximum of 3.8 dB at 8.9 GHz for NRCSF5 composite. The increase in SE with CS hybrid filler loading is due to the increase in conductivity and interfacial polarisation as reported elsewhere[46,47]. Thickness of the samples also influences the shielding efficiency with SE increasing with thickness as discussed in previous

reports[48]. The samples under study were prepared by film casting and have thickness below 0.7 mm. It is expected that thick samples with high concentration of conducting fillers will further improve SE of NR.
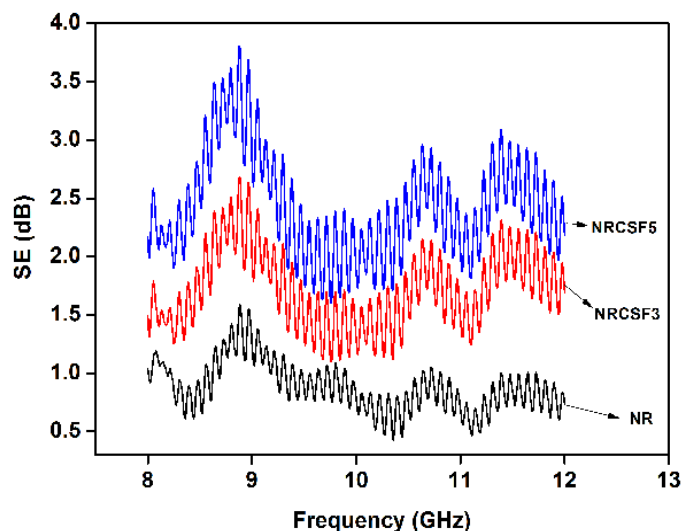
Fig. 6.A.17 Variation of SE with frequency of NRCSF composites

6.A.4 Conclusions

A novel NR composite with high dielectric constant and low dielectric loss was fabricated for the first time using a simple, efficient and eco-friendly method. MWCNTs decorated with nanosilica particles (CS hybrid) were prepared for the first time with the aid of ultrasonication assisted mixing of carboxylated MWCNTs and colloidal nanosilica. Hydrogen bonding possible between carboxyl groups on the nanotube side walls and silanol groups on nanosilica helped in the adsorption of nanosilica particles on the nanotube surface and also prevented re-aggregation of the tubes in water. Film casting method adopted in this case resulted in NRCSF composite with a segregated CS hybrid filler network. TEM and SEM images, and strain sweep studies of the composites revealed the segregated network of the hybrid filler. The composite shows significant improvement in mechanical properties and solvent resistance. Segregated network of conducting fillers

also assisted in achieving high dielectric constant (417 at 10^3 Hz) and low electrical percolation threshold (0.80 vol%). Insulating nanosilica decorated nanotubes reduces the dielectric loss for the composite. High thermal conductivity along with good distribution of the CS hybrid fillers in the segregated network enhances thermal stability of the composite. These elastomeric nanocomposites with high k and low loss can find application as capacitors for energy storage.

References

[1] Qi, L., Lee, B. I., Chen, S., Samuels, W. D., & Exarhos, G. J. (2005). High-Dielectric-Constant Silver–Epoxy Composites as Embedded Dielectrics. *Advanced Materials*, *17*(14), 1777-1781.

[2] Xu, J., Wong, M., & Wong, C. P. (2004, June). Super high dielectric constant carbon black-filled polymer composites as integral capacitor dielectrics. In *Electronic Components and Technology Conference, 2004. Proceedings. 54th* (Vol. 1, pp. 536-541). IEEE.

[3] Cao, M. S., Song, W. L., Hou, Z. L., Wen, B., & Yuan, J. (2010). The effects of temperature and frequency on the dielectric properties, electromagnetic interference shielding and microwave-absorption of short carbon fiber/silica composites. *Carbon*, *48*(3), 788-796.

[4] Li, Q., Xue, Q., Hao, L., Gao, X., & Zheng, Q. (2008). Large dielectric constant of the chemically functionalised carbon nanotube/polymer composites. *Composites Science and Technology*, *68*(10), 2290-2296.

[5] Khanam, P. N., Ponnamma, D., & AL-Madeed, M. A. (2015). Electrical properties of graphene polymer nanocomposites. In *Graphene-Based Polymer Nanocomposites in Electronics* (pp. 25-47). Springer International Publishing.

[6] Kohlmeyer, R. R., Javadi, A., Pradhan, B., Pilla, S., Setyowati, K., Chen, J., & Gong, S. (2009). Electrical and dielectric properties of hydroxylated carbon nanotube– elastomer composites. *The Journal of Physical Chemistry C*, *113*(41), 17626-17629.

[7] George, N., Chandra, J., Mathiazhagan, A., & Joseph, R. (2015). High performance natural rubber composites with conductive segregated network of multiwalled carbon nanotubes. *Composites Science and Technology*, *116*, 33-40.

[8]   Tai, X., hong Ma, J., Du, Z., Wang, W., & Wu, J. (2013).A simple method for synthesis of thermal responsive silica nanoparticle/PNIPAAm hybrids. *Powder technology*, *233*, 47-51.

[9]   Pérez-Quintanilla, D., delHierro, I., Fajardo, M., & Sierra, I. (2006). Adsorption of cadmium (II) from aqueous media onto a mesoporous silica chemically modified with 2-mercaptopyrimidine. *Journal of Materials Chemistry*, *16*(18), 1757-1764.

[10]   Shanmugharaj, A. M., Bae, J. H., Lee, K. Y., Noh, W. H., Lee, S. H., & Ryu, S. H. (2007). Physical and chemical characteristics of multiwalled carbon nanotubes functionalised with aminosilane and its influence on the properties of natural rubber composites. *Composites Science and technology*, *67*(9), 1813-1822.

[11]   Zheng, C., Chen, W., & Ye, X. (2012). Study on Au nanoparticles, TiO 2 nanoclusters, and SiO 2 nanoshells coated multi-wall carbon nanotubes/silica gel-glass. *Optical Materials*, *34*(7), 1042-1047.

[12]   Zhuravlev, L. T. (2000). The surface chemistry of amorphous silica. Zhuravlev model. *Colloids and Surfaces A: Physicochemical and Engineering Aspects*, *173*(1), 1-38.

[13]   Cerveny, S., Schwartz, G. A., Otegui, J., Colmenero, J., Loichen, J., & Westermann, S. (2012). Dielectric study of hydration water in silica nanoparticles. *The Journal of Physical Chemistry C*, *116*(45), 24340-24349.

[14]   Keddie, J. L. (1997). Film formation of latex. *Materials Science and Engineering: R: Reports*, *21*(3), 101-170.

[15]   Mensah, B.; Kim, H. G.; Lee, J.-H.; Arepalli, S.; Nah, C. (2016). Carbon Nanotube-Reinforced Elastomeric Nanocomposites: A Review. *Int. J. Smart Nano Mater,6*, 211–238.

[16]   Gao, J. F., Li, Z. M., Meng, Q. J., & Yang, Q. (2008). CNTs/UHMWPE composites with a two-dimensional conductive network. *Materials Letters*, *62*(20), 3530-3532.

[17]   Ismail, H., & Chia, H. H. (1998). The effects of multifunctional additive and vulcanisation systems on silica filled epoxidized natural rubber compounds. *European polymer journal*, *34*(12), 1857-1863.

[18]   Potts, J. R., Shankar, O., Du, L., & Ruoff, R. S. (2012). Processing–morphology– property relationships and composite theory analysis of reduced graphene oxide/natural rubber nanocomposites. *Macromolecules*, *45*(15), 6045-6055.

[19] Grunlan, J. C., Gerberich, W. W., & Francis, L. F. (2001). Electrical and mechanical behavior of carbon black–filled poly (vinyl acetate) latex–based composites. *Polymer Engineering & Science*, *41*(11), 1947-1962.

[20] Li, T., Ma, L. F., Bao, R. Y., Qi, G. Q., Yang, W., Xie, B. H., & Yang, M. B. (2015). A new approach to construct segregated structures in thermoplastic polyolefin elastomers towards improved conductive and mechanical properties. *Journal of Materials Chemistry A*, *3*(10), 5482-5490.

[21] Jin, S. H., Park, Y. B., & Yoon, K. H. (2007). Rheological and mechanical properties of surface modified multi-walled carbon nanotube-filled PET composite. *Composites Science and Technology*, *67*(15), 3434-3441.

[22] James, H. M., & Guth, E. (1943). Theory of the elastic properties of rubber. *The Journal of Chemical Physics*, *11*(10), 455-481.

[23] Fornes, T. D., & Paul, D. R. (2003). Modeling properties of nylon 6/clay nanocomposites using composite theories. *polymer*, *44*(17), 4993-5013.

[24] Mullins, L., & Tobin, N. R. (1965). Stress softening in rubber vulcanisates. Part I. Use of a strain amplification factor to describe the elastic behavior of filler-reinforced vulcanised rubber. *Journal of Applied Polymer Science*, *9*(9), 2993-3009.

[25] Francis, L. F., Grunlan, J. C., Sun, J., & Gerberich, W. W. (2007). Conductive coatings and composites from latex-based dispersions. *Colloids and Surfaces A: Physicochemical and Engineering Aspects*, *311*(1), 48-54.

[26] Zhan, Y., Lavorgna, M., Buonocore, G., & Xia, H. (2012). Enhancing electrical conductivity of rubber composites by constructing interconnected network of self-assembled graphene with latex mixing. *Journal of Materials Chemistry*, *22*(21), 10464-10468.

[27] Pang, H., Yan, D. X., Bao, Y., Chen, J. B., Chen, C., & Li, Z. M. (2012). Super-tough conducting carbon nanotube/ultrahigh-molecular-weight polyethylene composites with segregated and double-percolated structure. *Journal of Materials Chemistry*, *22*(44), 23568-23575.

[28] Payne, A. R., & Whittaker, R. E. (1971). Low strain dynamic properties of filled rubbers. *Rubber chemistry and technology*, *44*(2), 440-478.

[29] Fröhlich, J., Niedermeier, W., & Luginsland, H. D. (2005). The effect of filler–filler and filler–elastomer interaction on rubber reinforcement. *Composites Part A: Applied Science and Manufacturing*, *36*(4), 449-460.

[30] Das, A., Jurk, R., Stöckelhuber, K. W., Majumder, P. S., Engelhardt, T., Fritzsche, J.,... & Heinrich, G. (2008). Processing and properties of nanocomposites based on layered silicate and carboxylated nitrile rubber. *Journal of Macromolecular Science, Part A*, *46*(1), 7-15.

[31] Galimberti, M., Cipolletti, V., Musto, S., Cioppa, S., Peli, G., Mauro, M., ... & Kumar, V. (2014). Recent advancements in rubber nanocomposites. *Rubber Chemistry and Technology*, *87*(3), 417-442.

[32] F. W. Billmeyer. (1994). Text book of polymer science, Wiley Interscience, A Wiley-lnterscience Publication, John Wiley & Sons, Singapore.

[33] Abraham, J., Maria, H. J., George, S. C., Kalarikkal, N., & Thomas, S. (2015). Transport characteristics of organic solvents through carbon nanotube filled styrene butadiene rubber nanocomposites: the influence of rubber–filler interaction, the degree of reinforcement and morphology. *Physical Chemistry Chemical Physics*, *17*(17), 11217-11228.

[34] Huxtable, S. T., Cahill, D. G., Shenogin, S., Xue, L., Ozisik, R., Barone, P., ... & Keblinski, P. (2003). Interfacial heat flow in carbon nanotube suspensions. *Nature materials*, *2*(11), 731-734.

[35] Abdullateef, A. A., Thomas, S. P., Al-Harthi, M. A., De, S. K., Bandyopadhyay, S., Basfar, A. A., & Atieh, M. A. (2012). Natural rubber nanocomposites with functionalised carbon nanotubes: mechanical, dynamic mechanical, and morphology studies. *Journal of Applied Polymer Science*, 1(*125),* E76–E84.

[36] Grunlan, J. C., Mehrabi, A. R., Bannon, M. V., & Bahr, J. L. (2004). Water-Based Single-Walled-Nanotube-Filled Polymer Composite with an Exceptionally Low Percolation Threshold. *Advanced Materials*, *16*(2), 150-153.

[37] Shen, Y., Lin, Y. H., & Nan, C. W. (2007). Interfacial Effect on Dielectric Properties of Polymer Nanocomposites Filled with Core/Shell-Structured Particles. *Advanced Functional Materials*, *17*(14), 2405-2410.

[38] Das, A., Kasaliwal, G. R., Jurk, R., Boldt, R., Fischer, D., Stöckelhuber, K. W., & Heinrich, G. (2012). Rubber composites based on graphene nanoplatelets, expanded graphite, carbon nanotubes and their combination: a comparative study. *Composites Science and Technology*, *72*(16), 1961-1967.

[39] Dang, Z. M., Wang, L., Yin, Y. I., Zhang, Q., & Lei, Q. Q. (2007). Giant dielectric permittivities in functionalised carbon-nanotube/electroactive-polymer nanocomposites. *Advanced Materials*, *19*(6), 852-857.

[40] Lu, C., Hu, X. N., He, Y. X., Huang, X., Liu, J. C., & Zhang, Y. Q. (2012). Triple percolation behavior and positive temperature coefficient effect of conductive polymer composites with especial interface morphology. *Polymer bulletin*, *68*(7), 2071-2087.

[41] Grossiord, N., Loos, J., & Koning, C. E. (2005). Strategies for dispersing carbon nanotubes in highly viscous polymers. *Journal of Materials Chemistry*, *15*(24), 2349-2352.

[42] Yang, Y., Sun, H., Zhu, B., Wang, Z., Wei, J., Xiong, R., ... & Lei, Q. (2015). Enhanced dielectric performance of three phase percolative composites based on thermoplastic-ceramic composites and surface modified carbon nanotube. *Applied Physics Letters*, *106*(1), 9–14.

[43] Tangboriboon, N., Datsanae, S., Onthong, A., Kunanuruksapong, R., & Sirivat, A. (2013). Electromechanical responses of dielectric elastomer composite actuators based on natural rubber and alumina. *Journal of Elastomers & Plastics*, *45*(2), 143-161.

[44] Makled, M. H. (2012). Dielectric properties of high coercivity barium ferrite–natural rubber composites. *Journal of Applied Polymer Science*, *126*(3), 969-973.

[45] Matchawet, S., Kaesaman, A., Bomlai, P., & Nakason, C. (2016). Electrical, dielectric, and dynamic mechanical properties of conductive carbon black/ epoxidized natural rubber composites. *Journal of Composite Materials*, *50*(16), 2191-2202.

[46] Yuping, D., Shunhua, L., & Hongtao, G. (2005). Investigation of electrical conductivity and electromagnetic shielding effectiveness of polyaniline composite. *Science and Technology of Advanced Materials*, *6*(5), 513-518.

[47] Bryning, M. B., Islam, M. F., Kikkawa, J. M., & Yodh, A. G. (2005). Very Low Conductivity Threshold in Bulk Isotropic Single-Walled Carbon Nanotube–Epoxy Composites. *Advanced materials*, *17*(9), 1186-1191.

[48] Yim, Y. J., & Park, S. J. (2015). Electromagnetic interference shielding effectiveness of high-density polyethylene composites reinforced with multi-walled carbon nanotubes. *Journal of Industrial and Engineering Chemistry*, *21*, 155-157.

NR/CS HYBRID COMPOSITES WITH RANDOM NETWORK

6.B.1 Introduction

Studies on latex nanocomposites have attracted much attention, as their processing involves simple compounding methods along with the added advantage of uniform nanoparticle dispersion, excellent properties, and wide range of applications[1]. There are reports on the advantage of nanoclays over carbon black by latex compounding of rubber lattices[2,3]. Zhao et al.[4] found that a uniform dispersion of GO in the NR matrix was achieved with the latex mixing method which effectively improved the tensile strength and storage modulus of NR at very low filler contents. Potts et al.[5] investigated the dependence of property and morphology of the nanocomposites upon the processing method and found that coagulating a stable RGO suspension with NR latex resulted in segregated graphene network while two-roll milling yielded homogeneous dispersion in the NR matrix. They found that network morphology was highly beneficial for thermal and electrical conductivity properties whereas mechanical properties were found to be better for milled samples.

Furthermore synergistic effects of hybrid fillers containing CNTs have studied by many researchers and have reported improved mechanical and electrical properties. Ponnamma et al.[6] have studied the synergistic effect of MWCNT and reduced graphene oxides in NR for sensing application. Bokobza et al.[7] prepared SBR composites containing mixtures of CB and MWCNTs by solution blending method and the composites exhibited improved mechanical and electrical properties with low percolation threshold. Lorenz et al.[8] investigated the synergistic effects of CNT-hybrid filler systems on elastomers. Reinforcement of NR by MWCNT/silica hybrid filler system has been reported by Ismail et al.[9].

Latex stage mixing of the aqueous dispersions of nanofillers into rubber resulted in segregated network structure as discussed in the earlier chapters. In the latex film casting and curing method the segregated network is expected to remain as such which is beneficial for getting good electrical properties. But the latex coagulated nanocomposites would not be used directly in typical applications, but would instead be used as a masterbatch compound and would be mixed using a two-roll mill or internal mixer[10]. The intense shear forces generated by these mixing operations can affect the network morphology created by coagulation. In the present part of the chapter the effect of processing method on the filler morphology has been studied by co-coagulation of the NR latex and CS nanohybrid dispersion followed by mixing in an internal mixer. The filler morphology and properties of the NR/CS nanohybrid nanocomposites thus obtained (NRCSH) is investigated.

6.B.2 Experimental

6.B.2.1 Preparation of carboxylated multiwalled carbon nanotube-nanosilica hybrid (CS hybrid) dispersions

MWCNT was oxidized using conc.H_2SO_4/HNO_3 mixture as per procedure given in 4.A.2.1. of Chapter 4 to get carboxylated multiwalled carbon nanotube (MWCNTR). MWCNTR-nanosilica hybrid (CS hybrid) dispersions were prepared as per the procedure given in 6.A.2.1 of this chapter. The hybrid fillers containing 1, 2, 3 and 4 phr of MWCNTR along with 5 phr nanosilica were labeled as 1C5S, 2C5S, 3C5S and 4C5S respectively (phr is taken with respect to dry rubber).

6.B.2.2 Preparation of the composites by latex coagulation and Haake mixing (NRCSH composites)

Nanocomposites were prepared by latex coagulation method as follows. NR latices were weighed in separate containers, CS hybrid aqueous dispersions were added and mechanically stirred for 30 minutes. The latex

mixes were poured into trays and coagulated by rapid addition of 2% v/v acetic acid solution. The coagulum was washed several times with water and dried at 50 °C in an air oven.

The dried coagulum containing CS hybrid was mixed in a Haake mixer (at 70 °C, 8 minutes, 60 rpm) with compounding ingredients as per formulation given in Table 6.B.1 and procedure outlined in the ASTM D 3182. After mixing the batch was passed six times through tight nip in a two-roll mill and was finally sheeted out. The samples were kept overnight for maturation.

Table 6.B.1 Formulation of NRCSH composites

Ingredients	Amount (phr)
NR	100
Nanosilica	5.0
MWCNTR	0, 1.0, 2.0, 3.0, 4.0
Stearic acid	2.25
ZnO	5.0
Antioxidant SP	1.0
Accelerator MOR	0.75
Accelerator TMTD	0.2
Sulphur	2.5

The cure characteristics of the mixes were determined using Rubber Process Analyser. The optimum cure time, scorch time, maximum torque, minimum torque etc. were determined from the rheograph. The rubber compounds were compression moulded as per procedure outlined in chapter 2 (section 2.2.6) to get the nanocomposites. The composites were labeled as NRCSH1, NRCSH2, NRCSH3 and NRCSH4, where the number denotes the hybrids 1C5S, 2C5S, 3C5S and 4C5S respectively.

Concentration of nanofillers in each nanocomposite is given in Table 6.B.2.

Table 6.B.2 Concentrations of the nanofillers in the NRCSF nanocomposites

Composite	Nanosilica (phr*)	MWCNTR	
		phr*	vol %
NRCSH1	5	1	0.42
NRCSH2	5	2	0.838
NRCSH3	5	3	1.25
NRCSH4	5	4	1.68

* phr is with respect to dry NR

6.B.2.3 Characterisation

HRTEM analysis of the NRCSH composite was done to understand the CS hybrid filler distribution inside the rubber. Fracture surface morphology of the NRCSH nanocomposites were analysed using scanning electron microscopy (SEM). Mechanical properties of the samples were tested according to the relevant ASTM standards. Strain dependent dynamic mechanical properties were done using DMA. TGA and swelling studies were done to understand the thermal and solvent barrier properties. Dielectric and AC conductivity studies were done using Precision Impedance Analyser. DC electrical conductivity measurements were done using a Keithley 2400 source-measure unit. EMI shielding measurements were performed using Agilent Performance Network Analyser in the X band frequency range.

Detailed description on each characterisation method is given in Chapter 2.

6.B.3 Results and discussion

6.B.3.1 Latex stage mixing and coagulation process

Aqueous dispersions of carboxylated multiwalled carbon nanotube/nanosilica hybrid filler were found to be stable without settling which can be due to the presence of polar carboxyl groups on the nanotubes and silanol groups on silica. The H-bonding possible between the oxygen containing groups on the MWCNTRs and silanol groups on silica also adds to the

advantage in getting stable aqueous dispersions by preventing the rebundling of MWCNTRs. Latex stage mixing method involves the addition of aqueous filler dispersion to NR latex followed by mechanical stirring of the mixture. Coagulation was done by rapid addition of acetic acid to the mixture as suggested by Wu et al.[11].

Following the addition of the acetic acid to the mixture complete coagulation occurred within seconds. For neat NR latex and the latex containing 1C5S and 2C5S nanohybrids, serum after coagulation was colorless and the coagulum was a single mass. But on increasing the loading to 3C5S and 4C5S, the serum was slightly grey in colour and the coagulum contained solid particles of small sizes instead of a single mass. This indicates that flocculation of filler particles occur before the coagulation of NR latex particles as the filler concentration in latex increases.

6.B.3.2 Morphology and microstructure

Microstructure of the composite obtained from TEM is given in Fig. 6.B.1. The NRCSH composite showed homogeneous distribution of hybrid filler (CS hybrid) in the rubber matrix instead of a segregated structure as obtained in the film casting or simple hot pressing as reported elsewhere[12-14]. The reason is very clear that uniform distribution of nanosilica-carbon nanotube hybrid filler in the NR latex occurs during latex stage mixing; and on coagulation these fillers are pushed to the periphery of spherical rubber particles. This would have resulted in a segregated structure and remained intact on hot pressing without disturbing the filler distribution. But in this case when the dried coagulum is mixed in an internal mixer, definitely the spatial arrangement of fillers is getting disturbed resulting in random network. The composite after Haake mixing will have homogeneous distribution of fillers in the rubber matrix instead of web-like filler network. Intense shear forces in the internal mixer breaks the filler network in the coagulum and distributes the fillers evenly in the rubber.
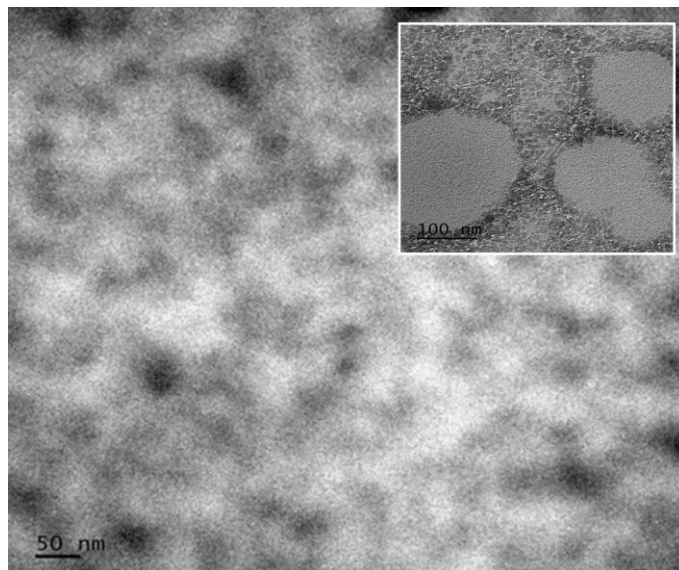
Fig. 6.B.1 TEM image of NRCSH3 composite. Inset shows TEM image of the NRCSF3 nanocomposite

Morphology of tensile and tear fractured surfaces of NRCSH3 nanocomposite are shown in Fig. 6.B.2. Fractured ends of the nanotubes are not visible from the images which can be either due to the nanosize of the tubes or mismatch in elongation between rubber and CNTs during rupture[15]. The fracture surface patterns differ significantly compared to those of NRCSF3 composites prepared by film casting method (given as inset in Fig. 6.B.2b and e). The difference can be attributed to the nature of filler distribution in the two composites. The film casting favours segregated structure whereas samples prepared by latex coagulation and Haake mixing have uniform distribution of hybrid fillers in the rubber matrix. Well-ordered segregated network structure in NRCSF composite leads to craters with special patterns whereas those patterns are absent in NRCSH composites prepared by Haake mixing indicating uniform homogeneous distribution of the fillers.
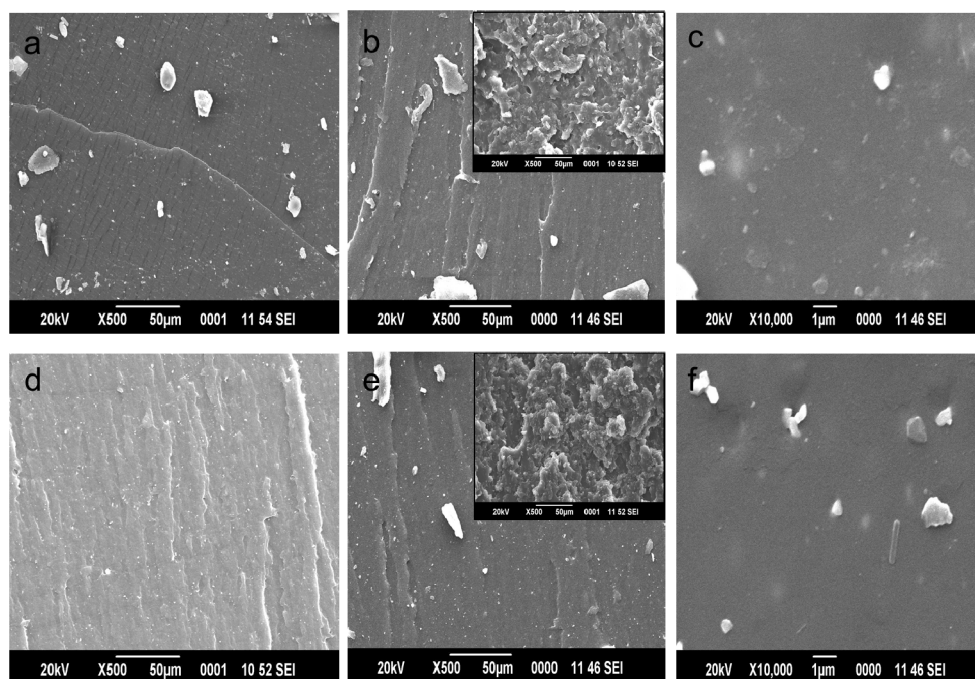
Fig. 6.B.2 SEM images of the fractured surfaces of NRCSH composites: tensile fractured surfaces of a) NR (b) and (c) NRCSH3; tear fractured surfaces of d) NR, (e) and (f) NRCSH3; (b) and (e) inset shows the tensile and tear fractured surface images of NRCSF3

Based on the microscopic observations a schematic representation of the formation of NRCSH nanocomposites is given in Fig. 6.B.3. Mixing of carboxylated multiwalled carbon nanotubes with colloidal nanosilica facilitates the adsorption of nanosilica on the surface of nanotubes. Mixing of this filler dispersion with NR latex followed by coagulation creates excluded volume and pushes the hybrid fillers to the interstitial spaces between the rubber particles to form a segregated network in the rubber matrix. Subsequent mixing with compounding ingredients in the Haake internal mixer disturb the web like network and a well dispersed NR-CS hybrid nanofiller composite is obtained.
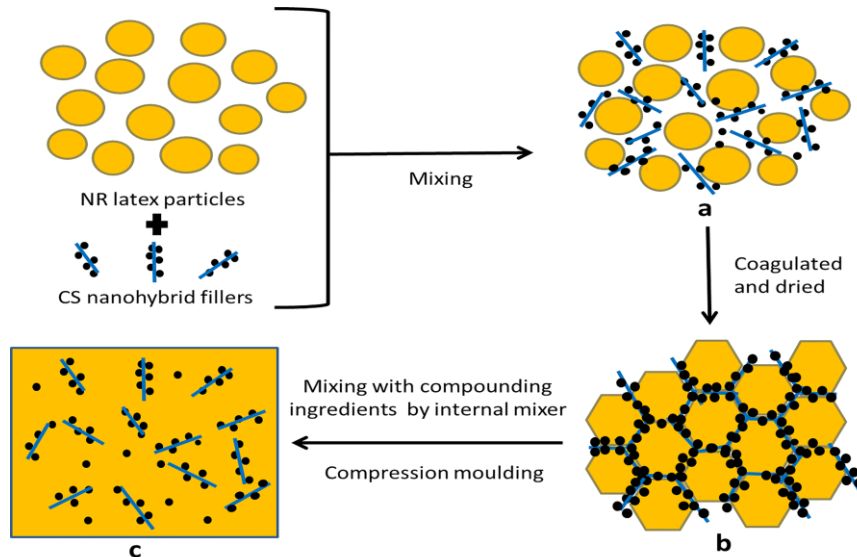
Fig. 6.B.3 Schematic representation of the preparation of NRCSH nanocomposites (a) nanosilica decorated multiwalled carbon nanotubes (CS nanohybrids) are uniformly distributed in the NR latex (b) segregated network of CS hybrids in the NR matrix after acid coagulation and drying (c) Mixing with compounding ingredients in an internal mixer destroys the network and uniformly distributes the fillers in the NRCSH composites

6.B.3.3 Cure characteristics of NRCSH composites
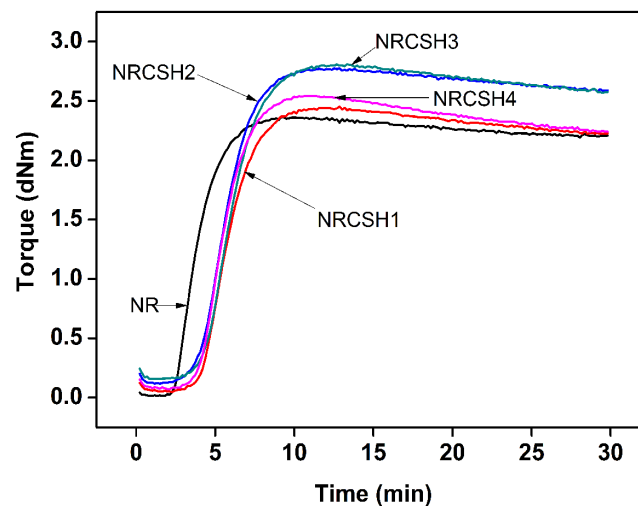
Fig. 6.B.4 Cure curves of NRCSH composites

Fig. 6.B.4 shows the cure graphs of NR and NRCSH nanocomposites at 150 ℃. Initial decrease in torque is due to the softening of the rubber matrix, which is followed by a sharp increase in torque due to the crosslinking of rubber.

Table 6.B.3 shows the vulcanisation characteristics of NR and NRCSH nanocomposites at 150 ℃. Minimum torque (M_L) represents viscosity of the unvulcanised compound and maximum torque (M_H) is an index of elastic modulus of the vulcanised rubber[16]. Minimum and maximum torque values of the NRCSH composites are higher compared to neat NR. Increase in M_L with addition of the hybrid filler indicates that inclusion of fillers reduces the mobility of rubber chains and increases viscosity[17]. Increase in M_H with hybrid filler addition suggests enhanced rubber-filler interaction and reinforcement of rubber. Torque difference; $\Delta M = M_H - M_L$ is a measure of crosslink density and gives the extent of polymer-filler interaction[18]. ΔM in the present study increases with filler addition and the maximum ΔM values are exhibited by NRCSH2 and NRCSH3 composites followed by a decrease, on further addition of the filler.

Table 6.B.3 Cure characteristics of NR and NRCSH nanocomposites

PROPERTIES	NR	NRCSH1	NRCSH2	NRCSH3	NRCSH4
Min. torque, M_L(dNm)	0	0.045	0.111	0.153	0.069
Max. torque, M_H(dNm)	2.37	2.46	2.78	2.82	2.55
$\Delta M = M_H - M_L$ (dNm)	2.37	2.42	2.67	2.66	2.48
Scorch time, T_{10} (min)	2.67	4.30	4.03	4.36	4.13
Opt. cure time, T_{90} (min)	5.90	8.06	7.81	8.42	7.58
Cure rate index(min^{-1})	30.96	26.59	26.46	24.63	28.99

Scorch time (T_{10}) represents the processing safety of the compound. Increase in scorch time observed for the composites indicates that the processing safety has been improved by the addition of the filler. Cure time (T_{90}) increased with filler addition as a result of the cure retarding nature of the

added fillers. Acidic carboxyl groups on the surface of MWCNTR and silanol groups on nanosilica interact with basic accelerator or other compounding ingredients and slow down the cure reaction[19].

6.B.3.4 Mechanical properties

Reinforcement of NR by the added CS hybrid fillers is obvious from the stress-strain curves of NR and NRCSH nanocomposites in Fig. 6.B.5. NR possess unique characteristic known as strain induced crystallisation which is the ability of rubber to crystallise under strain. The crystallites act as additional cross-links in the network and causes self-toughening of the elastomer. It is clear from the figure that strain induced crystallisation becomes more pronounced with addition of nanohybrid filler to NR.
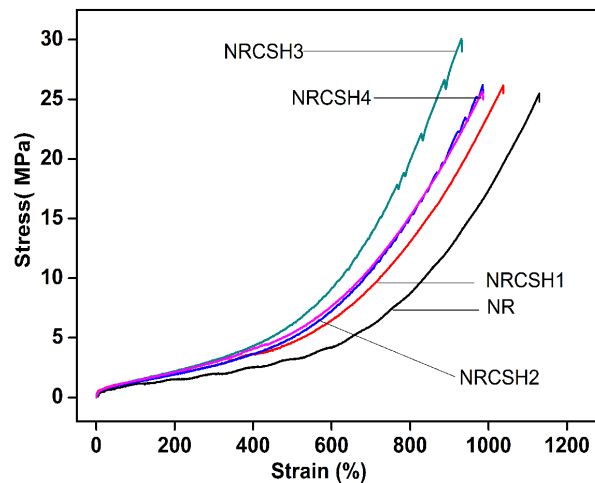
Fig. 6.B.5 Stress-strain behaviour of NR and NRCSH nanocomposites

The reinforcing effect of the nanohybrid fillers in NRCSH composites can be further understood from the Mooney-Rivlin plots according to Eq. 6.B.1.

$$\sigma^* = \frac{\sigma}{\alpha - \alpha^{-2}} = 2C_1 + 2C_2\alpha^{-1} \quad ....(6.B.1)$$

where σ^* is the reduced stress, σ is the nominal stress, α is the extension ratio and $2C_1$ and $2C_2$ are constants independent of α. σ^* is equal to the

elastic modulus E as per James and Guth approach[20]. Mooney–Rivlin curves in Fig. 6.B.6 display an increase in elastic modulus with filler loading at all deformations. Strain induced crystallisation which is characterised by an upturn in the curve, occurs at higher extension ratio (lower α^{-1}) for unfilled vulcanisates whereas the upturns for NRCSH composite appear at a lower extension ratio (higher α^{-1}). There is shifting of the curve upturns to higher α^{-1} with increasing hybrid filler loading. This may be due to the uniform dispersion of high aspect ratio CS nanohybrid fillers which would favour the strain induced crystallisation of NR. Large interfacial surface area of the nanohybrid fillers can also play an important role in causing early onset of strain induced crystallization. Combination of different factors like mechanical restraint by high aspect ratio fillers, alignment of fillers during stretching and enhanced strain induced crystallization by the nanohybrid fillers results in the modulus enhancement for the NRCSH samples. Similar results have been reported by others[21,22].
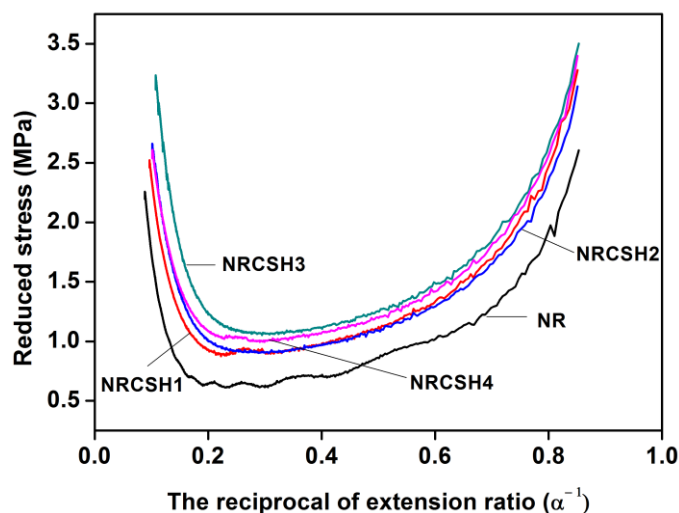
Fig. 6.B.6 Mooney-Rivlin plots for NRCSH nanocomposites

It is clear from Table 6.B.4 that mechanical properties of NR improve significantly by the addition of CS nanohybrids. Tensile strength, modulus

(300%) and tear strength increases with CS hybrid filler loading whereas elongation at break decreases. NRCSH3 composite shows best properties with 19% enhancement in tensile strength, 57 % in modulus, and 37 % in tear strength. The properties level off after NRCSH3 which can be due to aggregation of the fillers in the NR matrix at high loading. Improvement in mechanical properties can be explained in terms of better dispersion of nanosilica and carbon nanotubes in the rubber achieved by the latex stage addition of filler dispersion. Haake mixing breaks down the filler network in the coagulum and distributes the fillers evenly in the matrix. These uniformly distributed fillers can distribute the applied stress thereby improving tensile strength of the composites.

Table 6.B.4 Mechanical properties of NR and NRCSH nanocomposites

Sample Name	Tensile strength(MPa)	Elongation at break (%)	Modulus 300 % (MPa)	Tear strength (N/mm)
NR	25.4±0.4	1154±52	1.96±0.18	36.7±0.5
NRCSH1	26.1±0.5	1037±60	2.65±0.17	36.9±1.0
NRCSH2	28.2±0.2	985±34	2.66±0.05	46.6±1.0
NRCSH3	30.1±0.4	931±77	3.08±0.13	50.2±0.7
NRCSH4	26.3±0.8	984±58	2.95±0.11	33.9±1.1

Abrasion resistance index, Compression set, Hardness and Rebound resilience of NR and NRCSH composites is depicted in Fig. 6.B.7.

Abrasion resistance of a material is the ability to resist mechanical rubbing or erosion[23]. Abrasion resistance index has been enhanced by 60% for the NRCSH3 composite compared to NR, indicating better filler-rubber interaction. Evenly distributed hybrid fillers increase interfacial rubber-filler interaction and improve abrasion resistance[24].

Compression set is a measure of the material's ability to retain elastic properties under prolonged action of compressive stress at some higher temperature. Lowering of compression set with hybrid filler loading and

almost 31% reduction observed for NRCSH2 composite is an advantage in the field of rubber application.

Hardness, which is a measure of low strain elastic modulus, was found to be increasing with hybrid filler loading. NRCSH3 composite showed highest hardness with 53% improvement, compared to NR.
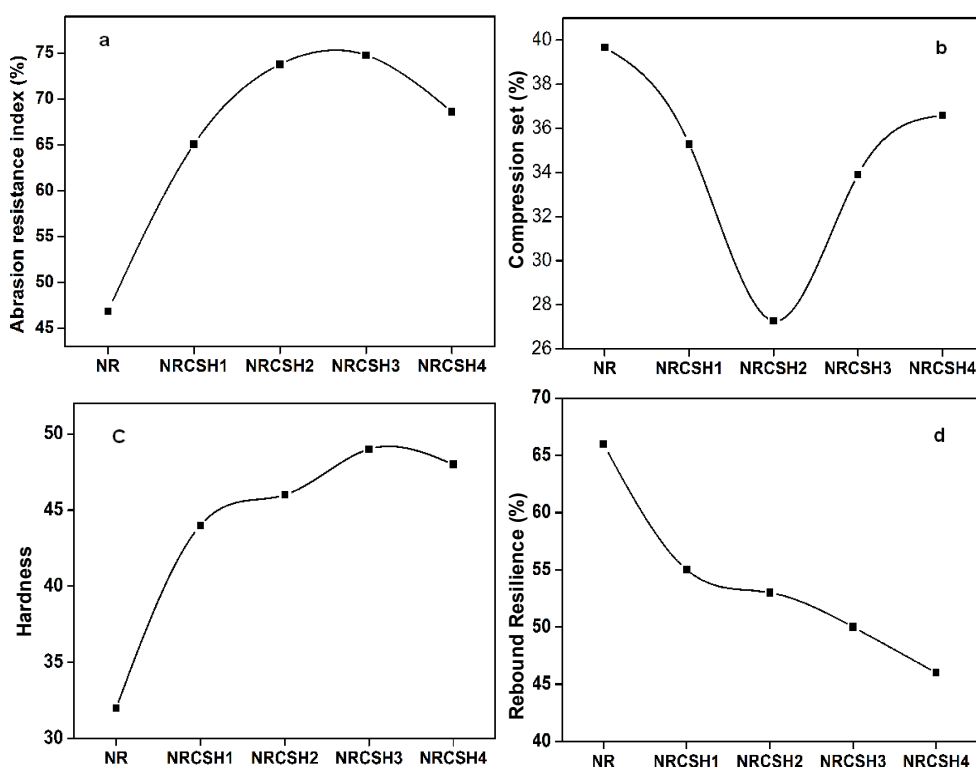
Fig. 6.B.7 Variation of Abrasion resistance index, Compression set, Hardness and Rebound resilience of NR and NRCSH composites with CS hybrid filler loading

Rebound resilience is the ratio of energy that is given up on recovery from deformation to the energy required to produce the deformation. Rebound resilience measures elasticity of the material and the property was found to decrease with CS hybrid filler addition. Almost 30% reduction in the resilience was observed for NRCSH4 nanocomposite.

Overall properties suggest good filler dispersion, better rubber-filler interaction and reinforcement for the NRCSH nanocomposites.

6.B.3.5 Comparison of mechanical properties of latex film cast samples with haake mixed samples

Fig. 6.B.8 compares the tensile strength, elongation at break, tear strength and modulus at 300% elongation of latex film cast (NRCSF) and Haake mixed (NRCSH) samples. NRCSF composites with segregated structure showed significant improvement in all the properties compared to the NRCSH samples. There is noticeable enhancement in tensile strength, tear strength and modulus while decrease in strain at break was observed for the NRCSF composites which can be attributed to the segregated structure. The trends suggest that the hybrid filler network located in the interstitial areas between the rubber particles increases stiffness but prevents the interparticle diffusion of rubber chains causing noticeable reduction in maximum elongation compared to neat rubber[25].

Dispersion morphology has an important role in reinforcement mechanism of the nanocomposites. Both NRCSF and NRCSH samples have well-distributed hybrid fillers in the rubber matrix. The hybrid filler consists of nanosilica particles decorated on the walls of nanotubes which helps in better dispersion of the filler in the rubber matrix. Similar studies regarding the improvement in mechanical properties achieved by employing surface modified MWCNTS in NR are reported elsewhere[26]. NRCSH samples have more uniform and homogeneous distribution of hybrid fillers compared to the film cast samples. Contrary to earlier reports the modulus values for Haake mixed samples are found to be higher than that for latex film cast samples which may be due to the high cross-link density for the former. Processing method has influence on the cross-link density of the samples as more crosslinks are possible in the case of compression moulded samples compared to the film cast ones. But the relative increase in modulus with

respect to neat rubber is still higher for the NRCSF composites and that can be credited to the segregated structure of the composites.
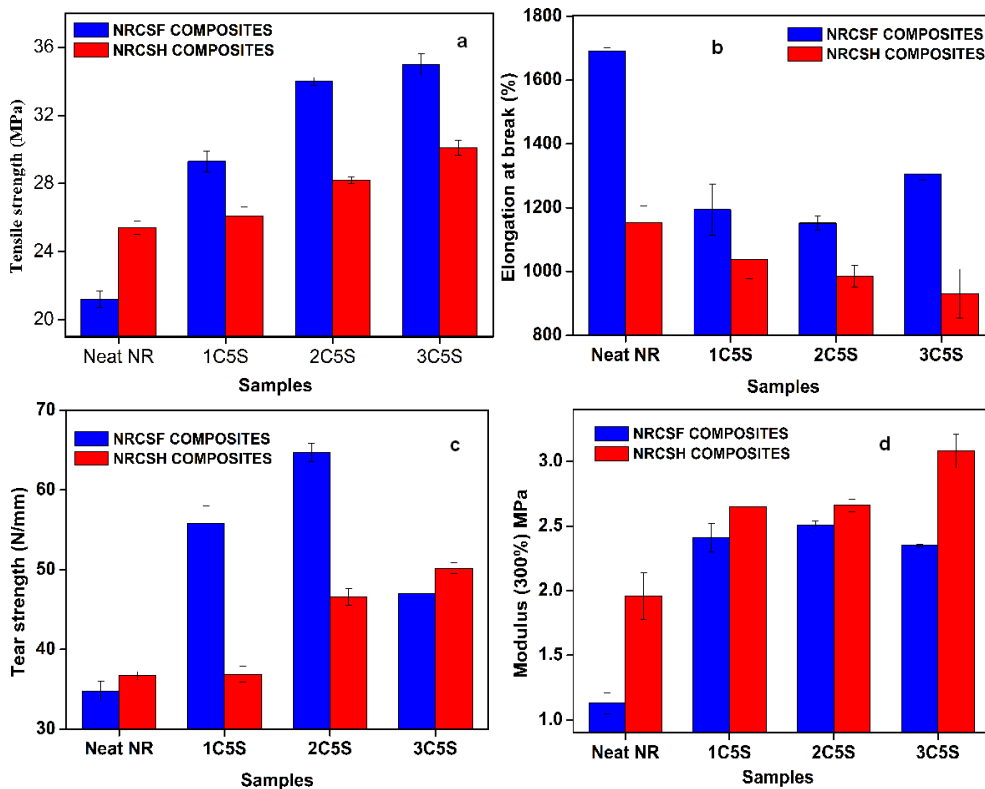
Fig. 6.B.8 Comparison of mechanical properties of NRCSF and NRCSH composites

6.B.3.6 Strain dependence of storage modulus

Strain dependence of storage modulus for the NRCSH nanocomposites is shown in Fig. 6.B.9 and that of NRCSF is given as the inset. In both cases strain dependency is more pronounced in the case of filled rubbers with increase in initial storage modulus with filler loading. E'_0-E'_∞ value which is the difference between high and low strain modulus is higher for NRCSF composites compared to NRCSH composites. This clearly indicates that break down of filler-filler network is more in the case of NRCSF composites due to

the presence of segregated filler network. Whereas the NRCSH composites contain uniformly distributed fillers, thereby reducing the filler-filler interaction and Payne effect[27].
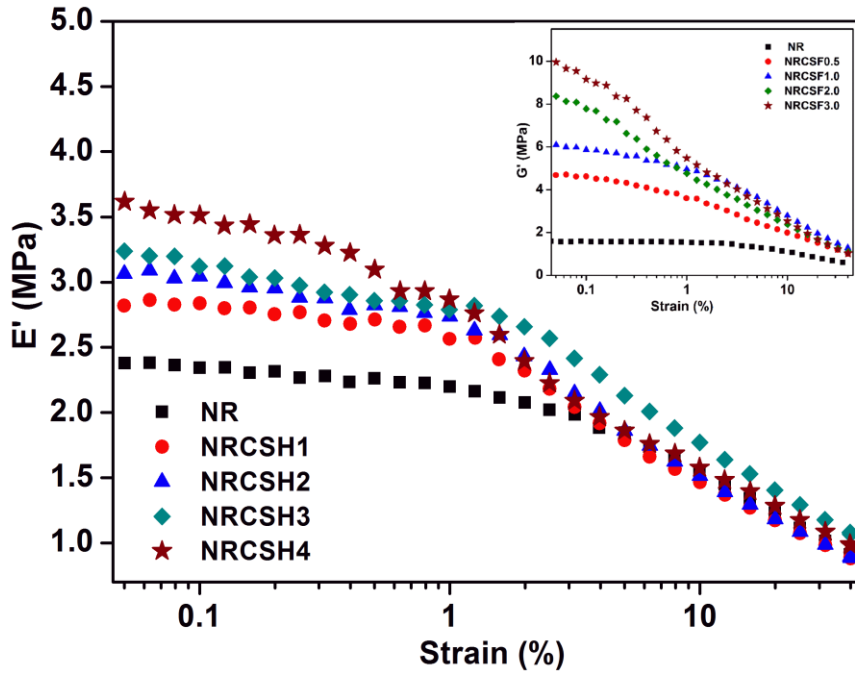
Fig. 6.B.9 Strain dependence of the storage modulus of NR and NRCSH nanocomposites

6.B.3.7 Crosslink density and solvent barrier properties

Variation of crosslink density and swelling index for the NRCSH nanocomposites is shown in Table 6.B.5. With increase in hybrid filler contents, the crosslink density increases whereas the swelling index decreases. This can be due to the physical crosslinks between the rubber chains and fillers, which restrict the motion of rubber chains and hinder the penetration of solvent through the rubber as reported elsewhere[28,29]. Decreased crosslink density and increased swelling index for the NRCSH4 composite suggest the possibility of filler aggregation at this filler concentration which is supported by the inferior mechanical properties observed for these samples.

Table 6.B.5 Crosslink density and Swelling index of NR and NRCSH composites

Samples	Crosslink density (x 10^{-5}mol/g)	Swelling Index (%)
NR	5.0	407
NRCSH1	6.5	352
NRCSH2	6.8	342
NRCSH3	7.0	334
NRCSH4	6.1	355

The sorption curves given in Fig.6.B.10 again confirms the improvement in crosslink density and hence reduction in solvent sorption with CS hybrid filler addition. Rate of solvent uptake is high in the beginning and reached a plateau known as equilibrium swelling for all the samples. Equilibrium swelling decreases with filler addition and minimum solvent intake is exhibited by the NRCSH3 composite. Higher solvent sorption observed with NRCSH4 composite can be related to the possibility of filler aggregation at this concentration that results in poor rubber filler interaction, which is confirmed by the lower crosslink density observed.
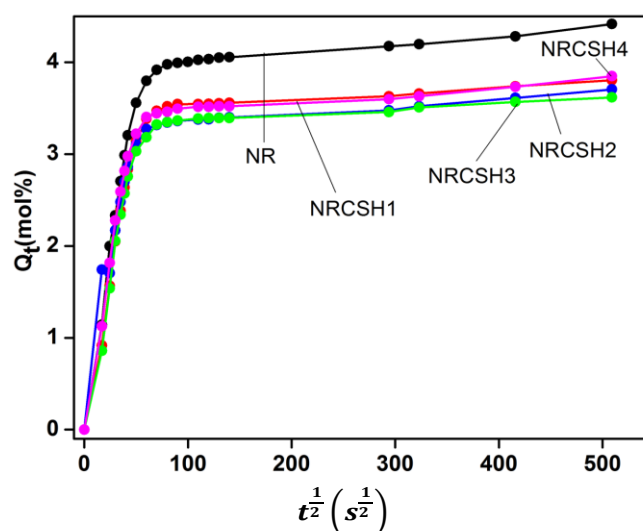
Fig. 6.B.10 Sorption curves of NR and NRCSH composites.

6.B.3.8 Thermal studies
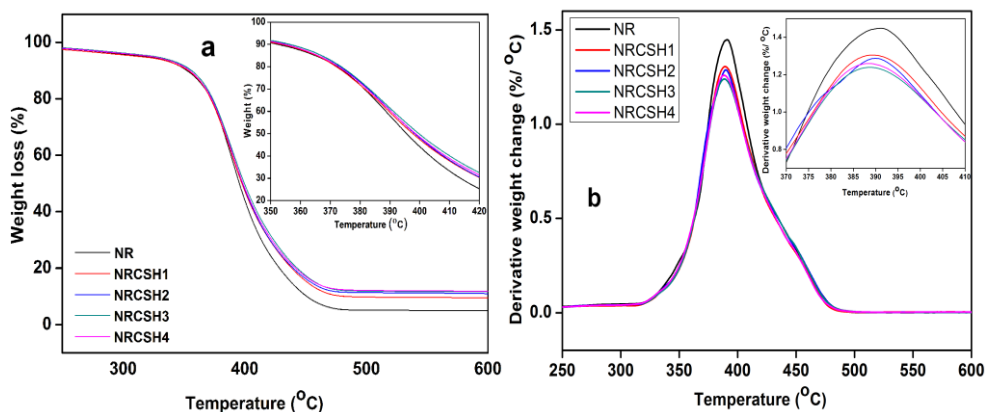
Fig. 6.B.11 (a) TGA and (b) DTG curves of NR and NRCSH nanocomposites

TGA and DTG curves (Fig.6.B.11a and b) and TGA data (Table 6.B.6) for the NRCSH composites reveal that the thermal stability of NR has not been affected by the addition of hybrid fillers. Only marginal improvement in thermal stability is observed for the NRCSH nanocomposites.

Table 6.B.6 TGA data for NR and NRSH nanocomposites

Property	NR	NRCSH1	NRCSH2	NRCSH3	NRCSH4
Onset degradation temperature (T_0,°C)	331	333	333	335	334
End set degradation temperature	483	478	477	477	475
Maximum degradation temperature (T_{max},°C)	391	390	389	389	389
Temperature at 50% degradation (T_{50},°C)	396	398	398	400	399
Residue at 600°C (%)	4.98	9.47	10.98	11.65	11.80

6.B.3.9 DC electrical conductivity

DC conductivity values obtained for the NRCSH composites (Fig. 6.B.12) are in good agreement with the arrangement of fillers proposed for the composite. There is no dramatic change in the conductivity with filler loading suggesting the absence of continuous conductive network for the composites. Moreover the presence of insulating silica particles around carbon nanotubes can hinder the proper contact between the conducting nanotubes and can result in poor conductivity.

Large difference in the electrical conductivity of the film cast samples (NRCSF) and the samples prepared by latex coagulation followed by mixing by an internal mixer (NRCSH) can be attributed to the difference in filler distribution in the two. The segregated filler network possible in the NRCSF composites makes the conductive filler network formation possible at very small concentration of the filler. Whereas in NRCSH, the mixing process breaks down the filler network and distributes the fillers in a more uniform and homogeneous way so that the conducting channels are formed at a higher filler fraction.
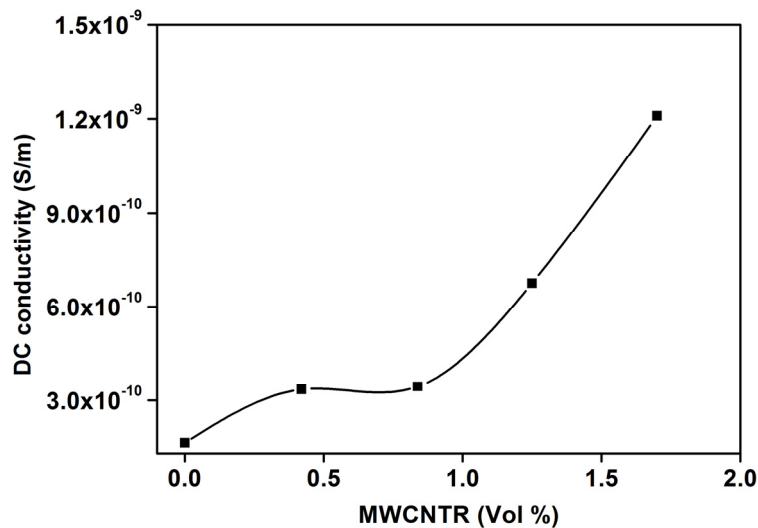
Fig. 6.B.12   DC conductivity versus MWCNTR concentration for the NRCSH composite

6.B.3.10 Dielectric studies

Variation of dielectric permittivity, dielectric loss and AC conductivity of NRCSH nanocomposites is shown in Fig.6.B.13.
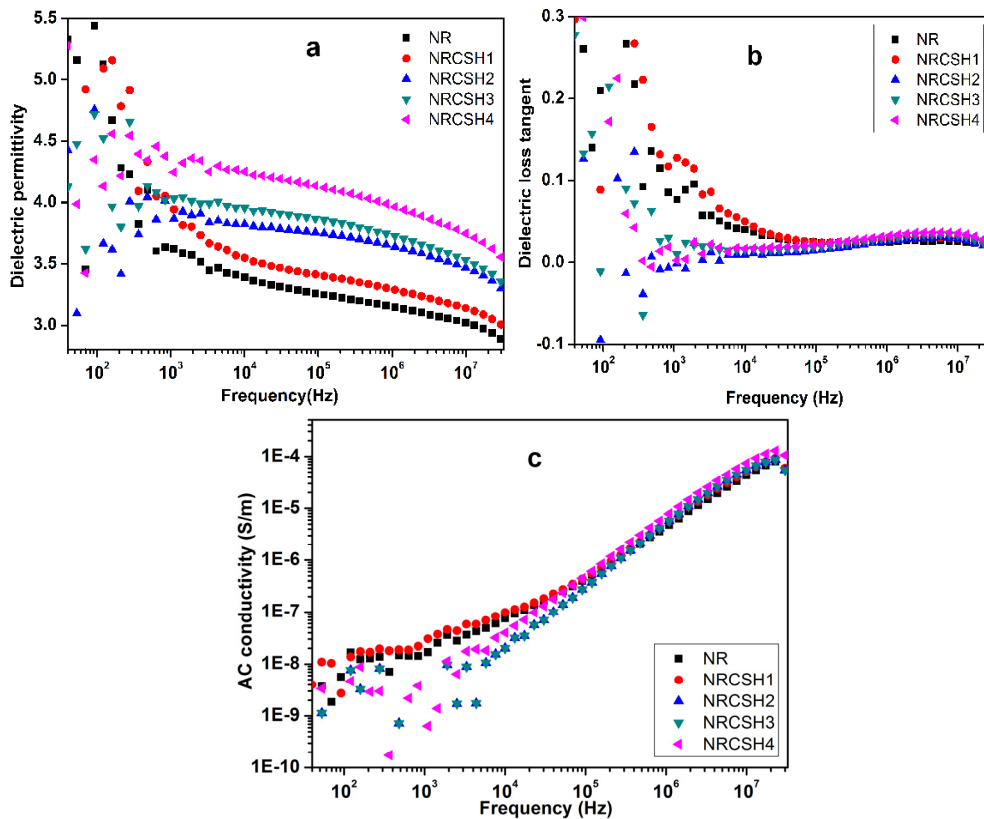
Fig. 6.B.13 Variation of (a) dielectric constant (b) dielectric loss tangent and (c) AC conductivity with frequency for NRCSH composites

The figure clearly shows that all the properties increase with hybrid filler addition which can be explained in terms of the increase in polarisation caused by increased amount of conducting fillers in the rubber matrix. Increase in dielectric constant for the nanocomposites can be explained in terms of the microcapacitor model[30]. According to this model uniformly distributed conducting hybrid fillers in an insulating rubber matrix is equivalent to a number of microcapacitors. With increase in hybrid filler concentration the

number of microcapacitors increases and causes gradual increase in dielectric permittivity. Both dielectric constant and dielectric loss decreased with increasing frequency which can be due to the insufficient time for the polymer chain relaxation at higher frequencies.

AC conductivity of the NRCSH nanocomposites (Fig. 6.B.13c) does not show any abrupt increase indicating that the percolation has not been achieved for the composite. The conducting hybrid fillers are homogeneously dispersed in the matrix and only non-Ohmic conduction occurs due to the tunnelling effect between conducting fillers. Moreover the presence of non- conducting nanosilica on the nanotubes prevents direct contact between the conducting CNTs and thus makes Ohmic conduction impossible.
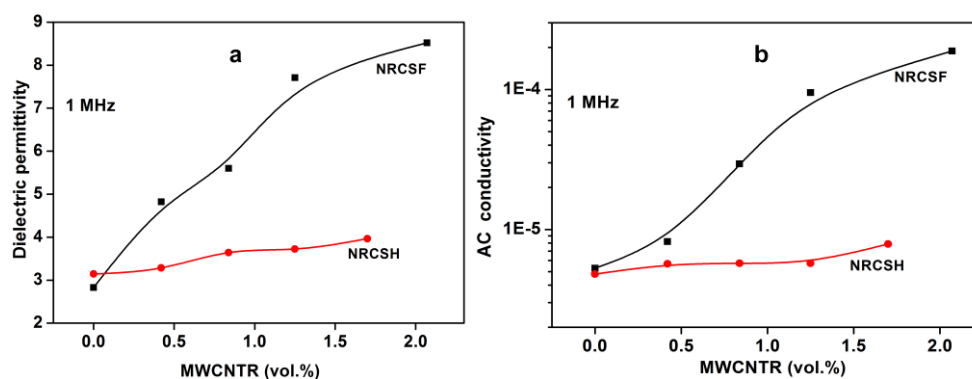
Fig. 6.B.14 (a) Comparison of dielectric permittivity and (b) AC conductivity of NRCSF and NRCSH composites at 1MHz

Comparison of dielectric permittivity (Fig. 6.B.14a) and AC conductivity (Fig. 6.B.14b) of NRCSF and NRCSH composites substantiates that the nature of filler distribution plays a major role in determining electrical properties of the composite. Significant improvement in dielectric constant and AC conductivity has been observed for the segregated structured NRCSF composites whereas only a marginal increase is observed for NRCSH composites with non-segregated structure. Segregated conductive polymer composites are well-known for their ultra-low electrical percolation threshold,

as the conducting fillers are confined to the periphery of polymeric granules and thereby utilizing minimum amount of the nanotubes to form a conductive network[31]. NRCSF composites are reported to have a percolation threshold of 0.80 vol % of MWCNTR in the hybrid filler (Chapter 6A). Large difference in conductivity for the two composites is a clear evidence for the type of filler network present in the systems.

6.B.3.11 EMI shielding effectiveness

EMI shielding effectiveness (SE) of the NRCSH composites in the frequency range 8-12 GHz is shown in Fig.6.B.15. Compared to NRCSF composites the SE observed in this case is small which can be related to the filler morphology and electrical properties.
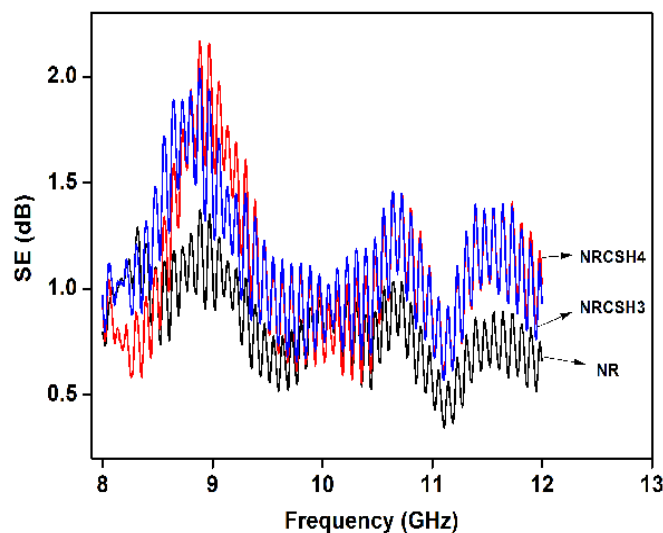
Fig. 6.B.15 Variation of SE with frequency of NRCSH composites

The NRCSH composites have poor electrical properties compared to NRCSF which have been discussed in the previous sections. Gupta et al.[32] and Huang et al.[33] have demonstrated that conductivity of the CNTs influences the shielding efficiency with highly conducting long nanotubes exhibiting better SE compared to short tubes. Random dispersion of conducting fillers makes

the connection between fillers possible only at high concentration leading to poor electrical properties at low loading. NRCSH composites contain CS hybrid fillers at random and have not attained percolation threshold even at 4 phr of MWCNT in hybrid filler. Silica coating over MWCNTs in the present filler morphology also does not help in getting good electrical properties leading to poor SE.

6.B.4 Conclusions

The processing method influences filler distribution inside the polymer matrix and hence properties of the composites. NRCSH composites prepared by Haake mixing possess random CS hybrid filler network whereas NRCSF composites contain segregated structure. NRCSH composites exhibit best mechanical properties at 3C5S nanohybrid loading. Improved solvent resistance and crosslink density observed for NRCSH composites indicate good rubber-filler interaction. Thermal stability of the rubber was unaffected by the added CS hybrid fillers. The electrical properties were inferior compared to the latex film cast samples. This can be attributed to the absence of continuous conductive filler network inside the polymer. The study reveals that random network of filler is beneficial in getting good mechanical properties whereas it has detrimental effect on electrical properties.

References

[1]   Kong, L., Chen, Y., Peng, Z., & Li, P. (2008). Latex-based nanocomposites. *Progress in polymer nanocomposite research*, 83-104.

[2]   Wang, Y., Zhang, L., Tang, C., & Yu, D. (2000). Preparation and characterisation of rubber–clay nanocomposites. *Journal of Applied Polymer Science*, 78(11), 1879-1883.

[3]   Zhang, L., Wang, Y., Wang, Y., Sui, Y., & Yu, D. (2000). Morphology and mechanical properties of clay/styrene-butadiene rubber nanocomposites. *Journal of Applied Polymer Science*, 78(11), 1873-1878.

[4]   Zhao, L., Sun, X., Liu, Q., Zhao, J., & Xing, W. (2015). Natural Rubber/ Graphene Oxide Nanocomposites Prepared by Latex Mixing. *Journal of Macromolecular Science, Part B*, *54*(5), 581-592.

[5]   Potts, J. R., Shankar, O., Murali, S., Du, L., & Ruoff, R. S. (2013). Latex and two-roll mill processing of thermally-exfoliated graphite oxide/natural rubber nanocomposites. *Composites Science and Technology*, *74*, 166-172.

[6]   Ponnamma, D., Sung, S. H., Hong, J. S., Ahn, K. H., Varughese, K. T., & Thomas, S. (2014). Influence of non-covalent functionalisation of carbon nanotubes on the rheological behavior of natural rubber latex nanocomposites. *European Polymer Journal*, *53*, 147-159.

[7]   Bokobza, L., Rahmani, M., Belin, C., Bruneel, J. L., & El Bounia, N. E. (2008). Blends of carbon blacks and multiwall carbon nanotubes as reinforcing fillers for hydrocarbon rubbers. *Journal of Polymer Science Part B: Polymer Physics*, *46*(18), 1939-1951.

[8]   Lorenz, H., Fritzsche, J., Das, A., Stöckelhuber, K. W., Jurk, R., Heinrich, G., & Klüppel, M. (2009). Advanced elastomer nano-composites based on CNT-hybrid filler systems. *Composites Science and Technology*, *69*(13), 2135-2143.

[9]   Ismail, H., Ramly, A. F., & Othman, N. (2013). Effects of silica/multiwall carbon nanotube hybrid fillers on the properties of natural rubber nanocomposites. *Journal of Applied Polymer Science*, *128*(4), 2433-2438.

[10]   Galimberti, M. (Ed.). (2011). *Rubber-clay nanocomposites: science, technology, and applications*. John Wiley & Sons.

[11]   Wu, Y. P., Wang, Y. Q., Zhang, H. F., Wang, Y. Z., Yu, D. S., Zhang, L. Q., & Yang, J. (2005). Rubber–pristine clay nanocomposites prepared by co-coagulating rubber latex and clay aqueous suspension. *Composites Science and Technology*, *65*(7), 1195-1202.

[12]   Gao, J. F., Li, Z. M., Meng, Q. J., & Yang, Q. (2008). CNTs/UHMWPE composites with a two-dimensional conductive network. *Materials Letters*, *62*(20), 3530-3532.

[13]   Tian, M., Zhang, J., Zhang, L., Liu, S., Zan, X., Nishi, T., & Ning, N. (2014). Graphene encapsulated rubber latex composites with high dielectric constant, low dielectric loss and low percolation threshold. *Journal of colloid and interface science*, *430*, 249-256.

[14] Francis, L. F., Grunlan, J. C., Sun, J., & Gerberich, W. W. (2007). Conductive coatings and composites from latex-based dispersions. *Colloids and Surfaces A: Physicochemical and Engineering Aspects*, *311*(1), 48-54.

[15] Mensah, B., Kim, H. G., Lee, J. H., Arepalli, S., & Nah, C. (2015). Carbon nanotube-reinforced elastomeric nanocomposites: a review. *International Journal of Smart and Nano Materials*, *6*(4), 211-238.

[16] Teh, P. L., Ishak, Z. M., Hashim, A. S., Karger-Kocsis, J., & Ishiaku, U. S. (2004). Effects of epoxidized natural rubber as a compatibilizer in melt compounded natural rubber–organoclay nanocomposites. *European Polymer Journal*, *40*(11), 2513-2521.

[17] Yuca,N. Karatepe,N. Yakuphanoğlu,N. (2011). World Academy of Science, Engineering and Technology, 79 ,611.

[18] Sezna, J. A., Pawlowski, H. A., & DeConinck, D. (1989). New test results from rotorless curemeters. In *Proceeding of 136th meeting of the ACS-rubber division*.

[19] M.P. Wagner. (1976). Rubber Chem. TedmoI, 49,703.

[20] James, H. M., & Guth, E. (1943). Theory of the elastic properties of rubber. *The Journal of Chemical Physics*, *11*(10), 455-481.

[21] Fornes, T. D., & Paul, D. R. (2003). Modeling properties of nylon 6/clay nanocomposites using composite theories. *polymer*, *44*(17), 4993-5013.

[22] Mullins, L., & Tobin, N. R. (1965). Stress softening in rubber vulcanisates. Part I. Use of a strain amplification factor to describe the elastic behavior of filler-reinforced vulcanised rubber. *Journal of Applied Polymer Science*, *9*(9), 2993-3009.

[23] Wanvimon Arayapranee, Dr MarcinAdamiak (Ed.) (2012). Rubber Abrasion Resistance, Abrasion Resistance of Materials, , ISBN: 978-953-51-0300-4.

[24] Arayapranee, W., Na-Ranong, N., & Rempel, G. L. (2005). Application of rice husk ash as fillers in the natural rubber industry. *Journal of applied polymer science*, *98*(1), 34-41.

[25] Steward, P. A., Hearn, J., & Wilkinson, M. C. (2000). An overview of polymer latex film formation and properties. *Advances in colloid and interface science*, *86*(3), 195-267.

[26] Peng, Z., Feng, C., Luo, Y., Li, Y., & Kong, L. X. (2010). Self-assembled natural rubber/multi-walled carbon nanotube composites using latex compounding techniques. *Carbon*, *48*(15), 4497-4503.

[27] Bokobza, L. (2012). Multiwall carbon nanotube-filled natural rubber: Electrical and mechanical properties. *Express Polymer Letters*, *6*(3), 213–223.

[28] Kader, M. A., Kim, K., Lee, Y. S., & Nah, C. (2006). Preparation and properties of nitrile rubber/montmorillonite nanocomposites via latex blending. *Journal of materials science*, *41*(22), 7341-7352.

[29] Yan, N., Wu, J. K., Zhan, Y. H., & Xia, H. S. (2009). Carbon nanotubes/ carbon black synergistic reinforced natural rubber composites. *Plastics, Rubber and Composites*, *38*(7), 290-296.

[30] Dang, Z. M., Wang, L., Yin, Y. I., Zhang, Q., & Lei, Q. Q. (2007). Giant dielectric permittivities in functionalised carbon-nanotube/electroactive-polymer nanocomposites. *Advanced Materials*, *19*(6), 852-857.

[31] Pang, H., Xu, L., Yan, D. X., & Li, Z. M. (2014). Conductive polymer composites with segregated structures. *Progress in Polymer Science*, *39*(11), 1908-1933.

[32] Gupta, T. K., Singh, B. P., Teotia, S., Katyal, V., Dhakate, S. R., & Mathur, R. B. (2013). Designing of multiwalled carbon nanotubes reinforced polyurethane composites as electromagnetic interference shielding materials. *Journal of Polymer Research*, *20*(6), 169.

[33] Li, N., Huang, Y., Du, F., He, X., Lin, X., Gao, H., ... & Eklund, P. C. (2006). Electromagnetic interference (EMI) shielding of single-walled carbon nanotube epoxy composites. *Nano letters*, *6*(6), 1141-1145.

.....ജ്ഞ.....

Chapter 7

CARBOXYLATED MULTIWALLED CARBON NANOTUBES IN CARBOXYLATED NITRILE BUTADIENE RUBBER LATEX

Carboxylated nitrile rubber (XNBR)/ Carboxylated MWCNT (MWCNTR) composites were prepared by adopting two processing techniques. XCF composites were prepared by the latex stage mixing of the MWCNTR aqueous dispersion followed by film casting and curing which resulted in segregated nanotube network due to the alignment of the MWCNTRs along the periphery of the rubber latex spheres on drying. XCH composites were prepared by co-coagulating the nanotube dispersion with NR latex followed by drying and mixing in an internal mixer which destroyed the segregated network structure yielding a random dispersion of fillers in the matrix. Comparison of properties of both vulcanisates revealed that incorporation of multiwalled carbon nanotubes in XNBR has significantly enhanced the mechanical and solvent barrier properties in both cases. However the electrical properties were highly dependent on the filler morphology inside rubber; with good electrical properties at very low percolation threshold for the XCF composites due to the segregated conductive network and poor electrical properties for the XCH composites due to the absence of conductive network.

XNBR/CARBOXYLATED MWCNT COMPOSITES WITH SEGREGATED NETWORK

7.A.1 Introducion

Carboxylated nitrile rubber (XNBR) is a high performance terpolymer of acrylonitrile, butadiene and monomers like acrylic and methacrylic acid[1]. XNBR shows excellent gum tensile strength compared to NBR. Nevertheless, improvement in the properties of XNBR by the addition of filler is reported elsewhere[2-7]. Tian et al.[8] have reported high performing graphene encapsulated XNBR composites having segregated graphene network with high dielectric properties at low percolation threshold. Yang et al.[9] studied the functional properties of expanded graphite filled XNBR composites and established that the composites had improved mechanical strength and electrical conductivity along with excellent gas barrier and wear properties. XNBR being a polar rubber with pendant carboxyl groups along the hydrocarbon chain is expected to interact with polar fillers more efficiently when compared to other nonpolar diene rubbers. Works on CNT filled XNBR composites with segregated network have not been reported in the literature. Nair et al.[10] have studied mechanical and electrical properties of the XNBR/MWCNT composites. They have used a surfactant (SDBS) assisted sonication of MWCNTs in water and latex stage blending of the CNT dispersion in XNBR and have reported significant enhancement in mechanical and electrical properties.

In the previous chapters formation of segregated and random network of nanofillers was studied using NR which is nonpolar rubber. In the present work, XNBR-a polar rubber, is chosen to understand the possibility of segregated filler network formation during latex stage mixing and the effect of processing method on the filler morphology. The study involves the incorporation of aqueous dispersion of carboxylated MWCNTs in XNBR latex and further processing in two different ways. The first processing method

proposes to add the compounding ingredients as aqueous dispersions to the above mix followed by bath sonication, film casting and curing. The second method involves the co-coagulation of the MWCNTR with XNBR latex, followed by compounding of the dried coagulum in an internal mixer. The processing method has an important role in deciding the filler morphology inside a polymer. This part of the study evaluates the mechanical and electrical properties of the XNBR/ MWCNTR composites prepared by latex stage processing.

7.A.2 Experimental

7.A.2.1 Preparation of carboxylated multiwalled carbon nanotube (MWCNTR) aqueous dispersion

MWCNTR and their aqueous dispersions were prepared as per the procedures given in 4.A.2.1 and 4.A.2.3 respectively. MWCNTR dispersion for each composition was prepared separately.

7.A.2.2 Preparation of XCF nanocomposites

XNBR latex (45% DRC) was diluted to 25% by adding distilled water and to that MWCNTR dispersion was added and the mixture was sonicated for 30 minutes using a bath sonicator so as to achieve uniform distribution of the filler in the latex. Then the latex was compounded as per formulation given in Table 7.A.1.

Table 7.A.1 Formulation of Latex

Ingredients	Amount (g)
XNBR latex (45% DRC)	222
MWCNTR	0, 0.1, 0.3, 0.5, 0.7, 1.0, 3.0, 5.0, 7.0
20% vulcastab VL solution	1.0
50% ZnO dispersion	4.0
50% ZDC dispersion	2.0
50% sulphur dispersion	2.0

The compounded latex was kept overnight for maturation, then cast on to flat glass trays, dried at 50 °C for 24 h and cured at 100 ^{0}C for 45 minutes in an air oven to get XCF nanocomposites. The composites are labelled as XCF composites with the content of MWCNTRs in phr suffixed. For example XCF0.1 refers to XNBR/MWCNTR composite containing 0.1 phr MWCNTR.

7.A.2.3 Characterisation

FTIR, SEM and HRTEM techniques were used for the characterisation of the XCF composites. The tensile and tear tests were done on UTM, as per ASTM D 412 and D 624 respectively. The strain-amplitude dependent dynamic mechanical properties of the vulcanisates were measured at room temperature by means of DMA.

Sorption behavior and cross-link density values of the samples were determined by equilibrium swelling method using methyl ethyl ketone (MEK) as the solvent. Thermogravimetric analysis, DC conductivity, AC conductivity, dielectric and EMI shielding studies of the composites were performed.

Detailed description on each characterisation is given in chapter 2.

7.A.3 Results and discussion

7.A.3.1 Interfacial interactions between XNBR and MWCNTR

For the XNBR/MWCNTR composite, H-bonding is possible between XNBR and MWCNTs due to the presence of –COOH and –OH functional groups on the surface of MWCNTRs and pendent –COOH groups on XNBR chains (Fig. 7.A.4a). FTIR spectra of XNBR and XCF composites given in Fig.7.A.1 confirm the presence of H-bonding. FTIR spectrum of neat XNBR (XCF0) shows characteristic peaks at 3000-3500 cm^{-1} (H-bonded O-H), 2850 and 2925 cm^{-1} (-CH$_2$ stretch), 2238 cm^{-1} (-CN) and

1716 cm^{-1} (C=O). XCF composites also show similar peaks and weakening of the peak corresponding to the C=O stretch in XCF composite indicates the presence of H-bond, that restricts free C=O stretching. C=O peak for 1.0 phr MWCNTR loading shows a blue shift from 1716 cm^{-1} to 1736 cm^{-1} and H-bonded –OH band shows broadening which again confirms the H-bond formation between XNBR and carboxylated MWCNTs. These H-bonds can improve the rubber-filler interactions resulting in good mechanical performance of the XCF nanocomposites.
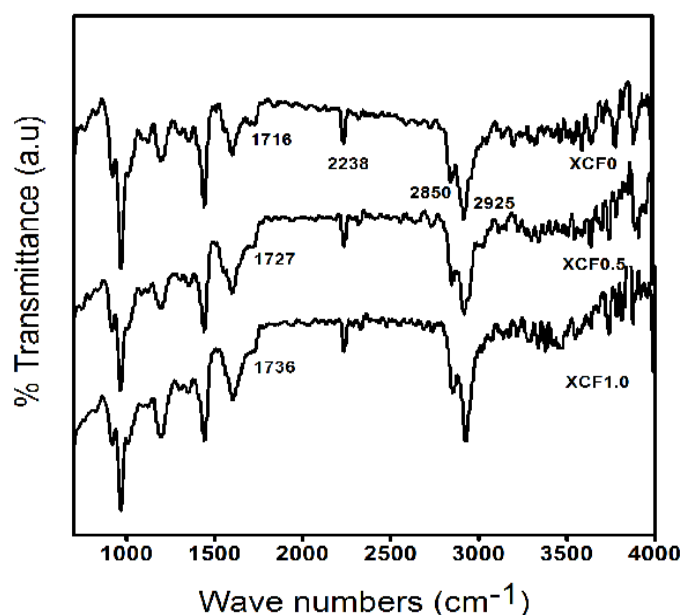
Fig. 7.A.1 FTIR spectra of neat XNBR (XCF0) and XCF composites

7.A.3.2 Microstructure of XCF composites

Fig. 7.A.2 shows the TEM images of the XCF composite film formed on the TEM grid that demonstrates the segregated network of MWCNTs in the XNBR. The image clearly shows that CNTs are wrapped around the XNBR microspheres of about 200 nm diameter and these tubes are interconnected to form beautiful network in the composite. In the TEM

images darker lines are the nanotubes and lighter portions are the rubber spheres.
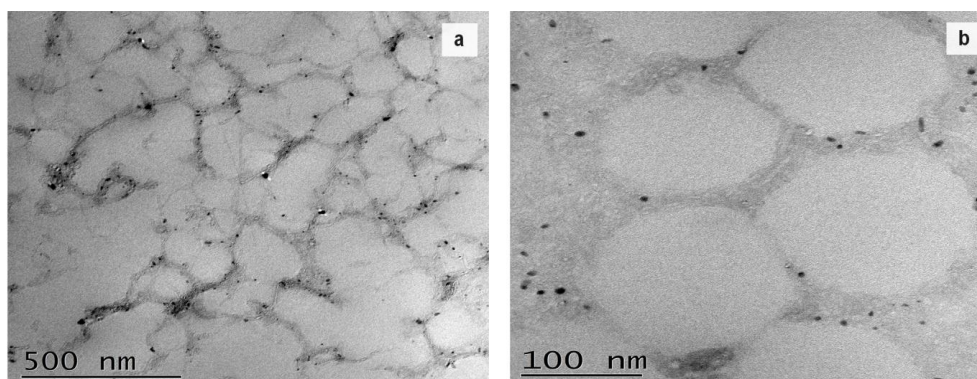
Fig. 7.A.2 TEM images of XCF0.5 composite film formed on the TEM grid which shows that carboxylated MWCNTs form a segregated structure in the rubber matrix

7.A.3.3 Fracture surface morphology

SEM images of the fractured surfaces of pure XNBR (XCF0) and XCF0.5 nanocomposite are shown in Fig. 7.A.3. The fracture patterns observed for the nanocomposite is entirely different from neat rubber. Fractured surfaces are smooth for neat rubber whereas they become rough in the composite. Magnified images of the XCF0.5 nanocomposite (Fig. 7.A.3e and f) clearly show the nanotube network around the broken rubber particles confirming the segregated network of MWCNTRs. Rupture patterns observed for the composite is in agreement with the concept that nanotubes are aligned along the periphery of rubber particles to form segregated network.
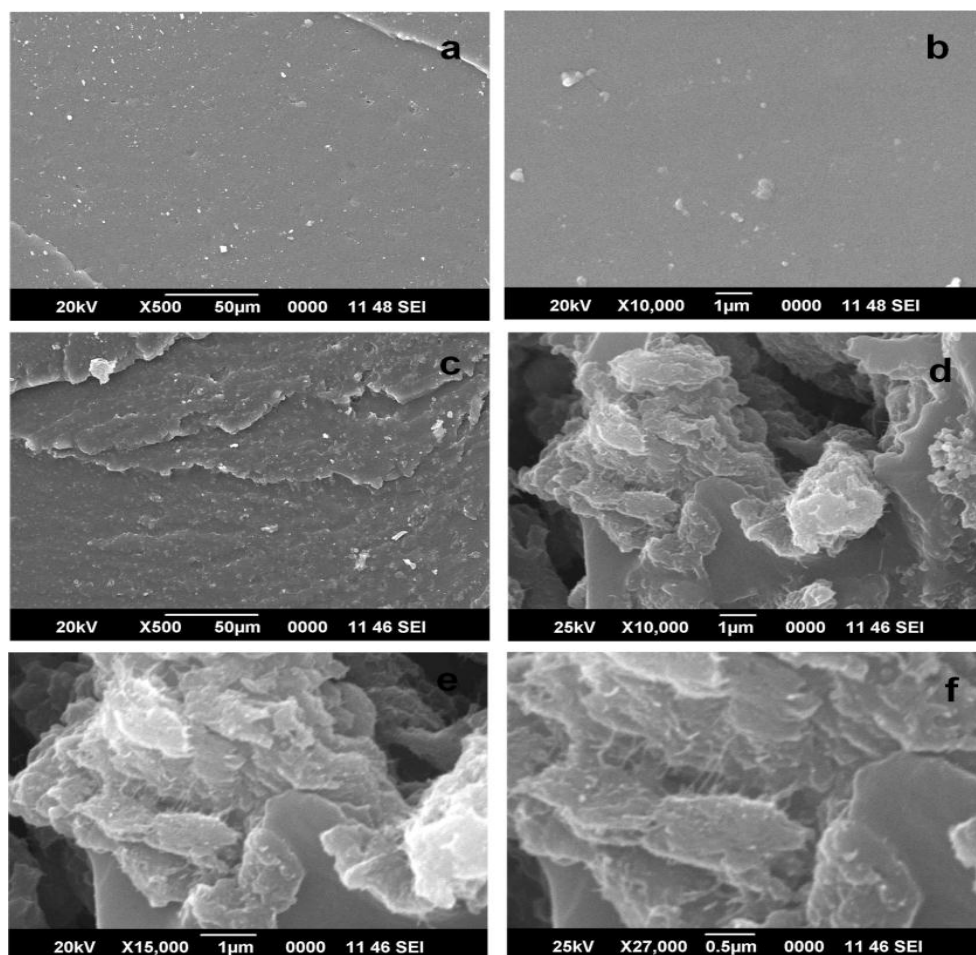
Fig. 7.A.3 SEM images of fractured surfaces of (a-b) XCF0 (c-f) XCF0.5 at different magnifications

7.A.3.4 Segregated network formation in XCF composites

Fig. 7.A.4 shows the schematic representation of the attachment of the carboxylated MWCNTs on XNBR latex particles and formation of segregated nanotube network in the rubber matrix. The assembly of nanotubes around XNBR latex spheres is facilitated by the H- bonding between the carboxyl groups in XNBR and oxygen containing groups in MWCNTR (Fig.7.A.4a) as suggested by Kang et al.[11]. According to them

the π-π interaction between the nanotubes and C=C, C≡N bonds of XNBR also plays significant role in the wrapping of MWCNTs around the XNBR latex particles. When the composite film is formed by casting followed by curing, web like network of nanotubes is formed since these are pushed to the periphery of the crosslinked rubber spheres, as shown in Fig. 7.A.4 (b & c). Zhan et al.[12] suggest that the segregated structure will be retained even after curing since the high viscosities of the rubber particles prevent the nanotubes from penetrating inside the crosslinked rubber.
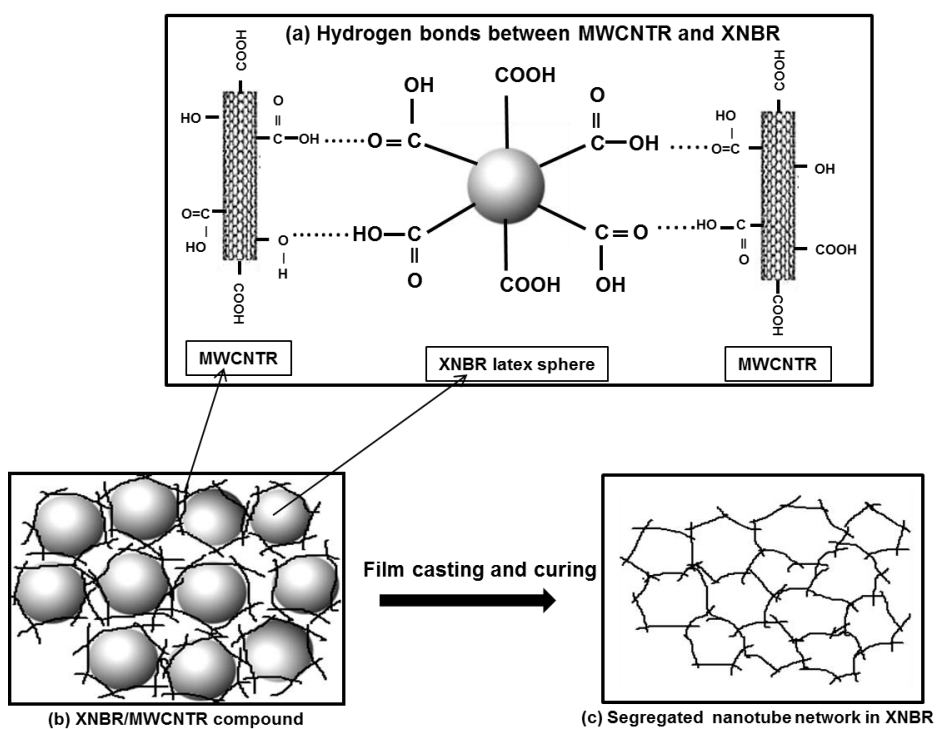
Fig. 7.A.4. Segregated network formation in XCF composites

7.A.3.5 Mechanical properties

Mechanical properties of the XCF composites are listed in Table 7.A.2. The properties are remarkably improved with nanotube loading, reach maximum at a particular loading and then decrease. The composites with

segregated structure are reported to have better electrical properties but inferior mechanical properties. Because the molecular diffusion between the polymer domains is prevented by the segregated fillers in the interfacial region[13,14]. The reason for better properties exhibited by the XCF0.5 composites in the present study can be explained as follows. At 0.5 phr MWCNTR, nanotubes form thin network around the XNBR spheres and intermolecular diffusion of rubber chains is possible which strengthens the polymer. But further increase in nanotube concentration can cause the aggregation of the nanotubes in between the rubber spheres causing the inter-diffusion difficult resulting in easy failure of the polymer. Compared to neat rubber all the composites exhibit improved mechanical properties. Almost 65 % improvement in tensile strength and 32% in modulus was observed for XCF0.3. Tear strength also increased by 22% for XCF0.7.

Reinforcement of NR by the MWCNTR in the composite can be explained in terms of the large aspect ratio and physical entanglement of CNTs with rubber. The nanotube network formed around the rubber particles divides the NR matrix into small units and gives a cellular structure. The cellular structure and occluded rubber (due to the confinement of rubber within the networks) in the NR-MWCNTR composite provides tremendous reinforcement[15].

Strong interfacial interaction between XCF and oxidised MWCNTs along with good filler dispersion increases the effectiveness of stress transfer from rubber to filler and results in enhanced tensile strength, tear strength and modulus[16-18]. High aspect ratio and large surface area of the nanotubes also contribute towards improved interaction with the rubber matrix. π-π interaction between the nanotubes and XNBR also plays an important role in reinforcement. Reduction in the properties at high nanotube loading can be attributed to the aggregation of nanotubes in the network preventing the diffusion of polymer chains.

Table 7.A.2 Mechanical properties of the XCF composites

Sample Name	Tensile strength(MPa)	Elongation at break (%)	Modulus 300 % (MPa)	Tear strength (N/mm)
XCF0	4.50±0.31	845±20	2.90±0.13	16.5±1.2
XCF0.1	6.86±0.45	833±15	3.49±0.08	16.6±5.4
XCF0.3	7.44±0.30	895±26	3.82±0.04	16.7±2.2
XCF0.5	6.50±0.15	863±18	3.62±0.10	18.5±1.9
XCF0.7	6.05±0.12	812±18	3.37±0.18	20.2±0.6
XCF1.0	5.63±0.10	838±33	2.90±0.10	15.4±3.4

7.A.3.6 Swelling studies

Further supporting evidence for the enhanced rubber-nanotube interactions is provided by the swelling behaviour. Crosslink density and swelling index of the composites against nanotube loading is presented in Table 7.A.3. It can be seen that the number of cross-links have been increased compared to the pure rubber sample and opposite behaviour is observed in the case of swelling index data. The composite containing 0.7 phr MWCNTR shows the highest crosslink density and lowest swelling index. The sorption curves given in Fig.7.A.5 also substantiates that addition of nanotube has lowered the solvent uptake. The curves consist of initial steeper region indicating high sorption rate and final steady region showing equilibrium solvent uptake. As the nanotube content increases the solvent uptake decreases which can be related to the segregated nanotube structure present inside the rubber. Nanotubes are distributed in the periphery of the rubber spheres creating tortuous path that can slow down the solvent penetration through the rubber[19]. Moreover strong interfacial bonding restricts the chain mobility and the polymer chains become less flexible. This increases the tortuosity and restricts the entrance of solvent molecules into the interfacial regions[20]. There is slight increase in the solvent uptake for the XCF1.0 composite which may be due to the agglomeration of the fillers in the segregated structure. The aggregation can lead to micro voids or free

volume in the segregated path which allows penetration of solvent into the rubber.

Table 7.A.3 Crosslink density and Swelling index of XCH composites

Sample name	Crosslink density (x 10^{-5} mol/g)	Swelling Index (%)
XCF0	0.5	436
XCF0.1	1.0	434
XCF0.3	1.3	432
XCF0.5	1.6	400
XCF0.7	2.4	375
XCF1.0	2.4	383
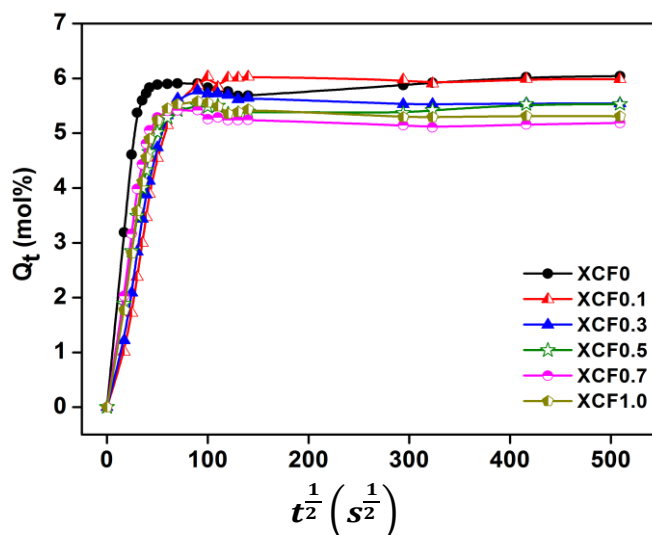
Fig. 7.A.5 Sorption curves of XCF composites

7.A.3.7 Strain-amplitude dependent dynamic mechanical properties

The strain dependence of storage modulus especially at low strain can deliver worthy information on the filler-filler networking in the rubber. Fig.7.A.6 shows variation in the storage modulus (E') of the vulcanisates with strain amplitude. A decrease in storage modulus with strain is observed for all compounds. Usually unfilled compounds exhibit strain independent dynamic behaviours, whereas in the present case a decrease in E' with strain

is observed for the XCF0 compound. This is due the breakage of ionic crosslinks that act as reinforcing sites. Same behaviour observed in the case of XCF composites is associated with the breakage of the filler network[21,22] (Payne effect). In the XCF composites filler-filler networks are successively broken on applying strain resulting in decrease in storage modulus. Increase in Payne effect with nanotube loading in XNBR confirms the existence of nanotube network inside XNBR.
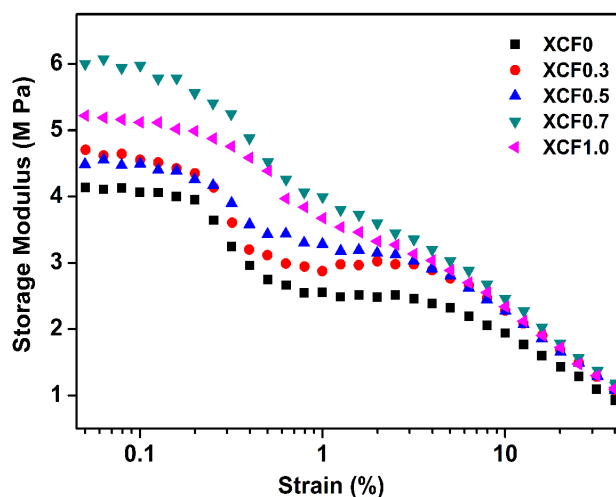
Fig. 7.A.6 Strain dependence of the storage modulus of XCF nanocomposites

However the modulus values (E′) of the composites are higher than the unfilled compound. Increase in E′ with MWCNTR loading can be ascribed to the hydrodynamic effect of the rigid fillers. Increase in filler concentration leads to increase in bound rubber or trapped rubber in the matrix. This causes increase in the effective volume of the filler causing enhancement in modulus of the rubber[23].

7.A.3.8 Thermal studies

Thermograms of XCF nanocomposites are presented in Fig. 7.A.7 and the relevant data is given in Table 7.A.4. Small increase in the T_{onset} and T_{50}

value for the composites indicates increased thermal stability of XNBR on addition of the oxidised nanotubes. Residual weight also increased with nanotube addition. Slight improvement in the thermal stability of the composites can be attributed to the easy dissipation of heat energy possible by the highly conducting segregated network of CNT inside XNBR[24]. Abdullateef et al.[25] have reported improvement in the thermal stability of NR by the addition of modified MWCNTs. Nanotube network present in these composites can prevent the diffusion of gaseous products resulting from thermal degradation causing raise in the degradation temperature. As per reports CNTs can act as thermal barriers and reduce the pyrolysis rate of the polymer due to reduction in the polymer chain mobility[26].
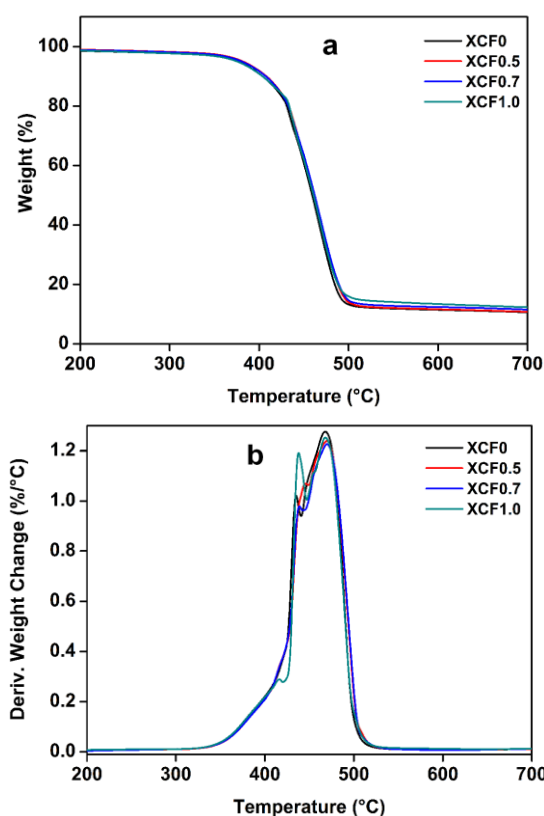
Fig. 7.A.7 (a) TGA and (b) DTG curves of XCF nanocomposites

Table 7.A.4 TGA results of XNBR and XNBR/MWCNTR composites

Compound name	T_{onset} (°C)	T_{50} (°C)	Residue (%) at 600 °C
XCF0	342	459	11.42
XCF0.5	344	461	11.61
XCF0.7	345	462	12.37
XCF1.0	345	460	13.38

7.A.3.9 DC electrical conductivity

Variation of DC electrical conductivity of the XCF composites as a function of MWCNTR loading is shown in Fig.7.A.8. Rapid increase in conductivity of the composites between 0 and 0.1 vol% of nanotube loading indicates the formation of percolative conductive network. The conductivity increases to 2.8 x 10⁻⁵ S/m for 7 phr or 3 vol% MWCNTR. Proposed model of segregated CNT distribution inside the rubber approves this low electrical percolation threshold. But the electrical conductivity values of the composites are lower compared to CPCs with segregated conductive fillers (s-CPCs)[27]. The lower conductivity value obtained in the present study is supported by the reports by Kohlmeyer et al.[28]
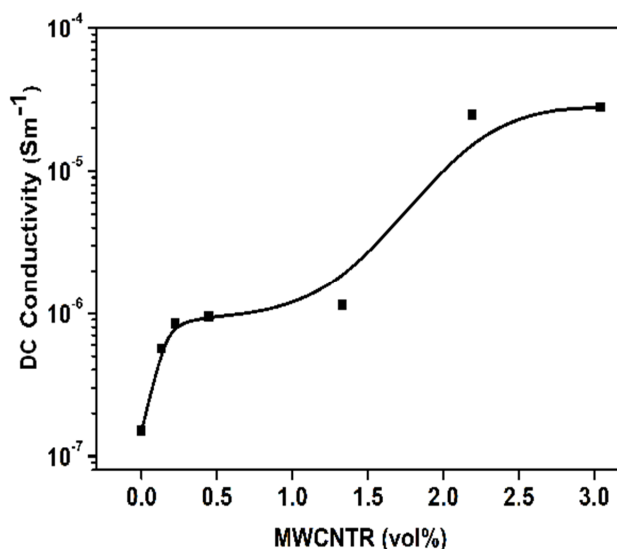
Fig. 7.A.8 Variation of DC conductivity of the XCF composites with MWCNTR

They have utilized both pristine (MWCNT$_{pristine}$) and hydroxylated MWCNTs (MWCNT$_{OH}$) for the preparation of Polydimethylsiloxane (PDMS) composites and obtained lower electrical conductivity for MWCNT$_{OH}$ – PDMS composites. According to them hydroxylation of MWCNTs interrupts the π-conjugation in the outer graphene layer of MWCNTs and lowers the surface electrical conductivity. In the present study lower conductivity of XCF composites can be attributed to the presence of –COOH and other oxygen containing groups on the nanotube surfaces.

7.A.3.10 Dielectric studies

Electrical properties are usually explained in terms of vol% of the conducting fillers rather than phr. For better understanding, the concentration of MWCNTR in XCF composites in both phr and vol% is given in Table 7.A.5.

Table 7.A.5 Concentration of MWCNTR in XCF composites

Composite	Concentration of MWCNTR	
	phr	vol%
XCF0.01	0.01	0.004
XCF0.05	0.05	0.0224
XCF0.1	0.1	0.04475
XCF0.3	0.3	0.134
XCF0.5	0.5	0.2233
XCF1.0	1.0	0.446
XCF3.0	3.0	1.33
XCF5.0	5.0	2.19
XCF7.0	7.0	3.04

Dielectric properties of XNBR and XCF composites are presented in Fig. 7.A.9. All the composites exhibit frequency dependent dielectric behaviour (Fig.7.A.9a). Dielectric constant is high at low frequency and the value decreases exponentially with increase in frequency. Dielectric constant of the composites vs MWCNTR concentration at 1 kHz is given in

Fig.7.A.9b. A sharp increase in dielectric constant is observed at very low content of MWCNTR (after 0.1 phr or 0.045 vol%) representing very low dielectric percolation threshold which can be attributed to the segregated structure of the nanotubes as discussed in the previous chapters. Dielectric constant at 100 Hz has been increased from 23 for pure XNBR to around 490 for 1 phr, and 7000 for 7 phr MWCNTR (About 20 and 300 fold increase) loading in the composite. The composites with large dielectric constants can find application as dielectric elastomers[29].
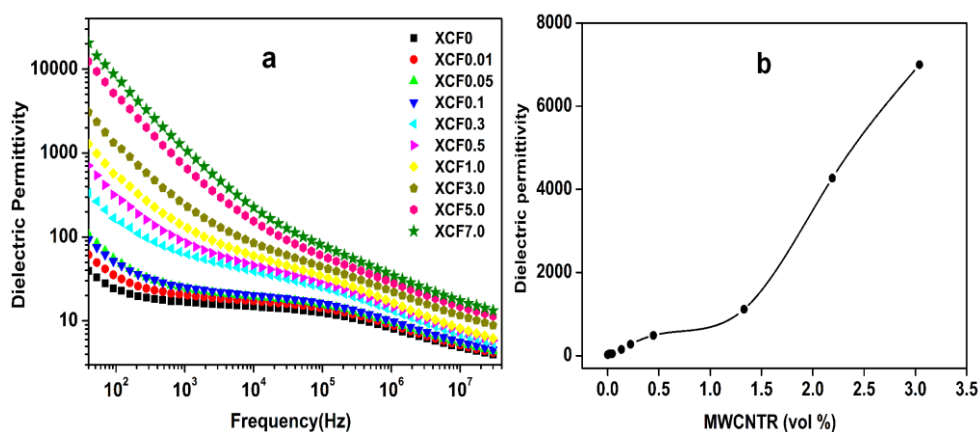
Fig. 7.A.9 (a) Dependence of dielectric constant of XCF composites on frequency at room temperature and (b)Variation of dielectric permittivity with MWCNTR loading at 1kHz.

The excellent dielectric constant displayed by the composites is due to the interfacial polarisation effect or Maxwell Wagner-Sillars (MWS) effect caused by the accumulation of charge carriers at the rubber-nanotube interfaces[30]. As the MWCNTR concentration increases interfacial polarisation also increases resulting in large dielectric permittivity. Moreover carboxylic groups attached to the CNTs are electron withdrawing and strengthen interfacial polarisation[31]. Below percolation threshold the conducting filler concentration is too small to cause accumulation of charges at the interfaces and hence the dielectric constant is almost independent of frequency. When

the nanotube concentration reaches percolation threshold, available interfaces increase due to the availability of large number of conducting nanotubes. This in turn leads to an increase in accumulation of free charges at the conductor-insulator interfaces and causes a sharp increase in the dielectric constant in the low frequency range. As the frequency increases the interfacial polarisation cannot cope up with electric field frequency and the MWS effect decreases.
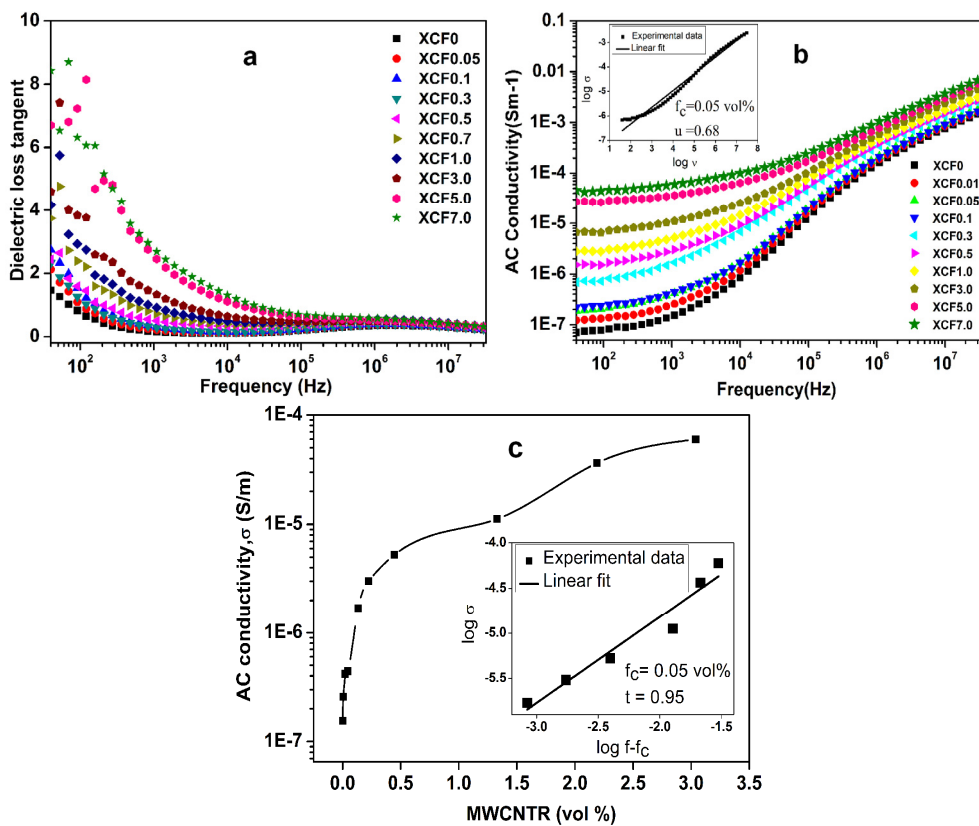
Fig. 7.A.10 Dependence of (a) dielectric loss tangent and (b) AC conductivity of XCF composites on frequency at room temperature. The (b) inset shows the best fit of the ac conductivity of the XCF composite with 0.05 vol% of MWCNTR to Eq. (7.A.2) (c) AC conductivity of the XCF composites as a function of MWCNTR concentration measured at 1 kHz and room temperature. Insets show the best fit of the conductivity to Eq. (7.A.1)

Dielectric loss also exhibits a decreasing trend with frequency (Fig.7.A.10a). At low frequencies induced dielectric polarisability is high due to large number of dipoles per unit volume and hence loss is also high. As the frequency increases, the decrease in polarisation results in low dielectric loss. An opposite behaviour is observed in the case of AC conductivity, which increases with frequency (Fig.7.A.10b). σ reached a value of 5.26×10^{-6} S/m at 1 kHz and 1.8×10^{-3} S/m at 10 MHz for 1 phr (0.45 vol%) MWCNTR. Compared to NR and its composites with MWCNTs, studied in the previous chapters, conductivity of neat XNBR and XCF composites is high. This is due to the presence of polar -CN and -COOH groups in XNBR that can contribute to the conductivity.

AC conductivity at 1kHz as a function of MWCNTR vol% is given in Fig.7.A.10c. Percolation threshold was estimated by fitting the conductivity (σ) to the well-known power law equation for the conducting region.

$$\sigma \propto (f - f_c)^t \text{ for } f > f_c \dots\dots\dots\dots\dots\dots\dots\dots\dots\dots\dots\dots (7.A.1)$$

where f is the volume fraction of the filler, f_c is the volume fraction at percolation threshold and t is the critical exponent in the conducting region. Best linear fit of the conductivity to the above equation (Fig.7.A.10c inset) gives percolation threshold f_c=0.05 vol% ~ 0.1 phr) and critical exponent t=0.95. Very low percolation threshold obtained for the composite can be credited to the segregated nanotube network inside the rubber and high aspect ratio of the filler[32,33]. Low percolation threshold is beneficial in maintaining low modulus and flexibility. The critical exponent 't' obtained from the data fitting deviates from the universal value (t_{un}~1.6-2). The deviation can be due to the complexity of segregated conductive network, filler morphology, distribution and dispersion of conductive fillers as reported elsewhere[34,35].

When f reaches f_c, the relation between conductivity and frequency can be related through percolation threshold power law as given in Eq. 7.A.2.

$$\sigma \propto \omega^{\mu}, \text{ as } f \rightarrow f_c \dots\dots\dots\dots\dots\dots\dots\dots\dots\dots\dots\dots\dots\dots\dots\dots\dots(7.A.2)$$

where $\omega = 2\pi\nu$, ν is the frequency and μ is the corresponding critical exponent. The value of μ obtained ($\mu = 0.68$) from the linear fit of the log-log plot of Eq. 7.A.2 using experimental data for $f = 0.045$ vol% (near f_c) is found to be close to the universal value ($\mu_{uni} = 0.70$).

Percolation threshold obtained in our study is very low compared to the reported values for elastomer/CNT composites in literature as summarized in Table 7.A.6[36].

Table 7.A.6 Percolation threshold of Elastomer/CNT composites[36]

Polymer	Filler	Processing	Percolation threshold
SBR	MWCNT	Melt	$(5)^b$
SBR/BR	MWCNT	Melt	$(<2)^a$
SBR/BR	MWCNT	Melt	$(<3)^a$
SBR/NBR	MWCNT	Melt	$(\sim 0.2 \text{ and } 1)^a$
NR/NBR	MWCNT	Melt	$(2)^b$
CIIR	MWCNT	Melt	$(6)^b$
IIR	MWCNT	Melt	$(6 \sim 8)^b$
CR	MWCNT	Melt	$(5)^b$
NBR	MWCNT	Solid (two-roll)	$(10)^b$
CR	MWCNT	Solid (two-roll)	$(3)^b$
NR	MWCNT	Solid (two-roll)	$(9 \sim 16)^a$
SR	MWCNT	Solvent	$(<0.1)^a$
SR	MWCNT	Solvent	$(\sim 1.0)^c$
SR	SWCNT	Solvent	$(4)^a$
PSF	MWCNT	Solvent	$(0.1 \sim 0.3)^a$
NR	MWCNT	Solvent	$(0.5-1)^b$
TPU	MWCNT	Solvent	$(0.5 \sim 10)^c$
EPDM	MWCNT	Solvent	$(4)^b$
MVQ	MWCNT	Solvent	$(1.6)^c$
MVQ	MWCNT/TRG	Solvent	$(2 \text{ and } 5)^a$
SBR	SWCNT	Solvent	$(0.27)^a$
SBR	MWCNT	Solvent	$(2 \text{ and } 3)^b$
PDMS	MWCNT	Manual	$(\sim 0.6)^a$
SR	MWNCT	High-shear	$(5 \text{ and } 10)^a$

^{a}wt%, ^{b}phr, ^{c}(vol%), *untreated CNT, ^{x}covalently treated CNT, ^{y}non-covalently treated CNT.

Ultralow percolation threshold obtained in the present study is credited to the presence of segregated nanotube network in XNBR matrix. Excellent dielectric properties exhibited by the XCF composites can be connected to the polar nature of XNBR. Very good dielectric properties obtained, at low concentration of CNTs for the XCF composites substantiates the presence of segregated structure inside the matrix.

7.A.3.11 EMI shielding effectiveness

EMI shielding effectiveness (SE) of the XCF composites in the frequency range 8-12 GHz is shown in Fig.7.A.12. SE of neat XNBR is very poor which is due to the electrically insulating nature and low dielectric loss tangent. SE increases with increase in concentration of MWCNTR in the composite and reaches a maximum SE of 5.3 dB at 8.9 GHz. Electromagnetic shielding is directly related to the electrical properties of the composite.
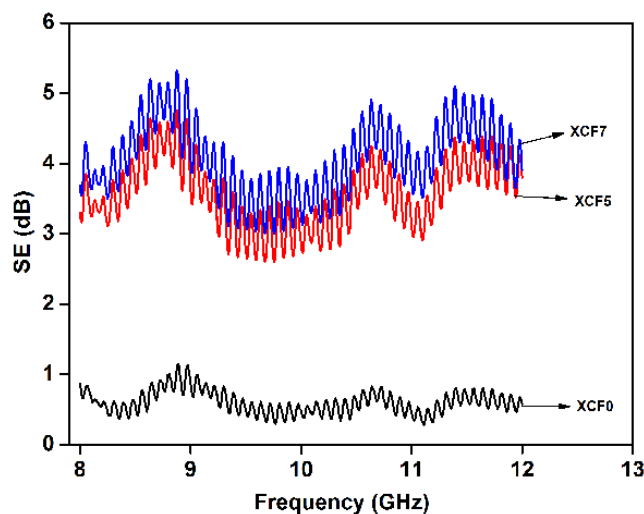
Fig. 7.A.11 Variation of SE with frequency of XCF composites

XCF composites have promising electrical properties as evident from the electrical conductivity measurements and dielectric studies. Earlier studies have shown that SE increases with permittivity and electrical conductivity[37,38].

Increase in SE with filler loading in the present study is due to the increase in the interfacial polarisation due to the accumulation of more and more charge carriers at the interfaces in the segregated structure. Strong interfacial polarisation is responsible for the high shielding efficiency[39].

7.A.4 Conclusions

Ultrasonication assisted latex stage mixing of MWCNTR aqueous dispersion with XNBR has been utilized in the fabrication of XCF composites. The composites exhibit excellent dielectric properties at ultralow percolation threshold (f_c=0.05 vol% ~ 0.1 phr) which is credited to the existence of 3D segregated MWCNTR network inside the rubber. Dielectric constant at 100 Hz has been increased from 23 for pure XNBR to around 490 and 7000 respectively for 1 and 7 phr MWCNTR. Nanotube network inside the composite is confirmed from HRTEM images and further supported by strain sweep studies. The rigid filler network along with good rubber-filler interaction possible via H-bonding between the surface groups on MWCNTR and XNBR contributes to the enhancement in mechanical properties of the composites. Segregated structure has no significant influence on the thermal stability of the rubber.

References

[1] Brown, H. P. (1957). Carboxylic elastomers. *Rubber Chemistry and Technology*, *30*(5), 1347-1386.

[2] Mousa, A., Heinrich, G., Gohs, U., & Wagenknecht, U. (2012). Mechanical properties of electron beam treated carboxylated nitrile butadiene rubber (XNBR) composites reinforced by organic/inorganic hybrid filler. *Journal of Composite Materials*, *46*(10), 1151-1157.

[3] Aliabadi, M. M., Naderi, G., Shahtaheri, S. J., Forushani, A. R., Mohammadfam, I., & Jahangiri, M. (2014). Transport properties of carboxylated nitrile butadiene rubber (XNBR)-nanoclay composites; a promising material for protective gloves in occupational exposures. *Journal of Environmental Health Science and Engineering*, *12*(1), 51.

[4]   Tian, M., Ma, Q., Li, X., Zhang, L., Nishi, T., & Ning, N. (2014). High performance dielectric composites by latex compounding of graphene oxide-encapsulated carbon nanosphere hybrids with XNBR. *Journal of Materials Chemistry A*, *2*(29), 11144-11154.

[5]   Basu, D., Das, A., George, J. J., Wang, D. Y., Stöckelhuber, K. W., Wagenknecht, U., ... & Heinrich, G. (2014). Unmodified LDH as reinforcing filler for XNBR and the development of flame-retardant elastomer composites. *Rubber Chemistry and Technology*, *87*(4), 606-616.

[6]   Bai, X., Wan, C., Zhang, Y., & Zhai, Y. (2011). Reinforcement of hydrogenated carboxylated nitrile–butadiene rubber with exfoliated graphene oxide. *Carbon*, *49*(5), 1608-1613.

[7]   Lu, L., Zhai, Y., Zhang, Y., Ong, C., & Guo, S. (2008). Reinforcement of hydrogenated carboxylated nitrile–butadiene rubber by multi-walled carbon nanotubes. *Applied Surface Science*, *255*(5), 2162-2166.

[8]   Tian, M., Zhang, J., Zhang, L., Liu, S., Zan, X., Nishi, T., & Ning, N. (2014). Graphene encapsulated rubber latex composites with high dielectric constant, low dielectric loss and low percolation threshold. *Journal of colloid and interface science*, *430*, 249-256.

[9]   Yang, J., Zhang, L. Q., Shi, J. H., Quan, Y. N., Wang, L. L., & Tian, M. (2010). Mechanical and functional properties of composites based on graphite and carboxylated acrylonitrile butadiene rubber. *Journal of applied polymer science*, *116*(5), 2706-2713.

[10]   Nair, K. P., Thomas, P., & Joseph, R. (2012). Latex stage blending of multiwalled carbon nanotube in carboxylated acrylonitrile butadiene rubber: mechanical and electrical properties. *Materials & Design*, *41*, 23-30.

[11]   Kang, H., Zuo, K., Wang, Z., Zhang, L., Liu, L., & Guo, B. (2014). Using a green method to develop graphene oxide/elastomers nanocomposites with combination of high barrier and mechanical performance. *Composites Science and Technology*, *92*, 1-8.

[12]   Zhan, Y., Lavorgna, M., Buonocore, G., & Xia, H. (2012). Enhancing electrical conductivity of rubber composites by constructing interconnected network of self-assembled graphene with latex mixing. *Journal of Materials Chemistry*, *22*(21), 10464-10468.

[13] Potts, J. R., Shankar, O., Du, L., & Ruoff, R. S. (2012). Processing–morphology–property relationships and composite theory analysis of reduced graphene oxide/natural rubber nanocomposites. *Macromolecules*, *45*(15), 6045-6055.

[14] Grunlan, J. C., Gerberich, W. W., & Francis, L. F. (2001). Electrical and mechanical behavior of carbon black–filled poly (vinyl acetate) latex–based composites. *Polymer Engineering & Science*, *41*(11), 1947-1962.

[15] Nah, C., Lim, J. Y., Cho, B. H., Hong, C. K., & Gent, A. N. (2010). Reinforcing rubber with carbon nanotubes. *Journal of applied polymer science*, 118(3), 1574-1581.

[16] Nair P. K. (2013). Studies on the use of Nanokaolin, MWCNT and Graphene in NBR and SBR, Ph. D Thesis, Department of Polymer Science and Rubber Technology Cochin University of Science and Technology, Cochin- 682 022, Kerala, India

[17] El-Nashar, D. E., Ward, A. A., Abd-El-Messieh, S. L., & Cairo, D. (2009). Physico-mechanical and dielectric properties of nitrile rubber filled with silica and mica. *Infrared spectroscopy*, *1*(2Mc), 3.

[18] Sangchay, W., Sikong, L., & Kooptarnond, K. (2008). Mechanical properties of MWNT-rubber composite. *CMU. J. Nat. Sci. Special Issue on Nanotechnology*, *7*(1), 137-143.

[19] Galimberti, M., Cipolletti, V., Musto, S., Cioppa, S., Peli, G., Mauro, M., ... & Kumar, V. (2014). Recent advancements in rubber nanocomposites. *Rubber Chemistry and Technology*, *87*(3), 417-442.

[20] Billmeyer. F. W (1994). Text book of polymer science, Wiley Interscience, A Wiley-lnterscience Publication, John Wiley & Sons, Singapore..

[21] Payne, A. R., & Whittaker, R. E. (1970). Dynamic properties of materials. *Rheologica Acta*, *9*(1), 97-102.

[22] Fröhlich, J., Niedermeier, W., & Luginsland, H. D. (2005). The effect of filler–filler and filler–elastomer interaction on rubber reinforcement. *Composites Part A: Applied Science and Manufacturing*, *36*(4), 449-460.

[23] Das, A., Jurk, R., Stöckelhuber, K. W., Majumder, P. S., Engelhardt, T., Fritzsche, J., ... & Heinrich, G. (2008). Processing and properties of nanocomposites based on layered silicate and carboxylated nitrile rubber. *Journal of Macromolecular Science, Part A*, *46*(1), 7-15.

[24] Huxtable, S. T., Cahill, D. G., Shenogin, S., Xue, L., Ozisik, R., Barone, P., ... & Keblinski, P. (2003). Interfacial heat flow in carbon nanotube suspensions. *Nature materials*, *2*(11), 731-734.

[25] Abdullateef, A. A., Thomas, S. P., Al-Harthi, M. A., De, S. K., Bandyopadhyay, S., Basfar, A. A., & Atieh, M. A. (2012). Natural rubber nanocomposites with functionalised carbon nanotubes: mechanical, dynamic mechanical, and morphology studies. *Journal of Applied Polymer Science*, 1(*125),* E76–E84.

[26] Perez, L. D., Zuluaga, M. A., Kyu, T., Mark, J. E., & Lopez, B. L. (2009). Preparation, characterisation, and physical properties of multiwall carbon nanotube/elastomer composites. *Polymer Engineering and Science*, *49*(5), 866.

[27] Bauhofer, W., & Kovacs, J. Z. (2009). A review and analysis of electrical percolation in carbon nanotube polymer composites. *Composites Science and Technology*, *69*(10), 1486-1498.

[28] Kohlmeyer, R. R., Javadi, A., Pradhan, B., Pilla, S., Setyowati, K., Chen, J., & Gong, S. (2009). Electrical and dielectric properties of hydroxylated carbon nanotube− elastomer composites. *The Journal of Physical Chemistry C*, *113* (41), 17626-17629.

[29] Ning, N., Ma, Q., Liu, S., Tian, M., Zhang, L., & Nishi, T. (2015). Tailoring dielectric and actuated properties of elastomer composites by bioinspired poly (dopamine) encapsulated graphene oxide. *ACS applied materials & interfaces*, *7*(20), 10755-10762.

[30] Tangboriboon, N., Datsanae, S., Onthong, A., Kunanuruksapong, R., & Sirivat, A. (2013). Electromechanical responses of dielectric elastomer composite actuators based on natural rubber and alumina. *Journal of Elastomers & Plastics*, *45*(2), 143-161.

[31] Li, Q., Xue, Q., Gao, X. L., & Zheng, Q. B. (2009). Temperature dependence of the electrical properties of the carbon nanotube/polymer composites. *Express Polym Lett*, *3*(12), 769-77.

[32] Lu, C., Hu, X. N., He, Y. X., Huang, X., Liu, J. C., & Zhang, Y. Q. (2012). Triple percolation behavior and positive temperature coefficient effect of conductive polymer composites with especial interface morphology. *Polymer bulletin*, *68*(7), 2071-2087.

[33] Grossiord, N., Loos, J., & Koning, C. E. (2005). Strategies for dispersing carbon nanotubes in highly viscous polymers. *Journal of Materials Chemistry*, *15*(24), 2349-2352.

[34] Makled, M. H. (2012). Dielectric properties of high coercivity barium ferrite–natural rubber composites. *Journal of Applied Polymer Science*, *126*(3), 969-973.

[35] Matchawet, S., Kaesaman, A., Bomlai, P., & Nakason, C. (2016). Electrical, dielectric, and dynamic mechanical properties of conductive carbon black/ epoxidized natural rubber composites. *Journal of Composite Materials*, *50*(16), 2191-2202.

[36] Mensah, B., Kim, H. G., Lee, J. H., Arepalli, S., & Nah, C. (2015). Carbon nanotube-reinforced elastomeric nanocomposites: a review. *International Journal of Smart and Nano Materials*, *6*(4), 211-238.

[37] González Sánchez, M., Mokry López, G., Morillas, N., Baselga Llidó, J., & Pozuelo de Diego, J. (2016). Carbon Nanotube Composites as Electromagnetic Shielding Materials in GHz Range.

[38] Jia, L. C., Yan, D. X., Cui, C. H., Jiang, X., Ji, X., & Li, Z. M. (2015). Electrically conductive and electromagnetic interference shielding of polyethylene composites with devisable carbon nanotube networks. *Journal of Materials Chemistry C*, *3*(36), 9369-9378.

[39] Yuping, D., Shunhua, L., & Hongtao, G. (2005). Investigation of electrical conductivity and electromagnetic shielding effectiveness of polyaniline composite. *Science and Technology of Advanced Materials*, *6*(5), 513-518.

XNBR/CARBOXYLATED MWCNT COMPOSITES WITH RANDOM NETWORK

7.B.1 Introduction

From an industrial point of view melt blending is the most preferred processing method to fabricate nanocomposites. But the method cannot ensure homogeneous dispersion of fillers which can lead to poor mechanical properties[1]. Latex compounding and co-coagulation method has been reported in the preparation of many elastomeric nanocomposites. A number of studies are available in the literature illustrating the advantage of this method in preparing elastomer/graphene nanocomposites[2-6]. This technology is reported to be one of the efficient methods since it requires mixing of two watery components. Since water is used as the solvent, this process is eco-friendly and cost effective[7]. Moreover the method ensures efficient dispersion of nanofillers and hence betterment of properties at very low filler loading.

Carboxylated nitrile rubber is known for its exceptionally good mechanical properties because of the presence of carboxyl groups which can form ionic crosslinks with metal ions during curing[8]. XNBR being a polar rubber with pendant carboxyl groups along the hydrocarbon chain is expected to interact with polar fillers more efficiently when compared to other non-polar diene rubbers. Bandyopadhyay et al.[9] have studied the rubber-filler interactions between XNBR and oxidised carbon black and have reported increased rubber-filler interactions due to the possibility of chemical bonding between COOH groups in XNBR and reactive groups on the filler surface. Reports on CNT based XNBR composites are rare in the literature. Nair et al.[10] have used latex stage mixing method to prepare surfactant treated MWCNTs in XNBR and have reported significant enhancement in mechanical and electrical properties. Lu et al.[11] have prepared hydrogenated carboxylated acrylonitrile-butadiene rubber (HXNBR)/ MWCNT composites in a two-roll

mill and reported 60% improvement in tensile strength at 4 phr MWCNT loading.

In this part of the study XNBR/MWCNTR system has been prepared using a facile and eco-friendly method based on latex co-coagulation technique followed by mixing in an internal mixer. The obtained nanocomposites were characterised by different methods. Effect of Haake mixing on segregated network discussed in chapter 7A was evaluated and properties were correlated with the filler morphology inside the rubber.

7.B.2 Experimental

7.B.2.1 Preparation of the XCH nanocomposites

MWCNTR and their aqueous dispersions were prepared as per the procedure given in 4.A.2.1 and 4.A.2.3 respectively. MWCNTR dispersion was added to the XNBR latex (diluted to 25% by adding distilled water) and the mixture was sonicated for 30 minutes using a bath sonicator. The latex mixes were poured into trays and coagulated by rapid addition of 5% $CaCl_2$ solution. The coagula were isolated by vacuum filtration, washed several times with water and dried at 50 °C in an air oven.

The dried coagulum was melt blended in a Haake mixer (at 70 °C, 8 minutes, 60 rpm) with compounding ingredients added in the same sequence as per the formulation given in Table 7.B.1 and procedure outlined in the ASTM D 3182. After mixing the batch was passed two times through tight nip in a two-roll mill and was finally sheeted out. The samples were kept overnight for maturation. The cure characteristics of the mixes were determined using Rubber Process Analyser and the composites were prepared as per procedure outlined in 2.2.5 of chapter 2. The composites were labelled as XCH composites with the content of MWCNTRs in phr suffixed. For example XCH0.3 refers to XNBR/MWCNTR composite containing 0.3 phr MWCNTR.

Table 7.B.1 Formulation of XCH composites

Ingredients	Amount (phr)
XNBR	100
MWCNTR	0, 0.3, 0.5, 1.0, 1.5
Sulphur	1.5
Stearic acid	2.0
ZnO	4.5
Antioxidant TQ	1.0
Accelerator CBS	1.0
Accelerator TMTD	0.3

7.B.2.2 Characterisation

Microstructure of the XCH nanocomposites was studied using SEM and HRTEM. Mechanical properties of the samples were tested according to the relevant ASTM standards. Strain dependent dynamic mechanical properties were evaluated using DMA. TGA and swelling studies were done to understand the thermal and solvent resistance properties. Dielectric properties, DC and AC conductivity of the composites were anaysed. EMI shielding measurements were performed to study the electromagnetic shielding efficiency of the composites.

Detailed description on each characterisation method is given in Chapter 2.

7.B.3 Results and discussion
7.B.3.1 Interfacial interactions between XNBR and MWCNTR

For the XNBR/MWCNTR composite, H-bonding is possible between XNBR and MWCNTs due to the presence of –COOH and –OH functional groups on the surface of MWCNTRs and pendent –COOH groups on XNBR chains (Fig. 7.B.4a). FTIR spectra of XNBR and XCH composites given in Fig. 7.B.1 confirm the presence of H-bonding. FTIR spectrum of neat XNBR (XCH0) shows characteristic peaks at 3000-3500 cm^{-1}(H-bonded

O-H), 2800 and 2925 cm^{-1} (-CH$_2$ stretch), 2237 cm^{-1} (-CN) and 1777 cm^{-1} (C=O). XCH composites also show similar peaks and weakening of the peak corresponding to the C=O stretch in XCH composite indicates the presence of H-bond, that restricts free C=O stretching. C=O peak for 1.5 phr MWCNTR loading shows a blue shift from 1769 cm^{-1} to 1775 cm^{-1} and H-bonded –OH band shows broadening which again confirms the H-bond formation between XNBR and carboxylated MWCNTs . These H-bonding interactions can improve the rubber-filler interactions resulting in good mechanical performance of the XCH nanocomposites.
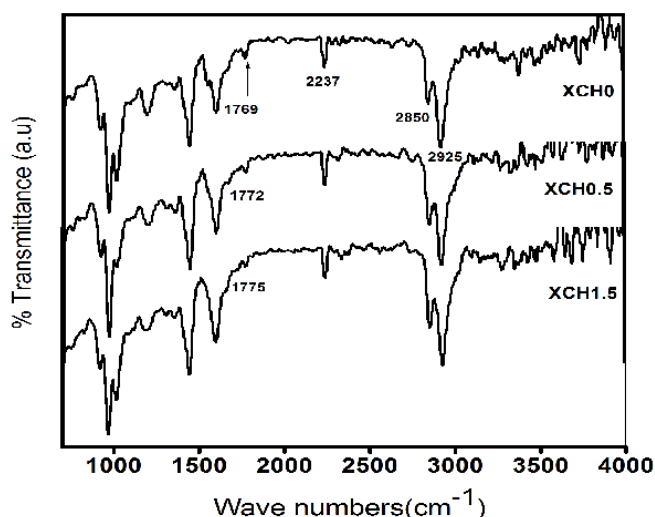
Fig. 7.B.1 FTIR spectra of neat XNBR (XCH0) and XCH composites

7.B.3.2 Morphology and microstructure

TEM images of the XCH1.5 nanocomposite are given in Fig. 7.B.2. As can be seen from the figure the CNTs are randomly distributed inside XNBR unlike in XCF composite (7.B.2 inset). The image provides clear evidence of the difference in the microstructure of the XCF and XCH nanocomposites. XCF contains segregated network of MWCNTs as these composites are prepared by film casting method which pushes the nanotubes to the periphery of the rubber particles during drying. In XCH composite

preparation intense shear forces in the internal mixer disturbs the web like nanotube network in the dried coagulum and results in an even dispersion of nanotubes in the composite. The difference in the distribution of MWCNTRs in XCF and XCH composites proves that processing method has important role in designing the filler morphology inside the polymer matrix[12,13].
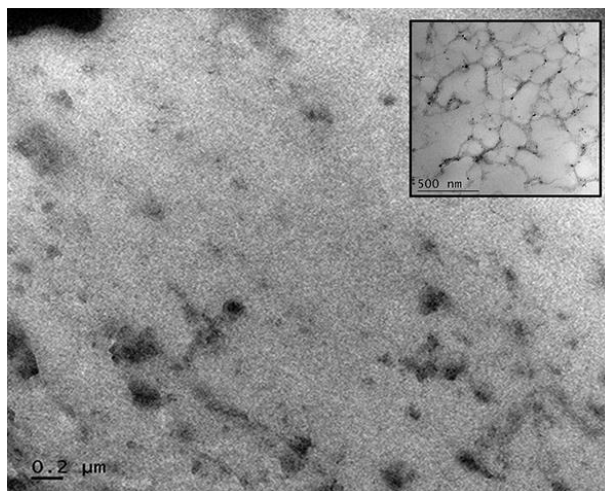
Fig. 7.B.2   TEM image of XCH composite containing 1.5 phr of MWCNTR. Inset shows TEM image of the XCF nanocomposite at 0.5 phr of MWCNTR

Fig.7.B.3 shows the surface morphology of tensile fracture surface of pure XNBR (XCH0) and XCH1.5 nanocomposite. Fracture surface of the composite is more uniform and devoid of cracks suggesting strong rubber-filler interaction. This strong interaction is possible through the H-bonding between carboxyl groups on XNBR and oxygen containing groups on MWCNTR (Fig. 7.B.4a). The observation is supported by the reports on the SEM observation of the fracture surface of NR-acid treated MWCNT composites by Peng et al. [14]. They have observed that the unmodified MWCNTs remain as agglomerates while the acid treated MWCNTs showed better dispersion. Though the broken ends of the nanotubes are not clearly visible in the SEM images the smooth fracture pattern can be believed to be due the better dispersion of the oxidised

MWCNTs and strong interaction between the rubber and filler. The fracture surface patterns of the XCH composite differ significantly from that of XCF (Fig.7.B.3f inset) composite prepared by film casting method. The difference is due to the difference in distribution of filler in the two composites. The film casting favours segregated structure whereas samples prepared by latex coagulation and Haake mixing have uniform distribution of hybrid fillers in the rubber matrix. Well-ordered segregated network structure in XCF composite leads to craters with special patterns whereas those patterns are absent in XCH composites indicating homogeneous distribution of the nanotubes in the rubber matrix.
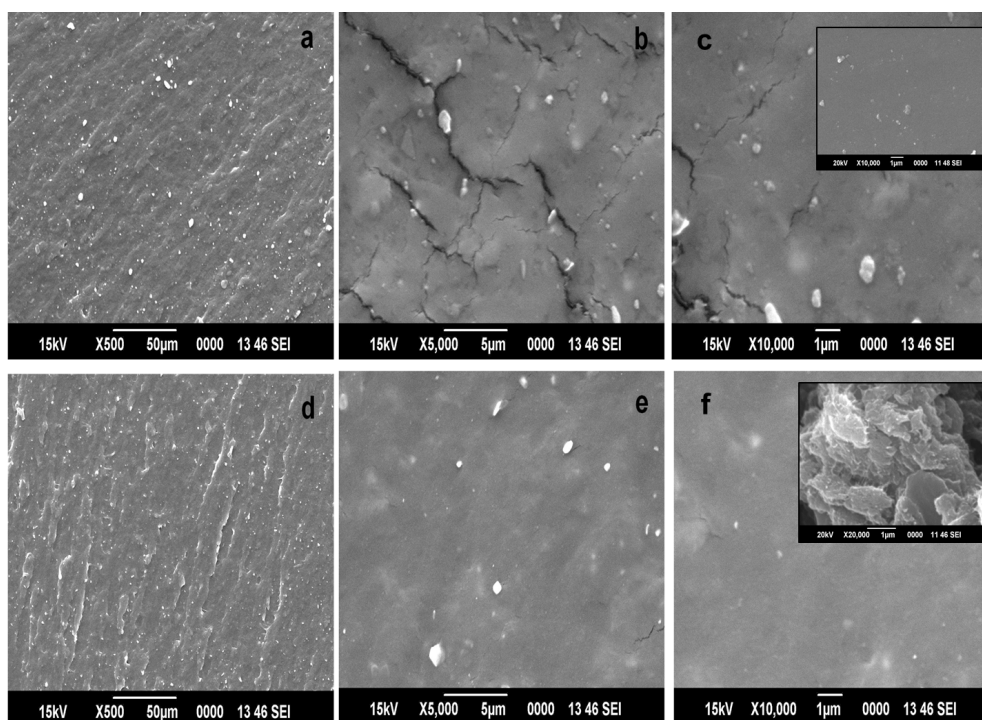
Fig. 7.B.3 SEM images of the tensile fractured surfaces of XCH composites (a-c) XCH0 and (d-f) XCH1.5. (c) and (f) inset shows the tensile fractured surface images of XCF0 and XCF0.5 respectively

Based on the TEM analysis and fracture surface analysis by SEM, schematic of the random network formation of MWNTRs in the XNBR composite is given in Fig. 7.B.4. H-bond formation possible between the oxygen containing groups on MWCNTR and carboxyl groups on XNBR is portrayed in the figure. The figure also clearly shows that segregated structure of the MWCNTs formed in the coagulum has been disturbed by the mixing process in Haake internal mixer and lead to the formation of random network of nanotubes in the final XCH composite.
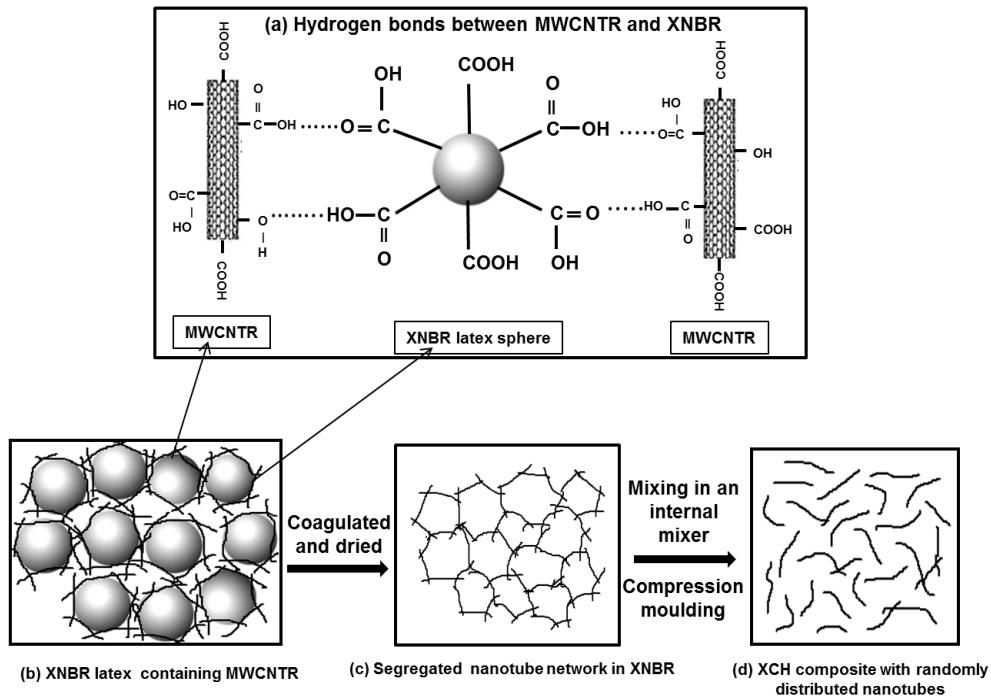
Fig. 7.B.4 Schematic for the preparation of XCH composites (a) H-bond formation between XNBR and MWCNTR (b) MWCNTR dispersion mixed with XNBR latex (c) Dried coagulum containing segregated nanotube network (d) network is disturbed by the intense shear forces in Haake to form random network in XCH composite

7.B.3.3 Cure characteristics of XCH composites

Cure graphs of XCH nanocomposites containing different concentrations of MWCNTR (0, 0.3, 0.5, 1.0 and 1.5 phr) at 150 °C are given in Fig.7.B.5. The curves show general trend with an initial decrease in torque due to the softening of rubber followed by an increase in torque value due to the formation of crosslinks in rubber and final levelling off shows completion of curing. Torque values of the nanocomposites containing MWCNTRs upto 1phr do not show marked difference from the neat rubber, whereas both minimum (M_L) and maximum torque (M_H) values for the XCH1.5 are high compared to others.
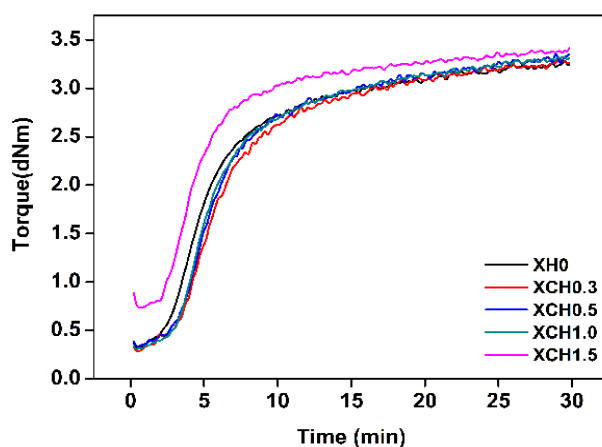
Fig. 7.B.5 Cure curves of NRCSH composites

Table 7.B.2 shows the vulcanisation characteristics in detail. M_L represents viscosity of the unvulcanised compound and M_H is an index of elastic modulus of the vulcanised rubber[15]. Addition of nanotubes upto 1.0 phr caused no marked change in M_L values of the neat rubber which may due the very small concentration of nanotubes present in the rubber. Noticeable increase in M_L observed for XCH1.5 indicates that the mobility of rubber chains has been reduced by the presence of nanotubes causing increase in viscosity of the composite[16]. M_H increased with nanotube addition suggesting enhanced rubber-filler interaction and reinforcement of rubber.

Scorch time (T_{10}) represents the premature vulcanisation or processing safety of the material. Both cure time and scorch time of the composite didn't vary much from the neat rubber by the incorporation of upto 1 phr MWCNTR. Increased cure rate index and decreased cure time for the XCH1.5 can be attributed to the enhanced dipole-dipole interaction or H-bonding among the oxygen containing groups on CNTs and carboxylic groups on XNBR[17]. In addition to sulphur and ionic crosslinks in the present system, MWCNTRs improved the degree of interaction as already discussed. This resulted in an increase in the degree of crosslinking, leading to an increase in cure rate and decrease in cure time for the XCH1.5.

Table 7.B.2 Cure characteristics of XNBR and XCH nanocomposites

PROPERTIES	XCH0	XCH0.3	XCH0.5	XCH1.0	XCH1.5
Min. torque M_L(dNm)	0.310	0.278	0.314	0.297	0.726
Max. torque M_H (dNm)	3.29	3.31	3.38	3.36	3.42
Scorch time, T_{10} (min)	2.63	3.15	3.15	3.20	2.40
Opt. cure time, T_{90} (min)	15.63	15.96	16.46	16.57	13.14
Cure rate index(min^{-1})	7.69	7.81	7.51	7.48	9.31

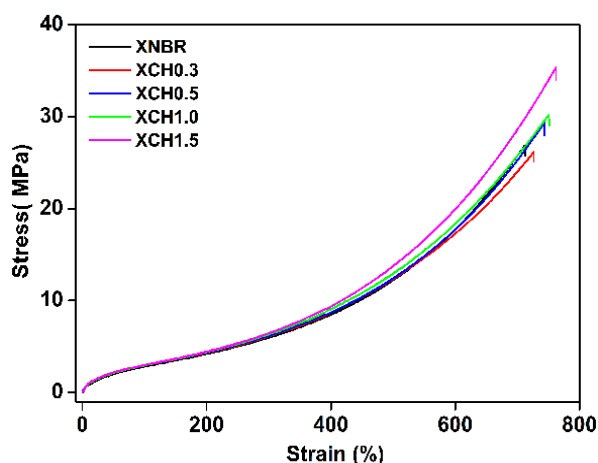## 7.B.3.4 Mechanical properties

Fig. 7.B.6 Stress-strain curves of XCH nanocomposites

Fig.7.B.6 shows the stress-strain behaviour and Table 7.B.3 shows the mechanical properties of XCH composites at different concentration of MWCNTR. XNBR, even in the gum form shows good tensile and tear properties due to the reinforcing action of ionic crosslinks present in the vulcanised rubber. Mechanical properties of XNBR were improved remarkably with nanotube loading. Tensile strength and modulus at 300% elongation increased by 35% and 8% respectively at 1.5 phr MWCNTR. Tear strength improved by 34% at 1.0 phr MWCNTR. The reinforcing efficiency of oxidised nanotubes in XNBR is attributed to the following reasons. Oxidised CNTs have abundant oxygen containing functional groups (hydroxyls, carboxyls etc.) [18,19] on the surfaces which could form H-bonds with carboxyl groups in the XNBR chains[20]. The large aspect ratio and surface area of CNTs could improve the interfacial interactions between the XNBR and CNTs[21]. Better dispersion of MWCNTs in the rubber achieved by the latex stage addition also contributes to the reinforcement. As per the scheme proposed, segregated network formed in the coagulum would be broken by the Haake mixing and the nanotubes are evenly distributed in the rubber matrix. These uniformly distributed fillers can bear the applied stress, thereby improving mechanical properties of the composites.

Table 7.B.3 Mechanical properties of XCH nanocomposites

Sample Name	Tensile strength(MPa)	Elongation at break (%)	Modulus 300 % (MPa)	Tear strength (N/mm)
XCH0	26.18±0.13	712±13	5.97±0.04	37.50±1.05
XCH0.3	29.42±1.13	727±25	6.12±0.09	39.81±0.34
XCH0.5	30.19±1.02	743±16	6.19±0.02	41.45±1.37
XCH1.0	30.19±0.85	751±7	6.33±0.12	50.37±1.65
XCH1.5	35.37±1.06	762±19	6.44±0.18	44.69±0.98

Abrasion resistance index, Compression set, Hardness and Rebound resilience of XNBR and XCH composites is given in Fig. 7.B.7.

XNBR shows exceptional mechanical properties, especially tensile strength and abrasion resistance even in the absence of fillers due to the presence of ionic microphases which act as reinforcement sites[22]. Very high abrasion resistance value of pure XNBR (Fig. 7.B.7) substantiates the statement. About 18% increment in abrasion resistance is observed by addition of 1 phr MWCNTR, indicating strong rubber-filler interaction.

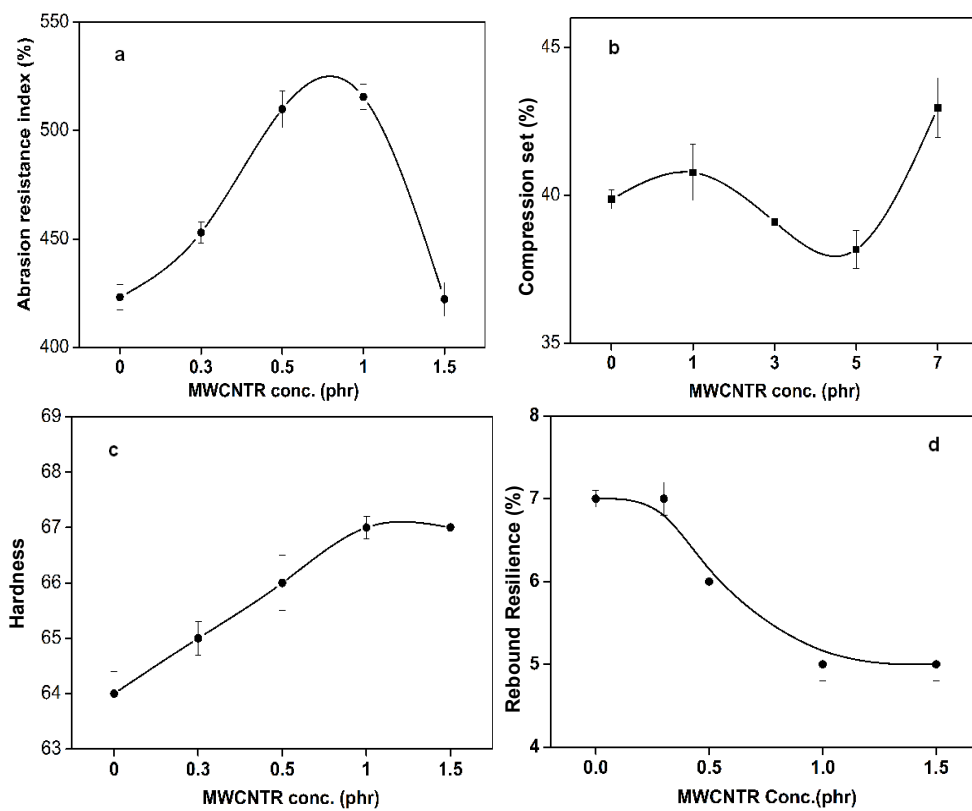**Fig. 7.B.7 Variation of Abrasion resistance index, Compression set, Hardness and Rebound resilience of XCH composites with MWCNTR loading**

Compression set is a measure of the material's ability to retain elastic properties under prolonged action of compressive stress at some higher temperature. Slight lowering of compression set with nanotube loading is observed upto 1 phr and an increasing tendency is observed thereafter.

Hardness, which is a measure of low strain elastic modulus, was found to be increasing with MWCNTR loading. XCH1.0 composite showed highest hardness with 67% improvement, compared to XNBR.

Rebound resilience was found to decrease with MWCNTR addition. Almost 29% reduction in the resilience was observed for XCH1.0. Better dispersion of nanotubes along with H-bonding possible between XNBR and MWCNTR explains the observed improvement in mechanical properties[23]. After 1 phr the properties level off which can be explained on the basis of dilution effect of fillers upon the reinforcing ionic microphases in crosslinked ionic polymers. Presence of fillers beyond a particular concentration retards the formation of ionic crosslinks resulting in reduced mechanical properties.

Overall properties suggest good filler dispersion, better rubber-filler interaction and reinforcement for the XCH nanocomposites.

7.B.3.5 Comparison of mechanical properties of latex film cast samples with Haake mixed samples

Fig.7.B.8 compares the tensile strength, elongation at break, tear strength and modulus at 300% elongation of latex film cast (XCF) and Haake mixed (XCH) samples. The composites prepared by latex film casting method exhibited inferior mechanical properties compared to the Haake mixed samples. This could be due to the poor crosslinking and possibility of defects and voids in the films prepared manually by casting onto glass plates. Whereas the XCH sample preparation involved hot pressing at 150 ℃ which would result in increased crosslink density, adhesion between rubber and CNTs and decreased porosity. Relative increase in the properties is more pronounced in the case of XCF composites which can be credited to the segregated structure. It has been previously discussed in section that the rigid nanotube network can provide high level of reinforcement in XCF composites.
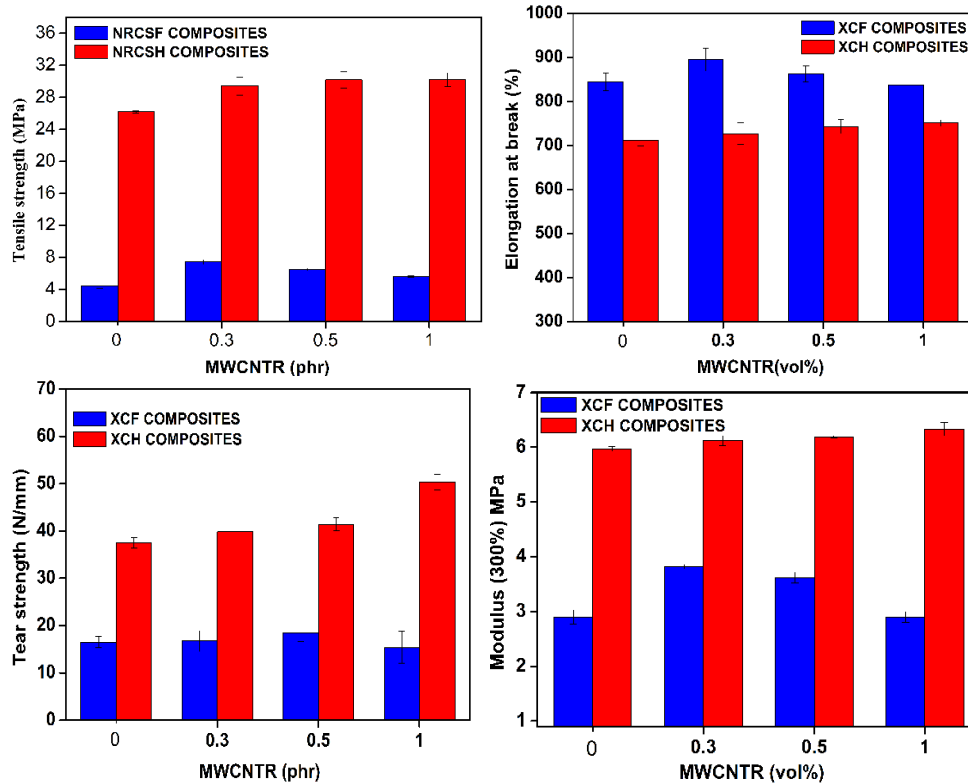
Fig. 7.B.8 Comparison of mechanical properties of NRCSF and NRCSH composites

Dispersion morphology of the filler within the matrix plays an important role in determining mechanical properties of the composites. Both XCF and XCH nanocomposites have well-distributed nanotubes in the matrix. Here the modulus values of the film cast samples are lower than those of Haake mixed samples. This observation is contradictory to the reports by Potts et al. [24] who studied the effect of processing method and nanocomposite morphology on the properties of reduced graphene oxide/Natural rubber nanocomposites. In their study they have observed a significant increase in the modulus for the solution treated samples, with large reduction in elongation at break with filler addition. On the other hand milled samples showed normal increase in modulus without a significant reduction in

elongation. They have connected the reason for this behaviour to the difference in filler morphology in the two viz. the web like network of fillers in the solution treated samples and uniformly distributed fillers in the milled samples. However on analysing the results of our study obtained for the XCF and XCH composites the relative increase in the modulus compared to their respective unfilled vulcanisates is high for the XCF samples but without sacrificing the elongation. High elongation exhibited by the composites with nanotube network points to the presence of strong interaction between the oxidised nanotubes and XNBR enhancing the rheological flow of the rubber[25].

7.B.3.6 Strain dependence of storage modulus

Variation of storage modulus (E') at low strain can be used to study the filler-filler interaction in the composite. From the Fig. 7.B.9 it is clear that strain dependent behaviour of storage modulus[26,27] (Payne effect) is more pronounced in the case of XCF composites compared to XCH composites (Fig. 7.B.9 inset). This clearly indicates that break down of filler-filler network is more in the case of XCF composites due to the presence of segregated filler network. Whereas the XCH composites contain uniformly distributed fillers, thereby reducing the filler-filler interaction and Payne effect[28].

Decrease in E' observed for XCH0 can be related to the breakage of ionic crosslinks whereas for XCH composites, breakage of filler-filler network along with ionic crosslinks explains the decrease in E' with strain. However the modulus values (E′) of the XCH composites are higher than the XNBR. Increase in E′ with MWCNTR loading can be ascribed to the hydrodynamic effect of the rigid fillers. Increase in filler concentration leads to increase in bound rubber or trapped rubber in the matrix. This causes increase in the effective volume of the filler causing enhancement in modulus of the rubber[29].
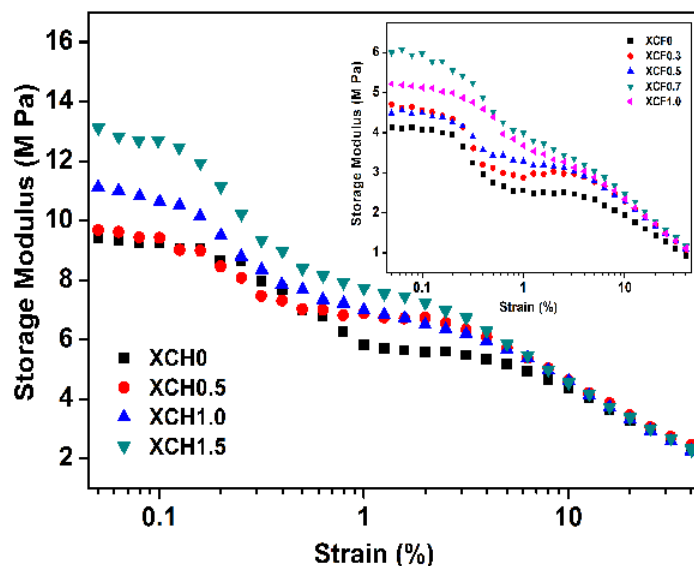
Fig. 7.B.9 Strain dependence of the storage modulus of XCH nanocomposites. The same graph for XCF composites is shown as inset

7.B.3.7 Crosslink density and solvent barrier properties

Table 7.B.4. Crosslink density and Swelling index of XCH composites

Sample name	Crosslink density (x 10^{-5} mol/g)	Swelling Index (%)
XCH0	3.7	203
XCH0.3	4.1	200
XCH0.5	4.3	195
XCH1.0	4.3	196
XCH1.5	4.8	187

Analysis of swelling behaviour confirms the enhanced XNBR-MWCNTR interaction. Crosslink density and swelling index of the XCH compounds is given in Table 7.B.4. Crosslink density increased whereas swelling index decreased indicating the increase in the number of crosslinks after incorporation of MWCNTR. The sorption curves given in Fig. 7.B.10

also substantiate the improved rubber-filler interaction. Equilibrium solvent uptake decreased with MWCNTR loading which could be related to the interfacial H-bonds between rubber and filler besides the sulphur and ionic crosslinks present in the system. With addition of oxidised nanotubes interfacial bonding increases which in turn decreases the polymer chain mobility and restricts the entrance of solvent molecules into the interfacial regions[30].
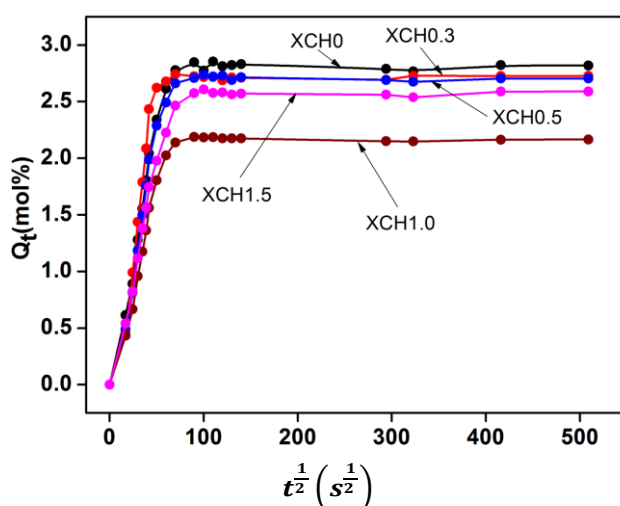
Fig. 7.B.10 Sorption curves of XCH composites

7.B.3.8 Thermal studies

TGA and DTG curves of XCH nanocomposites are presented in Fig. 7.B.11 and the relevant data is given in Table 7.B.5. Degradation of XCH composites starts at a higher temperature compared to neat XNBR which can be attributed to the easy dissipation of heat energy possible by the well dispersed CNTs inside XNBR[31]. Small increase in T_{50} also indicates slight improvement in thermal stability of the XCH composites. Residue at 600 °C, increases with filler addition. Even at low concentration of MWCNTRs, mobility of the rubber chains is restricted and allowed easy heat dissipation through the composite[32]. Abdullateef et al. have reported improvement in the

thermal stability of XNBR by the addition of modified MWCNTs [33]. High thermal stability and conductivity of MWCNTR also plays a major role in imparting slight improvement in thermal behaviour. As per reports presence of CNTs can act as thermal barriers and reduce the pyrolysis rate of the polymer due to reduction in the polymer chain mobility[34].
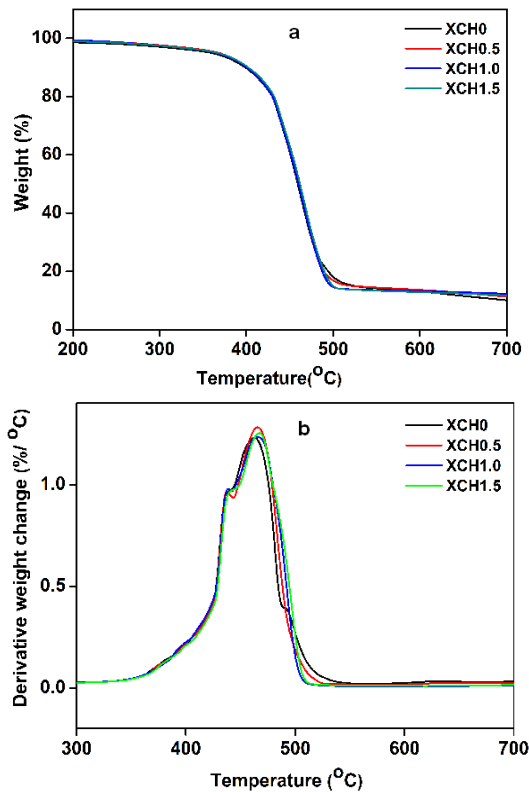
Fig. 7.B.11 (a) TGA and (b) DTG curves of XCH nanocomposites

Table 7.B.5 TGA results of XCH composites

Compound name	T_{onset} (ºC)	T_{50} (ºC)	Residue (%) at 600 ºC
XCH0	359	459	13.07
XCH0.5	373	460	13.13
XCH1.0	377	461	13.59
XCH1.5	370	461	16.02

7.B.3.9 DC electrical conductivity

DC conductivity of XCH composites is given in Fig. 7.B.12. There is no dramatic change in the conductivity with MWCNTR addition indicating absence of continuous conductive network inside the composites. The low conductivity values support the proposed CNT morphology (Fig.7.B.4) in XCH composite.
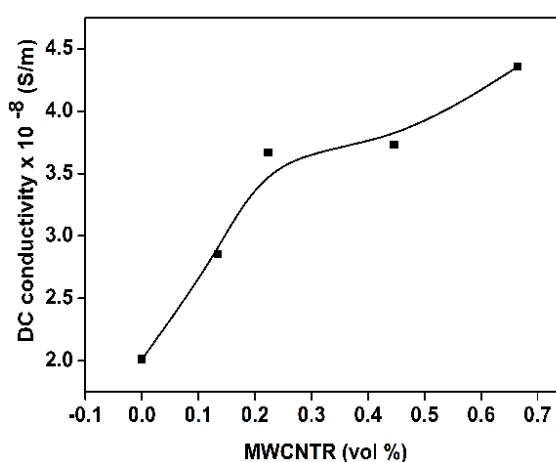
Fig. 7.B.12 Variation of DC conductivity of the XCH composites with MWCNTR loading

Difference in the conductivity of XCF and XCH composites can be explained in terms of the difference in filler distribution between the two. In XCF composites MWCNTRs form a segregated network which helps in creating percolative conductive network at low nanotube concentration. The presence of network at ultralow electrical percolation is reflected in their good DC conductivity behaviour which has been discussed 7.A of this chapter. XCH composites contain well dispersed nanotubes instead of segregated network that makes the tube-tube contact possible only at high concentration of CNTs[35]. For drastic change in the electrical conductivity the conducting CNTs should either make physical contacts or should be separated by very small gaps to allow the hoping or tunnelling of electrons across the gaps[36,37].

7.B.3.10 Dielectric studies

Fig.7.B.13 shows the variation of dielectric permittivity, dielectric loss and AC conductivity of XCH nanocomposites. The figure clearly shows that dielectric permittivity and loss tangent remain more or less the same for all nanocomposites. Inferior dielectric performance of XCH composites can be related to the random dispersion of MWCNTs in the Haake mixed samples. Here the dielectric percolation has not been achieved even at 1.5 phr MWCNTR loading. The results reveal that the segregated conductive network that existed in XCF was beneficial for attaining excellent dielectric properties whereas random dispersion of CNTs in XCH could not help in improving dielectric performance.
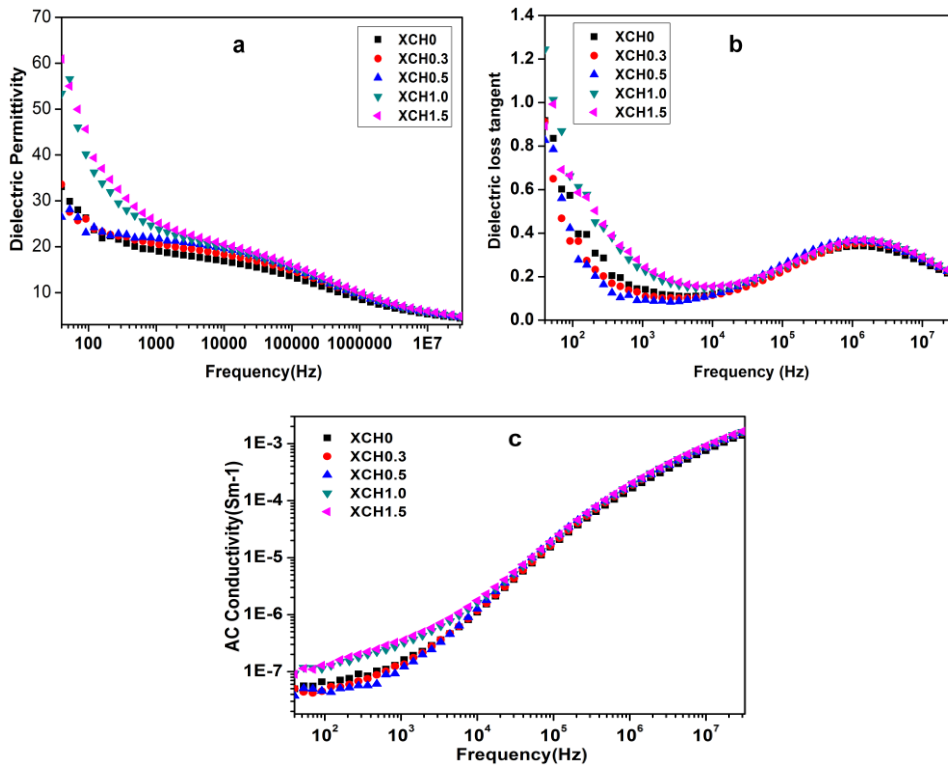
Fig. 7.B.13 Variation of (a) dielectric constant (b) dielectric loss and (c) AC conductivity with frequency for XCH composites

AC conductivity of the XCH nanocomposites (Fig. 7.B.13c) does not show any abrupt increase in the value indicating that the electrical percolation has not been achieved for the composite. The conducting MWCNTs are homogeneously dispersed in the matrix and are far apart to form a continuous conductive network.
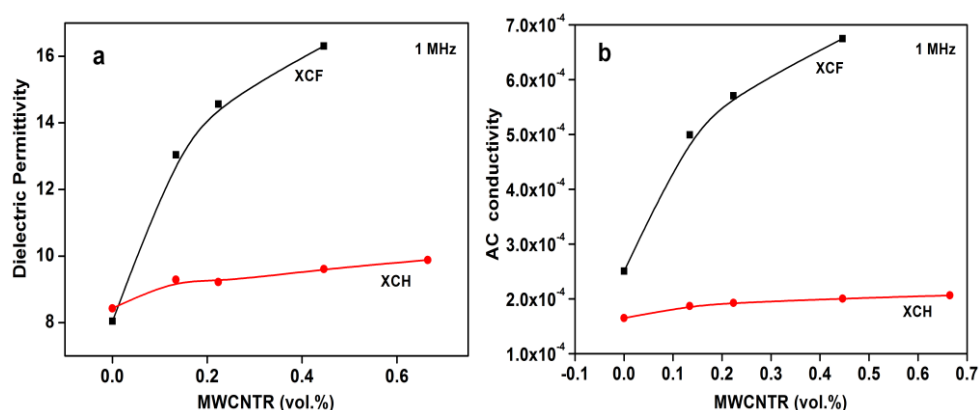
Fig. 7.B.14 (a) Comparison of dielectric permittivity and (b) AC conductivity of XCF and XCH composites at 1MHz

Comparison of dielectric permittivity (Fig.7.B.14a) and AC conductivity (Fig.7.B.14b) of XCF and XCH composites substantiates that the nature of filler distribution plays a major role in determining electrical properties of the composite. Significant improvement in dielectric constant and AC conductivity has been observed for the segregated structured XCF composites whereas only a marginal increase is observed for XCH composites with non-segregated structure. Segregated conductive polymer composites are well-known for their ultralow electrical percolation threshold as the conducting fillers are confined to the periphery of polymeric granules and thereby utilizing minimum amount of the nanotubes to form a conductive network [35]. XCF composites have a percolation threshold of 0.05 vol% of MWCNTR (Chapter 7A). Large difference in the electrical properties of the two composites is a clear evidence for the type of filler distribution present in the systems.

7.B.3.11 EMI shielding effectiveness

EMI shielding effectiveness (SE) of the XCH composites is shown in Fig. 7.B.15. Compared to XCF composites the SE observed in this case is small which can be related to the difference in filler morphology and electrical properties. The XCH composites have poor electrical properties compared to XCF which have been discussed in the previous sections. Gupta et al. [38] and Huang et al. [39] have demonstrated that conductivity of the CNTs influences the shielding efficiency with highly conducting long nanotubes exhibiting better SE compared to short tubes. XCH composites contain random nanotube network unlike segregated network in XCF and have not attained percolation threshold even at 1.5 phr of MWCNTR leading to poor EMI shielding efficiency.

Fig. 7.B.15 Variation of SE with frequency of XCH composites

7.B.4 Conclusions

Microstructure and electrical properties of the XCH composites were found to be entirely different from those of XCF composites. SEM and

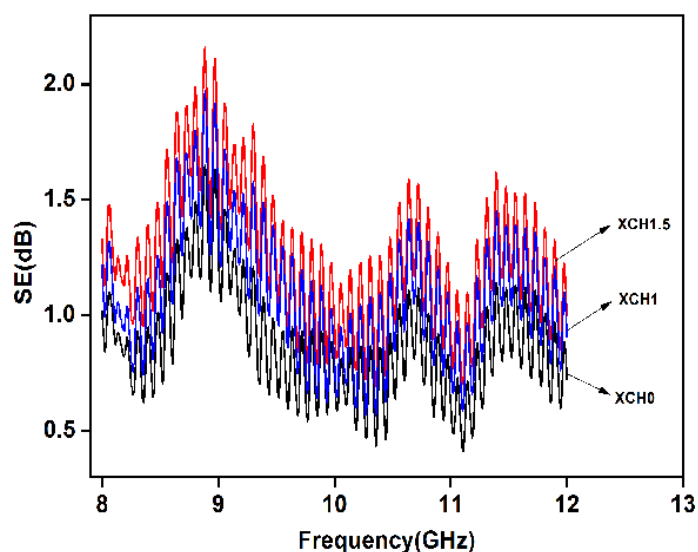TEM analysis of the XCH composites revealed that nanotubes are distributed evenly throughout the bulk of the XNBR matrix instead of segregating at the interfaces of XNBR granules as in XCF. The composites exhibited excellent mechanical properties. Tensile strength and modulus at 300% elongation increased by 35% and 8% respectively with 1.5 phr MWCNTR loading. Tear strength improved by 34% at 1.0 phr MWCNTR. The low conductivity behaviour and dielectric performance indicated the absence of continuous conductive filler network. The work reveals that the processing method has a significant influence on the filler morphology inside the polymer matrix and also on the properties of a composite. From the technological perspective XCH preparation method could be used industrially for applications which require mechanically strengthened XNBR. Improved solvent resistance and crosslink density observed for XCH composites indicated good rubber-filler interaction. Thermal stability of XNBR was unaffected by the addition of MWCNTRs.

References

[1] Yang, J., Tian, M., Jia, Q. X., Shi, J. H., Zhang, L. Q., Lim, S. H., ... & Mai, Y. W. (2007). Improved mechanical and functional properties of elastomer/ graphite nanocomposites prepared by latex compounding. *Acta Materialia*, *55*(18), 6372-6382.

[2] Yang, J., Zhang, L. Q., Shi, J. H., Quan, Y. N., Wang, L. L., & Tian, M. (2010). Mechanical and functional properties of composites based on graphite and carboxylated acrylonitrile butadiene rubber. *Journal of applied polymer science*, *116*(5), 2706-2713.

[3] Wang, J., Jia, H., Tang, Y., Ji, D., Sun, Y., Gong, X., & Ding, L. (2013). Enhancements of the mechanical properties and thermal conductivity of carboxylated acrylonitrile butadiene rubber with the addition of graphene oxide. *Journal of Materials Science*, *48*(4), 1571-1577.

[4] Liu, X., Sun, D., Wang, L., & Guo, B. (2013). Sodium humate functionalised graphene and its unique reinforcement effects for rubber. *Industrial & Engineering Chemistry Research*, *52*(41), 14592-14600.

[5]   Laskowska, A., Marzec, A., Zaborski, M., & Boiteux, G. (2014). Reinforcement of carboxylated acrylonitrile-butadiene rubber (XNBR) with graphene nanoplatelets with varying surface area. *Journal of Polymer Engineering*, *34*(9), 883-893.

[6]   Kang, H., Zuo, K., Wang, Z., Zhang, L., Liu, L., & Guo, B. (2014). Using a green method to develop graphene oxide/elastomers nanocomposites with combination of high barrier and mechanical performance. *Composites Science and Technology*, *92*, 1-8.

[7]   Tkalya, E., Ghislandi, M., Alekseev, A., Koning, C., & Loos, J. (2010). Latex-based concept for the preparation of graphene-based polymer nanocomposites. *Journal of Materials Chemistry*, *20*(15), 3035-3039.

[8]   Brown, H. P. (1957). Carboxylic elastomers. *Rubber Chemistry and Technology*, *30*(5), 1347-1386.

[9]   Bandyopadhyay, S., De, P. P., Tripathy, D. K., & De, S. K. (1996). Influence of surface oxidation of carbon black on its interaction with nitrile rubbers. *Polymer*, *37*(2), 353-357.

[10]   Nair, K. P., Thomas, P., & Joseph, R. (2012). Latex stage blending of multiwalled carbon nanotube in carboxylated acrylonitrile butadiene rubber: mechanical and electrical properties. *Materials & Design*, *41*, 23-30.

[11]   Lu, L., Zhai, Y., Zhang, Y., Ong, C., & Guo, S. (2008). Reinforcement of hydrogenated carboxylated nitrile–butadiene rubber by multi-walled carbon nanotubes. *Applied Surface Science*, *255*(5), 2162-2166.

[12]   Potts, J. R., Shankar, O., Murali, S., Du, L., & Ruoff, R. S. (2013). Latex and two-roll mill processing of thermally-exfoliated graphite oxide/natural rubber nanocomposites. *Composites Science and Technology*, *74*, 166-172.

[13]   Zhan, Y., Lavorgna, M., Buonocore, G., & Xia, H. (2012). Enhancing electrical conductivity of rubber composites by constructing interconnected network of self-assembled graphene with latex mixing. *Journal of Materials Chemistry*, *22*(21), 10464-10468.

[14]   Peng, Z., Feng, C., Luo, Y., Li, Y., & Kong, L. X. (2010). Self-assembled natural rubber/multi-walled carbon nanotube composites using latex compounding techniques. *Carbon*, *48*(15), 4497-4503.

[15] Teh, P. L., Ishak, Z. M., Hashim, A. S., Karger-Kocsis, J., & Ishiaku, U. S. (2004). Effects of epoxidized natural rubber as a compatibilizer in melt compounded natural rubber–organoclay nanocomposites. *European Polymer Journal*, *40*(11), 2513-2521.

[16] Yuca,N. Karatepe,N, Yakuphanoğlu,N. (2011). Thermal and Electrical Properties of Carbon Nanotubes Purified by Acid Digestion, World Academy of Science, *Engineering and Technology*, 79 , 611-616.

[17] Mousa, A., Heinrich, G., & Wagenknecht, U. (2011). Cure characteristics and mechanical properties of carboxylated nitrile butadiene rubber (XNBR) vulcanisate reinforced by organic filler. *Polymer-Plastics Technology and Engineering*, *50*(13), 1388-1392.

[18] Yudianti, R., Onggo, H., Sudirman, Y. S., Iwata, T., & Azuma, J. I. (2011). Analysis of functional group sited on multi-wall carbon nanotube surface. *Open Materials Science Journal*, *5*, 242-247.

[19] Datsyuk, V., Kalyva, M., Papagelis, K., Parthenios, J., Tasis, D., Siokou, A., ... & Galiotis, C. (2008). Chemical oxidation of multiwalled carbon nanotubes. *Carbon*, *46*(6), 833-840.

[20] Kim, H., Miura, Y., & Macosko, C. W. (2010). Graphene/polyurethane nanocomposites for improved gas barrier and electrical conductivity. *Chemistry of Materials*, *22*(11), 3441-3450.

[21] Bai, X., Wan, C., Zhang, Y., & Zhai, Y. (2011). Reinforcement of hydrogenated carboxylated nitrile–butadiene rubber with exfoliated graphene oxide. *Carbon*, *49*(5), 1608-1613.

[22] Eisemberg, A. (1970). Clustering of Ions in Organic Polymers. A Theoretical Approach, *Macromolecules*, 3 (2), 147–154.

[23] Arayapranee, W., Na-Ranong, N., & Rempel, G. L. (2005). Application of rice husk ash as fillers in the natural rubber industry. *Journal of applied polymer science*, *98*(1), 34-41.

[24] Potts, J. R., Shankar, O., Du, L., & Ruoff, R. S. (2012). Processing–morphology–property relationships and composite theory analysis of reduced graphene oxide/natural rubber nanocomposites. *Macromolecules*, *45*(15), 6045-6055.

[25] El-Nashar, D. E., Ward, A. A., Abd-El-Messieh, S. L., & Cairo, D. (2009). Physico-mechanical and dielectric properties of nitrile rubber filled with silica and mica. *Elastomers and Plastics*, 434–40.

[26] Payne, A. R., & Whittaker, R. E. (1971). Low strain dynamic properties of filled rubbers. *Rubber chemistry and technology*, *44*(2), 440-478.

[27] Fröhlich, J., Niedermeier, W., & Luginsland, H. D. (2005). The effect of filler–filler and filler–elastomer interaction on rubber reinforcement. *Composites Part A: Applied Science and Manufacturing*, *36*(4), 449-460.

[28] Bokobza, L. (2012). Multiwall carbon nanotube-filled natural rubber: Electrical and mechanical properties. *Express Polymer Letters,* 6(3), 213-223.

[29] Das, A., Jurk, R., Stöckelhuber, K. W., Majumder, P. S., Engelhardt, T., Fritzsche, J., ... & Heinrich, G. (2008). Processing and properties of nanocomposites based on layered silicate and carboxylated nitrile rubber. *Journal of Macromolecular Science, Part A*, *46*(1), 7-15.

[30] Billmeyer F.W. (1994). Text book of polymer science, Wiley Interscience, A Wiley-lnterscience Publication, John Wiley & Sons, Singapore.

[31] Huxtable, S. T., Cahill, D. G., Shenogin, S., Xue, L., Ozisik, R., Barone, P., ... & Keblinski, P. (2003). Interfacial heat flow in carbon nanotube suspensions. *Nature materials*, *2*(11), 731-734.

[32] Sui, G., Zhong, W. H., Yang, X. P., Yu, Y. H., & Zhao, S. H. (2008). Preparation and properties of natural rubber composites reinforced with pretreated carbon nanotubes. *Polymers for Advanced Technologies*, *19*(11), 1543-1549.

[33] Abdullateef, A. A., Thomas, S. P., Al-Harthi, M. A., De, S. K., Bandyopadhyay, S., Basfar, A. A., & Atieh, M. A. (2012). Natural rubber nanocomposites with functionalised carbon nanotubes: mechanical, dynamic mechanical, and morphology studies. *Journal of Applied Polymer Science*, 1(*125),* E76–E84.

[34] Perez, L. D., Zuluaga, M. A., Kyu, T., Mark, J. E., & Lopez, B. L. (2009). Preparation, characterisation, and physical properties of multiwall carbon nanotube/elastomer composites. *Polymer Engineering and Science*, *49*(5), 866.

[35] Pang, H., Xu, L., Yan, D. X., & Li, Z. M. (2014). Conductive polymer composites with segregated structures. *Progress in Polymer Science*, *39*(11), 1908-1933.

[36] Reffaee, A. S., El Nashar, D. E., Abd-El-Messieh, S. L., & Abd-El Nour, K. N. (2009). Electrical and mechanical properties of acrylonitrile rubber and linear low density polyethylene composites in the vicinity of the percolation threshold. *Materials & Design*, *30*(9), 3760-3769.

[37] Lorenz, H., Fritzsche, J., Das, A., Stöckelhuber, K. W., Jurk, R., Heinrich, G., & Klüppel, M. (2009). Advanced elastomer nano-composites based on CNT-hybrid filler systems. *Composites Science and Technology*, *69*(13), 2135-2143.

[38] Gupta, T. K., Singh, B. P., Teotia, S., Katyal, V., Dhakate, S. R., & Mathur, R. B. (2013). Designing of multiwalled carbon nanotubes reinforced polyurethane composites as electromagnetic interference shielding materials. *Journal of Polymer Research*, *20*(6), 169.

[39] Li, N., Huang, Y., Du, F., He, X., Lin, X., Gao, H., ... & Eklund, P. C. (2006). Electromagnetic interference (EMI) shielding of single-walled carbon nanotube epoxy composites. *Nano letters*, *6*(6), 1141-1145.

.....ഇരു.....

Chapter 8

SUMMARY AND CONCLUSIONS

Efficient dispersion of nanofillers in the polymer matrix plays a major role in the preparation of high performance polymer nanocomposites. Conventional methods of composite preparation were found to be ineffective due to the severe agglomeration of nanofillers in the polymer. In the present investigation an attempt has been made to prepare rubber nanocomposites with segregated structure of nanofillers. Segregated structure has more significance in the case of conductive fillers because of the ultra-low percolation threshold exhibited by these composites. Segregated electrically conductive polymer composites (s-CPCs) have conductive fillers segregated at the interfaces of the polymeric particles instead of being randomly dispersed in the polymer matrix. In the present investigation NR and XNBR were used as polymer matrices, MWCNT was chosen as the conductive nanofiller and nanosilica as the modifier to MWCNTs. In order to ensure efficient dispersion of nanofiller in the rubber, aqueous dispersion of the nanofiller was prepared and mixed with the rubber latex. A second processing route was adopted to study the effect of processing method on the distribution of nanofillers in the rubber nanocomposite and hence the properties, especially, the mechanical and electrical properties was studied.

MWCNTs are known for their exceptional mechanical and electrical properties and can contribute outstanding properties to polymer matrices.

The main difficulty in obtaining a homogeneous dispersion of CNTs is their tendency to remain as bundles due to strong van der Waals force of attraction. To overcome this difficulty two types of modifications were done on MWCNTs to disperse them uniformly in water so that these can be mixed with NR and XNBR latices efficiently. The use of non-ionic surfactant, Vulcastab VL as a dispersant for MWCNT in water is described in Part A of chapter 3. Concentration of VL and sonication energy required for stable nanotube dispersion has been optimised with the help of UV-vis spectral studies and particle size analysis based on dynamic light scattering. CNT to VL weight ratio has been optimised to be 1:1 for getting stable aqueous dispersions of MWCNTs. Minimum sonication energy required was 85000 J. Morphological studies using TEM confirmed the formation of surfactant wrapped exfoliated MWCNTs.

Surfactant treated nanotube dispersions were mixed with NR latex, compounded and film cast to get NR-MWCNT composites. TEM images of the composites revealed the presence of a segregated network of nanotubes throughout the NR matrix. The composites exhibited very good mechanical properties with 68% increase in tensile strength, 80% increase in tensile modulus and 55% increase in tear strength at 0.1phr MWCNT loading. A very low percolation threshold of 0.043 vol% obtained from electrical conductivity studies confirmed the presence of segregated nanotube network in which the individual CNTs are aligned along the periphery of the rubber particles in the composite. Dielectric properties of the composites were promising but the DC conductivity and AC conductivity (at low frequency) were far below the expected values due to the presence of insulating surfactant coating over the nanotubes.

The electrical properties of MWCNT based NR composites were improved by chemical modification of MWCNT (Chapter 4A), which involved acid treatment of MWCNTs. Polar hydrophilic groups such as

hydroxyl and carboxyl moieties introduced on the nanotube surface by oxidation with H_2SO_4/HNO_3 mixture assisted in getting stable aqueous dispersions of MWCNTs. FTIR spectra, Raman spectra, XPS and TGA confirmed the presence of carboxyl groups on the MWCNT surface. Morphological studies of MWCNTR using SEM and TEM further proved that the acid treatment shortens and purifies the nanotubes and helps in debundling of the MWCNTs into individual tubes.

Aqueous dispersions of oxidised MWCNTs (MWCNTRs) were mixed with NR latex, compounded and film cast to prepare NR-MWCNTR composites. The composites exhibited beautiful segregated MWCNTR network in NR giving rise to low electrical percolation threshold (0.086 vol% or 0.2 phr), good electrical conductivity and high dielectric constant. Along with increase in dielectric constant, there has been proportional increase in the dielectric loss for these composites. The composites exhibit good mechanical properties with 61% improvement in tensile strength, 75 % in tensile modulus and 59 % in tear strength at 0.5 phr of MWCNTR. The DC conductivity increases from 1.7×10^{-12} to 5.65×10^{-7} Sm^{-1} with 0.3 phr MWCNTR (0.1293 vol%). The inclusion of 1.0 phr MWCNTR in the NR matrix increased the dielectric constant from 4.7 for pure NR to 918 at 100 Hz. The AC conductivity reached a value of 10^{-4} S/m for the nanocomposite at 1 kHz. These, nanoscale, flexible, reinforced natural rubber based composites with high dielectric constant and dielectric loss can find application as electromagnetic wave absorbers in the low frequency region.

NR-MWCNTR composites prepared were of high dielectric loss and an attempt to reduce the dielectric loss by incorporation of insulating nanosilica along with carboxylated MWCNTs was done. Influence of colloidal nanosilica on the properties of NR is described in Chapter 5. NRSF composites prepared by film casting and curing of the nanosilica/natural rubber latex compound show segregated structure of nanosilica within the NR matrix. The rigid

network imparted significant improvement in tensile strength (60%), tear resistance (157%) and tensile modulus (90%) at 5 phr silica. The mol% uptake of toluene (Q_t) is reduced for the composite by 67% which could be explained in terms of the reduction in the ease of penetration of solvent due to the increase in tortuosity created by the segregated silica network in NR.

In order to understand how the processing method influences the filler morphology inside a rubber and hence the properties of the composites, NR/nanosilica composites were prepared using Haake mixer. Here also latex stage mixing of colloidal nanosilica with NR was done as the first step and then instead of film casting the mix was coagulated and the dried coagulum was mixed in the Haake internal mixer to get NRSH nanocomposites. Microstructure analysis of the composite using TEM revealed randomly dispersed nanosilica inside the rubber. This shows that the web-like nanosilica network in the coagulum has been broken by the intense shear forces in the internal mixer and the final sample contains uniformly distributed nanosilica in NR matrix. The composites exhibit significant improvement in the mechanical properties at 5 phr silica loading. NRSH5 nanocomposite exhibited good mechanical properties with 28% enhancement in modulus, 38% in tensile strength and 29% in tear strength. Difference in the filler morphology in NRSF and NRSH composites was supported by the SEM images of the tensile and tear fractured surfaces and strain sweep studies. On comparing NRSF and NRSH composites it is found that regardless of the processing conditions mechanical properties of both composites increased with silica loading and good mechanical properties were obtained at 5 phr.

Ultrasonication assisted mixing of carboxylated MWCNTs and colloidal nanosilica was done to coat nanotubes with nanosilica (CS hybrid) to reduce dielectric loss. Preparation of CS hybrid fillers involved very simple and environment friendly method using water as the solvent and ultrasonication as the processing tool. Hydrogen bonding possible between carboxyl groups

on the nanotube side walls and silanol groups on nanosilica helped in the adsorption of nanosilica particles on the nanotube surface. These hybrid fillers gave stable aqueous dispersions on ultrasonication. Film casting method adopted in this case resulted in NRCSF composite with a segregated CS hybrid filler network. TEM and SEM images, and strain sweep studies of the composites revealed the segregated network of the hybrid filler. The NRCSF2 composite exhibited excellent mechanical properties with 65% increase in tensile strength, 122% in tensile modulus and 86% in tear strength compared to neat NR and further addition of the nanohybrid filler reduced the properties. 58% reduction in swelling index was observed for NRCSF2 composite supporting the solvent resistance offered by the segregated CS hybrid in NR. The NRCSF composites exhibited high dielectric constant (417 at 10^3 Hz) and low electrical percolation threshold (0.80 vol%). Insulating nanosilica coated nanotubes reduced the dielectric loss for the composite and NRCSF composite exhibited better dielectric performance than the NR based composites reported elsewhere (Table 6.5). Comparison of dielectric properties of NRCSF with NR-MWCNTR at 1 kHz indicated that the dielectric loss of NRMWCNTR composite was very high (2.20) at a dielectric constant of 133 whereas the dielectric loss of NRCSF composite was low (1.6) at a dielectric constant of 417. At 1MHz frequency both NRMWCNTR and NRCSF exhibited same dielectric permittivity, but the dielectric loss tangents were quite low for the NRCSF composite compared to NRMWCNTR. In NRCSF, nonconducting silica can form insulating sheath around the carbon nanotubes and avoid direct contact of the conducting nanotubes. This reduces the leakage of current and the composite shows low dielectric loss. These elastomeric nanocomposites with high dielectric constant and low dielectric loss can find application as capacitors for energy storage.

NRCSH composites were prepared using the same method adopted for the preparation of NRSH nanocomposites. Here also the segregated CS filler network in the coagulum was disturbed by the intense shear forces between the rotors in the internal mixer resulting in random distribution of fillers in the composite. TEM, SEM and strain sweep studies provided clear picture of the difference in filler morphology of NRCSF and NRCSH nanocomposites. Tensile strength, modulus (300%) and tear strength increase with CS hybrid filler loading whereas elongation at break decreases. 19% enhancement in tensile strength, 57 % in modulus, and 37 % in tear strength were exhibited by NRCSH3 composite. Tensile strength, tear strength and modulus of NRCSF were higher compared to NRCSH which can be credited to the segregated structure. Higher modulus of NRCSH compared to NRCSF can be explained in terms of the crosslink density difference in the two; because more crosslink formation is possible in the case of compression moulded samples compared to the film cast ones. But the relative increase in modulus with respect to neat rubber is still higher for the NRCSF composites and that can be credited to the segregated structure of the composites. DC conductivity values obtained for the NRCSH composites are in good agreement with the arrangement of fillers proposed for the composite. There is no significant change in the conductivity with filler loading suggesting the absence of continuous conductive network for the composites. Moreover the presence of insulating silica particles around carbon nanotubes can hinder the proper contact between the conducting nanotubes and can result in poor conductivity. Comparison of dielectric permittivity and AC conductivity of NRCSF and NRCSH composites proves that the nature of filler distribution plays a major role in determining electrical properties of the composite. Significant improvement in dielectric constant and AC conductivity has been observed for the segregated structured NRCSF

composites while only a marginal increase is observed for NRCSH composites with non-segregated structure.

Possibility of segregated filler network formation during latex stage mixing and the effect of processing method on the filler morphology were studied using carboxylated nitrile rubber (XNBR) which is a polar rubber. XCF composites prepared by ultrasonication assisted latex stage mixing of MWCNTR aqueous dispersion with XNBR and film casting show segregated MWCNTR network in XNBR matrix. TEM of the composite film and SEM of the fracture surface along with strain sweep studies proved the presence of network. The rigid filler network along with good rubber-filler interaction possible via H-bonding between the surface groups on MWCNTR and XNBR contributed to the enhancement in mechanical properties of the composites. 65 % improvement in tensile strength and 32% in modulus were observed for XCF0.3. Tear strength also increased by 22% for XCF0.7. The composites exhibited excellent dielectric properties at ultralow percolation threshold (f_c=0.05 vol% ~ 0.1 phr) which is credited to the existence of 3D segregated MWCNTR network inside the rubber. Dielectric constant at 100Hz increased from 23 for pure XNBR to around 490 for 1 phr and 7000 for 7 phr MWCNTR.

XCH composites prepared by co-coagulation method and Haake mixing exhibited random nanotube network leading to excellent mechanical properties. Tensile strength at break increased by 35% at 1.5 phr MWCNTR and tear strength improved by 34% at 1.0 phr MWCNTR. Low electrical conductivity behaviour shown by all Haake mixed samples viz. NRSH, NRCSH and XCH composites indicate the absence of conductive network. Dielectric properties were also poor for these composites. The study reveals that the processing method has a significant impact on morphology which in turn affects the properties of the composites. Random network of filler is

beneficial in getting good mechanical properties whereas it has a detrimental effect on electrical properties.

Presence of segregated filler network in all the composites prepared by film casting was supported by strain sweep studies. These composites exhibited increase in Payne effect with filler loading suggesting decrease in modulus due to breakage of filler–filler networks with applied strain. Segregated structure had no significant influence on the thermal stability of the rubber. Improved solvent resistance and crosslink density of all the nanocomposites indicate good rubber filler interaction. The mechanical properties decrease after reaching an optimal concentration in all the composites which can be due to the agglomeration of the fillers.

This study could develop a technique for the successful fabrication of an elastomer composite with segregated network of nanofillers. The work has proved the efficacy of non-ionic surfactant in debundling the nanotubes and obtaining a good aqueous dispersion. Mechanical properties of the composites could be improved substantially even with very low filler concentrations. The segregated network of MWCNTs resulted in very low percolation threshold and improved electrical properties. Carboxylated MWCNTs could impart good dielectric properties barring an increase in dielectric loss. Nanosilica modified MWCNTs were successful in reducing the dielectric loss to considerably low values but not to the expected level for capacitor applications. An alternate processing method adopted (co-coagulation followed by mixing in Haake) proved that the method of processing a composite strongly influences the distribution of fillers in the polymer. The Haake mixing method resulted in random filler network which had a reducing effect on electrical properties.

Future scope of the work

There is ample scope for continuation of the studies on the rubber nanocomposites with segregated structure. Some of the possibilities are listed below.

- Preparation of Rubber/CNT nanocomposites with segregated network having high CNT content without sacrificing mechanical properties.

- Optimisation of silica coating over MWCNT and study of dielectric performance of the hybrid filler.

- Tuning the dielectric properties of the CNTs by modification to make them suitable for capacitor applications

- Study of actuated strain of the rubber/CNT composites for application as dielectric elastomer actuators.

- EMI shielding studies of NR/MWCNT composites with high CNT content.

.....ജാ.....

||||| List of Publications |||||

International Journals

[1] **Neena George,** Julie Chandra, A. Mathiazhagan, and Rani Joseph. "High performance natural rubber composites with conductive segregated network of multiwalled carbon nanotubes." *Composites Science and Technology* 116 (2015): 33-40.

[2] Julie Chandra, **Neena George** and Sunil K. Narayanankutty. "Isolation and characterization of cellulose nanofibrils from arecanut husk fibre." *Carbohydrate polymers* 142 (2016): 158-166.

[3] **Neena George**, Bipinbal P. K., Bhavya Bhadran, A. Mathiazhagan and Rani Joseph. "Segregated network formation of multiwalled carbon nanotubes in natural rubber through surfactant assisted latex compounding: A novel technique for multifunctional properties" *Polymer* 112 (2017): 264-277.

[4] **Neena George**, A. Mathiazhagan and Rani Joseph. "Natural rubber nanocomposites based on multiwalled carbon nanotube/nanosilica hybrid". *Plastics and Rubber Srilanka* 15(2016): 20-23.

[5] Ajalesh Balachandran Nair, **Neena George**, Rani Joseph. "Non-linear viscoelastic behaviour of rubber-rubber blend composites and nanocomposites: Effect of Spherical, Layered and Tubular fillers". *Advances in Polymer Science* 264(2014): 85-134.

[6] **Neena George**, Venugopal B., Honey John, A. Mathiazhagan and Rani Joseph, "Nanosilica decorated multiwalled carbon nanotubes (CS hybrids) in natural rubber latex". *RSC advances (communicated)*

[7] **Neena George**, Gean A. Varghese, A. Mathiazhagan and Rani Joseph, "Nanosilica as reinforcing filler in NR latex: role of processing method on filler morphology inside the rubber and properties of the nanocomposite", *European Polymer Journal (communicated)*.

Conference Proceedings

[1] **Neena George,** Anoop Anand K., Rosamma Alex and Rani Joseph, "Single walled carbon nanotubes reinforced Natural Rubber Composites through latex compounding", International Conference-ICMSRN 27-29 February, 2008, Kodaikanal.

[2]   **Neena George**, Anoop Anand K. and Rani Joseph, "Multi walled carbon nanotubes/Natural Rubber nanocomposites through latex compounding", National Symposium-POLYSYM '08, at NIT Calicut (Won first prize in the young researcher award contest)

[3]   **Neena George** and Rani Joseph, "Functionalized MWNTs in Natural Rubber Matrix: Mechanical Properties and Electrical Conductivity", International conference-APT '08, PS and RT, CUSAT, 27-29 September 2008.

[4]   **Neena George** and Rani Joseph, "*Carboxylated multiwalled carbon nanotube-natural rubber composites with high Dielectric constant and Electrical conductivity*", 24th Swedeshi Science Congress, Thunchath Ezhuthachan Malayalam University, Tirur, Malappuram, Kerala. 6-8 November 2014, ISBN: 978-81-928129-2-2 (179-183).

[5]   **Neena George**, Rani Joseph, A. Mathiazhakan, "*Synthesis and Characterization of Carboxylated Mutiwalled carbon nanotubes*", National seminar on " Characterization techniques in Chemistry", Dept. of Chemistry, KKTM Govt. College, Pullut, Kodungallur, 16-17 December 2014.

[6]   **Neena George** and Rani Joseph, "*Natural rubber composites with conductive segregated network of Multiwalled Carbon nanotubes*", National Conference on Materials Science and Technology, Indian Institute of Space Science and Technology, Thiruvananthapuram, 6-8 July 2015.

[7]   **Neena George**, A. Mathiyazhagan, Rani Joseph, "*Reinforcement of Natural rubber with Mutiwalled Carbon nanotube/Nanosilica hybrid filler*", National conference on "Advanced Functional Materials", Dept. of Chemistry, Mar Athanasius college, Kothamangalam, 15-16 September 2015.(Best Paper Award)

[8]   **Neena George**, A. Mathiyazhagan, Rani Joseph, "*Use of Nanosilica as reinforcing filler in Natural rubber latex*", National conference on Biopolymers and green composites (BPGC 2015- 3rd in series), Centre for Biopolymer Science and Technology (CBPST), 9-10 October 2015.(Second Best paper award)

[9]   **Neena George**, Silpa.V, B.Usha Kumari, and Rani Josep, "*NR latex filled with CNT-nano silica hybrid filler: mechanical and barrier properties*", UGC sponsored National seminar on "Nanochemistry: Techniques, Advancement and Applications", PG and Research Dept. of Chemistry, S.D College, Alappuzha, 16th October 2015.

[10]   **Neena George**, A. Mathiyazhagan, Rani Joseph, "*Study on dispersion stability of Multiwalled carbon nanotubes in aqueous surfactant solution*", International Conference on "Advances in Applied Mathematics, Material Science and Nanotechnology for Engineering and Industrial applications: IC-AMMN-2K16", FISAT, Angamaly, 7-9 January, 2016.

[11] **Neena George**, A. Mathiyazhagan, Rani Joseph, "*Mechanical and electrical properties of Natural Rubber/Carbon nanotube composites with segregated nanotube structure*", National seminar on frontiers in Chemistry, St Aloysious college, Thrissur, 2015.

[12] **Neena George**, A. Mathiyazhagan, Rani Joseph, "*Natural rubber - Multiwalled Carbon nanotube/Nanosilica hybrid filler Composites with segregated conductive network*", International conference-Advances in Polymer Technology (APT 2016) conducted by the Dept. of Polymer Science and Rubber Technogy, CUSAT, 25-26 February, 2016.

[13] **Neena George**, Bipinbal P.K., Bhavya Badran, A. Mathiyazhagan and Rani Joseph, *Natural rubber - multiwalled carbon nanotube composites with multifunctional properties through surfactant assisted processing*", National seminar on 'Advancements in Polymer Science and Technology', Post Graduate Department of Chemistry, St. Teresa's College, Ernakulam.

[14] Bhavya Badran, Dhanya Vijayan, **Neena George**, P.M. Sabura Begum and Rani Joseph, "*Studies on the influence of nanofillers on the mechanical properties of nitrile rubber*", National seminar on 'Advancements in Polymer Science and Technology', Post Graduate Department of Chemistry, St. Teresa's College, Ernakulam.

[15] Bhavya Badran, Dhanya Vijayan, **Neena George**, Julie Chandra C. S, P.M. Sabura Begum and Rani Joseph "*A Comparative study on the reinforcing effect of Organoclay in Nitrile rubber fabricated by mill mixing and latex compounding methods*", 29th Keral Science Congress, 28-30 January 2017.

[16] Bhavya Badran, **Neena George,** Bindusharmila T. K., Dhanya Vijayan, , P.M. Sabura Begum and Rani Joseph, "*Tailored Graphene based Nitrile Rubber Nanaocomposites for High Performance Applications*", SCICON 16, Amrita Vishwa Vidyapeedam Uvty., 19-21 December 2016.

[17] **Neena George**, A. Mathiyazhagan, Rani Joseph, "*Nanosilica decorated Multiwalled Carbon Nanotube/ Natural Rubber Nanocomposites: Study of Processing Morphology and Property relationships*", India Rubber Industry Forum-2016, 5-6 December 2016, Bengaluru.

[18] **Neena George** and Rani Joseph, "*Natural rubber nanocomposites with segregated and random network of multiwalled carbon nanotube/nanosilica hybrid fillers*", 191st Technical meeting, Rubber Division, American Chemical Society, 25-27 April 2017, Beechwood, Ohio, U.S.A.

Books

[1] **Neena George**, Ajalesh B Nair. *Engineering Chemistry :Theory and Practice Laboratory manual,* Educational Publishers and Distributors, 1st Edition 2015. ISBN 81-87198-25-7.

[2] K.E George, Rani Joseph, M. Ushamani, Tania Francis, **Neena George**, Ajalesh. B. Nair. *Engineering Chemistry :Theory and Practice,* Educational Publishers and Distributors, 1st Edition 2015. ISBN 81-87198-23-0.

…..ഇരു…..

▌▌▌ Curriculum Vitae ▌▌▌

Neena George
Kulappurathu House
Janatha Road, JRA 202A
Manjummel P.O.
Pin-683501, Ernakula
Kerala, India

Ph: 989531103
E mail: ninleo07@gmail.com

Qualification	:	M.Sc. Chemistry, B. Ed., NET, SET
Teaching Experience	:	1 year as Higher Secondary School Teacher 7 years as Assistant Professor in Chemistry
Official Address	:	Assistant Professor, Department of Chemistry Govt. College Chittur Palakkad - 678104 Kerala, India
Research experience	:	2 years as Junior Research Fellow in a DST funded project, Dept. of Polymer Science and Rubber Technology, CUSAT. 1 year as Technical Assistant, Regional Chemical Examiner's laboratory, Kakkanad.

Seminars and workshops attended

Subject	Duration	Place	Sponsoring Authority
One day workshop on "The art of writing research papers and doctoral thesis"	24 Nov 2007	STIC, CUSAT	CSC and STIC, CUSAT
National Seminar on "Nanoscience and programming in Chemistry"	8-9 Feb 2011	St. Thomas' College, Thrissur	The University Grants Commission, India

Interdisciplinary national seminar " Science Sans Borders"	7-8 Nov 2013	Maharaja's college, Ernakulam	The Directorate of Collegiate education, Govt. of Kerala
Symposium on "Recent Advances in Macromolecular science and Engineering"	30/12/2013 to 01/01/2014	School of Chemical Sciences, M. G University	Srinivasa Ramanujan Institute for Basic Sciences and KSCSTE
Workshop on "Research reporting and reference management tools"	19 March 2014	University Library, CUSAT	University Library, CUSAT
Two day Lecture workshop on 'Molecular Machines'	2-3 February 2017	Maharaja's College, Ernakulam	Indian Academy of Sciences in association with PG and Research department of Chemistry, Maharajas College

Book Chapters contributed

1) Ajalesh Balachandran Nair, **Neena George**, Rani Joseph. *Non-linear viscoelastic behaviour of rubber-rubber blend composites and nanocomposites: Effect of Spherical, Layered and Tubular fillers*, (Series title: Advances in Polymer Science 264), Springer, 2014, p 85-134.

Books Published

1) **Neena George**, Ajalesh B Nair. *Engineering Chemistry: Theory and Practice Laboratory manual,* Educational Publishers and Distributors, 1st Edition 2015. ISBN 81-87198-25-7

2) K.E George, Rani Joseph, M.Ushamani, Tania Francis, **Neena George**, Ajalesh. B. Nair. *Engineering Chemistry: Theory and Practice,* Educational Publishers and Distributors, 1st Edition 2015. ISBN 81-87198-23-0

.....ಬಂ.....

Appendix

Justification of the proposed work

Compared to intrinsically conducting polymers, electrically conductive polymer composites (CPCs) developed by mixing polymer with conductive filler have generated significant interest due to their ease of processing, low-cost and tunable electrical properties. They have been used in many applications as conductors, sensors, anti-static materials and electromagnetic interference (EMI) shields. In ordinary CPCs with random network of conductive fillers, insulator to conductor transition occurred only at high filler loading. In 1971 Turner and co-workers introduced the concept of "segregated conductive network" for nickel particle/high-density polyethylene (HDPE) composites. Segregated conductive polymer composite (s-CPC) contains conductive fillers that are segregated in the perimeters of the polymeric granules instead of being randomly distributed throughout the bulk CPC material. From there on s-CPCs have generated considerable interest because of their ultralow percolation concentration (0.005–0.1 vol%), superior electrical conductivity (up to 10^6 S/m), and reasonable electromagnetic interference (EMI) shielding effectiveness (above 20 dB) at low filler loadings. Segregated structures having good mechanical and barrier properties are also reported in the literature.

Many studies are concentrating in the field of carbon nanotube-rubber composites on account of their wide range of applications. Most of the studies reveal the difficulty in obtaining a homogeneous dispersion due to severe agglomeration of carbon nanotubes in the rubber matrix. For the same reason, efforts are made to reinforce rubber with carbon nanotubes by conventional mill mixing method were found to be ineffective. Latex nanocomposites prepared by mixing the dispersions of nanofillers to the polymer latices have

become attractive nowadays. This is due to better performance resulting from the homogeneous dispersion of nanofillers in the matrix.

An attempt to fabricate the rubber based nanocomposites having segregated network of nanofillers in the matrix is made in the present work. Latex stage mixing of the nanofillers has been done to ensure the formation of segregated network of the nanofillers. The nanofillers have been added as their aqueous dispersions to reduce the agglomeration and hence to improve the distribution in the bulk matrix. The effect of mill mixing on the segregated structure is also studied and the comparison of mechanical and electrical properties has been made.